UNIVERSITÁ DEGLI STUDI DI UDINE

Department of Medical and Biological Sciences
PhD Course in Clinical Sciences and Technologies
XXVII Cycle (2012-2014)

PhD Research Thesis

The Awakening of Numb Autophagy-Lysosome Pathway Contrasts Senescence in Human Cardiac Stem Cells obtained from Failing Hearts

PhD STUDENT
Giuseppe Gianfranceschi

SUPERVISORS
Prof. Giacinto Scoles
Prof. Carlo Alberto Beltrami

TUTOR
Dott. Antonio Paolo Beltrami

Academic Year 2014 - 2015

Cui ch'al nol crôt ai Sants,

ch'al crodi ai meracui!

ACKNOWLEDGMENTS

Although I do not think that words are enough I'll try anyway to thank all those who made possible the achievement of this title.

During my PhD program I have been fortunate to have three mentors: Professor Giacinto Scoles, Doctor Antonio Beltrami and Doctor Daniela Cesselli.

I am very grateful to all of them, particularly to:

Prof. Scoles who believed in me showing that is possible to be a professor in a "less academic" way, focusing on growing students' potential, and constantly animated by an insatiable curiosity as well as a passion for science and teaching;

Antonio who constantly stimulated me to move forward overcoming the inevitable failures encountered during the journey and for the backing given me not only for my studies;

Daniela for her pivotal and costant support both professional and extraprofessional she has provided to me.

I would also like to thank all the friend of CSL, particularly:

all the people who have assisted me achieving this great result: Emmanouil, Angela, Elisa M., Barbara, Elisa P., Marisa, Michela, Elisa A.;

"Glioma" and "Immunological Research" staffs who through a "healthy competition" gave me a constructive stimulus for my scientific growth: Damiano, Jenny, Rossana, Ivana, Federica, Andrea, Alice;

all of those who gave me suggestions in different aspects of this work: Stefania M., Veronica, Stefania Z., Natasha, Giorgia and Elisabetta;

the whole staff of diagnostic unit of the department of pathology, that unfortunately are too numerous to list;

Lorenzo Chiarandini for his precious technical assistance.

My most sincere thanks are extended to

Prof. Carlo Alberto Beltrami for his expert guidance and for helping me get over my personal problems;

Dr. Nicoletta Finato for providing the necessary pathologic competence useful for this study;

Lisa Barbiani for her support in dealing with bureaucratic issues;

Prof. Schneider for microarray analysis;

Prof. Ugolino Livi of Cardiac Surgery Unit of the University Hospital of Udine, who provided the human samples object of this project;

Director of Tigem, Prof. Andrea Ballabio who allowed me to access his list of TFEB target genes useful for my study;

Molino Moras srl who funded my PhD scholarship.

I would also like to thank the friends who I met during my stay at Udine, who gave their support outside the lab: Jessica, Matteo, Enrico, Serena, Monica, Anita, Anna, Leonardo, Stefano, Francesco.

Last but not least a special thank goes to my family that, despite the distance, has followed and supported me step by step during this adventure.

TABLE OF CONTENTS

ABSTRACT

Background: Cardiac Stem Cells (CSCs) expanded *in vitro* from explanted failing hearts (E-) are characterized, with respect to those obtained from healthy donors (D-), by: reduced proliferation and migratory capabilities, shorter telomeres, and a larger fraction of cells showing both telomere-associated damage foci and senescence markers.

Since the Autophagy-Lysosome Pathway (ALP) plays a pivotal role in cellular homeostasis by controlling both cellular clearance and response to nutrients, defects on ALP may be associated to aging and heart failure progression.

Aims: to monitor the efficiency of ALP in senescent CSCs isolated from patients with heart failure and to develop a drug-based strategy able to boost ALP, eventually contrasting senescence.

Methods and Results: 14 D-CSC and 20 E-CSC, obtained from healthy and failing human hearts, respectively, were compared in terms of cell surface immunophenotype and senescence marker expression. Although the two groups of cells shared a similar immunophenotype, E-CSC showed a significant enrichment in the fraction of senescent cells ($p16^+$, γ $H2A.X^+$ Ki67-).

Microarray analysis and Real Time PCR were performed to investigate transcriptional profile (3 D-CSC vs 3 E-CSC) and expression profile of 380 microRNAs (4 D-CSC vs 4 E-CSC), identifying 423 genes down-regulated in E-CSC ($p<0.05$), 23 of which are involved in ALP, in addition to 7 differently expressed miRNAs ($p<0.05$), that are able to target genes linked to ALP and cell senescence regulation.

Consistently, the lysosomal compartment of 7 D- and 5 E-CSC was monitored by FACS analysis after staining with lysotracker and acridine orange and E-CSC displayed lysosomes less functional than the D-CSC ones. To study in depth this element, confocal microscopy analysis was performed to evaluate the lysosomal presence of not degradable lipofuscin and of the endomembrane damage marker Galectin 3, together with the amount of nuclear active Transciption Factor EB (TFEB). Noteworthy E-CSC showed a higher abundance of lysosomal lipofuscin and Galectin 3, coupled with a reduced TFEB activation.

Given the link between mTOR and senescence and the pivotal role played by mTORC1 in controlling autophagy and TFEB activation, we evaluated mTORC1 activity by western blot analysis. In particular attention was focused on pS6K, Akt in parallel with the autophagic markers Atg3, Atg7, LC3II, p62. Altogether results demonstrated that E-CSC were characterized by an enhanced activity of mTORC1 and an arrest in autophagic degradation.

Moving from these elements we develop a three days drug treatment of E-CSC with 10nM Rapamycin (TORC1 inhibitor). This pharmacologic strategy was able to reduce mTORC1 activity, to

potentiate the lysosomal functionality, to improve the autophagic flux and to reduce the fraction of senescent cells.

Conclusions: this study demonstrated that E-CSC are characterized by a blunted ALP. The pharmacologic inhibition of TORC1, on one hand, reactivated the pathway and, on the other hand, contrasted senescence offering promising perspectives to improve E-CSC cardiac regenerative efficiency.

LIST OF ABBREVIATIONS

CSCs	Cardiac Stem Cells
D-CSC	Cardiac Stem Cells isolated from Donor hearts
E-CSC	Cardiac Stem Cells isolated from Explanted, failing hearts
HF	Heart Failure
MI	Myocardial Infarction
ALP	Autophagy Lysosome Pathway
CPDT	Cell Population Doubling Time
DDR	DNA Damage Response
AO	Acridine Orange

1. INTRODUCTION

1.1 HEART FAILURE

Heart Failure (HF) is the end result of any condition that impairs either the diastolic or the systolic function of the myocardium and is the leading cause of morbidity and mortality [1]. The European Society of Cardiology (ESC) estimates that in a population of 900 million (51 countries represented by ESC), there are at least 15 million people that suffer from HF [2]. Latest estimates from American Heart Association (AHA) suggest that in USA there are 6 million patients affected by HF [1]. The worldwide prevalence of HF (proportion of general population with HF) is between 2 and 3% and rises sharply at about 75 years of age, so that the prevalence in 70- to 80-year-old people is between 10 and 20% [2]. Rotterdam Study reports that the overall incidence (number of new cases of disease over a given period of time) rate of heart failure was, at the period of the study, 14.4/1,000 person-years and is significantly higher in men (17.6/1,000 man-years) than in women (12.5/1,000 woman-years) [3]. HF is the cause of 5% of acute hospitalizations and 10% of hospital bed [2]. It consumes about 2% of the entire national expenditure on health [4].

The overall prevalence is expected to increase in the future due to the combined effect of an aging population and an evolution in treatment of patients with cardiovascular diseases.

1.1.1 HF DEFINITION AND CLASSIFICATION

Descriptions of HF exist from ancient Egypt. Last definition depicts HF as "physician documentation or report of any of the following clinical symptoms of heart failure described as unusual dyspnea on light exertion, recurrent dyspnea occurring in the supine position, fluid retention; or the description of rales, jugular venous distention, pulmonary edema on physical examination, or pulmonary edema on chest x-ray. A low ejection fraction without clinical evidence of heart failure does not qualify as heart failure" [5].

The clinic diagnose of HF is complicated by the fact that clinical features in the early stage of the disease may be few and not heart specific [6]. Symptoms and exercise capacity are used to classify the severity of heart failure and monitor the response to treatment [7]. Despite outcome in heart failure is best determined not only by symptoms, but also by echocardiographic criteria, the functional classification of the New York Heart Association (NYHA) is used widely in clinical practice and research [7]. NYHA distinguishes four classes of HF patients [7, 8]:

Class I: asymptomatic - No limitation in physical activity despite presence of heart disease. This can be suspected only if there is a history of heart disease which is confirmed by investigations - for example, echocardiography.

Class II: mild - Slight limitation in physical activity. More strenuous activity causes shortness of breath - for example, walking on steep inclines and climbing several flights of steps. Patients in this group can continue to have an almost normal lifestyle and career.

Class III: moderate - More marked limitation of activity which interferes with work. Walking on the flat produces symptoms.

Class IV: severe - Unable to carry out any physical activity without having symptoms. Patients are breathless at rest and mostly housebound.

1.1.2 HF THERAPY

Once the type of HF has been recognized, the management plan can be determined. The aims of the management are different from patients to patients in connection with their specific NYHA class. In general the goals are to improve the quality of life and to reduce mortality, but also to reduce the risk of decompensation and hospitalization.

Until 1950 management consisted of strict bed rest, sedation, dietary sodium restriction, digitalis, venesection, and administration of morphine and mercurial diuretics [9]; all treatments not changed for about a half century. To present, procedures such as venesection and heavy sedation are no longer used and there are many different options for patients depending on the severity of their symptoms. These options include lifestyle modification, multiple drug therapies, the use of devices such as cardiac resynchronization, or an Implantable Cardioverter-Defibrillator (ICD) and surgery [6].

Drug therapy has advanced greatly in the past decade and generally consists of a drug combination reflecting the complexity and multifactorial nature of this disease [6].

Unfortunately, to date the final treatment for end-stage HF is represented by cardiac transplantation but it is severely limited by the availability of donor hearts in addition to lifelong immunosuppression for transplant recipients [10]. In order to overcome these limitations, several types of ventricular assist devices (VADs) have been developed. To date VADs are still routinely used only as bridges to transplantation but are also being tested as destination therapy by different clinical trial [11]. Obtained results are encouraging but there is still a long way to go. Indeed, the VADs are large (**Figure 1.1**) and require extensive surgical dissection and a large percutaneous lead. Moreover, many complications accompanied the use of these devices, resulting in a 2-year survival rate of only 20%. Because of this several efforts are being made to eliminate or reduce the incidence of these complications, as well as to miniaturize the implanted devices [11].

Developments in VAD technology are not the only ones to which it is addressed the hope of HF management. Indeed, gene therapy, pharmacogenetics and cell based therapies, although still considered experimental, offer promising perspectives, not only aimed to treat the symptoms of HF but also to counter the organic causes of heart failure, such as loss of myocyte [12].

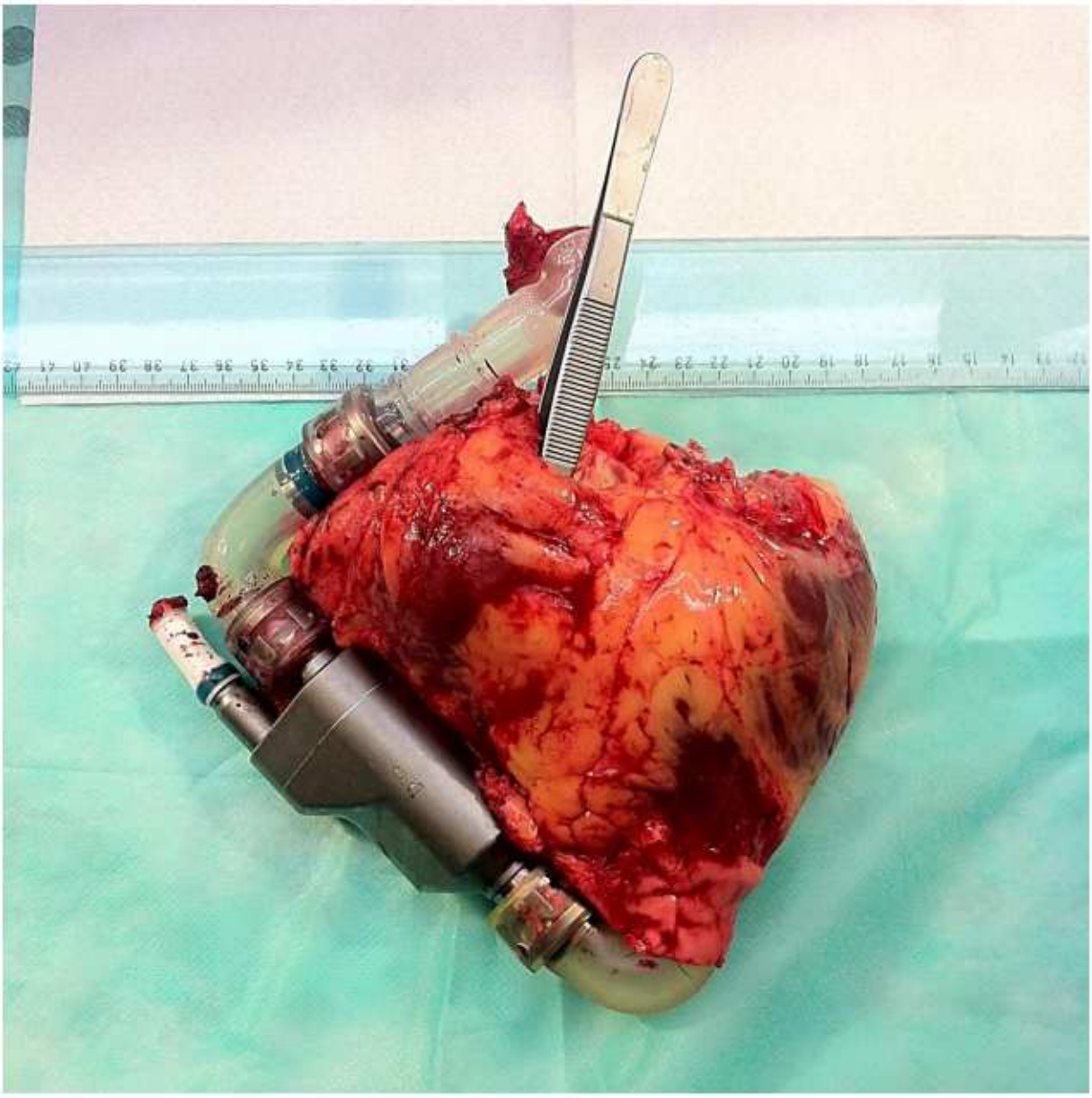

FIGURE 1.1. Explanted Heart with Ventricular Assistant Device.

1.2 STEM CELLS

The term "Stem Cell" was firstly proposed together with the existence of haematopoietic stem cells by Alexander Alexandrowitsch Maximow in 1908 [13], and it currently indicates immature precursor cells with the self-renewal ability and the great potential of multilineage differentiation [14].

1.2.1 DEFINITION AND CLASSIFICATION

A cell to be recognized as a stem cell has to satisfy four criteria (**Figure 1.2**) [14, 15]:

1. stem cells undergo multiple, sequential self-renewing cell divisions, a prerequisite for sustaining the population;
2. single stem cell-derived daughter cells differentiate into cells that have different, more restricted properties;
3. stem cells functionally repopulate the tissue of origin when transplanted in a damaged recipient;
4. stem cells contribute differentiated progeny in vivo even in the absence of tissue damage.

Depending on their differentiation potential (**Table 1.1**), stem cells are classically grouped as:

a. Totipotent (or Omnipotent) Cells differentiate in each extraembryonic and embryonic tissue. These cells are derived from embryos at the 4-8 cell stage, after 1-3 days after fertilization.
b. Pluripotent Cells are embryonic cells at the blastocyst stage, after 4-14 days after fertilization. These cells are capable of differentiating in tissues of embryonic origin organized in three different germ layers (ectoderm, mesoderm and endoderm), including germ cells.
c. Multipotent Cells have the capacity to multiply and remain in culture, but not the one to be indefinitely renewed. These cells differentiate into different tissues but (with the exception of spermatogonial stem cells) cannot differentiate into germ cells. Adult stem cells belong to this category.
d. Oligopotent Cells form 2 or more lineages within a specific tissue.
e. Unipotent Cells present in adult tissues, potentially more limited as well as organ-specific, are able to self-renew and to differentiate into the cell type of the belonging tissue ensuring its repair and maintenance [16].

Finally there is a classification based on origin (**Table 1.1**) that categorizes stem cells in:

a. Embryonic Stem Cells (ESCs) and Embryonic Germ Cells (EGCs) are pluripotent cells, derived from either the inner cell mass of the blastocyst or from primordial germ cells, respectively;
b. Fetal Stem Cells (FSCs) are multipotent cells, derived from fetal blood and bone marrow as well as from other fetal tissues;
c. Adult (or Somatic) Stem Cells (ASCs) are oligopotent cells, derived from adult tissue;
d. Induced Pluripotent Cells (IPSs) are pluripotent cells that are produced from adult somatic cells that are genetically reprogrammed to an 'ESC-like state'[16].

1.2.2 CARDIAC STEM CELLS

Recent studies in animal models and humans have shown that both the cardiomyocytes and the vascular cells can regenerate *de novo* in the adult heart, refuting the paradigm according to which the heart would be a post-mitotic organ composed of terminally differentiated cells that carry their function throughout the entire organism life [17].

The demonstration that humans can divide and amplify small myocytes after an infarction [18, 19] or a pressure overload [20, 21], and the evidence that the mammalian heart has a reserve of stem cells have led to consider the possibility of reconstituting, after a heart attack, the necrotic myocardium and to repair the dilation and thinning of the ventricular wall.

Cardiac stem cells (CSCs) identified by the expression of stem cell antigens c-kit (Stem Cell Factor Receptor), MDR-1 (Multi Drug Resistance Protein) and Sca-1 (Stem Cell Antigen) were found in hearts of different mammalian species; these cells have typical properties of stem cells, since they are multipotent, clonogenic and capable of self- renewal [22].

Candidate stem cells were also obtained from human heart samples by an *in vitro* selection under stringent conditions that could discourage the expansion of differentiated cell contaminants. In this manner, Cardiosphere Derived Cells (CDCs) and Multipotent Adult Stem Cells (MASCs) were identified in human hearts [23]. These cells are positive for c-kit, also known as CD117, are able to differentiate into the three major heart cell lines (myocytes, smooth muscle, and endothelial cells) and, when injected locally in the infarcted myocardium of immunodeficient mice and immunosuppressed rats, are capable of regenerating damaged tissue, giving rise to new cardiomyocytes and coronary vessels cells [24].

Although it has now been established that there is a population of CSCs in human adult heart, their origin remains still much debated. Some authors argue that resident cardiac stem cells, after being generated during embryonic development, remain *in situ* in an undifferentiated state, staying mainly in the apex and in the atrium [25, 26]; other studies have recently suggested the epicardium as a possible reserve of multipotent stem cells [27, 28]. In contrast, studies of sex-mismatched cardiac

transplants support the hypothesis of an extracardiac origin, suggesting that CSCs would derive from the bone marrow and would migrate into the site of damage after an appropriate stimulation [29, 30]. Intriguingly, a recent work by our laboratory has shown that, the transcriptional profile of human CSCs is similar to that of mesothelial cells, supporting the notion that these cells may be derived from the epicardium [31].

A reasonable correlation between these two hypotheses has been found by recent *in vitro* experimental approaches that have shown as bone-marrow-derived mesenchymal stem cells promote the proliferation and differentiation of CSC residents, through a paracrine mechanism [32, 33].

1.2.3 Clinical Trials to Treat Heart Failure with Cardiac Stem Cells

The robust evidence of the efficacy of CSC use for the therapy of injured myocardium in animal models [25, 34] encouraged the birth of several clinical trials designed to establish the safety, the feasibility and, more recently, the effectiveness of autologous CSC transplantation for the treatment of cardiovascular diseases.

The first clinical trial testing the therapeutic potential of CSCs in humans has been the Stem Cell Infusion in Patients with Ischemic Cardiomyopathy (SCIPIO) trial [35, 36]. In this trial, autologous c-kit$^+$ CSCs were isolated and expanded *ex vivo* from patients undergoing coronary artery bypass surgery after Myocardial Infarction (MI). Participants were then randomized to receive either intracoronary infusion of these c-kit$^+$ CSCs or conventional therapy. Preliminary results reported the feasibility and safety of the isolation and expansion of c-kit$^+$ CSCs, and their subsequent intracoronary delivery [36]. Regarding the effectiveness of this procedure, researchers described a significant improvement in both global and regional left ventricular function and a reduction in infarct size in the c-kit$^+$ CSC group when compared to conventional therapy. However, the trial was not designed to test efficacy [35].

In addition to SCIPIO, CADUCEUS (Cardiosphere-Derived Autologous Stem Cells to Reverse ventricular dysfunction) has been the only other clinical trial to have published results [37]. CADECEUS study evaluated the safety of autologous intracoronary CDC delivery in post-MI patients [38]. Endomyocardial biopsies were obtained by percutaneous techniques, and were used for CDCs isolation. These latter were then expanded *ex vivo*, and 2–4 weeks after were delivered by intracoronary injection into the infarct-related arteries. Results from the CADUCEUS trial show that CDC therapy appears to be safe. Magnetic resonance imaging revealed that at 3 months, CDC treatment reduced scar mass, increased viable heart mass as well as increased regional systolic wall thickening, when compared to controls [38]. These encouraging results led to further investigation of allogeneic CDC therapy in the larger ALLSTAR clinical trial (NCT01458405).

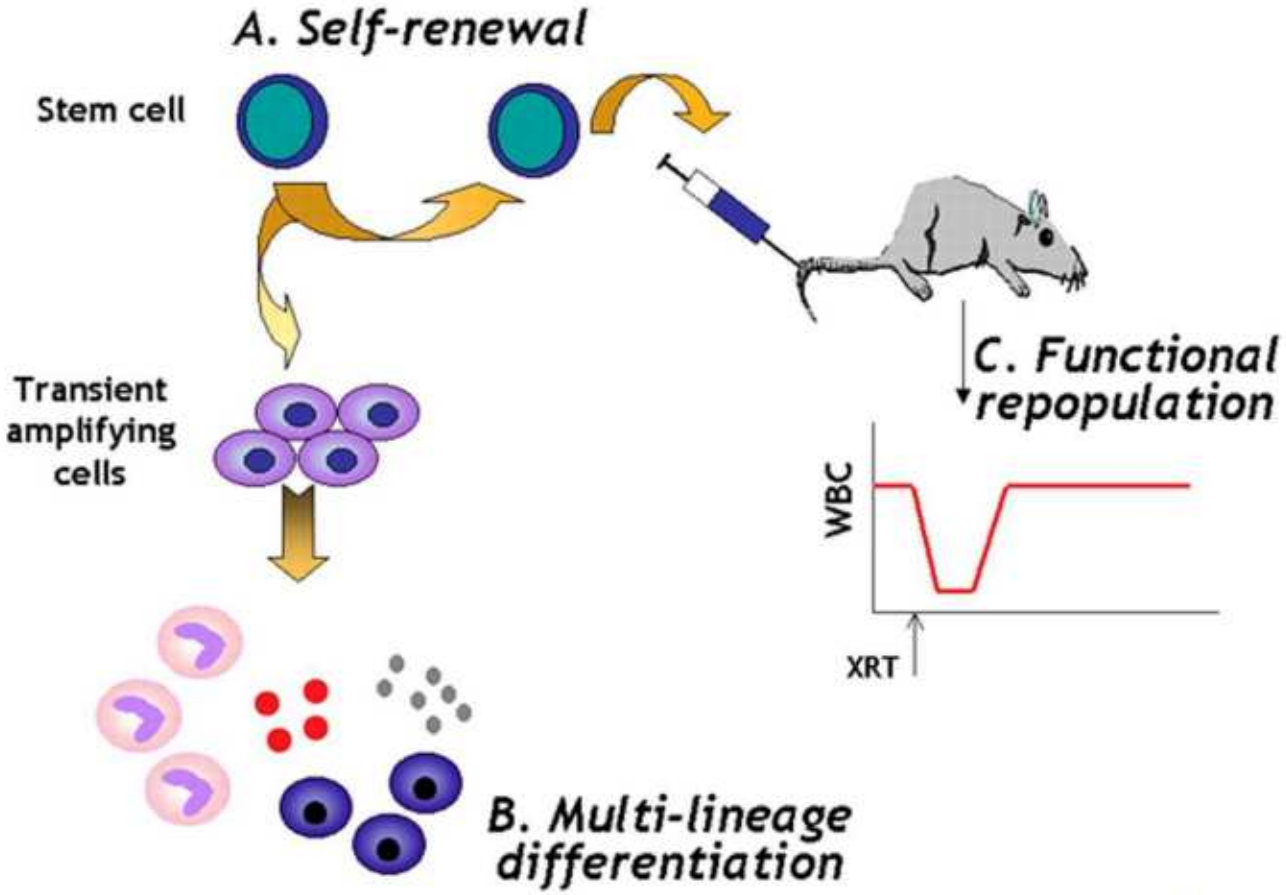

FIGURE 1.2. Criteria of Stem Cell Recognition. The picture illustrates three abilities that a cell has to exhibit to be considered a stem cell: self-renewal; multilineage differentiation; recovery of a damaged tissue *in vivo* for the lifetime of the recipient. The figure has been extracted from Verfaillie, C.M. et al., *Stem cells: hype and reality*. Hematology Am Soc Hematol Educ Program, 2002: p. 369-91.

TABLE 1.1. Stem Cell Classification Based on Their Differentiation Potential and Origin.

DIFFERENTIATION POTENTIAL[§]	ORIGIN[§]
Totipotent or Omnipotent	
Pluripotent	ESCs, iPSCs
Multipotent	Fetal Stem Cells
Oligopotent	Adult or Somatic Stem Cells
Unipotent	

[§] As in Kolios, G. et al., *Introduction to Stem Cells and Regenerative Medicine.* Respiration, 2013. **85**(1): p. 3-10

1.3 CELL SENESCENCE

Cellular senescence can be defined as a stable arrest of the cell cycle coupled to stereotyped phenotypic changes [39]. The term senescence (from Latin *senescere*, to grow old) was first used in 1961 by *Hayflick* and *Moorhead* to describe the irreversible growth arrest that characterizes diploid fibroblasts expanded in culture above a fixed number of population doublings (**Figure 1.3**) [40]. In this manner *Hayflick* and *Moorhead* broke up the immortality dogma of individual human cell. Hypothesized as a tumor suppressive mechanism, the existence of cell senescence met originally skepticism that has been gradually fading by the growing supporting evidence, and now it is globally accepted.

Mechanisms able to induce senescence can be divided in two principal groups:

1. Intrinsic Mechanisms originating internally to the cell;
2. Extrinsic Mechanisms coming from the outside of the cell.

Intrinsic inducers are either the progressive shortening of telomeres with cell divisions (replicative senescence) or the onset of irreparable DNA lesions that induce a persistent DNA Damage Response (DDR), which keeps the cells metabolically active but arrests their growth (telomere-independent, premature senescence) [41]. In the latter, intrinsic cell senescence is induced by activated oncogenes and DNA double-strand break–inducing agents. In this regard, 50 oncogenic or mitogenic alterations that are able to induce senescence have been described [42]. Once senescence has been established, senescent cells show remarkable changes in gene expression, including changes in known cell-cycle inhibitors or activators. Among these, the cyclin-dependent kinase inhibitor $p16^{INK4A}$ is one of the most important since its expression correlates with the chronological age of essentially all tissues studied, both in mice and humans [43]. In addition to changes in gene expression, senescent cells present also a reorganization of chromatin into discrete foci that are known as senescence-associated heterochromatin foci (SAHFs). SAHFs are generated in response to activated oncogene in a cell type- and insult-dependent manner and are often associated with the expression of $p16^{INK4A}$ [44].

Regarding extrinsic inducers, Interleukin (IL)-1ß, IL-6, IL-8, angiotensin II, Insulin-like Growth Factor-Binding Protein 7 (IGFBP7), Growth-Regulated Oncogene protein Alpha (GRO α), Plasminogen Activator Inhibitor 1 (PAI1) and glycation end products have been described to induce senescence in different cell types [41, 45].

Intrinsic and extrinsic inducers are interconnected by the fact that senescence cells exhibit peculiar altered secretome known as Senescence-Associated Secretory Phenotype (SASP) by which they are able to influence their microenvironment, to remodel the extracellular matrix, and to stimulate inflammation creating the conditions to induce cellular senescence in neighboring cells in a paracrine fashion [41].

1.3.1 CONNECTION BETWEEN CELL SENESCENCE AND HEART FAILURE

Growing demonstrations describe a cause-effect correlation among cellular senescence, aging and cardiovascular disease, including heart failure [46]. In fact, histological studies described the association with cardiac aging, senescence and death of CSCs and cardiac myocytes (**Figure 1.4**) [47, 48]. In line with these statements, other scientists illustrated that, while in acute ischemic heart disease, the pathologic condition is followed by CSC activation and recruitment toward injured areas, chronic cardiomyopathy is coupled with stem cell senescence and apoptosis [26]. Noteworthy, *Cesselli et al.* demonstrated that age and pathological conditions are both associated with a reduction in CSC telomerase activity and with an increased accumulation *in vitro* of cells exhibiting shorter telomeres, telomere-induced dysfunction foci, and expressing $p16^{INKA}$ and $p21^{CIP}$. Additionally, these cells were characterized by impaired proliferative, migratory and clonogenic capabilities and by an altered gene expression profile, enriched in transcripts of proteins involved in the SASP, such as IL-6 and IGFBP7 [46]. More recently, the effects of anthracycline administration on global heart condition and CSCs were assessed in mice [49]. This study proved that the drug induced toxicity in cardiomyocytes was coupled with a drug induced oxidative stress in CSCs promoting their senescence and apoptosis. Interestingly, authors demonstrated also that the exogenous administration of CSCs was able to regenerate cardiac myocytes and vascular structures, and then to improve ventricular performance and rate of animal survival, supporting the reparative role played by CSCs.

1.3.2 CSC SENESCENCE AND CELL THERAPY

The discovery that the heart is composed not only by terminally differentiated cells, but also of primitive cells, able to proliferate and differentiate toward a cardiac lineage [50], eventually improving the recovery of the organ, prompted the experimental activity of several laboratories aimed at developing stem cell based therapies for myocardial repair [37]. The results achieved by the clinical trials involving the use of stem cells of different origins for HF treatment are promising [35, 36, 38], however several evidences indicate that both ageing and chronic age-related pathologies, including atherosclerosis [51] or end-stage HF [46], are associated with stem cell senescence and functional impairment.

In addition to these numerous *in vitro* evidences of the impaired regenerative potential of end-stage CSCs, our group has recently demonstrated the influence that the senescence of CSCs exerts on their *in vivo* regenerative potential. Specifically, we showed not only that senescent CSC isolated from explanted end-stage heart are unable to protect *in vitro* rat adult cardiac myocytes, exposed to Simulated Ischemia/Reoxygenation (SI/RO), from apoptosis and senescence, but also that the same cells are characterized by an impaired regenerative ability when injected in the peri-infarct region of an infarcted mouse heart [52].

Altogether actual evidences indicated that senescence jeopardizes the regenerative potential of CSC resident in failing heart and suggested further improvements to achieve better results.

Text-Fig. 1.—Diagrammatic representation of the history of cell strains and the phenomenon of cell alteration. Phase I, or the primary culture, terminates with the formation of the first confluent sheet. Phase II is characterized by luxuriant growth necessitating many subcultivations. Cells in this phase are termed "cell strains". An alteration may occur at any time giving rise to a "cell line" whose potential life is infinite. Conversely, cell strains characteristically enter Phase III and are lost after a finite period of time.

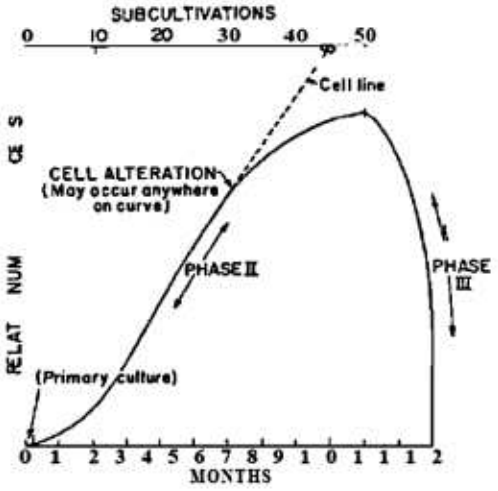

FIGURE 1.3. Hayflick and Moorhead Experiment that Suggested the Existence of Senescence in 1961. The graph, in the right, illustrates the irreversible growth arrest that characterizes diploid fibroblasts expanded in culture above 50 divisions, while in the left the related caption is reported. The figure has been extracted from Hayflick, L. er al., *The serial cultivation of human diploid cell strains*. Exp Cell Res, 1961. 25: p. 585-621.

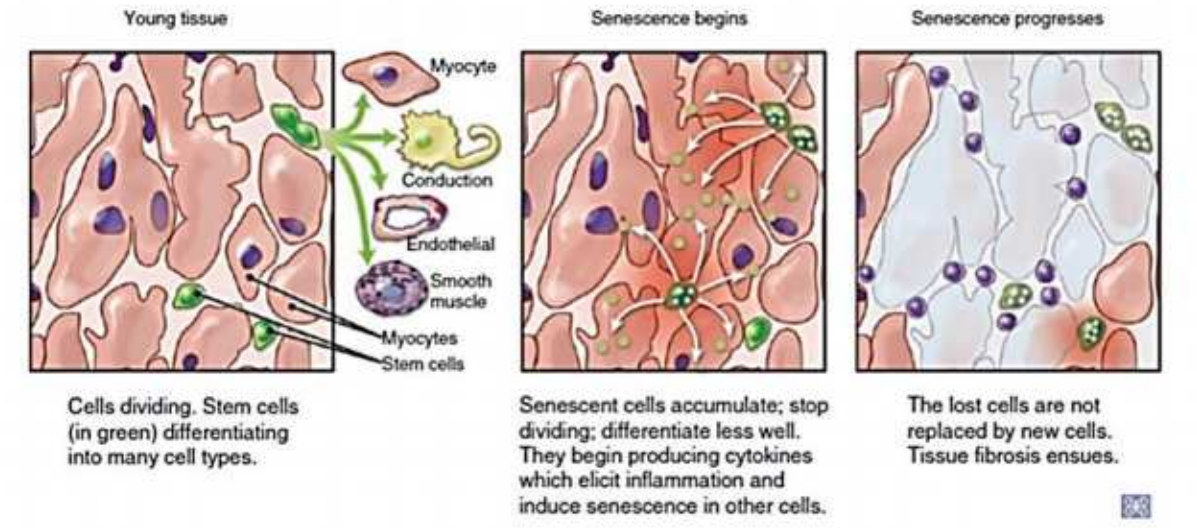

FIGURE 1.4. Effects of Cell Senescence on CSCs and then on Cardiac Tissue. Representative model of chronological or pathological evolution of cardiac tissue from young tissue, with effective CSCs, to senescent one with senescent CSCs unable replace the lost myocardium. The figure has been extracted from Beltrami, A.P. at al., *Stem cell senescence and regenerative paradigms*. Clin Pharmacol Ther, 2012. 91(1): p. 21-9.

1.4 AUTOPHAGY-LYSOSOME PATHWAY (ALP)

1.4.1 LYSOSOMES

Lysosomes (from Greek *lysis*, dissolution or destruction, and *soma*, body) are membrane-enclosed organelles, heterogeneous in morphology (spheroid, ovoid or occasionally tubular [53]), present in several copies in all eukaryotic cell types with the exception of erythrocytes. These organelles were discovered at the end of the 1940s from *Christian De Duve et al.*, as a result of studying the intracellular distribution of acid phosphatase by using centrifugal fractionation of liver tissue homogenate. The experiment gave birth to the hypothesis that acid phosphatase could be contained in membrane delimited vesicles. The hypothesis was confirmed with other four hydrolases and in 1955 *De Duve* gave the name "lysosomes" to the vesicles [54], that were firstly photographed with electron microscope by *Novikoff* in 1956 (**Figure 1.5**)[55]. For this discovery De Duve received the Nobel Price award in 1974 [56].

As intelligible from the name, the principal function of lysosomes is the degradation that ensures continuous renewal and recycling of cellular constituents and avoids accumulation of worn out components. The degrading function is performed by more than 80 different acid hydrolases (proteases, lipases, nucleases, glycosidases, phospholipases, phosphatases and sulfatases) that are active at the acidic pH of the lysosomal lumen and are able to degrade an array of biological polymers. The function of lysosomes is mediated by their membranes and by the capability of these latter to fuse with other membranes [57]. Lysosomal membranes contain proton pumps (vacuolar ATPase), responsible for maintaining the concentration of intralysosomal H^+ 100-fold higher than that of cytosol, permeases responsible for recycling essential nutrient from the degraded products back to cytosol, and other proteins such as Lysosomal Associated Membrane Protein 1 and 2 (LAMP1 and LAMP2) that are essential both to protect lysosomal membrane from internal enzymes and other dangerous agents [58], and to regulate lysosomal movement, cellular distribution, exocytosis and many other functions [59].

Lysosome network is considered the final destination of degradative pathways including heterophagy (endocytosis, phagocytosis), and autophagy (**Figure 1.6**). The other degradation pathway is the ubiquitin-proteasome system, depending on ubiquitin, a small protein of 76 amino acids responsible for the demolition of many cytosolic, nuclear and endoplasmic proteins [60].

Besides the degradation, lysosomes are also responsible for exocytosis useful to eliminate toxic substances from the cell [61], to release cellular products such as cytokines [62], and to repair the plasma membrane in both normal and pathological conditions [63]. Moreover, given their high levels of hydrolytic enzymes, for which *Christian De Duve* termed lysosomes "suicide bags", these organelles are involved in programmed cell death by a mechanism known as selective Lysosomal Membrane Permeabilization (LMP) [64]. In fact LMP relocates lysosomal contents to cytoplasm, in

particular cathepsins. These latter remain active at neutral pH, and induce the activation of apoptotic effectors that provoke controlled cell death, are used in differentiation and development processes, and have been recently exploited for the development of cancer treatments [65].

1.4.2 AUTOPHAGY

Autophagy (or autophagocytosis) (from the Greek *auto-*, self and *phagein*, to eat), is the basic catabolic mechanism that involves cell degradation. Three types of autophagy have been described, depending on the manner in which substrates reach the lysosome (**Figure 1.6**): macroautophagy, microautophagy and Chaperone-Mediated Autophagy (CMA) [66]. During macroautophagy, cytoplasmic components, damaged proteins and whole organelles are degraded and recycled to generate building block that are used by anabolic processes [67]. The CMA is a process by which cytoplasmic proteins, containing a specific amino acid motif, are incorporated into lysosomes through an action performed in combination by a chaperone protein (usually Heat Shock Cognate protein 70, Hsc70) and lysosomal receptor protein LAMP2A [67]. Microautophagy is the term used to describe the process through which macromolecules are directly relocated to lysosomal lumen for degradation. Among the three types described above the macroautophagy pathway is the best characterized and it is normally named autophagy [67].

The autophagic process can be essentially schematized by three consecutive steps: autophagy induction, autophagosome generation, and its fusion with lysosome [67]. In the first step different stress stimuli, such as lack of nutrient, induce the inhibition of mammalian Target Of Rapamycin (mTOR) and so trigger autophagy [68]. Subsequently, cytosolic proteins and organelles are captured by the autophagosome, a double membrane vesicle probably originated from the endoplasmic reticulum. In order to guarantee a selective autophagy, cargo destined to be degraded have to be recognized by a binding with specific receptor proteins, including p62/SQSTM1 (Sequestosome1) [69]. The autophagosome generation is coordinated by complexes of Autophagy related (Atg) proteins [70]. Specifically LC3 conjugation system is an ubiquitin like system constituted by Atg3, Ag4, Atg7 and by the microtubule-associated proteins 1 Light Chain 3 (LC3BI) [71]. After induction of autophagy, soluble cytosolic LC3BI is first cleaved by a protease Atg4, and then transferred by Atg7 to Atg3 in order to be conjugated to Phosphatidylethanolamine (PE), generating la lipid-conjugated LC3BII form that is incorporated within the autophagosomes membrane. During the last steps of autophagy autophagosomes fuses with a lysosome, by a process depending on the endosomal protein Rab7, LAMP1 and LAMP2 [67, 72]. The newly formed autophagolysosome proceeds to degrade the internal cargo by lysosomal proteases. Finally the degraded products are released back to the cytosol upon collapse of the structure.

1.4.3 ASSOCIATIONS BETWEEN MTOR PATHWAY AND ALP

The mTOR pathway is considered the main regulator of cell growth and plays a key role in the aging process [73]. mTOR is a serine / threonine kinase and is the initial component of the pathway. In fact, it is the catalytic subunit of two distinct protein complexes: mTORC1 and mTORC2 [74]. mTORC1 contains mTOR, RAPTOR (Regulatory Associated Protein of mTOR), mLST8 / GβL and PRAS40, while mTORC2 is constituted by mTOR and the proteins: Rictor (Rapamycin-Insensitive Companion of mTOR), mSIN1, PROTOR and mLST8 / GβL [75]. Growth factors, such as Insulin Growth Factor (IGF), activate both the complexes and are upstream effectors of the PI3K / PTEN signaling network, which acts via the serine/threonine kinase Akt [76]; in addition mTORC1 is also regulated by the availability of nutrients including amino acids and glucose. Two important substrates have been demonstrates downstream of mTORC1: S6 kinase (S6K) and the translation inhibitor 4E-BP1; both of them mediate important links between mTORC1 and the cell growth machinery mostly by influencing the cap-dependent translation [77].

The mTOR inhibitor Rapamycin (or Sirolimus) is a macrolide produced by bacteria (*Streptomyces Hygroscopicus)* that acts by forming a complex with the intracellular protein FKBP12, which then binds to FRB domain of mTOR and inhibits the phosphorylation of its substrates through an allosteric mechanism. Rapamycin is effective specifically on mTORC1 whereas mTORC2, in some types of cells, is sensitive to prolonged treatment with the same drug. In *Saccharomyces cerevisiae*, Rapamycin induces a state similar to starvation: it arrests cell cycle in G1/S phase, reduces protein synthesis to 20%, and stimulates autophagy [78, 79]. Although less intense, in mammalian cells the effects of Rapamycin are similar to those demonstrated for the yeast [80-82].

Several discoveries reported the central role played by the unexpected link between ALP and mTORC1 in controlling the cellular response to nutrients [65]. In amino acids rich condition, mTORC1 moves to the lysosome membrane where it is activated by its modulator Rheb. Activated mTORC1 phosphorylates its downstream effectors, including S6K, resulting in metabolism modulation and in autophagy inhibition [83]. *Narita et al.* demonstrated that in senescent cells that show high levels of autophagy and an intense synthesis of secretory proteins, lysosomes connect spatially mTOR and autophagy in a compartment that authors defined as TOR-Autophagy Spatial Coupling Compartment (TASCC). TASCC pairs protein degradation and synthesis, two processes, one catabolic and other anabolic, that were previously considered incompatible. *Korolchuk et al.* clarified the importance of the position of lysosomes within the cell. In fact, during starvation, lysosomes form clusters in the perinuclear region, where are concentrated the autophagosomes, thus promoting the processes of degradation and recycling useful to supply necessary nutrients to the cell. On the contrary, when nutrients are abundant, lysosomes relocate through the microtubules to the cell periphery, where mTORC1 inhibits again autophagy [84]. In addition, *Yu at al.* showed that prolonged starvation induces mTORC1 not merely to inhibit autophagy, but also to control the recycling of lysosomal membrane proteins through a process known as Autophagic Lysosome Reformation

(ALR). This latter is an evolutionary preserved mechanism that generates a proteolysosome, which then evolves into a mature and functional lysosome [85].

1.4.4 THE TFEB ROLE

Given that the degradation needs of cells significantly change according to various elements, including tissue type, age and environmental conditions, ALP must be able to adequately respond to these changes of necessity, but the mechanism at the base of ALP regulation was unknown until six years ago. In 2009 *Sardiello and his colleagues* reported that many lysosomal genes exhibit coordinated behavior and are regulated by Trascription Factor EB (TFEB) [86]. This latter is one member of the microphthalmia Transcription Factor (Mit / TFE, subfamily of transcription factors basic Helix-Loop-Helix, bHLH, leucine zipper) family, is a master gene that positively regulates the genes belonging to the CLEAR (Coordinated lysosomal Expression and Regulation) network, targeting, inter alia, genes encoding for lysosomal hydrolases, lysosomal membrane proteins and components of the vacuolar H^+ -ATPase (V-ATPase). In this manner, TFEB is able to induce biogenesis of lysosomes and increases the degradation of complex molecules such as glycosaminoglycans [86].

TFEB also intervenes in response to starvation and controls autophagy inducing the autophagosome formation and its fusion with lysosomes, thus stimulating autophagic flux and degradation of long-lived proteins [87, 88]. *Settembre et al.* demonstrated that TFEB positively influences 11/51 macroautophagy related genes, specifically UVRAG, WIPI, MAPLC3B, SQSTM1, VPS11, VPS18, and ATG9B [88]. Immunoblotting studies have shown that stress or starvation conditions activate TFEB by targeting its phosphorylation status (TFEB shows a reduced molecular weight) and inducing its transfer into the nucleus [87]. A study of high-throughput mass spectrometry predicted 11 different residues that could be phosphorylated in TFEB, suggesting a complex regulation of its activity with different phosphorylation sites potentially involved [88]. Specifically were identified three Serines (142, 332 and 402) that are phosphorylated in conditions of nutrient (Ser^{142}, Ser^{332}, Ser^{402}); among these Ser^{142} plays a crucial role in the subcellular localization and activity of TFEB [87]. In addition to Ser^{142}, Ser^{211} has been demonstrated also perform the same functions [88].

As seen above (see **par. 1.4.3**), an instrument sensitive to the nutritional status of the cell has been identified on the surface of the lysosome and involves mTORC1 together with V-ATPase [83]. The interaction between amino acids and V-ATPase activate Rag Guanosine Triphosphatase (GTPase), which in turn recruits mTORC1 to the lysosome surface where it interacts with TFEB. Under healthy conditions there is a partial localization of TFEB to the lysosome due to a transient bond with mTORC1 useful to TFEB phosphorylation and its cytoplasmic localization. Indeed mTORC1 inhibits

nuclear transfer of TFEB phosphorylating its two key residues (Ser^{142}, Ser^{211}), which were demonstrated to be two substrates resistant to Rapamycin (**Figure 1.7**) [88].

The growing interest in TFEB had incited several studies that demonstrated, among other discoveries, that TFEB controls cellular clearance not only by stimulating ALP [61, 89]. *Palmieri et al.* identified 471 TFEB direct targets that represent essential components of the CLEAR network. The study of functional meaning of these genes clarified that TFEB through CLEAR network is able to regulate in a coordinated fashion lysosomal biogenesis and degradation capability, the autophagy, but also other lysosomal related functions such as exocytosis, endocytosis, phagocytosis and immune response [89]. Given these properties, TFEB is now investigated to evaluate the effectiveness and the safety of its use in therapeutic strategy for the treatment of disorders associated with intracellular storage. Preliminary results showed that activation of TFEB enforce exocytosis increasing both the number of lysosomes in proximity of plasma membrane and their fusion with the membrane, facilitating the disposal of cell waste materials. This strategy reduced the pathological accumulation of proteins on cell model of Huntington's disease [86], and improves the phenotype of the cells derived from murine models of Parkinson disease [90], and of some lysosomal storage disorders [61].

1.4.5 ALP DYSFUNCTION AND HF

ALP is the main intracellular proteolytic system. It is responsible for degradation and recycling of more than 98% of long-lived proteins, especially in tissues such as the liver and muscles [60]. Given the pivotal role played by ALP in quality control of proteins and organelles to maintain cell homeostasis and function by controlling both cellular clearance and response to nutrients, defects on the pathway cause aberrant accumulation of undigested materials that may provoke serious disease, mostly if ALP defects affect long-lived cells, such as cardiac myocytes. In these latter the contractile activity of the heart submits the proteins to constant wear so that efficient quality control mechanisms are essential for guaranteeing the cardiomyocytes physiological function that depends on a critical balance between protein synthesis and protein turnover (**Figure 1.8**) [91, 92].

The vital importance of autophagy is revealed by the fact that its failure leads to cardiomyopathy in both clinical and experimental models, which have indicated the gene Atg5 as one of the markers of these pathological conditions. In fact, an accumulation of damaged proteins and organelles, due to the dysfunction of Atg5, leads to sarcomere disorganization, cardiac hypertrophy, followed by dilated cardiomyopathy and, finally, by heart failure [67, 82]. Similarly, a defect in the lysosome membrane protein LAMP2 is characterized by muscle weakness and cardiomyopathy in mice and Danon disease in patients [92].

Moreover, aging is accompanied by a reduced renewal of cardiomyocytes due to a reduction in both the differentiation of stem cells into cardiac myocytes, and in the division of these latters. As a result it is observed a progressive accumulation within the lysosomes of undigested waste materials.

Among these lipids, metals and oxidatively modified proteins create autoflorescent pigments that cannot be degraded by lysosomal hydrolases and are known as lipofuscin. The age related deposition of lipofuscin progressively reduces degradative potential of lysosomes and impairs autophagy exposing cardiomyocytes to all the problems that ensue [93]. On this line, *Terman et al.* reported that aged lipofuscin-rich cardiac myocytes become overloaded with damaged mitochondria, leading to increased oxidative stress, apoptotic cell death, less of myocardial tissue, and finally development of HF [94].

Actually, the effects of ALP on the pathophysiology of HF are not well defined. Autophagy may play a protective role antagonizing ventricular hypertrophy by decreasing tissue mass through protein degradation. However, the rate of autophagy effectiveness declines with age-related store of lipofuscin that results in enhanced oxidative stress, collapse of the cellular catabolic machinery, and cell death. *Shimomura et al.* showed that autophagy intervenes during HF but it is associated not only with functional degradation of damaged proteins but also with progressive destruction of cardiomyocytes [95]. Additionally it has been reported that, in load-induced heart failure, the excessive and prolonged autophagy produce autophagic cell death and loss of cardiomyocytes and exacerbating the heart failure course [96].

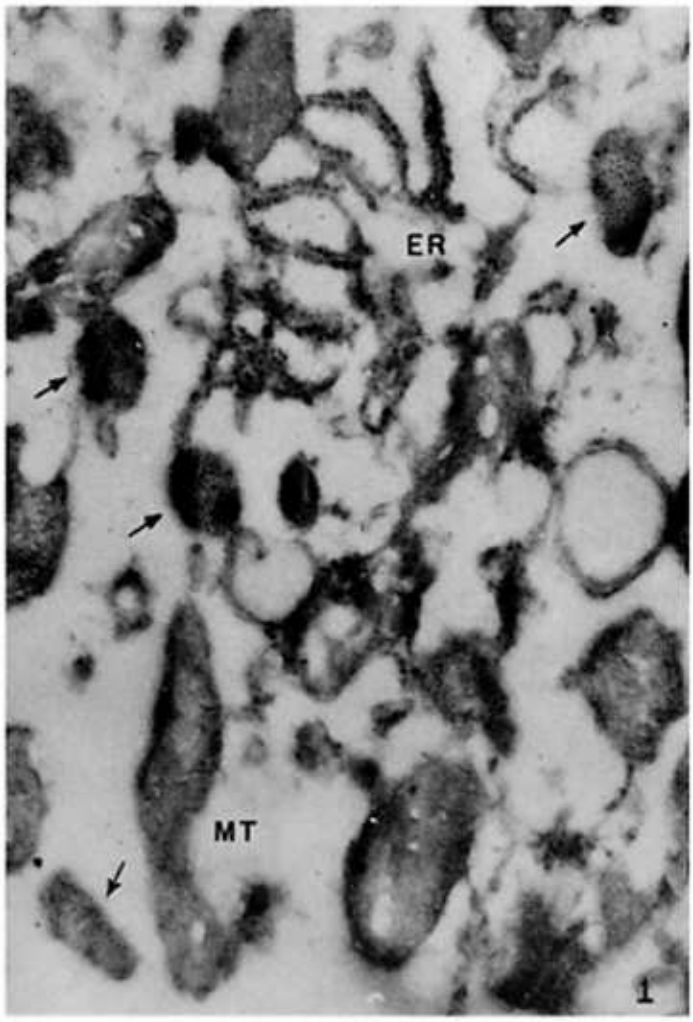

FIGURE 1.5. First Electron Micrograph of Lysosomes. The figure is a reproduction of the first electron microscope image showing the existence of lysosomes (black sharp arrows) in a fragment of liver containing also mitochondria (MT) and endoplasmic reticulum (ER). The figure has been extracted from Novikoff, A.B. et al., *Electron microscopy of lysosomerich fractions from rat liver.* J Biophys Biochem Cytol, 1956. 2(4 Suppl): p. 179-84.

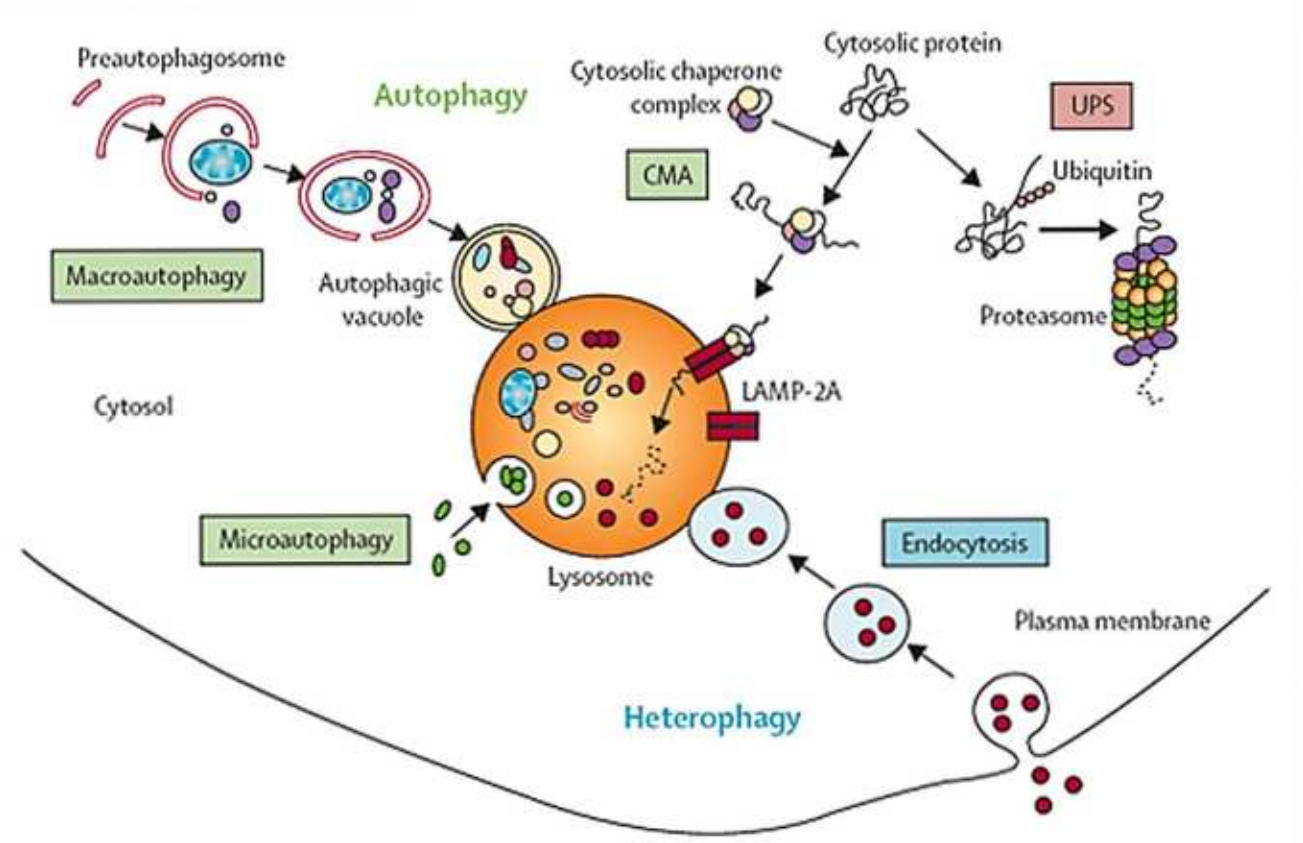

FIGURE 1.6. Model of Cellular Degradative Pathways. The cartoon summarizes the degradation mechanisms of the cell. Abbreviations: Ubiquitin Proteasome System (UPS), Chaperone Mediated Autophagy (CMA). The figure has been downloaded by https://www.mdc-berlin.de.

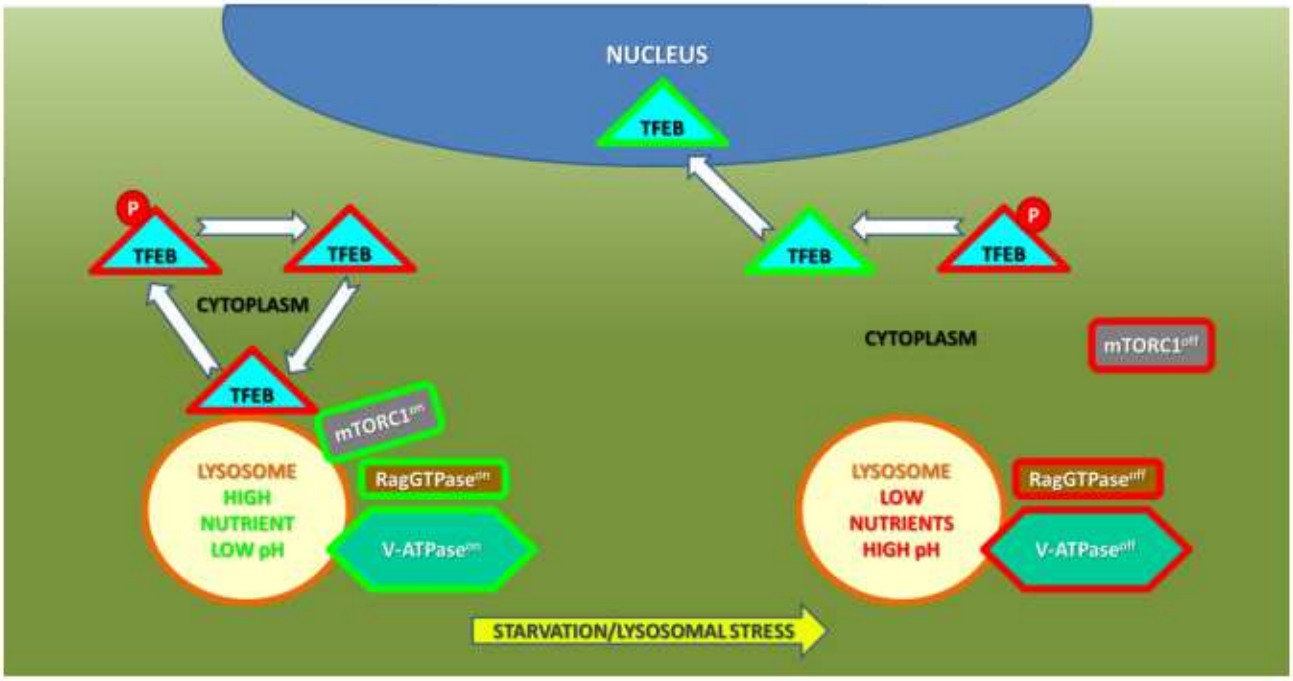

FIGURE 1.7. Model of TFEB Regulation by mTORC1. During nutrient rich condition (left) and in the absence of lysosomal stress, mTORC1 is recruited on lysosomal membrane by active Rag-GTPase. In this manner active mTORC1 phosphorylates TFEB impeding its relocation to nucleus. During Starvation or Lysosomal stress (right) condition, the inactivation of Rag-GTPase produces mTORC1 detachment from the lysosome and thus its inactivation. As a direct consequence TFEB is no longer phosphorylated and is able to reach nucleus and so to induce the transcription of its targets.

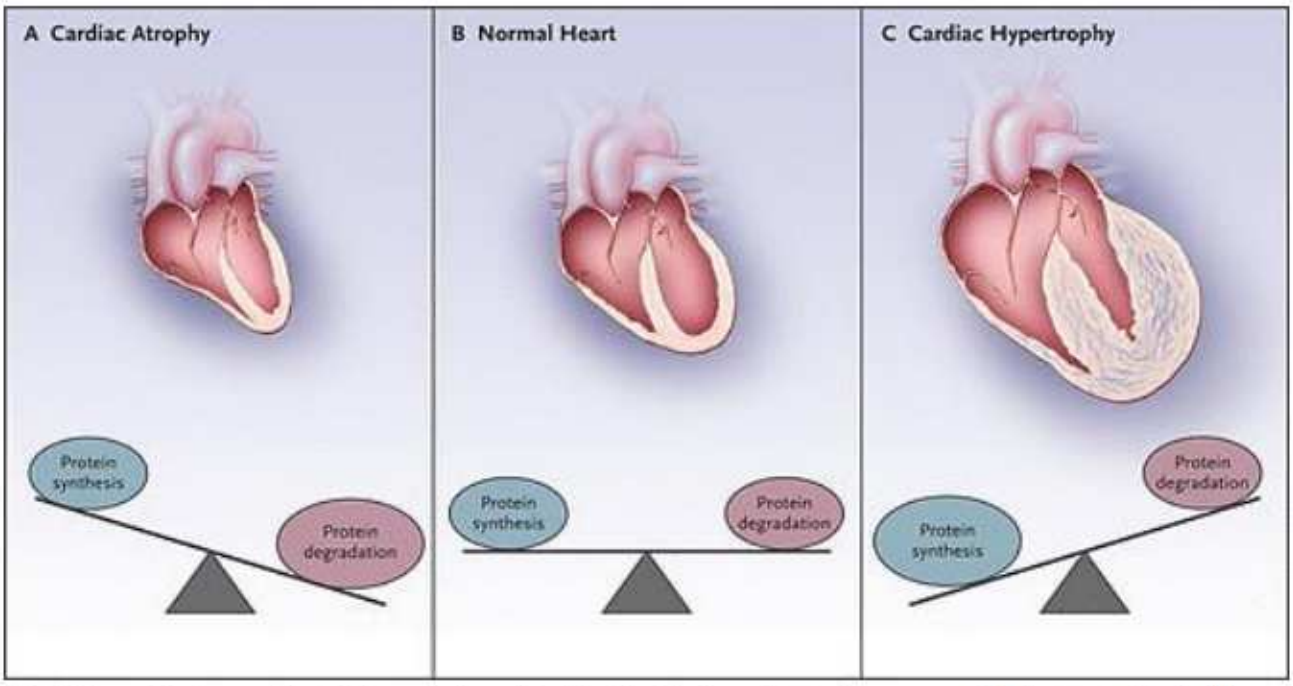

FIGURE 1.8. Cartoon of the Balance between Protein Synthesis and Protein Turnover. In the heart, the imbalance between protein synthesis and protein degradation leads to cardiac atrophy if protein degradation outclasses protein synthesis (**A**), on the contrary if the production of new proteins is higher than its decomposition heart becomes hypertrophic(**C**). The optimal condition is guaranteed by a tradeoff between protein degradation and synthesis (**B**). The figure has been extracted from Willis, M.S. et al., *Proteotoxicity and cardiac dysfunction--Alzheimer's disease of the heart?* N Engl J Med, 2013. 368(5): p. 455-64.

2. RATIONALE AND AIMS

Despite improved therapies, cardiovascular diseases remains the leading cause of death and disabilities in Western world [1], being responsible for the death of 235.5/100,000 people, in the United States (versus 185.9 / 100,000 deaths for cancer)[97], and for causing 40% of all deaths in European Union, for a total of 2 million per year (leading cause of premature death before the age of 75).

Heart Failure (HF) is defined as the inability of the heart to supply physiological circulation without supernormal filling pressure [98], its aging-related incidence has substantially increased, due to the improvement in life expectancy and survival after acute myocardial infarction. Although significant progress has been made on HF pharmacological therapy, heart transplantation is still the only life-saving approach for patients with end stage HF. However this procedure is limited by donor availability and lifelong immunosuppression for transplant recipients [99]. Because of this, identification and development of new therapies that assist or outclass the effectiveness of the present one, is of undisputed relevance.

To this aim, promising prospects have opened when it was shown that the heart is not a terminally differentiated organ, but has its intrinsic self-renewal ability. Specifically, it was discovered the existence of Cardiac Progenitor Cells (CPCs) Lin- cKIT^{+} resident in the heart [18]. These self-renewing, clonogenic, and multipotent cells are able to promote healing of an acute myocardial infarction [25]. On the wake of these evidences and of the progression in regenerative medicine, several laboratories have been interested in developing cell replacement therapies based on the use of Cardiac Stem Cells (CSCs). The results, although encouraging, have shown that the framework is complicated by CSC senescence, that is associated both with aging and with chronic age-related pathologies, such as atherosclerosis [51], or heart failure [46]. Specifically CSCs isolated from end-stage failing explanted hearts are characterized by reduced levels of telomerase activity, a larger fraction of primitive cells showing telomere dysfunction, expressing senescence markers, and with reduced proliferative and migratory abilities [46], attributes considered to be decisive for the regenerative potential of this autologous cell source. For this reasons, it would be crucial to identify cell senescence key pathways that could be targeted in order to improve the CSCs regenerative ability and therefore to ameliorate the feasibility of autologous therapy.

Growing evidences report that the animal lifespan is related to the capacity of the cells to prevent the accumulation of damaged macromolecules and organelles and so, on the Autophagy-Lysosome Pathway (ALP), responsible of maintaining cellular homeostasis regulating both cellular clearance

and response to nutrients [100]. The efficacy of ALP declines with aging, causing dangerous imbalances in protein homeostasis [100]. Although the mechanism responsible for the age-related ALP dysfunctions are unknown, part of the problem may be related to a progressive increase in concentration of free radicals within the lysosomes and to an intralysosomal-accumulation of undegradable lipofuscin, which decreases the digestive potential of these organelles and make it unable to fuse with autophagosomes, paralyzing in this manner the autophagic flux [101]. Because of the pivotal role played by ALP, defects of this pathway cause aberrant accumulation, within the cells, of undigested materials and are associated with many different diseases, including cardiovascular disorders [102]. Indeed, the failure of ALP and the resulting accumulation of damaged proteins leads to cardiac hypertrophy, followed by dilated cardiomyopathy and, finally, by HF[82].

For the reasons described above, the aim of the present study was firstly, to monitor the efficacy of ALP in senescent CSCs isolated from and-stage failing hearts. After the demonstration that these cells were characterized by a reduced ALP, the second aim was to develop a drug-based strategy that could boost ALP, eventually contrasting senescence.

More specifically, the project was organized in the following different steps:

1. characterization of the CSCs obtained from explanted hearts (E-CSC), in terms of cell surface immunophenotype, proliferative ability, expression of markers associated with senescence and apoptosis;
2. identification of E-CSC transcriptome imbalances, connected with ALP and cell senescence;
3. evaluation of E-CSC post-transcriptional regulation at the expense of ALP and cell senescence;
4. assessment of extension and functionality of E-CSC lysosomal compartment;
5. test of E-CSC autophagic flux;
6. fine-tuning of pharmacologic-treatment of E-CSC with drug able to stimulate autophagy;
7. check of drug-treatment effects on senescence and ALP.

3. MATERIALS AND METHODS

3.1 PATIENT ENROLLMENT AND ETHICS

In this study, patients with end-stage heart failure (Stage D AHA classification) who underwent cardiac transplantation, at the University Hospital of Udine, were enrolled. In order to be enrolled in the waiting list for organ transplantation, patients were subjected to an in-depth evaluation of their clinical status, which included: coronary angiography, cardiopulmonary exercise test, pulmonary function test, echocardiography, cardiac catheterization, assessment of pulmonary vascular resistance, electrocardiography and tests aimed at excluding the presence of malignancies and other vascular diseases. Furthermore, expert pathologists had access to the explanted organs, allowing the hearts to be evaluated macroscopically and histologically. For every patient enrolled in our case study, inspection of the coronary arteries confirmed the presence of stenosing atherosclerotic plaques shown by angiography, while histologic examination of the myocardium revealed the presence of segmental fibrosis and replacement fibrosis, defined as in [103]. Clinical characteristics of patients and hearts are reported in **Table 3.1**, **3.2**, **3.3** and **3.4**.

The study, in accordance with the Declaration of Helsinki, was approved by the Ethics Committee of Udine (2 August 2011, reference number 47831) and written informed consent was obtained from each patient.

TABLE 3.1. DEMOGRAPHIC, ANATOMIC AND FUNCTIONAL CHARACTERISTICS OF THE SUBJECTS AND HEARTS INCLUDED IN THE STUDY. Clinical characteristics of the patients whose hearts were studied. Data are presented as means±SD.

	No. of Patients	Age (yr)	Sex (M/F)	Duration of Disease (mo)	Time from Heart Failure to Transplantation (mo)
Ischemic Cardiopathy	20	60±7	19/1	119±94	42±44
Control	14	49±11	8/6	-	-

TABLE 3.2. DEMOGRAPHIC, ANATOMIC AND FUNCTIONAL CHARACTERISTICS OF THE SUBJECTS AND HEARTS INCLUDED IN THE STUDY. Echocardiographic, Hemodynamic and Pathologic measurements. Data are presented as means±SD.

	Ischemic Cardiopathy (N=20)	Normal Value §
Left Ventricular Diameter (mm)		
Systolic	63.9±21.1	20-35
Diastolic	78.2±30.6	37-56
Ratio of Wall Thickness to Chamber Radius	0.26±0.08	0.32-0.39
Fractional Shortening (%)	17.1±5.7	34-44
Left Ventricular End-Diastolic Volume (ml/m2 of Body-Surface Area)	122±36	44-96
Ejection Fraction (%)	24.7±9.4	>50
Stroke-Volume Index (ml/beat/m2)	28±11	20-41
Cardiac Output (ml/min)	4138±1367	5000-7000
Cardiac Index (ml/min/m2)	2220±775	2600-4200
Mean Pulmonary-Artery Edge Pressure (mmHg)	27±6	1-10
Heart Weight (g)	521±120	<350

§ Normal value as in Olivetti, G. et al., *Apoptosis in the failing human heart.* N Engl J Med. 1997. **336**(16):p.1131-41. Plus-minus values are means ± SD.

TABLE 3.3. DEMOGRAPHIC, ANATOMIC AND FUNCTIONAL CHARACTERISTICS OF THE SUBJECTS AND HEARTS INCLUDED IN THE STUDY. Comorbidities. Data are presented as frequency (%) of patients with a positive history for the indicated comorbidity.

	ISCHEMIC CARDIOMYOPATHY (%)
RENAL FAILURE	35
HYPERTENSION	55
DYSLIPIDEMIA	85
HYPERCHOLESTEROLEMIA	85
HYPERTRIGLYCERIDEMIA	40
TYPE 1 DIABETES	0
TYPE 2 DIABETES	50
HYPERURICEMIA	45

TABLE 3.4. DEMOGRAPHIC, ANATOMIC AND FUNCTIONAL CHARACTERISTICS OF THE SUBJECTS AND HEARTS INCLUDED IN THE STUDY. Drug therapy. Data are presented as frequency (%) of patients with a positive history for the indicated drug.

	DRUG (%)
ANTIARRHYTHMIC	53
ACE-INHIBITORS	82
DIURETICS	100
ANTICOAGULANTS	53
ANTIPLATELET	65
INOTROPIC	47
β BLOCKERS	100
NITRO DERIVATIVES	29
LIPID LOWERING/ STATINS	88
ANTI HYPERGLYCAEMIC/ INSULIN	24
ANTACIDS	65

3.2 CARDIAC STEM CELLS ISOLATION AND *IN VITRO* EXPANSION

Atrial samples were collected both from donor hearts (n=14) and from explanted hearts (n=20) of ischemic patients undergoing cardiac transplantation at the University Hospital of Udine.

Human Cardiac Stem Cell lines (CSCs) were isolated, as in [104, 105]. Specifically, isolation was performed by washing atrial fragments (3-6g) in Basic Dissociation Buffer (BDB - see **par. 3.13**) to eliminate blood from the tissue. Pericardial, adipose tissue and macroscopically apparent areas of fibrosis were then removed. The tissue underwent mechanic disaggregation with scalpels and scissors until fragments have a dimension not larger than 1 mm^3. The tissue was then washed with BDB and the cell solution was centrifuged 5 minutes at 500g and supernatant discarded. The pellet was enzymatically dissociated by incubation in a 0.25% Collagenase type II solution (Worthington Biochemical Corporation). The enzyme/cell solution was incubated for 15-20 minutes at 37°C in a tube rotator. Collagenase activity was stopped by the addition of 0.1% bovine serum albumin (BSA, Sigma-Aldrich) solution in BDB. Cell suspension was first centrifuged at 100g for 1 minute to remove myocytes and subsequently at 500g for 5 minutes. The resulting pellet was resuspended in 1ml of BDB and filtered through a pre-wet strainer (BD Falcon) in order to select a population less than 40 µm in diameter. The filtered suspension was centrifuged at 500g for 5 minutes. The supernatant was discarded and cell pellet was resuspended in 1ml of Human MesenCult Proliferation Medium (STEMCELL Technologies). Cells were cultured in the presence of 100U Penicillin and 100µg/L Streptomycin (Life Technologies). Cells were plated at a concentration of $1.5 \cdot 10^6$ in a 100-mm dish and maintained at 37°C, 5% CO_2.

To induce CSC differentiation, cells were exposed for 2-3 weeks to media added with the appropriate cytokines, as in [46, 106]. After treatment, cells were fixed and processed for immunofluorescence as described below (see **par. 3.6**).

3.2.1 DETACHMENT AND EXPANSION OF CSCS

To detach cells from substrate, the plate was washed twice with 5ml of HBSS. 2ml of TrypLE Express solution (Gibco - Life Technologies) was added to the cells and incubated at 37°C, until the cells were observed to dissociate, after which 7ml HBSS were added to the cells to inhibit enzymatic activity. Cell suspension was centrifuged at 500g for 5 minutes and the supernatant was discarded. The cell pellet was resuspended in 1ml of culture medium. The cells were plated at a density of 5,000 cells/cm^2. After the second passage, the tissue culture plastic was coated with 10µg/ml human Fibronectin (Sigma-Aldrich) in HBSS and medium was switched to expansion medium (see **par. 3.13**).

3.3 CSC GROWTH KINETIC (CPDT)

For the determination of the population doubling time, CSCs were seeded into 6well-plates at a density of $3 \cdot 10^3$ cells/cm^2 in expansion medium. Medium was replaced with fresh one every 4 days and, every 24 hours, cells were detached and counted using Burker Counting Chamber. Population doubling time was calculated during the log-phase of growth.

3.4 CELL MIGRATION: SCRATCH ASSAY

In order to evaluate *in vitro* cell migration of drug-treated or untreated CSCs, a scratch assay was performed [105]. In 96well-plates at high confluence, scratches were created in the center of the well utilizing 10µl tips. Phase contrast images of the scratches were acquired immediately and after 2, 8 and 24 hours, until their complete closure. Images were then compared and quantified by the software ImageJ. The rate of cell migration, expressed as µm/h, was calculated in the interval of time between 2 and 8 hours from the creation of the scratch, measured in 3 different points of the scratch. Then the average migration speed was calculated. Each condition was performed at least in quadruplicated.

Images were acquired using the microscope Leica DMI6000B equipped with a 10x objective (numerical aperture: 0.25).

3.5 FLOW CYTOMETRY ANALYSIS

To perform flow-cytometry (FACS) analysis, growing cultures of CSCs in expansion medium were detached from the culture substrate. Detached cells were washed to discard the detaching agent, resuspended in 200µl of calcium and magnesium free Phosphate Buffered Saline (PBS) and then appropriately stained.

3.5.1 STAINING FOR CELL SURFACE IMMUNOPHENOTYPE

To assess the surface immunophenotype, detached cells were incubated with the appropriate antibody (listened in **Table 3.1**) for 20 minutes at room temperature, in the dark. The c-Kit antigen required a different procedure as it was an unconjugated antibody. After the first incubation with the c-Kit antibody (30 minutes at 37°C), cells were washed with PBS and incubated with a labelled secondary antibody for 20 minutes at 37°C. Isotype matched antibodies were employed as negative controls. After incubation, cells were washed, resuspended in 250µl of PBS and analyzed.

3.5.2 STAINING FOR APOPTOSIS AND NECROSIS

To assess the fraction of apoptotic and necrotic cells, we employed the Annexin V-FITC Apoptosis Detection Kit (eBioscience), following manufacturer's instructions. Briefely, detached cells were washed once with PBS and then once in 1xBinding Buffer (provided in the kit). Washed cells were incubated 15-20 minutes at room temperature with fluorochrome-conjugated Annexin V diluted (1:20) in 1xBinding Buffer. After incubation, cells were washed with 1xBinding Buffer, resuspended in 200µl of 1x Binding Buffer added with 5µl of Propidium Iodide Staining Solution and analyzed.

3.5.3 STAINING FOR THE MONITORING OF LYSOSOMAL COMPARTMENT

Lysosomal compartment was evaluated in terms of size or functionality incubating detached cells 2 hours at 37°C with 75nM LysoTracker Red DND-99 (Life Technologies), or 15 minutes at 37°C with 1µM Acridine Orange (Sigma-Aldrich) respectively. Both the dyes were diluted in Opti-MEM (Life Technologies). After incubation cells were washed, resuspended in 500µl of PBS and analyzed.

3.5.4 ANALYSIS

Cell analysis was carried out with a FACSCanto analyzer (Becton Dickinson). Cells of interest were gated on the basis of their physical parameters (SSC and FSC). Cell doublets were gated out plotting fluorescence area vs width. Mean fluorescence intensity was computed by dividing the mean fluorescence of labeled cells by the mean fluorescence of the negative control.

TABLE 3.5. CELL SURFACE IMMUNOPHENOTYPE ANTIBODIES EMPLOYED IN FLOW CYTOMETRY.

ANTIGEN	PRIMARY ANTIBODY	COMPANY	TIME, TEMP	SECONDARY ANTIBODY
CD13	CONJUGATED MOUSE	eBioscience	20', RT	-
CD44	CONJUGATED MOUSE	BD	20', RT	-
CD49A	CONJUGATED MOUSE MONOCL	BD	20', RT	-
CD49B	CONJUGATED MOUSE MONOCL	BD	20', RT	-
CD49D	CONJUGATED MOUSE	eBioscience	20', RT	-
CD73	CONJUGATED MOUSE MONOCL	BD	20', RT	-
CD105	CONJUGATED MOUSE MONOCL	Serotec	20', RT	-
KDR	CONJUGATED MOUSE MONOCL	Serotec	20', RT	-
C-KIT	UNCONJUGATED RABBIT POLYCLONAL	Dako	30', 37°C	ALEXA488, (20' 37°C)

3.6 IMMUNOFLUORESCENCE CONFOCAL ANALYSIS

3.6.1 CELL STAINING

For immunofluorescence analyses, cultured cells, at the fourth passage *in vitro*, were fixed incubating them, for 20 minutes at RT, with 4% paraformaldehyde (PFA, Sigma-Aldrich) in PBS. Fixed cells were washed three times with PBS and then incubated, for 10 minutes at RT, with 0.1% (v/v) Triton-X 100 (Sigma-Aldrich) in PBS to permeabilize their membranes. After three washes with PBS, cells were incubated with a primary antibody, washed three times with PBS and incubated with the appropriate labeled secondary antibody. The cells were again washed with PBS three times before staining of nuclei with 1µg/ml of 4', 6-diamidino-2-phenylindole (DAPI, Sigma-Aldrich) diluted in PBS. All the information concerning the antibody used, their dilution, incubation time and temperature are reported in **Table 3.6**. Specifically the following antibody or combinations of antibodies were used:

a. Anti-c-Kit to evaluate undifferentiated cells;
b. Anti-Cardiac Myosin Heavy Chain to evaluate differentiation towards cardiac lineage;
c. Anti-Smooth Muscle Actin to evaluate differentiation towards smooth muscle cell lineage;
d. Anti-CD31 to evaluate Platelet endothelial cell adhesion molecule (PECAM-1);
e. Anti-$p16^{INK4A}$ to evaluate senescence;
f. Anti-Ki67 to evaluate proliferation;
g. Anti-γ H2AX + Ki67 to evaluate DDR;
h. Anti-LAMP-2 to evaluate lysosomes;
i. Anti-Galectin 3 + LAMP-2 to evaluate damaged lysosomal membranes;
j. Anti-TFEB to evaluate transcription regulation of ALP genes.

Apoptotic cells were identified by TdT-mediated dUTP-X nick end labeling (TUNEL) assay ApopTag Plus Fluorescein In Situ Apoptosis Detection Kit, EMD Millipore Corporation), following manufacturer's instructions. Briefly, CSCs, at the same passage *in vitro* as above, were fixed with 1% PFA in PBS, for 10 minutes at RT. The cells were washed twice with PBS and permeabilized with pre-cooled Ethanol: Acetic Acid (Sigma-Aldrich) 2:1 for 5 minutes at -20°C. The cells were incubated with 50µl Equilibration Buffer (provided in the kit). The supernatant was then aspirated and the cells were incubated with the TdT Working Solution and the digoxigenin-labeled nucleotides (70% Reaction Buffer: 30% TdT Enzyme), in a humidified chamber for 1 hour at 37°C. The 50µl of Stop/Wash buffer was incubated on the cells for 10 minutes at RT, after which the cells were incubated with 50µl anti-digoxigenin fluorescein antibody. This incubation was performed for 30 minutes at RT, in the dark. To stain the cell nuclei, the cells were incubated for 5 minutes at RT, in the dark, with a solution of 1µg/ml DAPI diluted in PBS.

Vital staining of CSCs with 75nM LysoTracker Red DND-99 (Life Technologies), or 1μM Acridine Orange (Sigma-Aldrich), was performed incubating living CSCs with the specific dye for 2 hours or 15 minutes, respectively. Both the dyes were diluted in expansion medium. After incubation, CSCs were washed two times with HBSS, and fixed for 20 minutes at RT, with 4% PFA. Fixed cells were stained with 1μg/ml of DAPI or permeabilized with Triton-X 100 and then stained with primary antibody as seen above.

3.6.2 QUANTITATIVE ANALYSIS

To evaluate differentiated, senescent, proliferative and apoptotic cells, image analyses were performed employing a Leica DMI6000B setup (Leica microsystems) equipped with a 40X oil-immersion objective (numerical aperture: 1.25) or a 63X oil-immersion objective (numerical aperture: 1.40). Experiments were performed in duplicate. For each marker, at least 400-500 cells were analyzed. Positive cells for each marker were expressed as percentage of the total cells.

To assess the myocyte differentiation capacity, a score was used. This score was calculated as the product of the fraction of α-sarcomeric actin positive cells and an index expressing the level of α-sarcomeric actin filament organization , which ranged from 1 (not-organized) to 3 (well defined filaments) as done in [46].

The emission spectrum of lipofuscin was determined, with confocal microscope, by a λ-scanning on unstained cells (**Figure 3.1**). Depending on the spectral profile of autofluorescence, lipofuscin fluorescence was collected at λ =508-530nm after exciting the sample at λ =488nm.

To obtain quantitative data of the lysosomal levels of lipofuscin, lysosomal membrane levels of Galectin 3 and nuclear levels of TFEB, images of immunofluorescently labeled cells were acquired with a Leica TCS SP2 Confocal microscope (Leica microsystems) equipped with 63X oil-immersion objective (numerical aperture: 1.40). Scrupulous care was taken to keep constant all the acquisition parameters. A quantitation of the total fluorescence of lysosomal lipofuscin, lysosomal Galectin 3 and nuclear TFEB stainings were obtained employing ImageJ software[107]. A threshold was applied to LAMP-2 or DAPI images both to measure colocalization areas and to create a mask to measure the average intensity of lipofuscin autofluorescence, Galectin 3 fluorescence or TFEB fluorescence. Lipofuscin, Galectin 3 or TFEB Integrated Fluorescence Intensity (IFI) was computed for each lysosomal compartment or nucleus multiplying each involved area for the respective mean grey value of lipofuscin, Galectin 3 or TFEB respectively.

TABLE 3.6. ANTIBODIES EMPLOYED IN IMMUNOFLUORESCENCE ANALYSIS.

ANTIGEN	PRIMARY ANTIBODY*	COMPANY	TIME, TEMP, DILUTION*	SECONDARY ANTIBODY*,§
C-KIT	RABBIT POLICLONAL	DAKO	2H, 37°C, 1:30	ALEXA555, 1:800, 1H 37°C
CARDIAC MYOSIN HEAVY CHAIN	MOUSE MONOCLONAL	ABCAM	O/N, 4°C, 1:100	ALEXA488, 1:600, 1H 37°C
SMOOTH MUSCLE ACTIN	MOUSE MONOCLONAL	DAKO	2H, 37°C, 1:50	ALEXA555, 1:800, 1H 37°C
CD31	MOUSE MONOCLONAL	DAKO	2H, 37°C, 1:50	ALEXA555, 1:800, 1H 37°C
A-SARCOMERIC ACTIN	MOUSE MONOCLONAL	SIGMA-ALDRICH	O/N, 4°C, 1:100	ALEXA555, 1:800, 1H 37°C
P16INK4A	MOUSE MONOCLONAL	CIN-TEK	O/N, 4°C, PREDILUTED	ALEXA488, 1:600, 1H 37°C
γH2AX	MOUSE MONOCLONAL	MILLIPORE	2H, 37°C, 1:500	ALEXA555, 1:800, 1H 37°C
KI67	RABBIT POLICLONAL	LEICA-NOVOCASTRA	O/N, 4°C, 1:1000	ALEXA488, 1:600, 1H 37°C
GALECTIN 3	GOAT POLICLONAL	R&D	O/N, 4°C, 1:1000	ALEXA647, 1:600, 1H 37°C
LAMP-2	MOUSE MONOCLONAL	SANTA CRUZ	2H, 37°C, 1:100	ALEXA555/647, 1:800, 1H 37°C
TFEB	RABBIT POLICLONAL	ABCAM	O/N, 4°C, 1:75	ALEXA647, 1:800, 1H 37°C

* Incubations were done in humidified chamber, in the dark.

§ All from Invitrogen and produced in donkey.

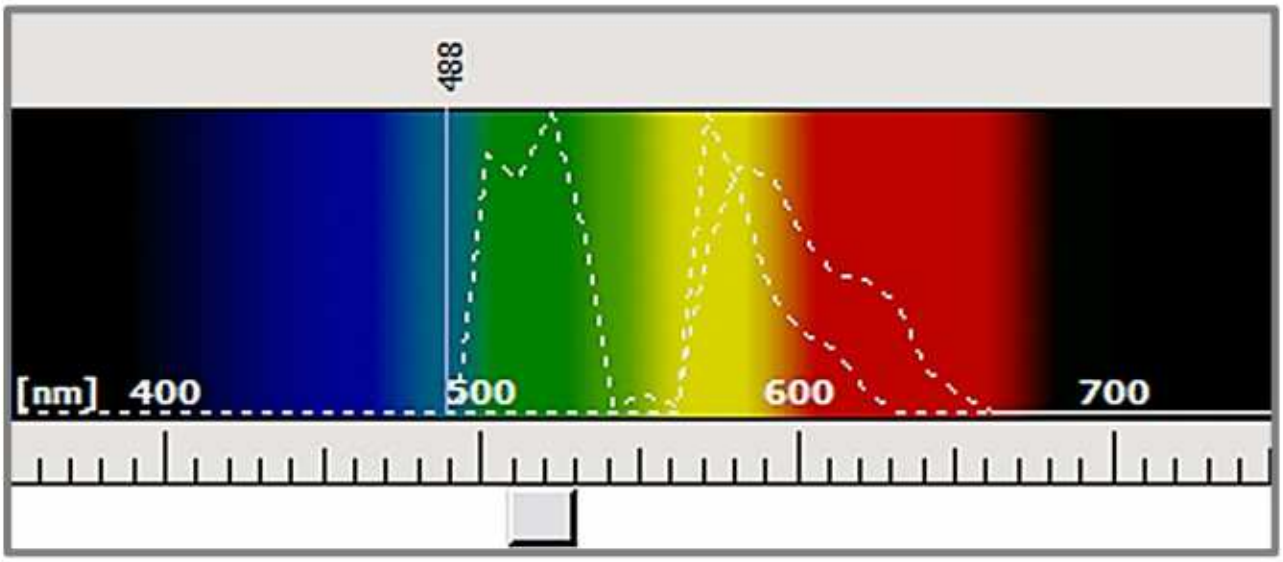

FIGURE 3.1. Emmission Spectrum of Lipofuscin. The panel reports the emission spectrum of lipofuscin as resulted by a λ-scanning performed by confocal microscope (white dotted lines), exciting unstained cell at λ=488nm (light blue line). The hole in the spectrum profile, between 530nm and 570nm, is due to the manufacture of the instrument specifically to a dichroic mirror which makes to collect light at that wavelength impossible. The gray band on the bottom of the figure indicates the interval of wavelength (λ=508-530nm) at which the signal was collected for the present study.

3.7 WESTERN BLOT ANALYSIS

3.7.1 PROTEIN COLLECTION AND EXTRACTION

For the preparation of total cell lysates, cells were detached as seen above (**par. 3.2.1**) and washed with ice-cold PBS, counted, pelleted and frozen. Cell pellet was resuspended in lysis buffer (see **par. 3.13**), at a cell density of 10^7 cells/ml and rotated for 30 minutes at 4°C. After centrifugation at 12,000g for 10 minutes at 4°C, the supernatant was collected as total cell lysate and stored at -80°C until required.

3.7.2 MEASUREMENT OF PROTEIN TOTAL CONTENT

Concentration of protein extracts was measured using the Bradford assay (Bio-Rad). The Bradford reagent was initially diluted to working dilution with distilled water. BSA standards were prepared, ranging from 0µg/ml to 20µl/ml and diluted in 1x Bradford reagent (final volume 1ml). 2µl protein lysate was then diluted in 998µl Bradford reagent, before the lysates and standards absorbance was measured with a spectrophotometer set at 595nm. The protein concentration of the lysates was calculated using a standard curve generated from the known concentration of the protein standards.

3.7.3 ELECTROPHORESIS AND IMMUNOBLOTTING

For used solutions, see **par. 3.13**. 30µg of total cell lysate was prepared for electrophoresis in sample loading buffer. Samples were boiled at 95°C for 5 minutes and then spun down. Samples were separated by a 12% SDS-PAGE gel. The resolving gel is prepared at the right density for the protein of interest and polymerized between two glass plates in a gel caster. The gel was leveled using saturated butanol. After the resolving gel was polymerized, the stacking gel was poured on the first gel, with a comb inserted at the top to create the sample wells. Once polymerized the combs were removed. The gel was put into the Bio-Rad Tetra running tank with 500ml of 1x running buffer, then the samples and 10µl of protein ladder were loaded into the wells. The voltage was set a 120V for 1 hour.

Separated proteins were then transferred to nitrocellulose membranes (Schleicher & Schuell). The "sandwich" was prepared with a sponge, 3x filter paper (Bio-Rad), gel, membrane, 3x filter paper and sponge and placed in the cassette. Paper and sponges were soaked in transfer buffer and the tank was filled with running buffer. The voltage was set at 30V for 12 hours at 4°C. The resulting transferred proteins and membrane were then ready to be used in the antibody hybridization method.

3.7.4 ANTIBODY HYBRIDIZATION

Membranes were saturated by incubation at RT for 1 hour with 5% (w/v) nonfat dry milk (Bio-Rad) in TBS-T and incubated overnight at 4°C with the antibodies listed in **Table 5**. After three washes with TBS-T, membranes were incubated with an anti-rabbit antibody coupled to the enzyme peroxidase (HRP) (Sigma-Aldrich). After 2 hours of incubation at RT, membranes were washed 3 times with TBS-T and last with distilled water, to remove the Tween-20 detergent.

3.7.5 ANALYSIS

The blots were developed using the ECL enhanced chemiluminescence procedure (GE Life Science), which consists of incubating of the membrane with a chemiluminescence solution, resulting in the production of a chemiluminescent signal that is captured onto a film. Equal loading was confirmed by the use of a polyclonal anti-actin antibody (Sigma-Aldrich). The bands were visualized and analyzed using ChemiDoc XRS (Bio-Rad) and associated software. Polyclonal anti-actin antibody (Sigma-Aldrich) was used to normalize the protein content in the total extracts.

TABLE 3.7. ANTIBODIES EMPLOYED IN WESTERN BLOT ANALYSIS.

ANTIGEN	ANTIBODY	COMPANY	TIME, TEMP, DILUTION
MTOR	RABBIT MONOCLONAL	CELL SIGNALING	1:1000, O/N 4°C
P-MTOR^{SER248}	RABBIT MONOCLONAL	CELL SIGNALING	1:1000, O/N 4°C
P70 S6K	RABBIT MONOCLONAL	CELL SIGNALING	1:1000, O/N 4°C
P-P70 S6K^{THR389}	RABBIT MONOCLONAL	CELL SIGNALING	1:1000, O/N 4°C
ATG3	RABBIT POLYCLONAL	CELL SIGNALING	1:1000, O/N 4°C
ATG7	RABBIT POLYCLONAL	CELL SIGNALING	1:1000, O/N 4°C
AKT	RABBIT MONOCLONAL	CELL SIGNALING	1:1000, O/N 4°C
P-AKT^{SER473}	RABBIT MONOCLONAL	CELL SIGNALING	1:1000, O/N 4°C
P62 SQSTM1	RABBIT POLYCLONAL	LIFESPAN BIOSCIENCES	1:1000, O/N 4°C
LC3B	RABBIT MONOCLONAL	CELL SIGNALING	1:1000, O/N 4°C
ACTIN	RABBIT POLYCLONAL	SIGMA ALDRICH	1:1000, O/N 4°C

3.8 TRANSCRIPTIONAL PROFILE

3.8.1 GENE EXPRESSION PROFILING BY MICROARRAY

CSCs obtained from age- and sex-matched donor and explanted hearts (N = 3 each) were used for the analysis of the transcriptional profile that was performed through LNCIB 28K cDNA microarray slides (supporting 28.000 cDNA clones). The gene expression data were obtained in prof. Schneider's laboratory, as in [46].

3.8.2 FUNCTIONAL ANNOTATION ANALYSIS

Differentially expressed gene lists were subjected to functional analysis using R(version 3.1.2)/Bioconductor (version 3.0) environment implemented with clusterProfiler[108] (available at http://bioconductor.org/packages/release/bioc/html/clusterProfiler.html), ReactomePA (available at http://bioconductor.org/packages/release/bioc/html/ReactomPA.html), and DOSE[109](available at http://bioconductor.org/packages/release/bioc/html/DOSE.html) that automate the process of biological-term classification and the enrichment analysis of gene clusters. Specifically:

a. clusterProfiler functions enrichGO and enrichKEGG were used to calculate enrichment test for Gene Ontology[110] (GO), terms related to biological processes, molecular functions, and cellular components and Kyoto Encyclopedia of Genes and Genomes (KEGG)[111] pathways;
b. ReactomePA function enrichPathway was used to calculate enrichment test for Reactome [112] pathways;
c. DOSE function enrichDO was used to calculate enrichment test for Disease Ontology (DO) [113] terms.
d. The KEGG pathway maps with integrated data results of enriched tests were created by R(version 3.1.2)/Bioconductor (version 3.0) environment implemented with Pathview (available at http://pathview.r-forge.r-project.org/) [114].

To assess the presence of Autophagy-Lysosome pathway related genes and TFEB gene targets, R(version 3.1.2) environment was used to match differently expressed gene lists both with a list of 435 genes extracted form a System Biology study on Autophagy-Lysosome pathway[115] and with a list of 471 identified TFEB direct gene targets that prof. Ballabio make available for the study [89].

3.9 MICRORNA EXPRESSION ANALYSIS

3.9.1 RNA EXTRACTION, RETROTRANSCRIPTION AND REAL-TIME PCR REACTIONS

CSCs obtained from age- and sex-matched donor and explanted hearts (N = 4 each) were used for the analysis of microRNA expression. Total RNA was extracted with miRVana kit, following the manufacturer's instructions (Life Technologies). The concentration of total RNA and its quality were determined by measuring the absorbance at 260nm (A260) using a Nanodrop spectrophotometer (Nanodrop 1000, Thermo Scientific) according to the manufacturer's instructions.

To reverse transcribe the RNA, the miRNA Reverse Transcription Kit (Life Technologies) and Megaplex RT Primers, Human Pool A v2.1 (Life Technologies) were used, as per manufacturer's instructions. Briefly, the reaction of reverse transcription included dNTPS (100mM), Multiscribe Reverse Transcriptase, $MgCl_2$ (25mM), 10x RT buffer, RNase inhibitor (20U/µl), nuclease-free water, Megaplex RT Primers (10x) and 350-1,000ng of total RNA. The reaction was run on a thermal cycler at the conditions reported in Table 3.

To assess the expression profile of microRNAs, TaqMan Array Human MicroRNA A Cards v2.0 (Life Technologies) were used. The TaqMan Array contains 384 TaqMan MicroRNA Assays 377 for the quantitation of human microRNAs; 3 for endogenous controls to use in data normalization; 1 not related to human to use as a negative control. The PCR-reaction mix was prepared mixing 444µl of nuclease-free water with 6µl of transcription product and 450µl of TaqMan Universal PCR Master Mix, No AmpErase UNG, 2x (Life Technologies). The preparation of Taqman Arrays followed the manufacturer's instructions. The run was performed using the Applied Biosystems 7900HT System (Life Technologies) implemented with the Low Density Array Thermal Cycling Block and with the Sequence Detection Systems (SDS, version v2.1) software. Specific information of TaqMan Array Cards was imported from the SDS setup file provided with the Taqman Arrays. The SDS software uses this setup file to configure the plate document plate grid and setup table. PCR reactions were run following thermal cycling parameters listed in **Table 3**.

3.9.2 RELATIVE QUANTIFICATION AND DATA ANALYSIS

Relative Quantification was calculated using the $2^{-\Delta\Delta Ct}$ method previously described in [116]. The expression of the endogenous control U6 snRNA was employed as a reference to normalize the expression levels. Results were expressed in fold-change respect to the control CSC line.

The differential microRNAs expression between CSCs obtained from donor and explanted hearts was established by Kruskal-Wallis test performed with SPSS20 for Macintosh software.

3.9.3 IDENTIFICATION AND FUNCTIONAL ANNOTATION ANALYSIS OF MICRORNA GENE TARGETS

To identify experimentally validated gene targets, the lists of differently expressed microRNA were matched with TarBase (version 5.0, downloaded at http://diana.cslab.ece.ntua.gr/tarbase/tarbase_download.php) [117, 118].

MiRNA target Gene lists were subjected to functional analysis using R (version 3.1.2)/Bioconductor (version 3.0) environment implemented with clusterProfiler as seen above (see **par. 3.8.3**).

TABLE 3.1 THERMAL-CYCLING CONDITIONS OF REVERSE TRANSCRIPTION AND REAL-TIME PCR REACTION.

REVERSE TRANSCRIPTION				REAL-TIME PCR REACTION		
STEP	TEMP	TIME		STEP	TEMP	TIME
CYCLE (40 CYCLE)	16°C	2 MIN		-	-	-
	42°C	1 MIN		HOLD	95°C	10 MIN
	50°C	1 SEC		CYCLE (40 CYCLE)	95°C	15 SEC
HOLD	85°C	5 MIN			60°C	60 SEC
HOLD	4°C	∞		HOLD	4°C	∞

3.10 PHARMACOLOGICAL TREATMENT OF CSCS

In order to perform a pilot titration study, E-CSC were exposed to either 1nM-, 10nM-, 100nM-, and 1μM-Rapamycin (Sigma-Aldrich) for three days in culture and analyzed immediately thereafter to detect the fraction of: apoptotic and necrotic cells by FACS (see **par. 3.5**), senescent-, DDR positive-, and cycling-cells by immunofluorescence (see **par. 3.6**).

Once identified the drug concentration minimizing acute toxicity, D-CSC and E-CSC at the fourth passage in culture were exposed to 10nM Rapamycin for three days. As a control, cells were treated with the vehicle alone (DMSO). Vehicle-treated and drug-treated cells were then switched for 24 hours to a drug-free medium and subsequently properly assayed in the *in vitro* experiment (**Figure 3.1**).

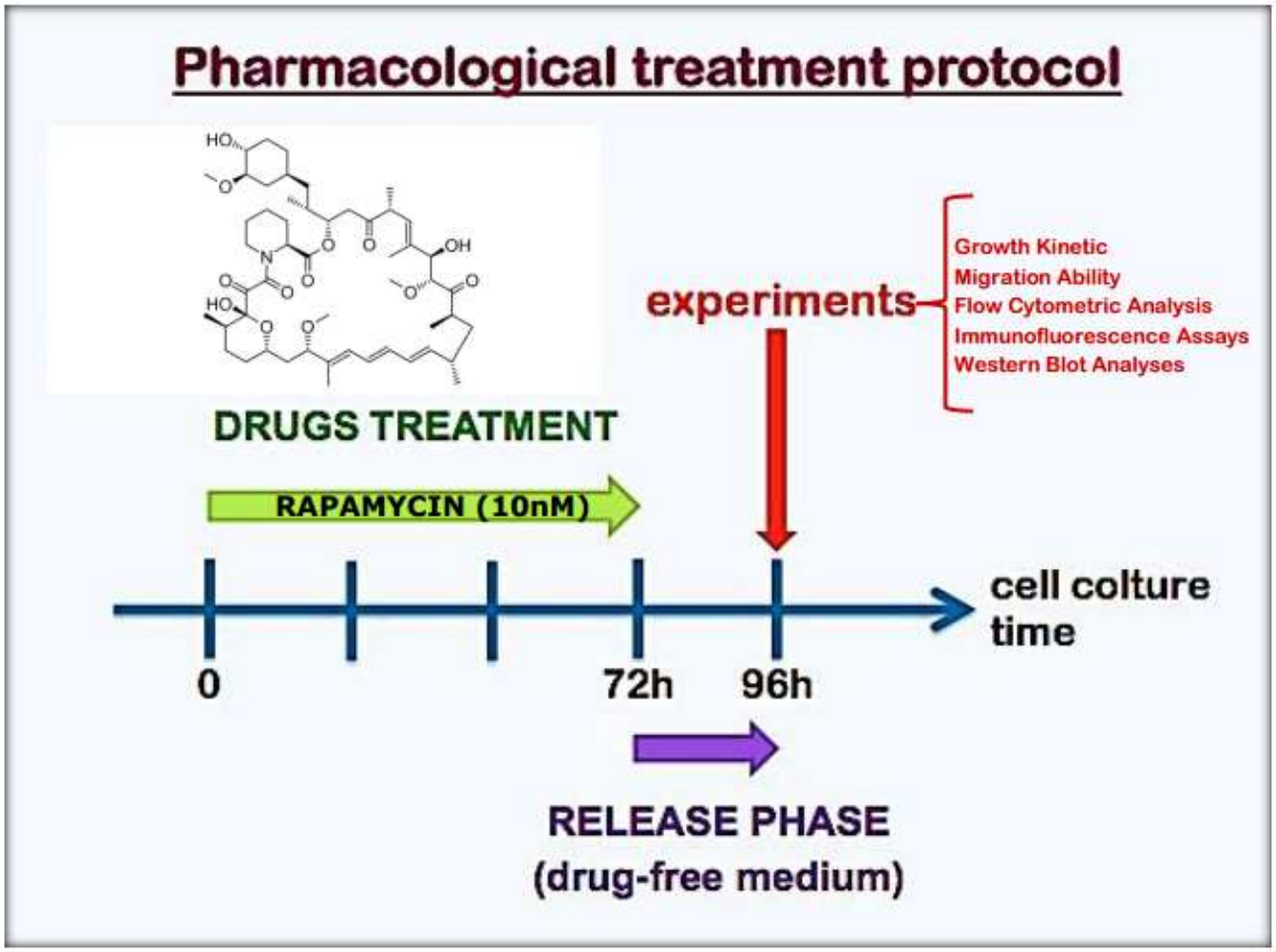

FIGURE 3.2. Experimental Design.

3.11 STATISTICAL ANALYSES

Characteristics of the study population are described using means±SEM. Data were analyzed for normal distribution by Kolmogorov-Smirnov test. T-test or Mann-Whitney test, as appropriate, was used to compare continuous variables between two groups. Drug-treatment assays were analyzed by repeated measurements one-way Anova followed by Bonferroni post-test or by Kruskal-Wallis followed by Dunn's post-test, as appropriate. In order to distinguish the effects of age and pathology on CSC senescence parameters (dependent variables), a univariate general linear model was employed in which pathology was considered as fixed factor and age as covariate.

Probability values (p) less than 0.05 were considered significant. Results are shown as means±SEM.

Analyses were conducted with Prism, version 4.0c and SPSS20 for Macintosh software.

3.12 IMAGE PROCESSING

Adobe Photoshop software was utilized to compose, overlay the images and to adjust contrast (Adobe).

3.13 SOLUTIONS AND CULTURE MEDIA

All chemical reagents have been purchased from (Sigma-Aldrich) otherwise differently specified.

Basic Dissociation Buffer (BDB)

Minimum Essential Medium Joklik (J-MEM, Life Technologies) reconstituted in 1L ultrapure H_2O, 3mM HEPES, 2mM Glutamine, 20U Insulin, 100µg/L Streptomycin, 100U Penicillin; pH to 7.3 with NaOH.

HBSS (Calcium free, Magnesium free Hank's Balanced Salt Solution)

Add the content of 1 package in 1L ultrapure H_2O, adjust the pH to 7.3.

Expansion Medium for CSCs (starting from the second passage in culture)

60% low glucose DMEM (Life Technologies), 40% MCDB-201, 1mg/ml linoleic acid-BSA, 10^{-8}M dexamethasone, 10^{-4}M ascorbic acid-2 phosphate, 5g/ml insulin, 5g/ml transferrin, 30nM sodium selenite, 2% fetal bovine serum (STEMCELL Technologies), 1x Penicillin/Streptomycin (from 100x concentrated stock, Life Technologies), 10ng/ml human PDGF-BB (Peprotech), 10ng/ml human EGF (Peprotech); adjust the pH to 7.4.

Muscle Cell Differentiation Medium

Expansion medium for CSCs containing 9% Fetal bovine serum (Euroclone), 10ng/ml basic fibroblast growth factor (bFGF, Peprotech), 10ng/ml Vascular Endothelial Growth Factor (VEGF, Peprotech), and 10ng/ml Insulin-like Growth Factor 1 (IGF-1, Peprotech).

Endothelial Cell Differentiation

EGM-2 Endothelial Cell Growth Medium-2 (Lonza).

PBS (Phosphate Buffered Saline) with Calcium and Magnesium

137mM NaCl, 27mM KCl, 4.3mM Na_2HPO_4, 1.4mM KH_2PO_4, 0.1mM $MgCl_2$, 0.1mM $CaCl_22H_20$; adjust the pH to 7.4.

PFA Solution (4%w/v)

4% PFA in PBS gently heated at 55°C and agitated with a magnetic flea, until the powder dissolved. Solution prepared in a chemical hood and pH to 7.4.

Lysis Buffer for Protein Extraction

50mM TrisHCl (pH 7.4), 150mM NaCl, 1mM EDTA, 1% v/v Triton X-100, 1x protease inhibitor cocktail, 0. mM phenylmethylsulfonyl fluoride (PMSF), 1mM NaF, 1mM Na_3VO_4.

Western Blot Solutions

- Resolving Gel 12% Acrilamide

Distilled water 3.3ml, 30% Acrilamide mix 4ml, TrisHCl pH 8.8 2.5ml, 10% SDS 100µl, 10% APS 100µl, TEMED 4µl.

- Stacking Gel

Distilled water 3.4ml, 30% Acrilamide mix 830µl, TrisHCl pH 8.8 630µl, 10% SDS 50µl, 10% APS 50µl, TEMED 5µl.

- TBS 10x pH=7.5

Tris 100mM, NaCl 150mM in distilled water. Adjust pH to 7.5. Store at RT.

- TBS-T

TBS (1x) + 0.1% (v/v) Tween-20.

- Transfer Buffers

Dissolve 3g Tris base and 11.3g Glycine in a final volume of 800ml in distilled water. Add 200ml Methanol. Store at 4°C.

- Running Buffer 10x

For a final volume of 2L in distilled water: Tris 60.6 g, Glycine 288 g, SDS 20g.

- SDS Samples Loading Buffer 5x

250mM TrisHCl pH6.8, 10% SDS, 30% Glycerol, 5% β -mercaptoethanol, 0.02% bromophenol blue.

4. RESULTS

4.1 CARDIAC STEM CELLS ISOLATED FROM FAILING EXPLANTED HEART ARE SENESCENT

Human Cardiac Stem Cells (CSCs) of the present study were isolated by mechano-enzymatic dissociation [104, 105] from atrial fragments (**Figure 4.1**) of healthy donor hearts (D-CSC, n=14) and from explanted hearts of heart failure patients (E-CSC, n=20). Obtained cells resulted able to be expanded in vitro as proliferating cultures of undifferentiated c-Kit positive cells (**Figure 4.2A**), cloned, and differentiated towards myocyte (**Figure 4.2B**), smooth muscle (**Figure 4.2C**), and endothelial (**Figure 4.2D**) lineages[46, 105].

4.1.1 CELL SURFACE IMMUNOPHENOTYPE

Cell surface immunophenotype of undifferentiated D-CSC and E-CSC was evaluated by FACS analysis (**Figure 4.3**). Both classes of CSCs display a comparable mesenchymal surface phenotype (CD13, CD44, CD73, CD105, CD49b and CD49d.). Markers of the hematopoietic/endothelial cell lineage (CD133, CD34, CD45, Abcg2 and KDR) are not detected (data not shown). CD49a/α1 integrin, that increases with cardiac aging and disease[119], is more represented in CSCs from failing hearts.

4.1.2 E-CSC ARE LESS PROLIFERATING AND MORE APOPTOTIC

Growth properties of CSCs were determined at the forth passage of cultured cells. Cell Population doubling time (CPDT) is 1.7 fold shorter in D-CSC than E-CSC (**Figure 4.4A**).

Markers of cell proliferation (Ki67) and apoptosis (TdT) were assessed by immunofluorescence microscopy. E-CSC are less proliferating (**Figure 4.4B-D**) and more apoptotic if compared with D-CSC (**Figure 4.4E-G**). Although both age and pathology may influence the evaluated markers, univariate linear model analysis showed that the pathological status is, in the present case study, the only independent predictor for Ki67 ($p<0.0001$) and TUNEL ($p=0.02$) levels in CSCs[46].

4.1.3 E-CSC ARE ENRICHED IN SENESCENCE MARKERS

The expression of senescence markers were assessed in D-CSC and E-CSC by immunofluorescence microscopy. CSC obtained from explanted hearts shows significantly higher expression of senescence associated cyclin dependent kinase inhibitor $p16^{INK4A}$ (**Figure 4.5 A, B, C**) as well as a significantly higher percentage of cells with persistent DNA-Damage Response (DDR). DNA damage foci positive cells were identified by the presence of the histone protein γ-H2A.X (at least 5 foci of positivity per nucleus) in the absence of cell proliferation (Ki67 negativity, **Figure 4.5 D, E, F**) [120]. As seen above the pathological status is the only independent predictor of the fraction of CSCs expressing either $p16^{INK4A}$ ($p<0.0001$) or γ-H2A.X ($p=0.004$).

These results, together with results of **par. 4.1.2** display that E-CSC, compared to D-CSC, are significantly enriched in cells showing typical senescence features.

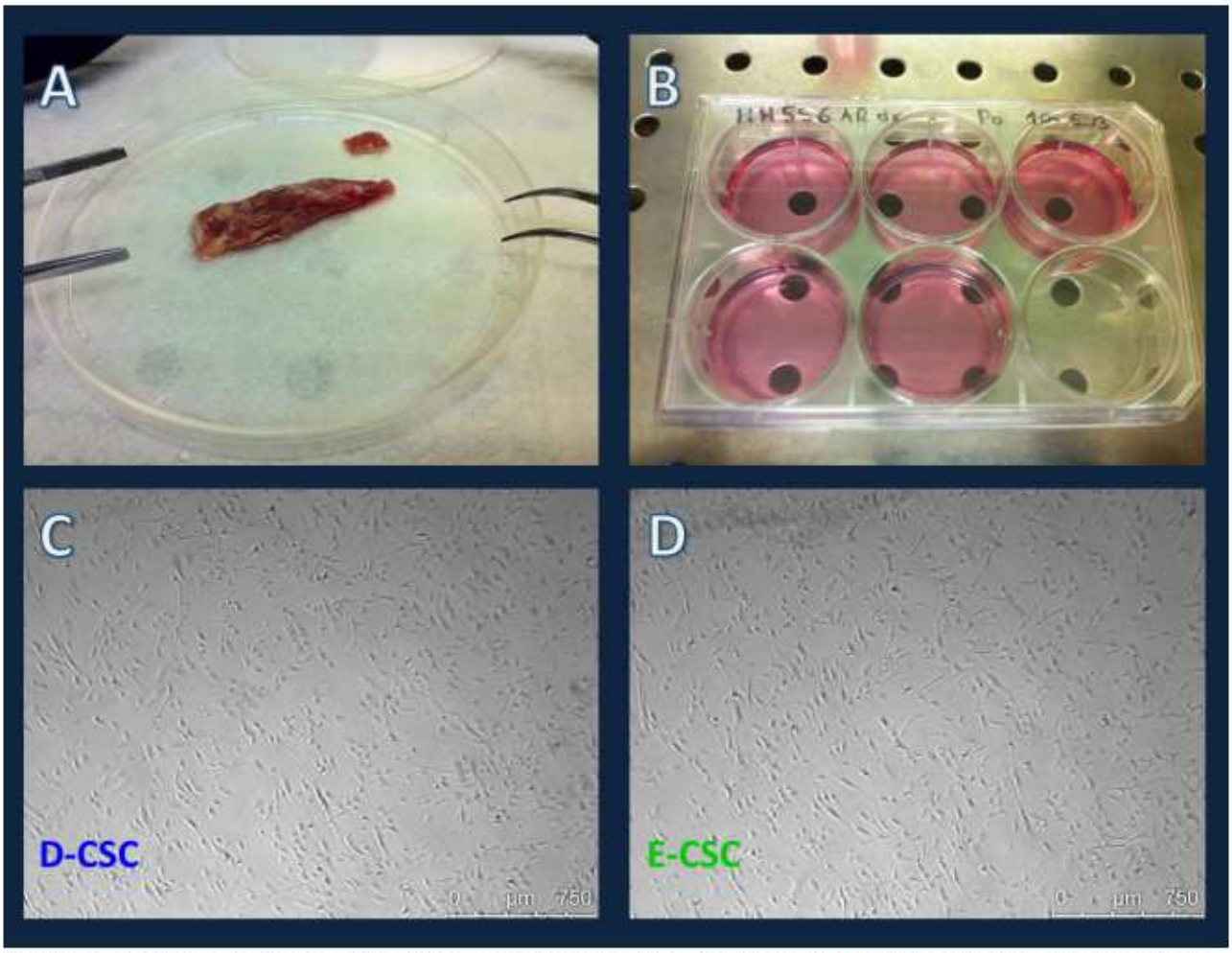

FIGURE 4.1. Schematic Phases of Isolation and Culture of CSCs. Representative pictures of atrial samples that show the extreme points of an isolation: from the atrial sampling (**A**), to the culture (**B**) of obtained cells, Representative phase-contrast images of CSC isolated from donor heart (**C**) and from explanted failing heart (**D**).

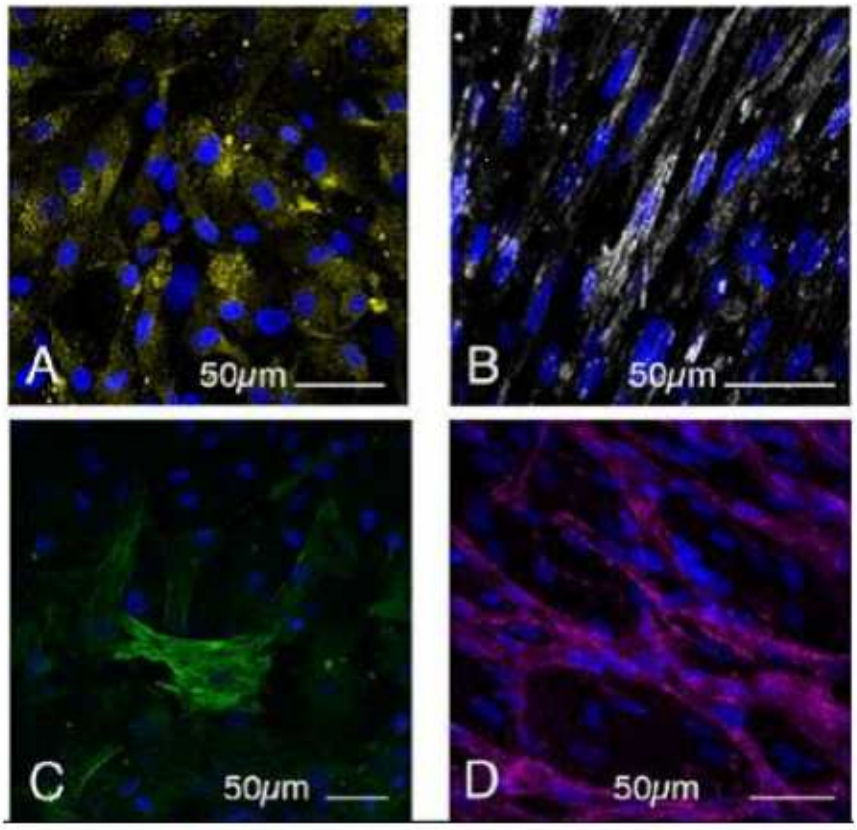

FIGURE 4.2. CSC Characteristics. Representative confocal images that show the expression of c-Kit (**A**, yellow), Cardiac Myosin Heavy Chain (**B**, white), Smooth Muscle Actin (**C**, green), and CD31 (**D**, purple).

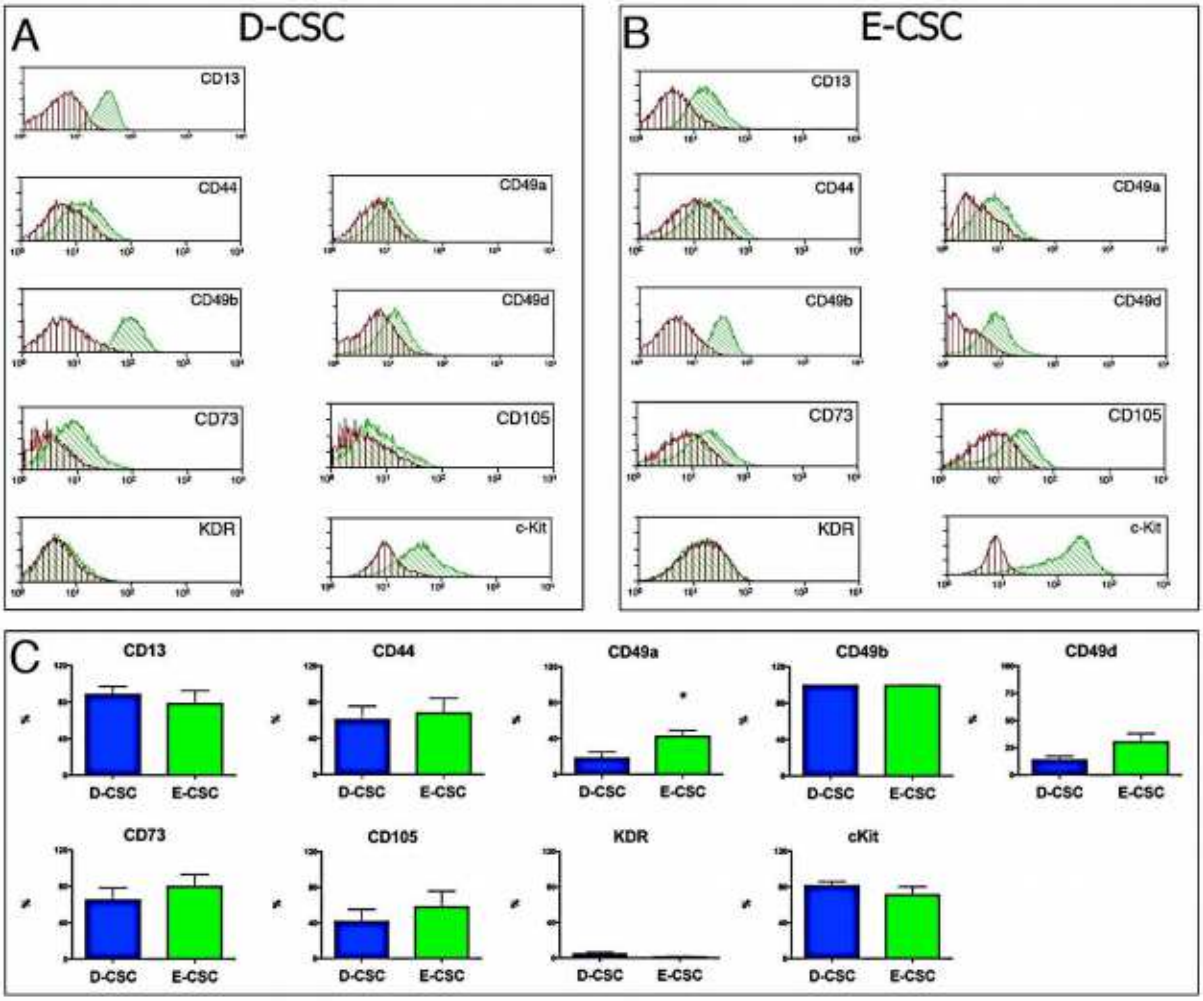

FIGURE 4.3. Cell Surface Immunophenotype. Representative Flow-Cytometry histograms of cultured D-CSC (**A**) and E-CSC (**B**). The specific antibody staining profile (green histogram) is superimposed to the isotype control IgG staining profile (red histogram). **C**: bar graphs summarize quantitative Flow-Cytometry data, that are expressed as frequency (%) of D- and E-CSC positive to the markers indicated. Values are means±SEM. * $p<0.05$ vs D-CSC.

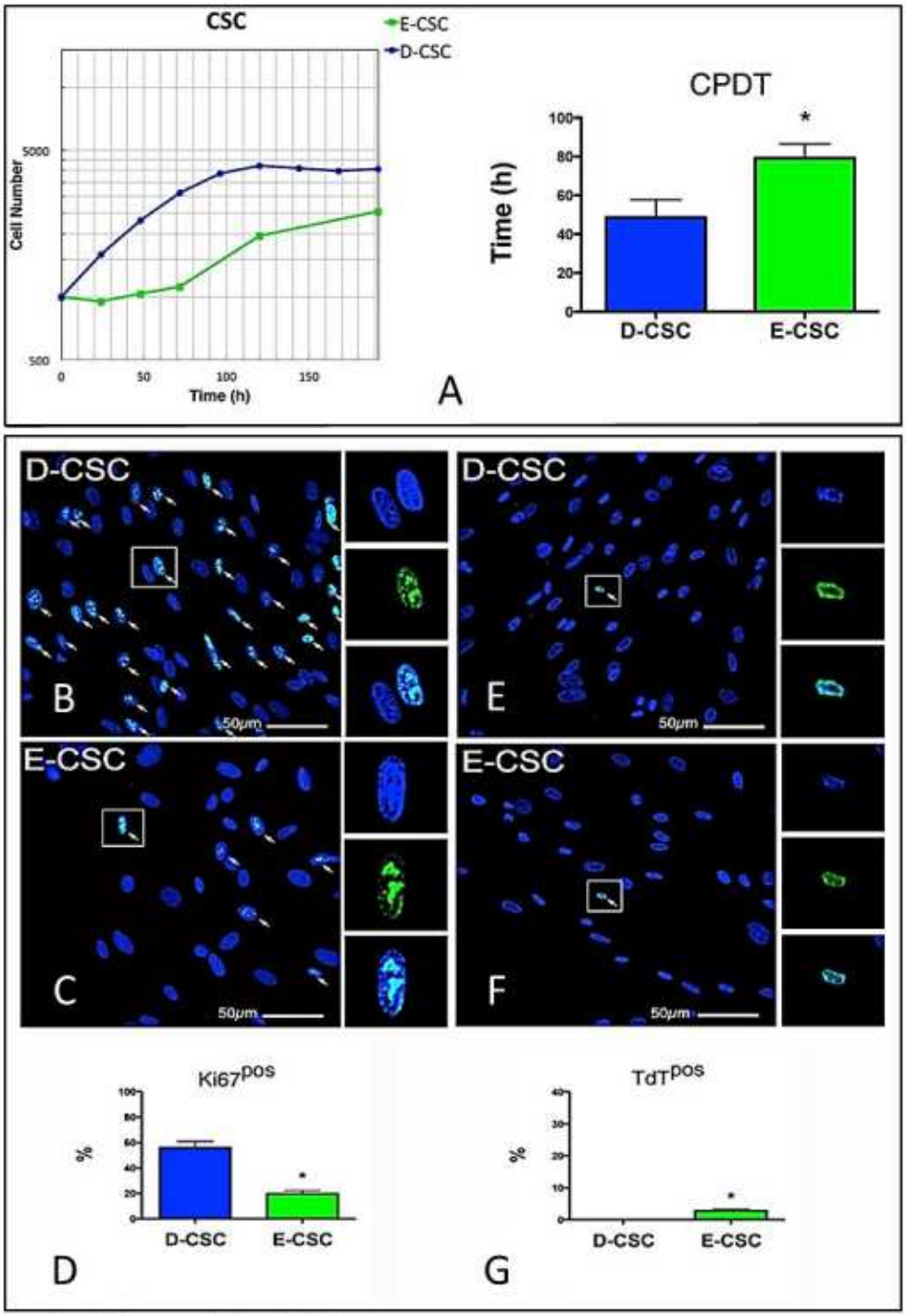

FIGURE 4.4. Functional Characteristics of CSCs. A: representative growth curves of D- and E-CSC (left); histograms summarizing cell population doubling time (CPDT, right). **B-G**: Expression of proliferation and apoptosis markers in CSC. Representative confocal images of cultured D-CSC (**B**, **E**) and E-CSC (**C**, **F**) illustrating: the presence of D-CSC (**B**) and E-CSC (**C**) cycling cells (Ki67, arrows, green); the presence of apoptotic D-CSC (**E**) and E-CSC (**F**) (TUNEL, arrows, green). Nuclei are shown by the blue fluorescence of DAPI. Histograms (**D**, **G**) represent the fraction of cells (%) positive to the specific immuno-stainings. All the values showed by histograms (**A**, **D**, **G**) are means±SEM. * $p<0.05$ vs D-CSC.

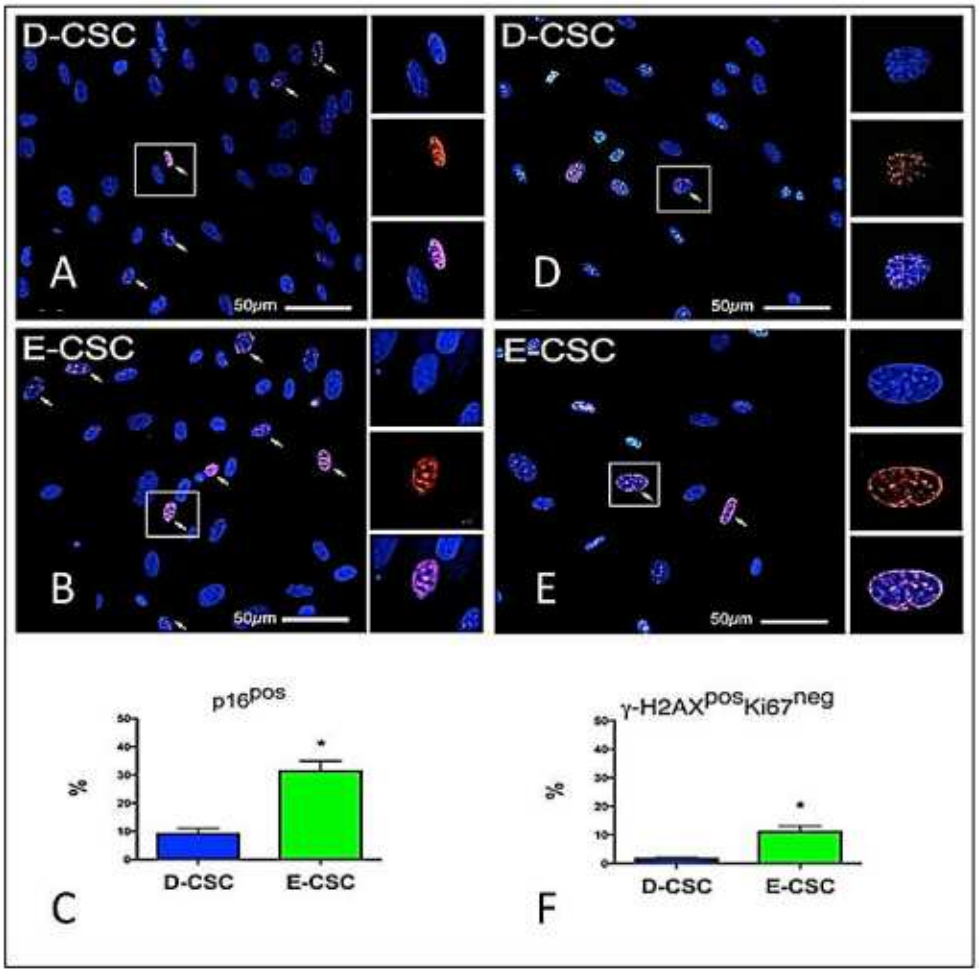

FIGURE 4.5. Expression of Senescence Markers. Representative confocal images of cultured D-CSC (**A**, **D**) and E-CSC (**B**, **E**) illustrating the nuclear expression of p16INK4A (arrows, red) both in D-CSC (**A**) and E-CSC (**B**); the presence of cells showing a persistent DDR as reported by expression of γ-H2A.X (at least n=5 foci of positivity per nucleus) in the absence of proliferative marker (Ki67, green) both in D-CSC (**D**) and E-CSC (**E**). Nuclei are shown by the blue fluorescence of DAPI. Histograms (**C**, **F**) represent the fraction of cells (%) positive to the reported marker. All Values are means±SEM. * $p<0.05$ vs D-CSC.

4.2 GENE EXPRESSION

With the aim to identify transcriptome imbalances associated with cell senescence and Autophagy-Lysosome Pathway (ALP) dysfunction, the transcriptional profiles of CSCs obtained from donor and failing explanted hearts were determined by microarray analysis. Original gene expression data obtained in prof. Schneider's laboratory [46] were reanalyzed according to last version of gene annotation (http://www.ncbi.nlm.nih.gov/gene). Only Genes that showed a significant ($p<0.05$) expression difference of at least 1.7-fold between D- and E-CSC were considered. 372 genes and 423 genes were found to be up-regulated and down-regulated in CSCs from failing hearts, respectively (**Supplementary Table S1, S2**).

4.2.1 FUNCTIONAL ANNOTATION OF DIFFERENTLY EXPRESSED GENES

To understand the functional meaning of transcriptome analysis results, the functional annotation of differently expressed gene lists were examined in four different pathway databases: Gene Ontology, KEGG, Reactome and Disease Ontology.

In Gene Ontology "Biological Process" category: 330 and 242 ontologies resulted enriched in up-regulated and down-regulated E-CSC gene lists respectively (p.adjust<0.01, **Supplementary Table S3, S4**). A part from similar ontologies, genes associated with "response to stress", "response to wounding", "wound healing" and "inflammatory response", together with "cardiovascular system development" ontologies are more expressed in E-CSC.

In Gene Ontology "Cellular Component" category: 47 and 44 ontologies resulted enriched in up-regulated and down-regulated E-CSC gene lists respectively (p.adjust<0.01, **Supplementary Table S5, S6**). Noteworthy transcriptome of E-CSC presented a deficit in genes associated with "lysosome" and "lytic vacuole" (ADA, CTSK, CTSL, DAB2, FNBP1, MLC1, TMEM9, DPP7, LUM, ASAH1, OCA2, CTSA, WDR48, TCN2, GPR137B, USP5, CAT, **Figure 4.6**).

In Gene Ontology "Molecular Function" category: 33 and 18 ontologies resulted enriched in up-regulated and down-regulated E-CSC gene lists respectively (p.adjust<0.01, **Supplementary Table S7, S8**). In agreement with what seen above, the link with the inflammation is confirmed; indeed transcription profile of E-CSC appeared to be enriched in genes involved in "cytokine binding".

The enrichment test for KEGG, Reactome and Disease Ontology pathways linked the list of genes more expressed in E-CSC with 3 pathways annotated in KEGG, and 4 pathways annotated in Reactome (p.adjust<0.05, Supplementary **Table S9, S10**). Specifically these enriched pathways concern pathological inflammatory conditions, "hemostasis", platelet activation and interestingly the

"protein processing that involves the endoplasmic reticulum" (**Figure 4.7**). KEGG, Reactome and Disease Ontology pathways did not result enriched in genes down-regulated in E-CSC.

Summarizing, bioinformatics research indicated that transcripts of genes encoding proteins connected with the structure of lysosomes and lytic vacuole are less expressed in CSCs isolated from explanted hearts. These cells are also characterized by an overexpression of genes involved in cellular response to stress, in inflammatory conditions, and in protein degradation by proteasome.

4.2.2 AUTOPHAGY-LYSOSOME PATHWAY RELATED GENES ARE UNDER-EXPRESSED IN E-CSC.

Once established that the transcriptome of E-CSC was deficient in lysosomal mRNAs, the list of E-CSC down-regulated genes was also matched with the list of Autophagy-Lysosome Pathway (ALP) associated genes [115]. This comparison enabled the identification of 23 ALP related genes that are down-regulated in E-CSC as reported in **Table 4.1**.

4.2.3 A SUBSET OF E-CSC DOWNREGULATED GENES ARE DIRECT TARGETS OF TFEB

Since growing evidences report that Transcription Factor EB (TFEB) plays an integrated control of cellular clearance pathways regulating the transcription of a set of genes known as CLEAR (Coordinated Lysosomal Expression and Regulation) gene network, the presence of validated targets of TFEB [89] was evaluated among the E-CSC down-regulated genes. This investigation unearthed 21 genes, less expressed in E-CSC, that are part of CLEAR network (**Table 4.2**)

This result together with the bioinformatics results seen above indicates a dysregulation within the CSCs obtained from failing hearts, at expense of a set of genes involved in cellular clearance processes.

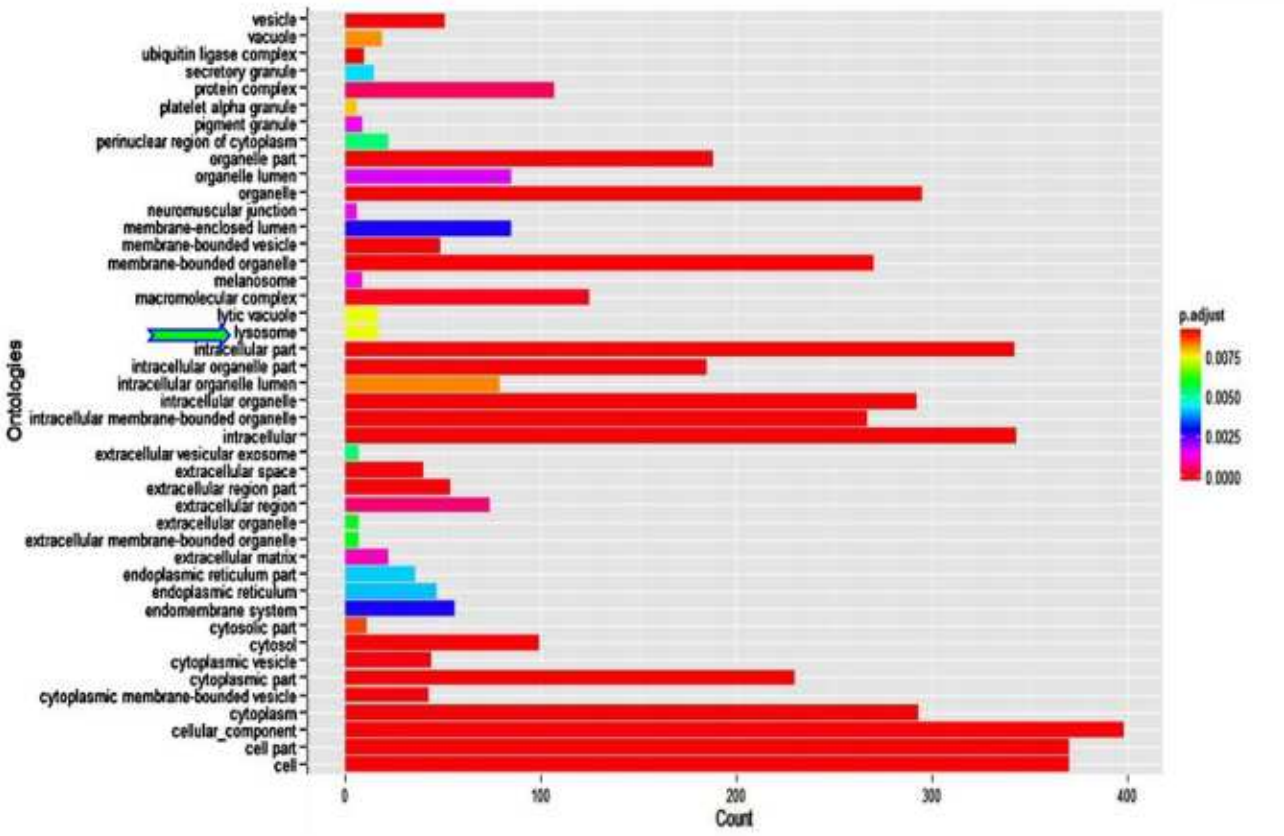

FIGURE 4.9. Gene Ontologies of Cellular Component Category Enriched in Down-Regulated E-CSC Genes. Barplots graphically represent the results of enrichment tests for Gene Ontology annotations of Cellular Component Category, calculated on the lists of genes that are under-expressed in E-CSC. Bar length is proportionally to the count of gene targets associated with the specific Cellular Component Ontologies. As reported by legends on the left, the bar colors depend on the p.value that characterize the match between the genes of interest and the Ontology. Green arrows point out Lysosome Ontology because of its relevance for the present study.

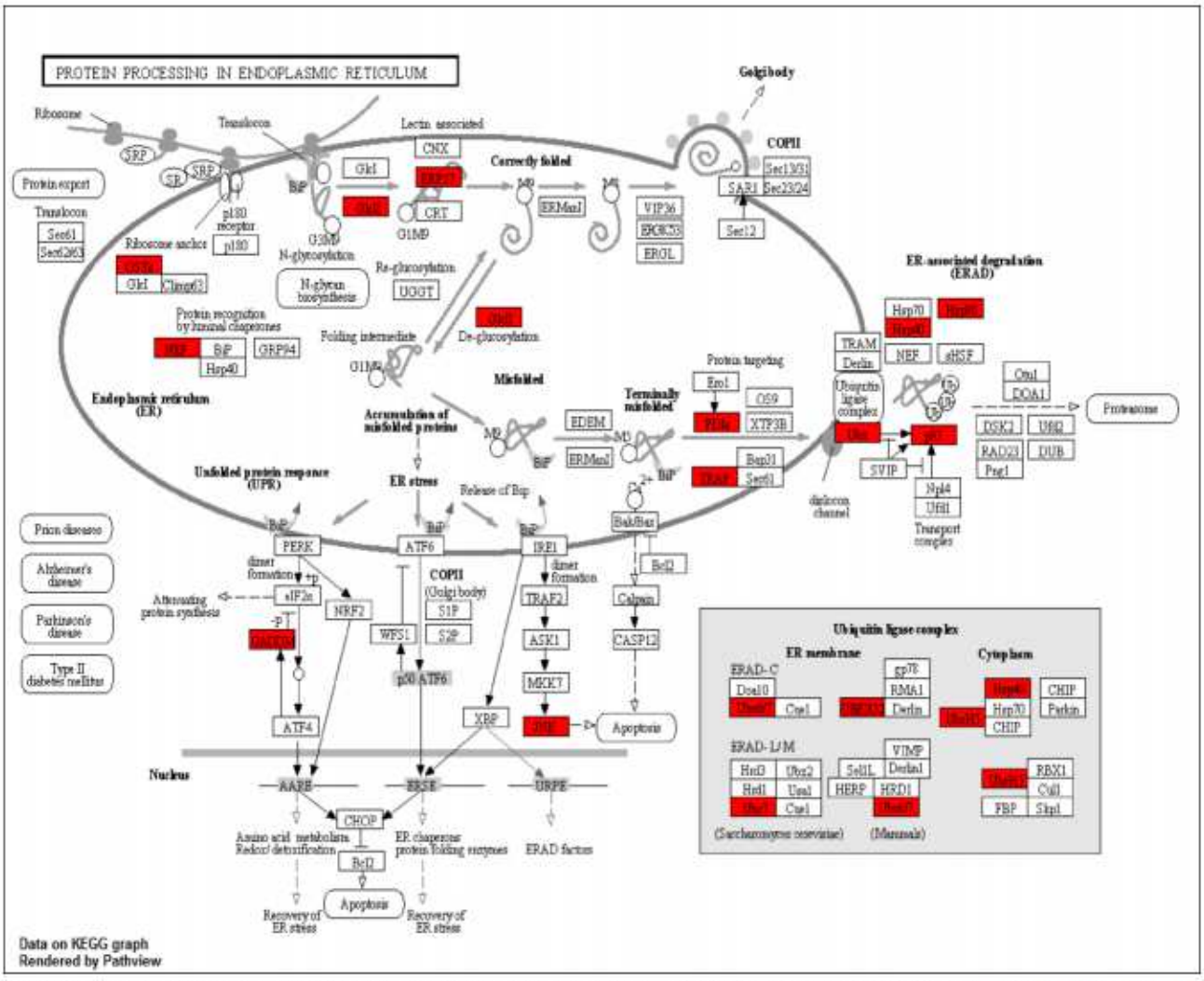

FIGURE 4.8. KEGG Map of Protein Processing in Endoplasmic Reticulum Pathway (hsa04151). The map illustrates the Protein processing in endoplasmic reticulum pathway as reported in KEGG annotation. Red rectangles underline genes of Protein processing in endoplasmic reticulum pathway that are up-regulated in E-CSC compared with D-CSC.

TABLE 4.1. LIST of GENES DOWN-REGULATED IN E-CSC THAT ARE ASSOCIATED WITH ALP.

GENE SYMBOL	ENTREZ GENEID	GENE NAME	CATEGORY§
ATG12	9140	Atg12 Autophagy Related 12 Homolog (S. Cerevisiae)	Autophagy
WDR45L	56270	Wdr45-Like	Autophagy
ARNT	405	Aryl Hydrocarbon Receptor Nuclear Translocator	Autophagy Regulators
B2M	567	Beta-2-Microglobulin	Autophagy Regulators
ITGB4	3691	Integrin, Beta 4	Autophagy Regulators
TGM2	7052	Transglutaminase 2 (C Polypeptide, Protein-Glutamine-Gamma-Glutamyltransferase)	Autophagy Regulators
ADA	100	Adenosine Deaminase	Lysosomal Regulators
FNBP1	23048	Formin Binding Protein 1	Lysosomal Regulators
TMEM9	252839	Transmembrane Protein 9	Lysosomal Regulators
USP5	8078	Ubiquitin Specific Peptidase 5 (Isopeptidase T)	Lysosomal Regulators
WDR48	57599	Wd Repeat Domain 48	Lysosomal Regulators
ASAH1	427	N-Acylsphingosine Amidohydrolase (Acid Ceramidase) 1	Lysosome
CTSA	5476	Cathepsin A	Lysosome
CTSK	1513	Cathepsin K	Lysosome
CTSL1	1514	Cathepsin L1	Lysosome
DPP7	29952	Dipeptidyl-Peptidase 7	Lysosome
WDR41	55255	Wd Repeat Domain 41	Lysosome
DAB2	1601	Dab, Mitogen-Responsive Phosphoprotein, Homolog 2 (Drosophila)	Lysosome
MLC1	23209	Megalencephalic Leukoencephalopathy With Subcortical Cysts 1	Lysosome
GPR137B	7107	G Protein-Coupled Receptor 137b	Lysosome
TCN2	6948	Transcobalamin Ii	Lysosome
CAT	847	Catalase	Lysosome
LUM	4060	Lumican	Lysosome

§ALP related category, as reported in Jegga, A.G., et al., *Systems biology of the autophagy-lysosomal pathway.* Autophagy, 2011. **7**(5): p. 477-489.

TABLE 4.2. LIST of GENES DOWN-REGULATED IN E-CSC THAT ARE DIRECTED TARGET OF TFEB.

GENE SYMBOL	ENTREZ GENEID	GENE NAME
ST3GAL1	6482	ST3 beta-galactoside alpha-2,3-sialyltransferase 1
CTSA	5476	cathepsin A
GPNMB	10457	glycoprotein (transmembrane) nmb
SLC39A1	27173	solute carrier family 39 (zinc transporter), member 1
LZTS2	84445	leucine zipper, putative tumor suppressor 2
CSF1R	1436	colony stimulating factor 1 receptor
GRN	2896	Granulin
EEF1A1	1915	eukaryotic translation elongation factor 1 alpha 1
SHMT1	6470	serine hydroxymethyltransferase 1 (soluble)
ASAH1	427	N-acylsphingosine amidohydrolase (acid ceramidase) 1
SSR3	6747	signal sequence receptor, gamma (translocon-associated protein gamma)
DENND6A	201627	DENN/MADD domain containing 6A
SDF4	51150	stromal cell derived factor 4
STX4	6810	syntaxin 4
ATP6AP1	537	ATPase, H+ transporting, lysosomal accessory protein 1
CAMKK1	84254	calcium/calmodulin-dependent protein kinase kinase 1, alpha
DPP7	29952	dipeptidyl-peptidase 7
CHAF1A	10036	chromatin assembly factor 1, subunit A (p150)
FAF1	11124	Fas (TNFRSF6) associated factor 1
INSIG1	3638	insulin induced gene 1
SLC31A2	1318	solute carrier family 31 (copper transporter), member 2

4.3 MICRORNA EXPRESSION PROFILING

Given the crucial role conducted by microRNAs in regulating cellular pathways, RNA of undifferentiated CSCs (4 E-CSC and 4 D-CSC) at the fourth passage was extracted and probed by Real-Time PCR, in order to define the expression profiles of several microRNAs. Among the 380 microRNAs detectable by the TaqMan Array Human MicroRNA A Cards v2.0, 189 miRNAs were found to be expressed. Among these, hsa-miR-10b-5p and hsa-miR-199b-5p resulted expressed only in D-CSC, while hsa-miR-450b-5p was expressed only in E-CSC, that were also characterized by a down-regulation of other 4 miRs: hsa-miR-146b-5p, hsa-miR-155-5p, hsa-miR-299-5p, hsa-miR-493-3p ($p<0.05$, **Figure 4.8**).

4.3.1 MIRNAS DOWN-REGULATED IN E-CSC TARGETS CELL SENESCENCE AND MTOR PATHWAY GENES

Once identified the differently expressed microRNAs, the research of their target genes was performed by a bioinformatics analysis. In order to obtain only reliable results, the study was focused on Tarbase database so that only the experimentally validated miRNA targets were considered. Because of the stringent criteria applied, no genes were found target of hsa-miR450b-5p or hsa-miR-493-3p, while 987 genes resulted targets of the other five miRs over-expressed in D-CSC.

These genes were subjected of enrichment test on KEGG, Reactome and Disease Ontology databases, and were found to be associated with 32 pathways annotated in KEGG, 47 pathways annotated in Reactome and 7 pathways annotated in Disease Ontology (p.adjust<0.05, Supplementary **Table S11**, **S12**, **S13**). Most of these pathways are keys signaling pathway directly or indirectly connected with cell senescence, such as "cell senescence", "oncogene induced cell senescence" "insulin signaling pathway", "wnt signaling pathway", "p53 signaling pathway", "apoptosis" and others (**Figure 4.9**). Noteworthy the enrichment test on KEGG pathways revealed the specific involvement of "mTOR signaling pathways" (**Figure 4.10**).

Altogether these results suggested that CSCs isolated by donors actively perform post-transcriptional regulation to control mTOR pathway and other key senescence pathway by the expression of a set of microRNAs that are down-regulated in CSCs obtained from explanted hearts.

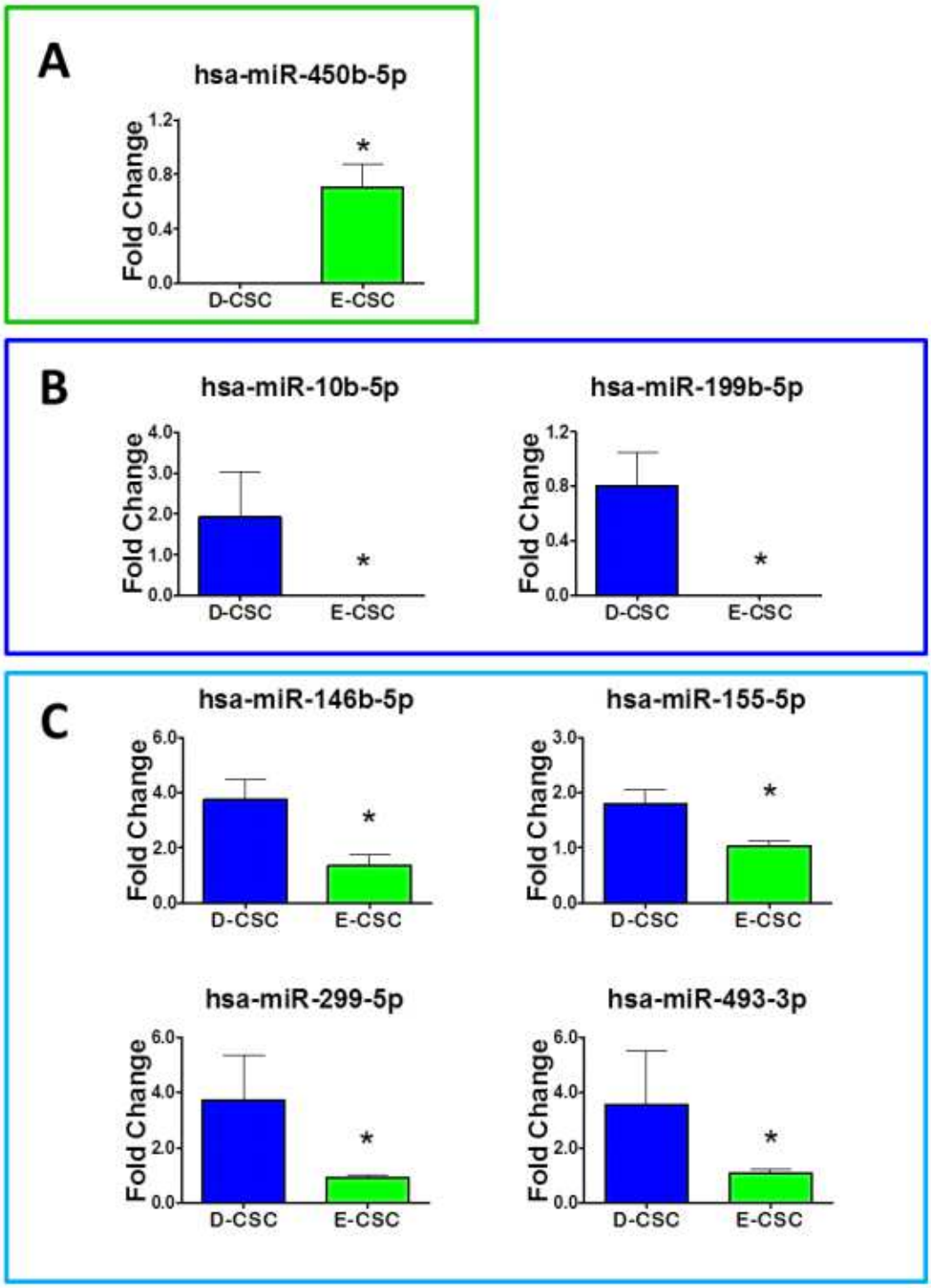

FIGURE 4.8. MicroRNAs Profiling Results. The histograms (**A**, **B**, **C**) show the expression levels of microRNAs that resulted differently regulated in E-CSC compared to D-CSC. Specifically the bar graphs report the expression levels of: miRNA found to be present only in E-CSC (**A**), or in D-CSC (**B**); miRNA over-expressed in CSC isolated from donor hearts (**C**). All Values are means±SEM. * $p<0.05$ vs D-CSC.

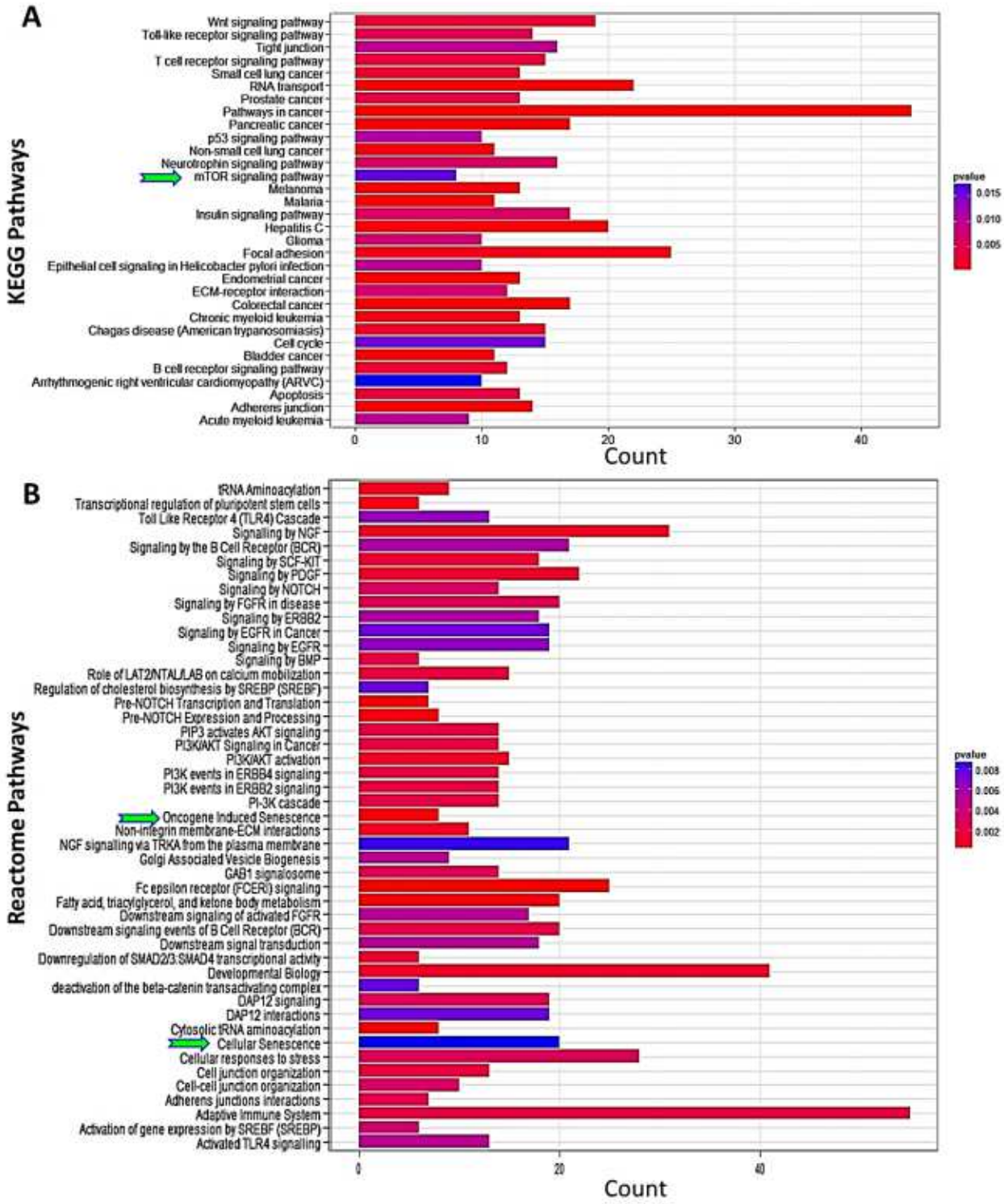

FIGURE 4.9. Pathways Enriched in Validated Gene Targets of D-CSC Up-Regulated microRNAs. Barplots graphically represent the results of enrichment tests for KEGG (**A**) and Reactome (**B**) pathways calculated on the lists of genes that are targeted by the microRNAs over-expressed in D-CSC. Bar length is proportionally to the count of gene targets associated with the specific pathways reported on the left. As reported by legends on the left, the bar colors depend on the p.value that characterize the match between the genes of interest and the pathways. Green arrows point out relevant pathways for the present study.

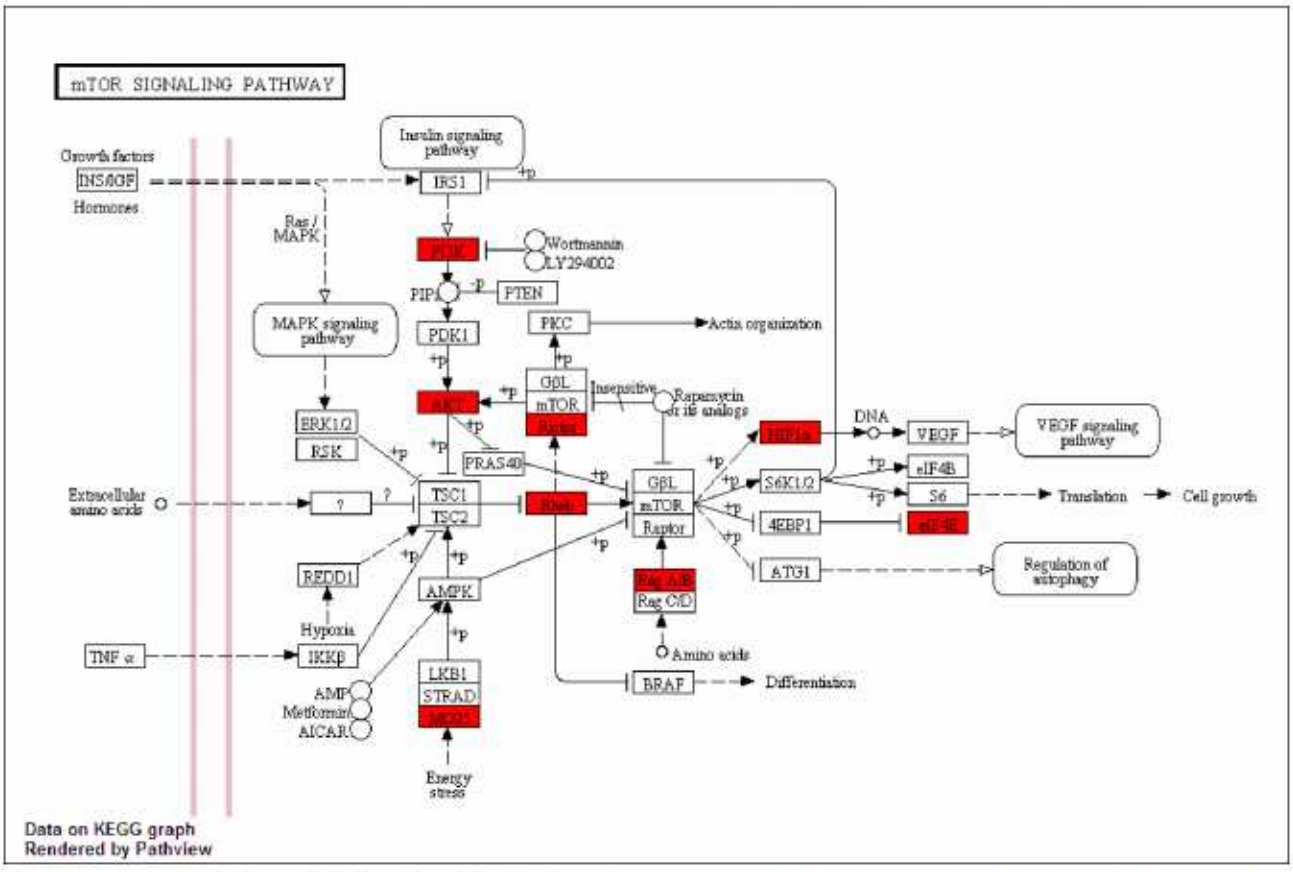

FIGURE 4.10. KEGG Map of mTOR Signaling Pathway (hsa04150). The map illustrates the mTOR signaling pathway as reported in KEGG annotation. Red rectangles underline mTOR signaling pathway related genes that are validated targets of microRNAs up-regulated in D-CSC compared with E-CSC.

4.4 FUNCTIONALITY OF E-CSC LYSOSOMAL COMPARTMENT WAS JEOPARDIZED

Once identified the differences in transcriptional and post-transcriptional regulation of genes ALP and Senescence associated, the study moved to the evaluation of functionality of lysosomes. For this purpose, FACS analysis was performed, after staining undifferentiated E- and D-CSC (N=5 each), at the forth passage, with Acridine Orange (AO). This latter is a metachromatic dye that precipitates within acid lysosomes exhibiting a red fluorescence (maximum emission at 640nm) that shifts towards green (maximum emission at 535nm) when intralysosomal pH is increased [121]. FACS analysis reported that Red Fluorescence of stained E-CSC is more than three-fold less intense than the D-CSC one, sign of a less functional lysosomal compartment (**Figure 4.11**).

Undifferentiated CSCs were stained with LysoTracker Red DND-99 to exclude that different intensity of red fluorescence is due to a more extensive lysosome equipment. FACS analysis didn't underline significant differences in terms of size of lysosomal compartment (**Figure 4.12**).

The reasons of less functional lysosomes were studied in depth evaluating the presence both of intralysosomal material, connected with aging and known as lipofuscin, and of Galectin 3, a recently established marker of damaged endomembranes [122]. Quantification of Integrated Fluorescence Intensity (IFI) showed that the E-CSC lysosomes, compared to those of D-CSC, are characterized by higher levels of lipofuscin and Galectin 3 (**Figure 4.13**).

Since eukaryotic cells rely on the master ALP regulator Transcription Factor EB to promote the clearance of lysosomes [61], the activation status of TFEB was appraised. Immunofluorescence confocal analysis demonstrated that the amount of nuclear activated TFEB is significantly higher in D-CSC with respect to E-CSC (**Figure 4.14**).

Altogether these results suggest that CSCs isolated from failing explanted hearts are characterized by a compromised lysosomal compartment and, as a consequence, by reduced digestive potential.

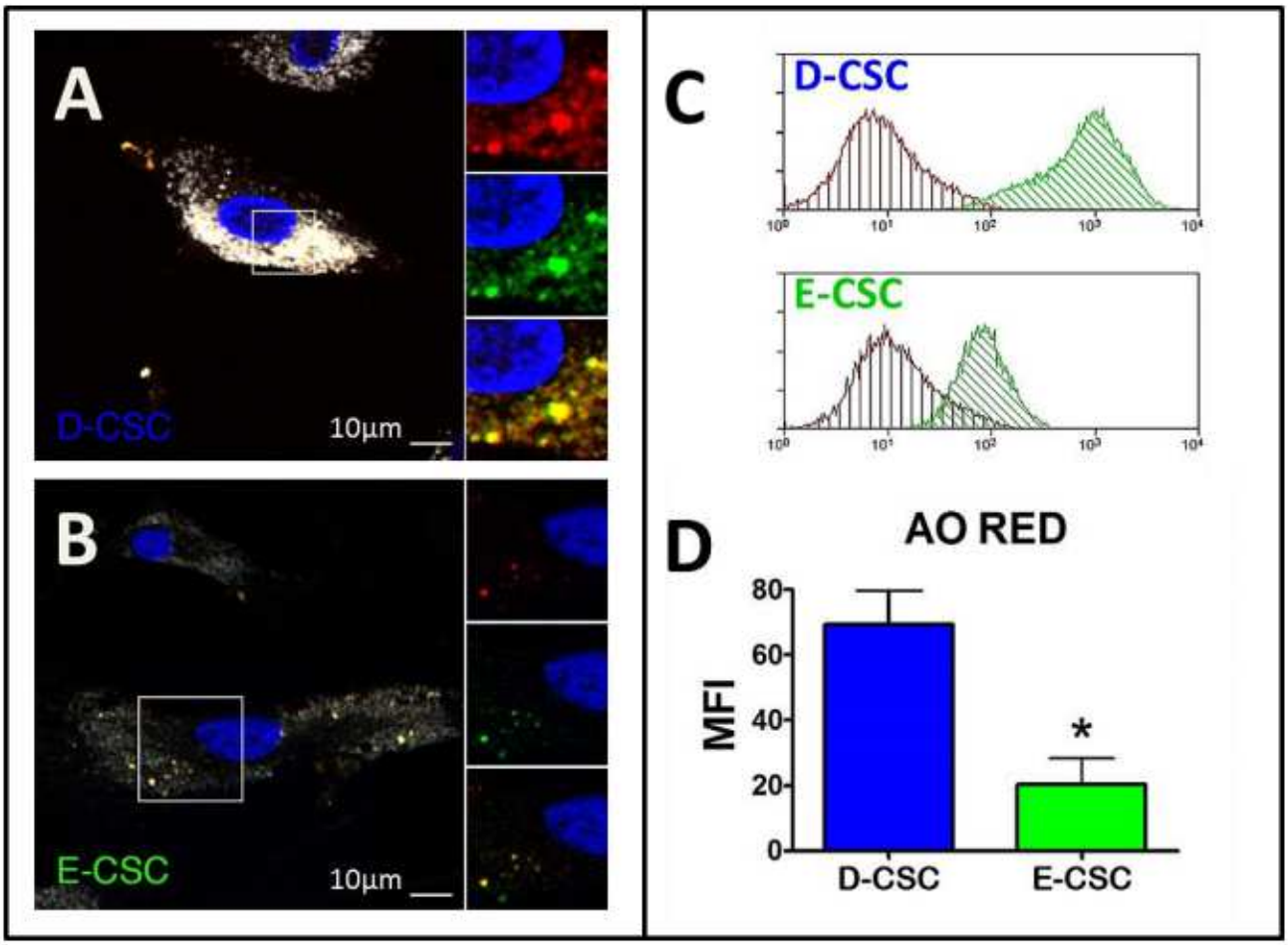

FIGURE 4.11. Lysosomal Functionality Assay in CSCs. Illustrative confocal images of cultured D-CSC (**A**) and E-CSC (**B**) stained with Acridine Orange (red and green) and LAMP2 (grey). Nuclei are shown by the blue fluorescence of DAPI. Split channel images of the cells comprised in the squares are shown at a higher magnification in the right portion of each figure. **C**: representative Flow-Cytometry histograms of cultured D- and E-CSC analyzed after incubation with Acridine Orange. The red florescence emission of stained cells is reported by green histograms that are superimposed with control profiles of unstained cells (red histograms). Bar graph in **D** summarizes quantitative Flow-Cytometry result that is expressed as Mean Fluorescence Intensity (MFI) of red emission from cells stained with Acridine Orange (AO). All Values are means±SEM. * $p<0.05$ vs D-CSC.

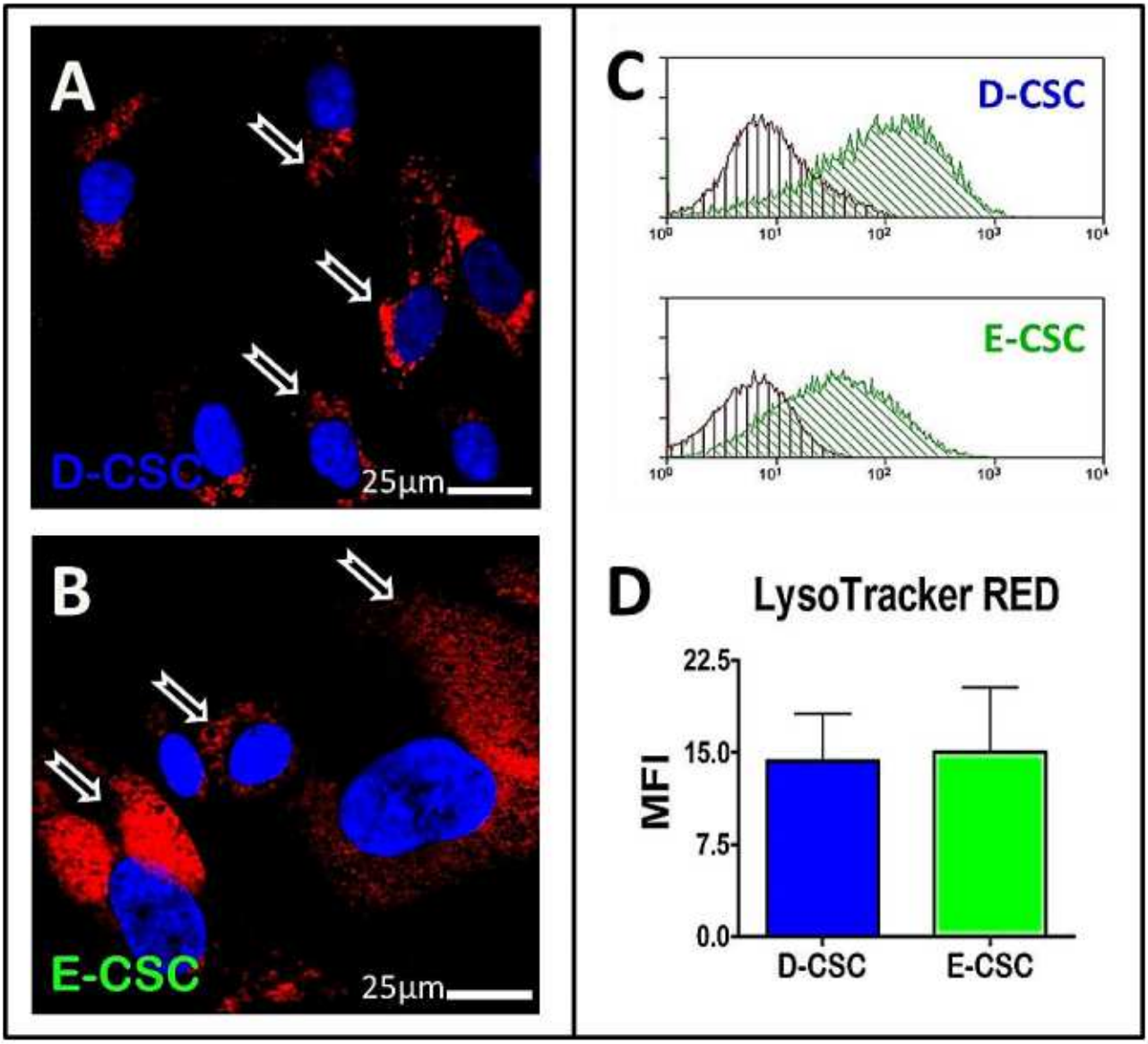

FIGURE 4.12. Evaluation of Lysosomal Compartment Size in CSCs. Representative confocal images of D-CSC (**A**) and E-CSC (**B**) lysosomes, stained with LysoTracker Red DND-99 (red) and pointed out by explicative arrows. Nuclei are shown by the blue fluorescence of DAPI. **C**: representative Flow-Cytometry histograms of cultured D- and E-CSC analyzed after incubation with LysoTracker Red DND-99. The red florescence emission of stained cells is reported by green histograms that are superimposed with control profiles of unstained cells (red histograms). Bar graph in **D** summarizes quantitative Flow-Cytometry result that is expressed as Mean Fluorescence Intensity (MFI) of red emission from cells stained with LysoTracker Red DND-99. All Values are means±SEM. * $p<0.05$ vs D-CSC.

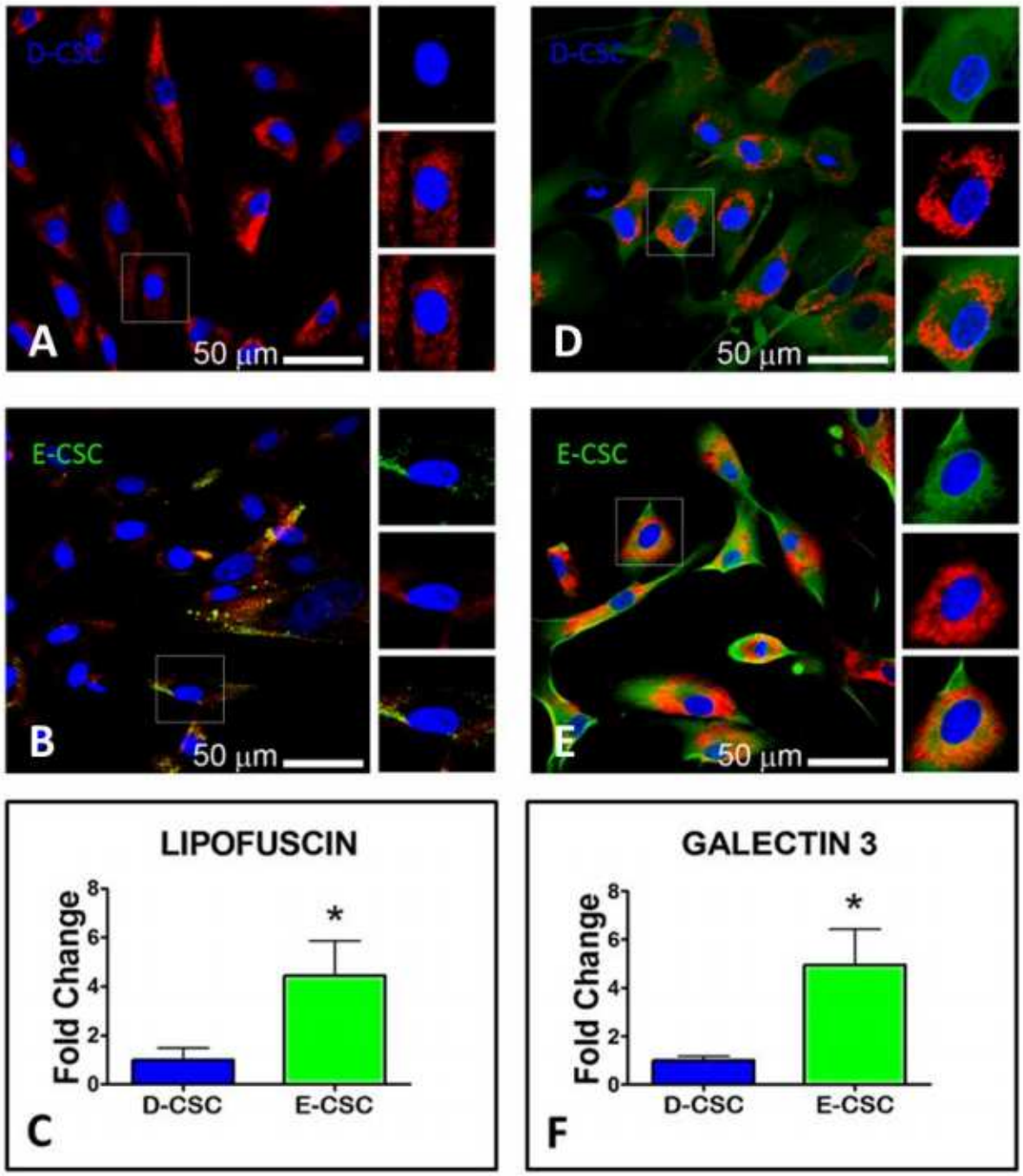

FIGURE 4.13. Lisosomal Level of Lipofuscin and Galectin 3 in CSCs. Representative confocal images of cultured D-CSC (**A**, **D**) and E-CSC (**B**, **E**) illustrating colocalization of lysosomes (marked by LAMP-2, red) with autofluorescent lipofuscin (**A**, **B**), or with Galectin 3 (**D**, **E**) . Nuclei are shown by the blue fluorescence of DAPI. Split channel images of the cells comprised in the squares are shown at a higher magnification in the right portion of each figure.. Histograms (**C**, **F**) summarize results of the quantification of the lipofuscin (**C**) or Galectin 3 (**F**) Integrated Fluorescence Intensity for lysosomal compartment. All Values are means±SEM. * $p<0.05$ vs D-CSC.

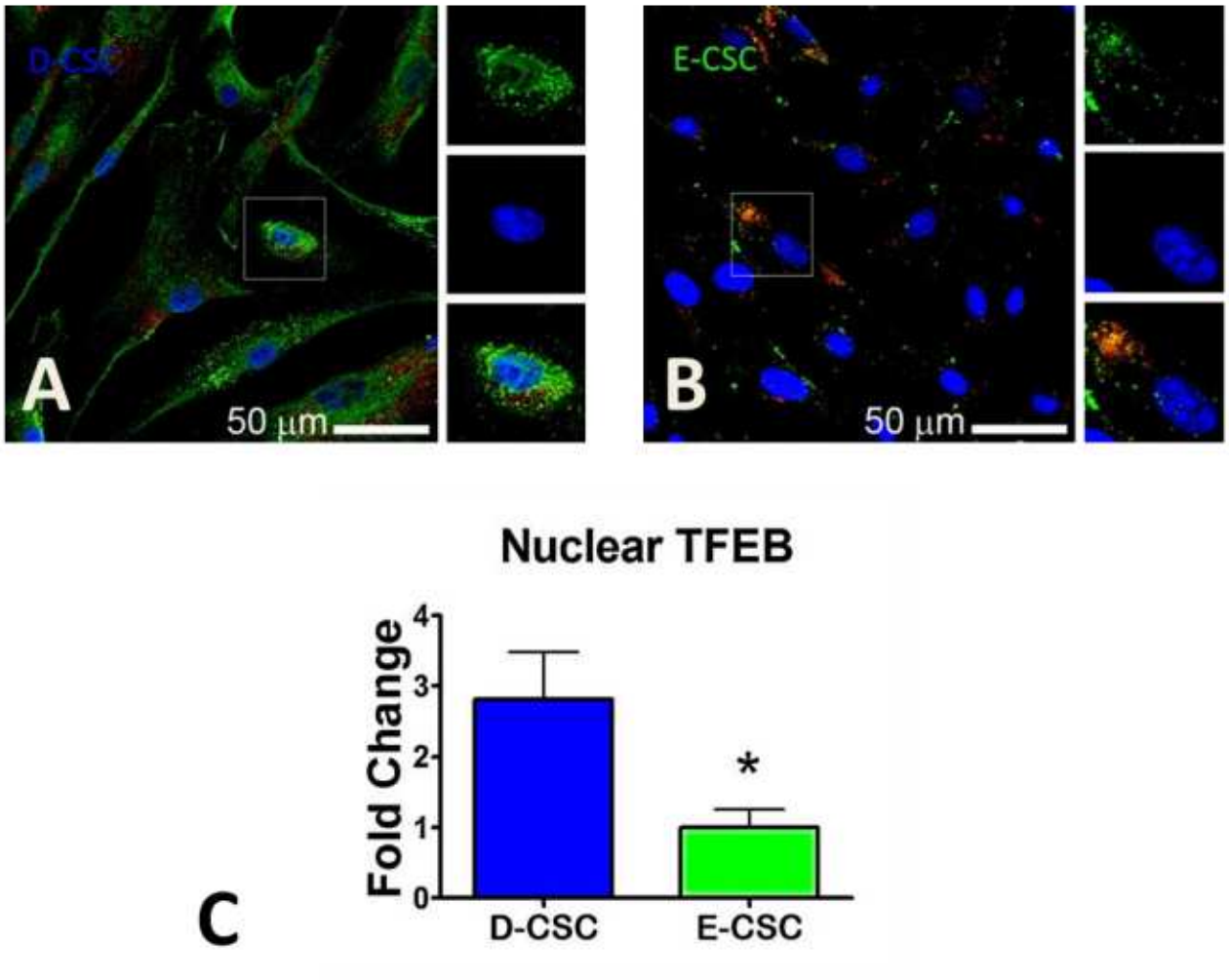

FIGURE 4.14. Evaluation of Active Nuclear TFEB on CSCs. Representative confocal images of cultured D-CSC (**A**), and E-CSC (**B**), after immunostaining with antibody against TFEB (green), and LAMP-2 (red). Nuclei are shown by the blue fluorescence of DAPI. Split channel images of the cells comprised in the squares are shown at a higher magnification in the right portion of each figure. Histogram (**C**) reports the result of the quantification of the TFEB Integrated Fluorescence Intensity for nuclear compartment. All Values are means±SEM. * $p<0.05$ vs D-CSC.

4.5 mTORC1 Constitutive Activation in E-CSC Impairs the Autophagic Machinery

Given the link between cell senescence and mTOR [123, 124] and the pivotal role played by the latter, in regulating autophagy, mTOR signaling pathway was assayed. Western Blot results, although not highlighting differences in the levels of total mTOR between the two group of cells (data not shown), reported a constitutive activation of mTORC1 complex in E-CSC as supported by higher phosphorylation on Thr^{389} of mTORC1 downstream effector S6K (**Figure 4.15 A**), coupled with decreased Ser^{473} phosphorylation of Akt (**Figure 4.15 B**), known to be negatively regulated by mTORC1 [125].

As a consequence of these results the study moved to the evaluation of autophagic marker levels. The LC3 conjugation system proteins LC3BII, Atg3, Atg7 resulted less expressed in D-CSC compared with E-CSC that also showed higher levels of p62/SQSTM1 (**Figure 4.16**). This latter is a receptor for cargo destined to be degraded by autophagy and its expression inversely correlates with autophagic activity [126].

All these results advised that autophagic flux of E-CSC is hindered by a marked activation of mTORC1 complex.

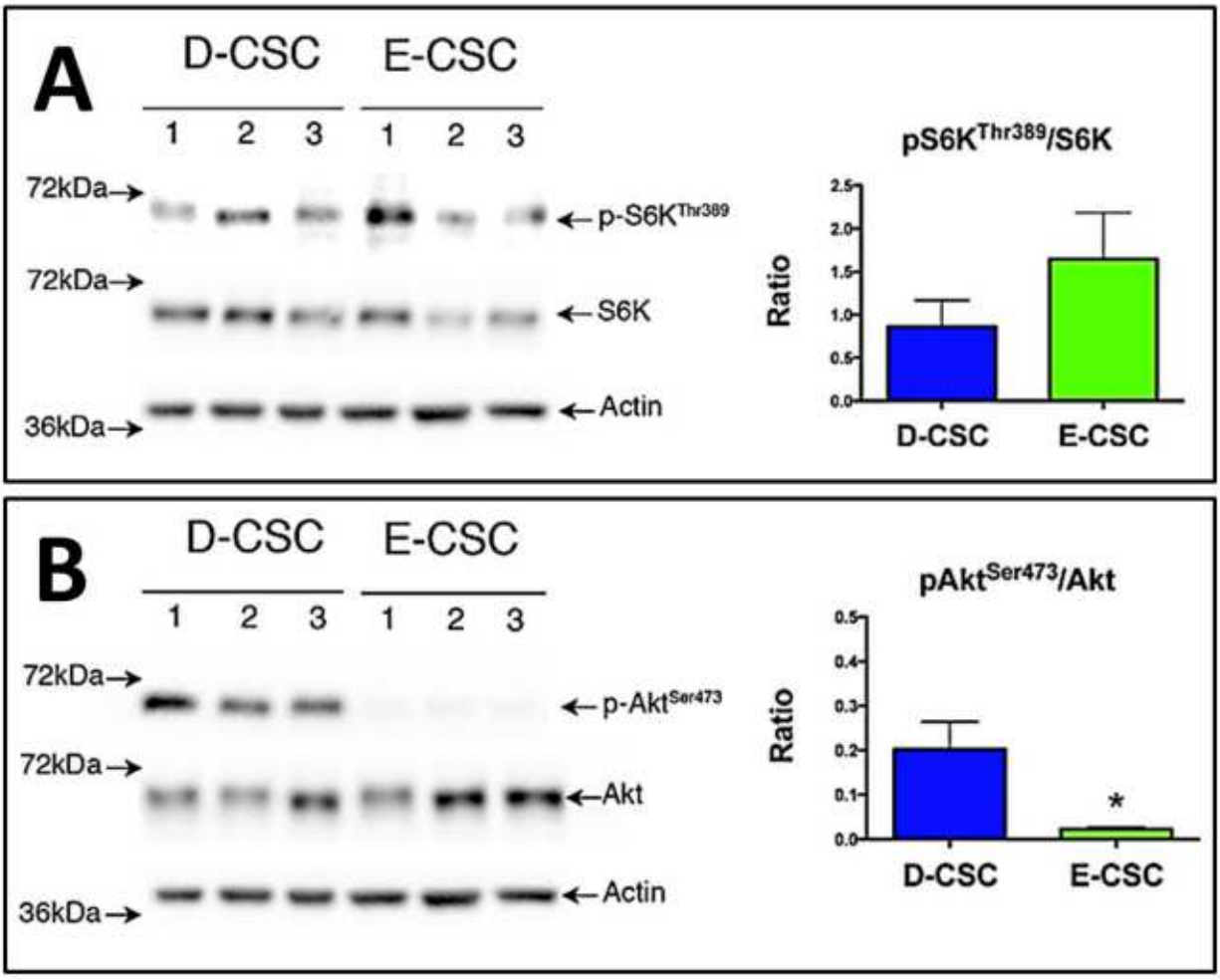

FIGURE 4.15. mTOR Signaling Pathway Evaluation on CSCs. In the left, representative Western Blots of cell extracts obtained from 3 D-CSC and 3 E-CSC. Blotted proteins were incubated with antibodies directed against S6K, phospho-S6KThr^{389} (**A**), Akt, phospho-AktSer^{473} (**B**), and Actin. Histograms in the right show the respective results of the densitometric analyses normalized versus Actin. * $p<0.05$ vs D-CSC.

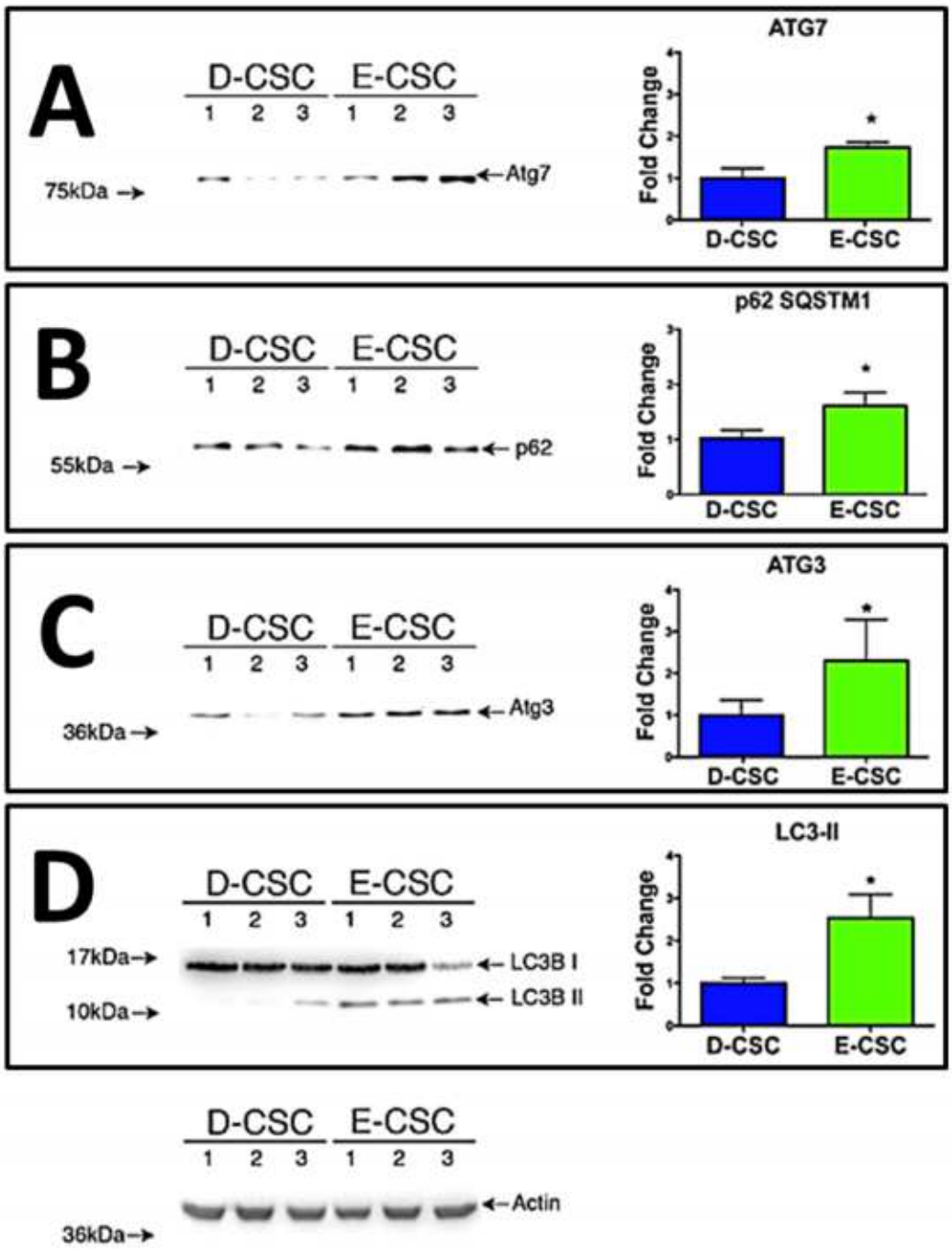

FIGURE 4.16. Autophagic Markers Evaluation on CSCs. In the left, representative Western Blots of cell extracts obtained from 3 D-CSC and 3 E-CSC. Blotted proteins were incubated with antibodies directed against Atg7 (**A**), p62/SQSTM1 (**B**), Atg3 (**C**), LC3B (**D**) and Actin. Histograms in the right show the respective results of the densitometric analyses normalized versus Actin. * $p<0.05$ vs D-CSC.

4.6 FINE TUNING OF PHARMACOLOGIC TREATMENT

Moving from the results that CSCs isolated from end-stage failing hearts are senescent and characterized by an impaired ALP coupled with a constitutive activation of mTORC1 complex, the next goal was to develop a pharmacologic strategy designed to revert senescence by targeting the dysfunction of ALP. Given its faculty to interfere with mTOR signaling pathway, Rapamycin was the drug of choice.

4.6.1 RAPAMYCIN TITRATION STUDY

A pilot titration study was performed to evaluate the safety, tolerability, and acute effects of four ascending concentrations 1nM, 10nM, 100nM and 1μM of Rapamycin in order to identify the suitable dose. Specifically growing undifferentiated E-CSC were cultured for three days in the presence of these increasing drug doses and were analyzed immediately thereafter to establish the effects of each concentration on apoptosis, necrosis and senescence.

After staining with Annexin V-FITC Apoptosis Detection Kit (eBioscience), FACS analysis showed that fraction of apoptotic cells (Annexin V positive cells) tended to increase depending on Rapamycin concentration (**Figure 4.17 A**), differently from the fraction of necrotic cells (Propidium Iodide positive cells, **Figure 4.17 B**).

Immunofluorescence microscope revealed that: proliferation, testified by Ki67 expression, didn't result substantially affected by the drug (**Figure 4.17 C**); the expression of nuclear $p16^{INK4A}$ was reduced by 10nM- and 100nM-Rapamycin treatments but it was increased by 1μM treatment (**Figure 4.17 D**). This latter dose of Rapamycin was also the only one increasing the fraction of cells with DDR (γ-H2A.X positive, Ki67 negative cells) that otherwise was not influenced by lower drug dosage.

Based on these results, the present study was focused on 10nM Rapamycin dose that reduce the fraction of senescent E-CSC and is below the threshold of cytotoxicity.

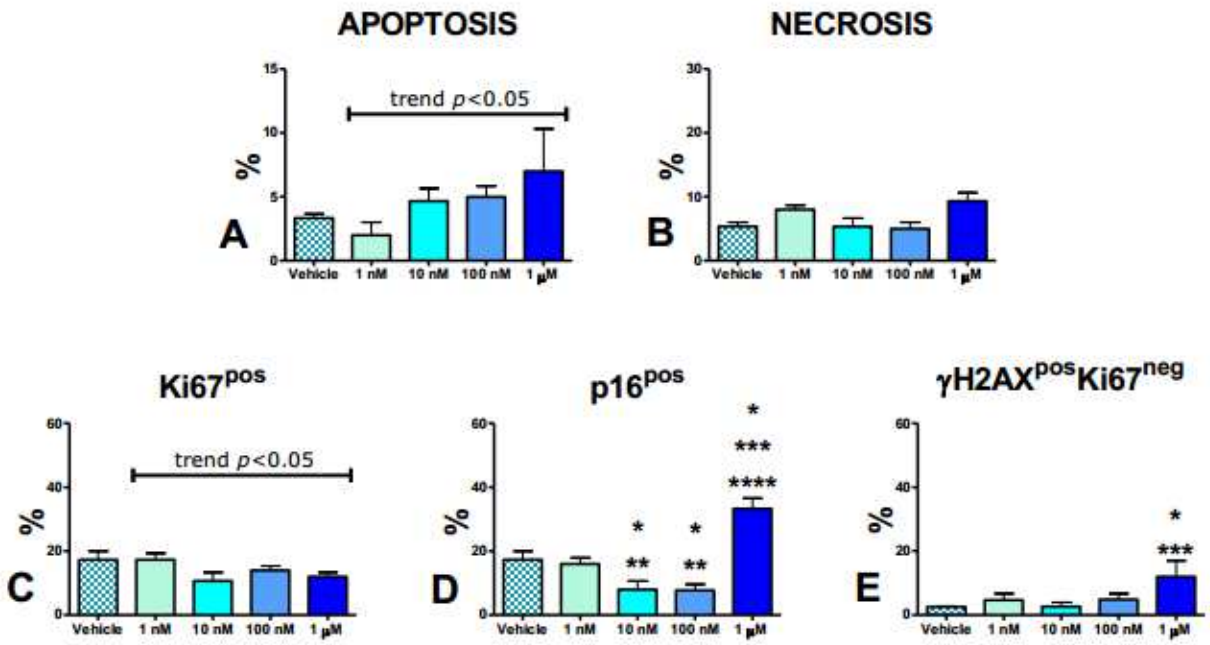

FIGURE 4.17. Pilot Titration Study. E-CSC were exposed for three days to 1nM, 10nM, 100nM and 1μM Rapamyicin. Histograms (**A**, **B**, **C**, **D**, **E**) represent the fraction (%) of apoptotic (annexin V positive, **A**), necrotic cells (propidium iodide positive, **B**), cycling cells (Ki67 positive, **C**), senescent cells (p16 positive, **D**) and DDR positive cells (γ-H2A.X positive Ki67negative, **E**). Results are presented as mean and SEM. *, **, ***, ****, p<0.05 vs Rapamycin's vehicle, 1nM-, 10nM-, 100nM-Rapamycin.

4.7 RAPAMYCIN CONTRASTS SENESCENCE IN E-CSC

Once identified the suitable dosage (see **par. 4.6**), undifferentiated CSCs, at the fourth passage, were cultured in a medium added with 10nM Rapamycin for three days. As a control, cells were treated with the vehicle alone (DMSO). Vehicle-treated and drug-treated cells (**Figure 4.18**) were then subjected to a 24 hours release period with drug-free medium and subsequently properly studied for immunophenotype, senescence markers, and functional properties.

4.7.1 RAPAMYCIN DOES NOT MODIFY THE CELL SURFACE IMMUNOPHENOTYPE

With the aim to demonstrate that pharmacologic treatment did not alter the mesenchymal immunophenotype, treated E- and D-CSC were analyzed as seen above (see **par. 4.1.1**).

FACS analysis of drug-treated D- and E-CSC showed that cell immunophenotype was not significantly modified by the drugs (**Figure 4.19**). The only exception regards the expression of the cardiac aging and disease associated CD49a/α1 integrin, which was significantly reduced in treated E-CSC (**Figure 4.19 A**).

4.7.2 FUNCTIONAL PROPERTIES ARE NOT ALTERED BY RAPAMYCIN

Given that Rapamycin mainly acts inhibiting mTOR signaling pathway, thus inhibiting cell growth, the proliferative capability of treated CSCs were judged. Growth Kinetics demonstrated that CPDT didn't differ between drug and Vehicle-treated cells (**Figure 4.20 A**). These results were confirmed by nuclear expression of Ki67 (Figure **4.20 B**).

Moreover treated E-CSC were evaluated for their differentiation and migration properties. α-sarcomeric actin was utilized as myogenic markers, while CD31 as endothelial marker. Applying the score that considers both the expression of α-sarcomeric actin and the level of filament organization, Rapamycin did not interfere with the myogenic differentiation ability (**Figure 4.21 A**). Differently the same drug was able to improve the capacity of E-CSC to differentiate into endothelial cells (CD31 positive cells, **Figure 4.21 B**). Finally, scratch assays didn't report substantial differences between the motility of treated and untreated cells (**Figure 4.21 C, D**).

4.7.3 RAPAMYCIN REDUCED P16^{INK4A} POSITIVE CELLS

The efficacy of pharmacologic strategy on reducing senescence was assayed by its ability to reduce the senescence markers in E-CSC. Results showed that Rapamycin was effective in decreasing the expression of p16^{INK4A} (**Figure 4.22 A**). No changes in the fraction of cells with DNA-damage foci were observed (**Figure 4.22 B**), while a slight increase in the fraction of apoptotic E-CSC was reported (**Figure 4.22 C**).

Interestingly, the treatment of D-CSC with the drug (**Figure 4.22 D, E**) did not exert any effect.

These results together with results of **par. 4.7.1** and **par.4.7.2** demonstrated that three days treatment with 10nM Rapamycin is able to contrast senescence of E-CSC without prejudice their functional ability.

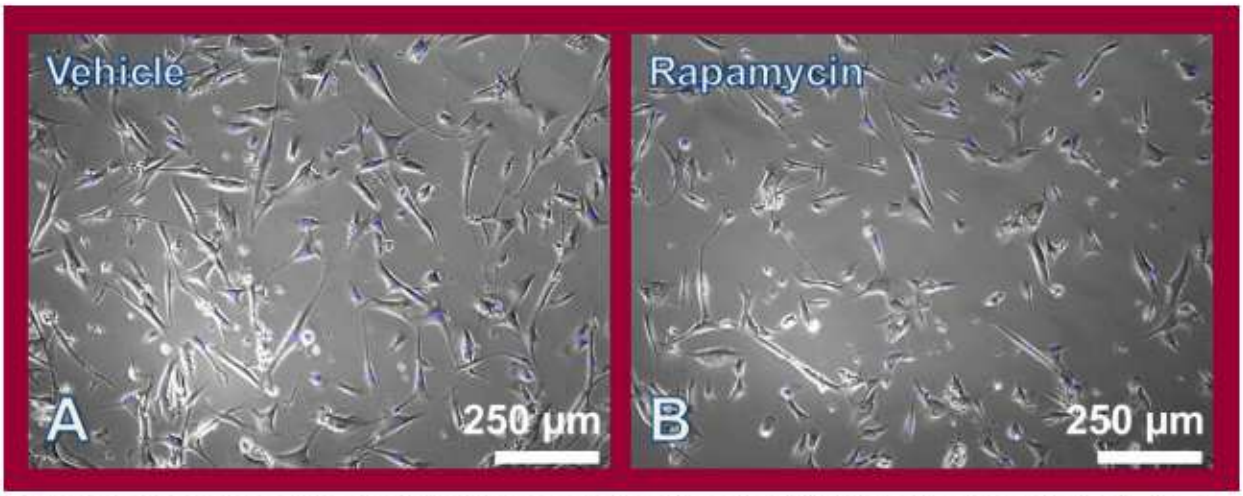

FIGURE 4.18. Phase Contrast Representative Pictures of CSCs Treated with Vehicle (A) or Rapamycin (B). Nuclei are illustrated in blue.

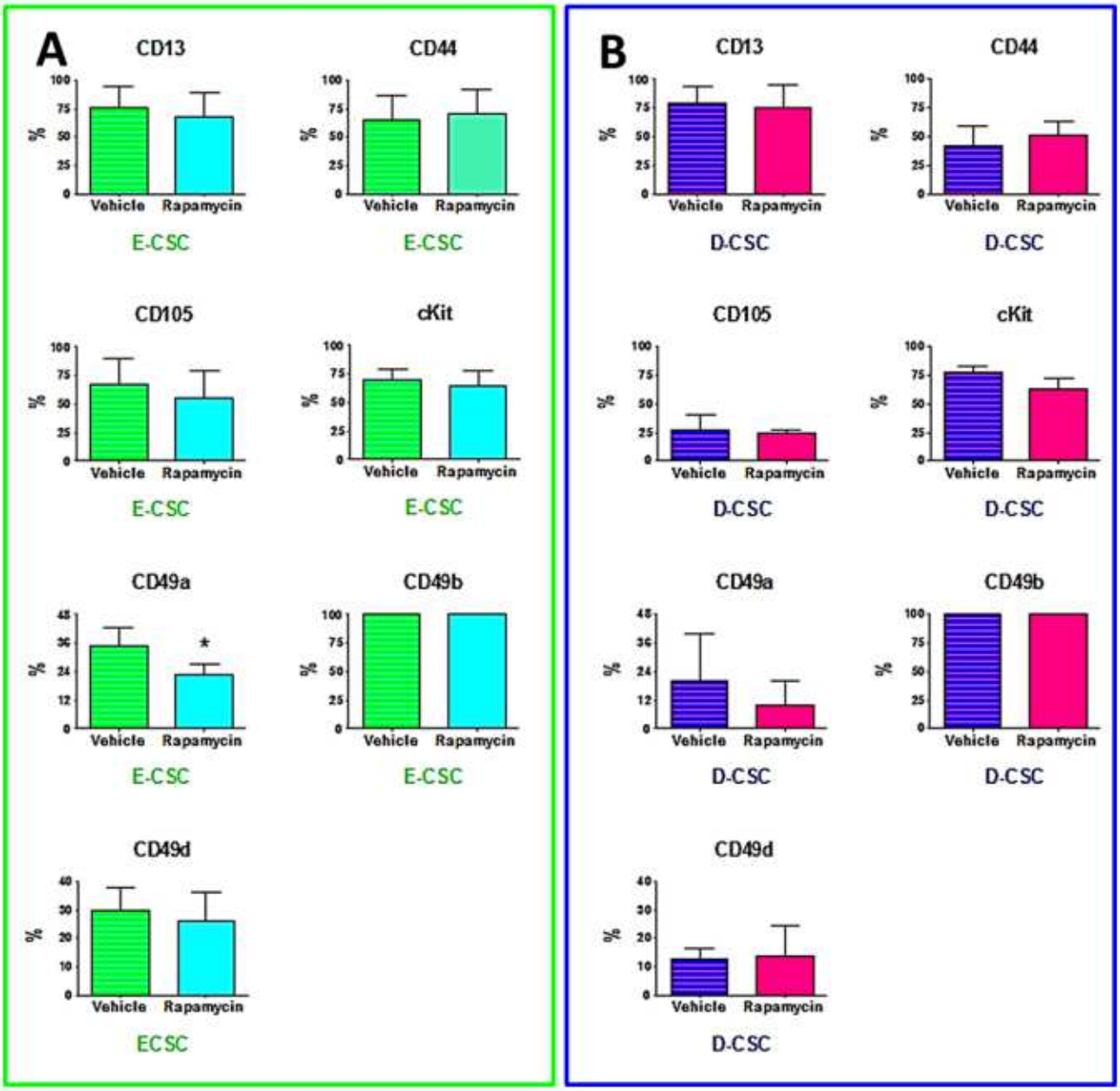

FIGURE 4.19. Effects of 10nM Rapamycin Treatment on Cell Surface Immunophenotype. Histograms (**A**, **B**) summarize quantitative Flow-Cytometry data, that are expressed as frequency (%) of Vehicle and Rapamycin treated CSCs expressing the indicated antigen. Specifically, panel on the left (**A**) shows results of E-CSC treatment, while panel on the right displays results of D-CSC treatment. Values are means±SEM. * $p<0.05$ vs Vehicle-treated CSCs.

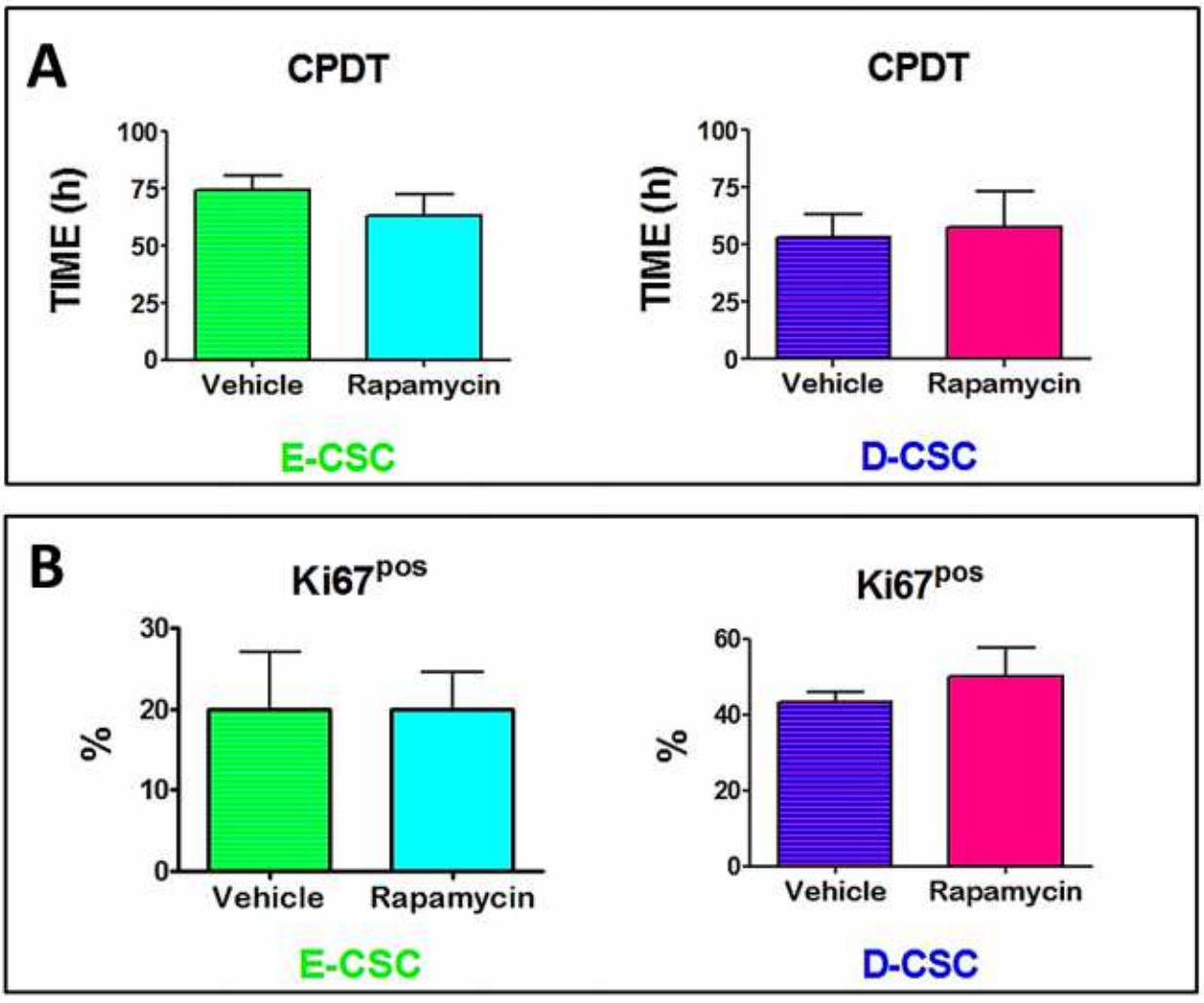

FIGURE 4.20. Effects of Rapamycin Treatment on Cellular Growth. A: histograms summarize cell population doubling time (CPDT) of Vehicle- and drug-treated E-CSC (left) or D-CSC (right). **B**: graph bars represent the effects of Rapamycin treatment on the fraction (%) of cycling (Ki67 positive) E-CSC (left) or D-CSC (right). All the values showed by histograms (**A**, **B**) are means±SEM. * $p<0.05$ vs Vehicle-treated CSCs.

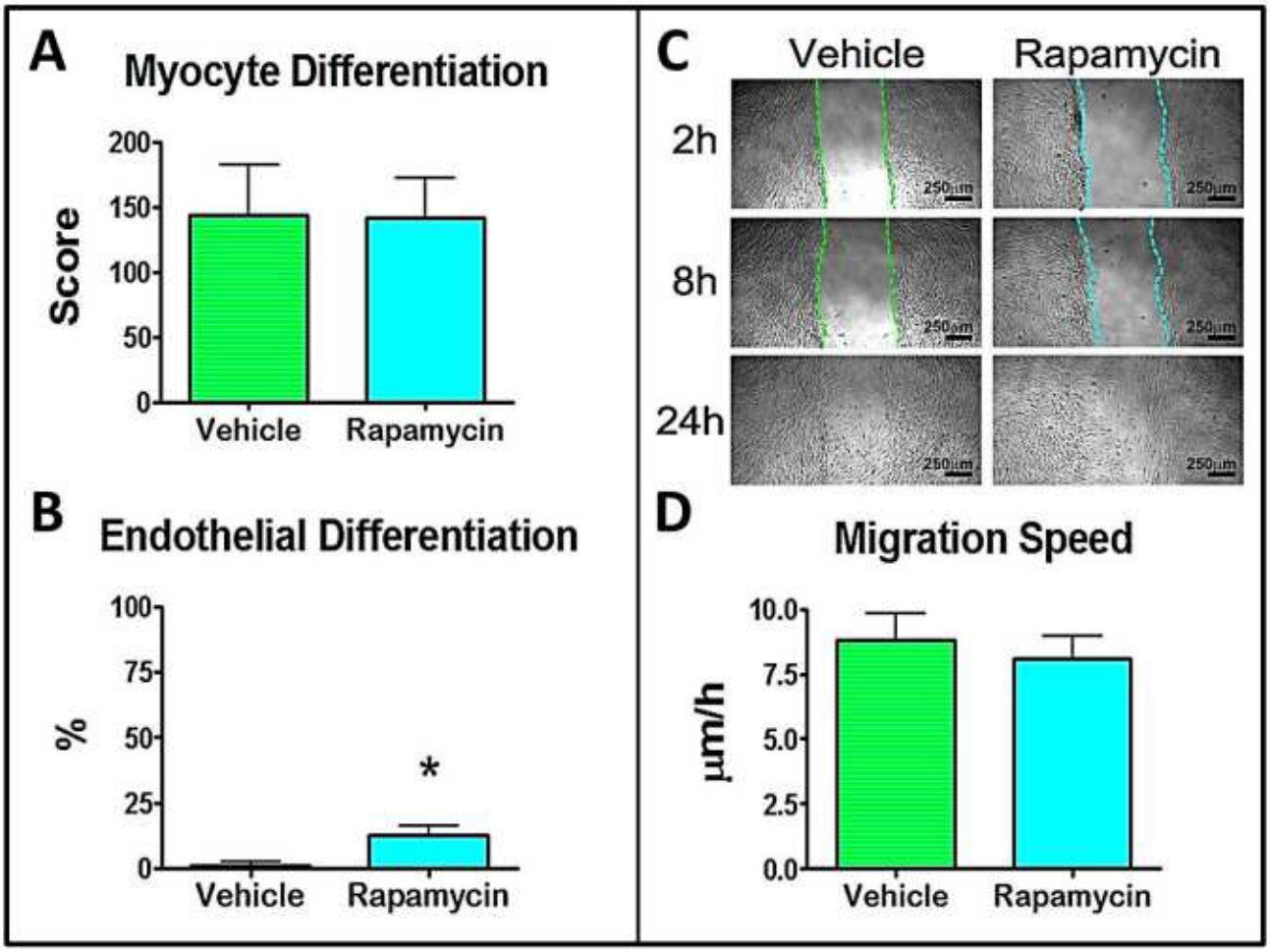

FIGURE 4.21. Effects of Rapamycin Treatment on E-CSC Differentiation and Cell Motility. **A**. **B**: histograms show results of myocyte and endothelial differentiation of E-CSC treated with Rapamycin or Vehicle. Specifically, **A**: result of quantitative scoring of myocyte differentiation (see **par. 3.6.2**); **B**: result of quantitative analysis of the fraction (%) of CD31 positive cells. **C**: representative phase contrast images of scratch assay performed to evaluate cell motility of drug- or Vehicle-treated CSCs. The dotted lines illustrate the margins of the scratches on Vehicle- (green) or drug- (light blue) treated E-CSC (see **par. 3.4** for details). **D**: histograms summarize E-CSC migration speed. Values are means±SEM. * $p<0.05$ vs Vehicle-treated CSCs.

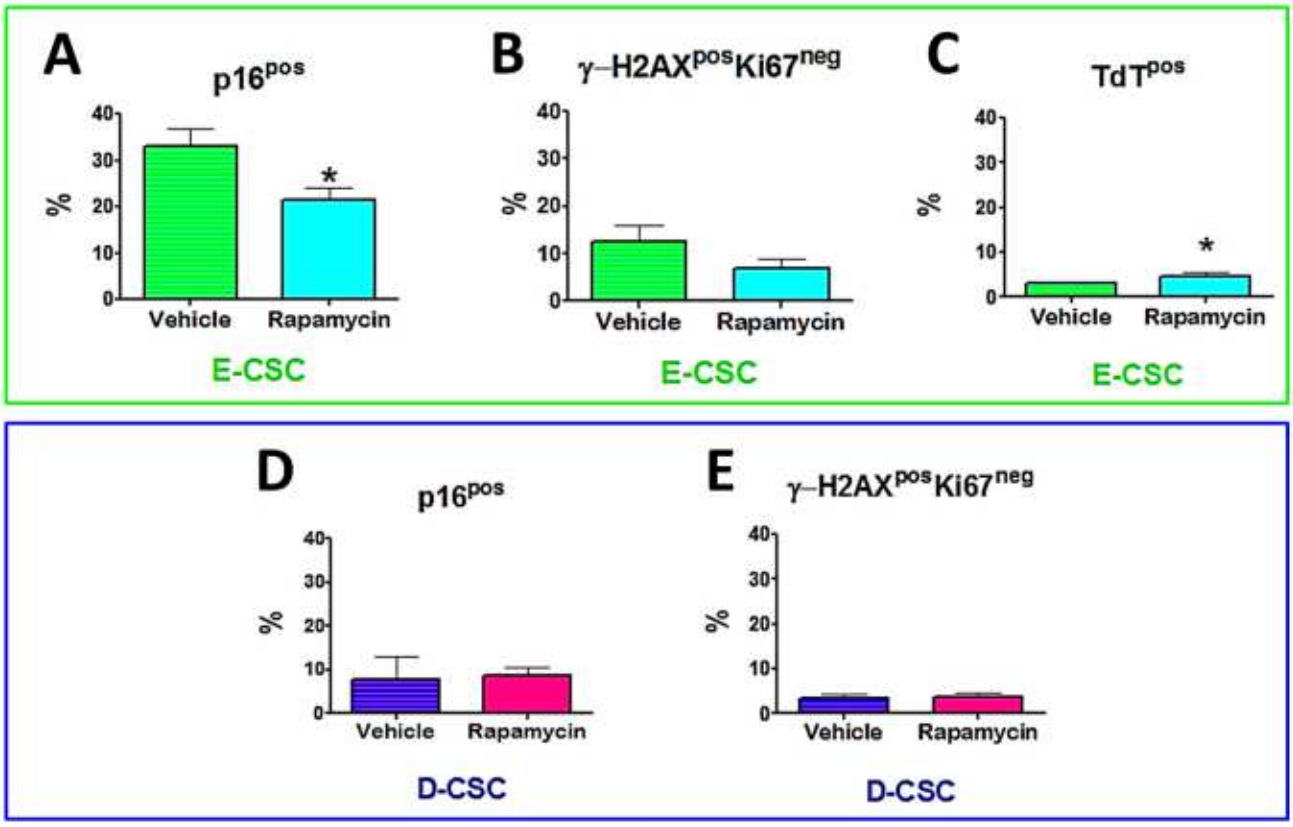

FIGURE 4.22. Effects of Rapamycin Treatment on CSCs. Histograms summarize the effects of Vehicle or Rapamycin on E-CSC senescence (**A**, **B**) and apoptosis (**C**) or on D-CSC senescence (**D**, **E**). Data are reported as fraction (%) of cells expressing the indicated marker. Values are means±SEM. * $p<0.05$ vs Vehicle-treated CSCs.

4.8 RAPAMYCIN RESTORES THE FUNCTION OF E-CSC'S LYSOSOMAL COMPARTMENT

As the second principal aims of the present study, the effect of the pharmacological conditioning on the function of lysosomes was investigated.

FACS analysis demonstrated that Rapamycin was able to potentiate the functionality of the lysosomal compartment, as suggested by the significant increase in red fluorescence of treated E-CSC stained with Acridine Orange (**Figure 4.23 A**). Unexpectedly, after LysoTracker Red DND-99 staining, the extension of lysosomal equipment of preconditioned E-CSC, compared to that of Vehicle-treated cells, resulted reduced, although not significantly (**Figure 4.23 B**).

Data obtained from confocal images demonstrated that the one dose therapy was able to downsize the mass of lipofuscin (**Figure 4. 24 A**), without affecting the amount of lysosomal Galectin 3 (**Figure 4. 24 B**).

Moreover, quantitative measurement of nuclear Trascription Factor EB proved that the active form of TFEB was significantly higher in drug-treated E-CSC compared to Vehicle-treated ones (**Figure 4.24 C**).

Altogether these results suggested that the conditioning of E-CSC for three days with 10nM Rapamycin is effective in reverting their dysfunctional lysosomal compartment, thereby ameliorating their degradative potential.

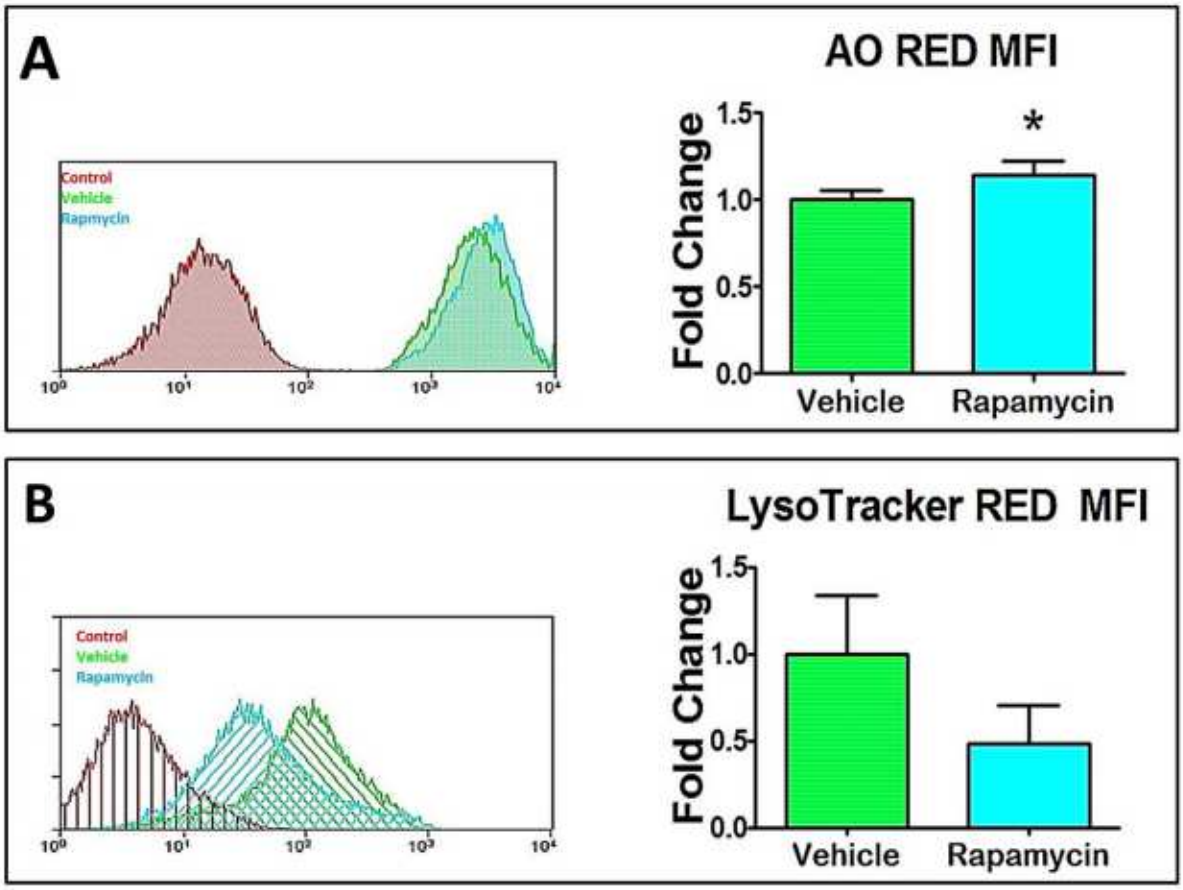

FIGURE 4.23. Effects of Rapamycin Treatment on Lysosome Size and Functionality of E-CSC. On the left: representative Flow-Cytometry histograms of Vehicle- and Rapamycin-treated E-CSC, analyzed after incubation with Acridine Orange (**A**) or LysoTracker RED DND-99 (**B**). The red florescence emission of stained cells treated with Rapamycin is reported by green histograms that are superimposed with control profiles of Vehicle-treated stained cells (cyan blue histograms) and of unstained cells (red histograms). Bar graphs in the right summarize quantitative Flow-Cytometry results, that are expressed as Mean Fluorescence Intensity (MFI) of red emission from cells stained with Acridine Orange (AO, **A**) or LysoTracker (**B**). All Values are means±SEM. * $p<0.05$ vs Vehicle-treated E-CSC.

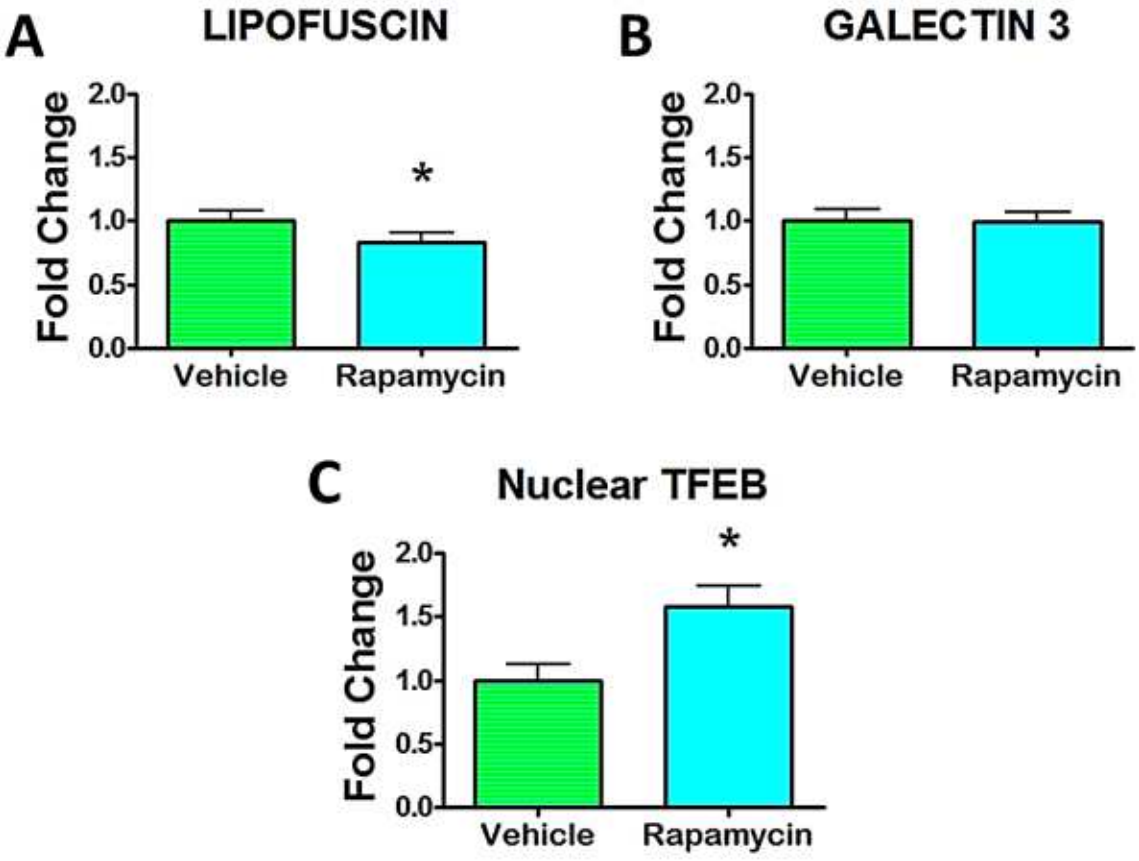

FIGURE 4.24. Effects of Rapamycin Treatment on Lysosomal Levels of Lipofuscin and Galectin-3 as well as on Nuclear Activated TFEB. Histograms (**A**, **B**, **C**) summarize results of the quantification of the lipofuscin (**A**), or Galectin 3 (**B**) IFI for lysosomal compartment together with the quantification of TFEB IFI for nuclear compartment. All Values are means±SEM. * $p<0.05$ vs Vehicle-treated E-CSC.

4.9 RAPAMYCIN AWAKENS THE E-CSC AUTOPHAGIC FLUX

Last, the effects of drug treatment on E-CSC mTOR signaling pathway were explored.

As expected, Western Blot analysis showed that Rapamycin was useful in inhibiting the constitutive active mTORC1 as indicated by a decrease in phosphorylation of S6K on Thr^{389} coupled with an increased phosphorylation of Akt on Ser^{473} (**Figure 4. 25 A, B**).

In agreement with these results, the pharmacologic inhibition of mTORC1 was effective in reducing p62/SQSTM1 protein expression in treated E-CSC (**Figure 4.25 C**), without modifying the levels of Atg3, Atg7 and LC3BII (**Figure 4. 25 D, E, F**).

Summarizing, these results constitute the final confirmation that the pharmacological strategy that we experimented is effective in reactivating the autophagic flux of E-CSC.

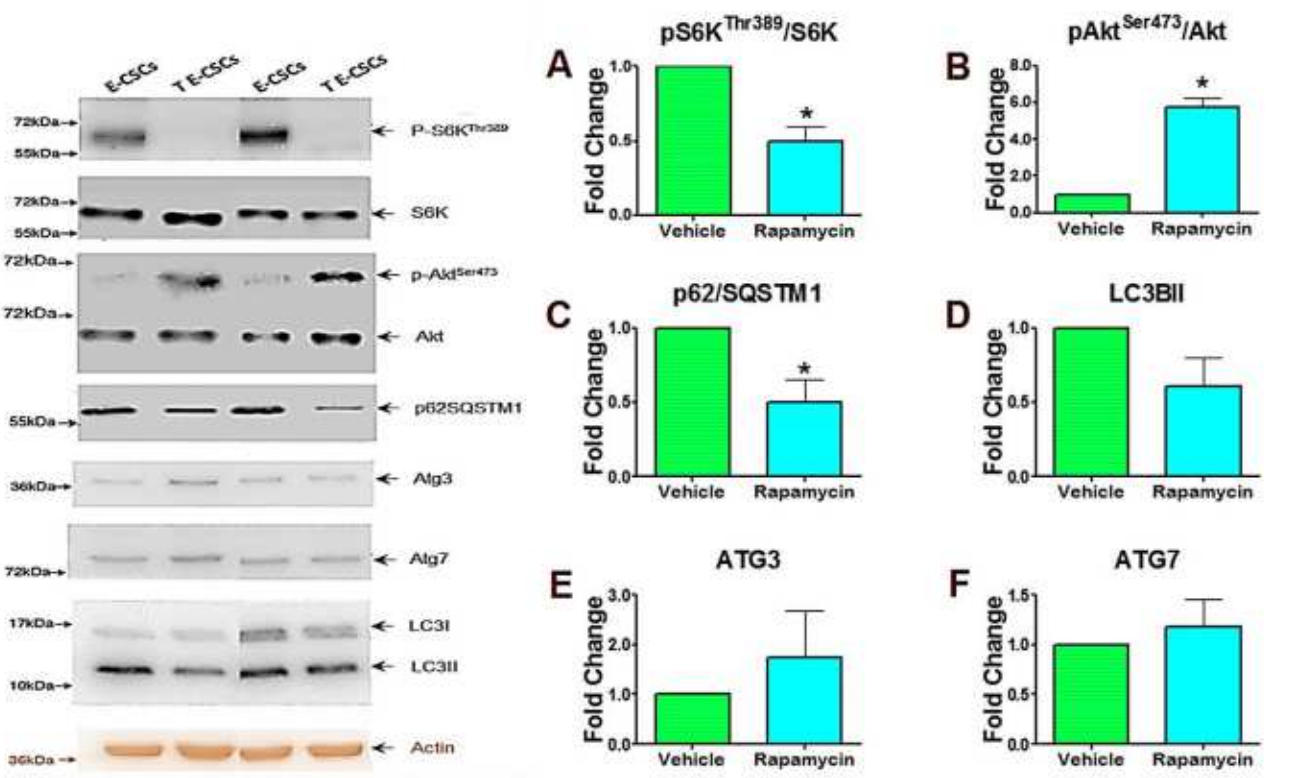

FIGURE 4.25 Effects of Rapamicyn Treatment on mTOR Signaling Pathway. In the left, representative Western Blots of cell extracts obtained from 2 Vehicle-treated, and 3 Rapamycin-treated E-CSC. Blotted proteins were incubated with antibodies directed against S6K, phospho-S6KThr^{389}, Akt, phospho-AktSer^{473}, p62/SQSTM1, Atg3, Atg7, LC3II, and Actin. Histograms (**A**, **B**, **C**, **D**, **E**, **F**) in the right show the respective results of the densitometric analyses normalized versus Actin. * $p<0.05$ vs Vehicle-treated E-CSC.

5. DISCUSSION

To date, despite medical and pharmacological advances, heart diseases hold the first place as cause of death and disability. The evolution in the management of acute cardiovascular disease has been followed by a growing number of patients with chronic debilitation due to Heart Failure (HF) [1]. Current end-stage HF treatments are limited to cardiac transplantation or the option of permanent mechanical assistance of the circulation [99], two strategies that, although beneficial for the patient, remain not fully satisfactory; therefore additional therapies are highly desirable. Once the heart had been demonstrated to be not a terminally differentiated organ [18], hopes were pinned on the isolation and characterization of the Cardiac Stem Cells (CSCs) present in the adult, relying on the possibility to use these cells in cell replacement therapy. The results, although encouraging, have been limited by the discovery that both aging and chronic age-related pathologies, such as atherosclerosis [51], or heart failure [46] are associated with stem cell senescence. Specifically, our group demonstrated that CSCs isolated from end-stage failing explanted hearts (E-CSC) are characterized by reduced levels of telomerase activity, a larger fraction of primitive cells showing telomere dysfunction, expressing senescence markers, and with reduced proliferative and migratory abilities [46], features able to limit the regenerative potential of this autologous cell source. Thus, in order to identify pharmacological interventions aimed at improving the effectiveness of CSC based therapies, it would be mandatory to identify key pathway alterations associated with E-CSC cell senescence. For this reason, we focused our attention on Autophagy-Lysosome Pathway (ALP), a highly conserved process, whose activity increases during multiple forms of cardiovascular stress, including pressure overload and chronic ischemia [127], while its defects are associated with aging and heart failure progression [82].

At present, the efficacy of ALP in CSCs obtained from normal hearts (D-CSC) has not yet been directly compared with that of E-CSC. This was the first aim of this study.

In the first part of the work, we characterized D- and E-CSC, showing that they display a similar mesenchymal immunophenotype, enriched in the expression of c-Kit (about 80% of cell positivity) and negative for endothelial and hematopoietic markers. Noteworthy, CD49a/ α 1 integrin, that increases with cardiac aging and disease [119], is more represented in E-CSC. These latter cells are also more apoptotic than D-CSC and display a blunted growth capability, as demonstrated by a 1.7 fold longer Cell Population Doubling Time (CPDT), coupled with a reduced expression of the proliferation marker (Ki67). Moreover, cultures of CSCs obtained from failing hearts are enriched in cells expressing p16INK^{4A} and presenting a persistent DNA-Damage Response (DDR), as suggested by the presence of the histone protein γ -H2A.X in the absence of cell proliferation. All these results

are in full harmony with the recently demonstrated discovery that CSCs residing in hearts of HF patients are senescent and functionally impaired [46].

Subsequently, we performed a new analysis of CSCs' transcriptome. This latter differs between the two groups of cells, since 372 genes and 423 genes are up- and down-regulated in E-CSC, respectively. Bioinformatics analysis on the functional meaning of these two lists of differently expressed genes underlined that the set of genes overexpressed in E-CSC are involved in: response to stress, wound healing and inflammatory processes. These data support the notion that the milieu (i.e. that of a failing heart) conditions their gene expression profile, possibly by epigenetic alterations. In line with our data, a recent work by Vecellio and colleagues demonstrates that cardiac derived mesenchymal stem cells isolated from diabetic hearts retain an epigenetic memory of their diseased organ of origin [128]. Interestingly, the expression of a subset of genes implicated in protein degradation bypassing ALP are more expressed in E-CSC, suggesting that a plausible compensatory mechanism is made necessary by an inadequate ALP. This latter is supported by the fact that genes encoding for proteins, that are attributable to the structure of lysosomes and other lytic vacuoles, are down-regulated in explanted cells. Further confirmations arrived from the identification of 23 different genes that are associated to ALP and are under-expressed in E-CSC. To complete the framework, the involvement of Transcription Factor EB (TFEB) was considered, given its centrality in controlling cellular clearance pathways, promoting the transcription of a set of genes known as CLEAR (Coordinated Lysosomal Expression and Regulation) gene network [86, 129]. This work newly demonstrated that 21 TFEB direct target genes that are less expressed in decompensated heart derived-CSC, suggesting that TFEB is less active in E-CSC than in D-CSC. The reduced activity of this transcription factor may, in fact, account for the diminished transcription of ALP genes [88]. This is the last evidence of transcriptome imbalances associated with ALP of CSCs obtained from end-stage failing hearts.

Subsequently, the work moved to the assessment of microRNA post-transcriptional regulation. miRNA expression profiling revealed 2 and 1 microRNAs that are expressed only D-CSC (hsa-miR-10b-5p, hsa-miR-199b-5p) and only in E-CSC (hsa-miR-450b-5p) respectively, and other 4 miRs (hsa-miR-146b-5p, hsa-miR-155-5p, hsa-miR-299-5p, hsa-miR-493-3p) that are less expressed in explanted cells compared to cells from donor hearts. To conduct a study as rigorously as possible, the research of microRNA target genes was limited only to those that had been experimentally validated in order to minimize false positives. Although these stringent criteria kept out from the study the hsa-miR-450b-5p (only expressed in E-CSC) and one of the miRs up-regulated in D-CSC (hsa-miR-493-3p), it was able to identify 987 genes that are targets of the other microRNA that are less expressed in E-CSC. Remarkably, enrichment test calculation, conducted on KEGG and Reactome database, connected directly or indirectly this targetome to cell senescence and mTOR. The relevance of these discoveries is manifested by considering the proper role of microRNA in inhibiting the expression of its target, in view of what our results suggest that either D-CSC limit cell senescence and mTOR pathway post-transcriptionally or these pathways are less restrained in E-CSC.

The newly recognized disparities in transcriptional and post-transcriptional regulation of ALP- and Senescence-associated genes drove our research towards the direct examination of lysosomal size and functionality. Not surprisingly, FACS analysis, although excluding differences in terms of lysosomal compartment extension, reported that lysosomes of CSCs obtained from heart of patients with HF are less acidic and so less functional.

To further validate these functional differences in the ALP, we assessed the amount the undigested material, known as lipofuscin, that was accumulated within the lysosomes, jeopardizing their digestive capability, and their fusion with the autophagosomes [101]. The differences, that were striking even from a qualitative point of view, were quantified by the confocal microscopy imaging, followed by the analysis of Integrated Florescence Intensity. Quantitatively, we showed that the load of lipofuscin is more than 5-fold higher in lysosomes of E-CSC. Furthermore we demonstrated that explanted CSCs express also higher level of lysosomal-localized Galectin 3 (Gal-3). This latter is a lectin with high affinity for ß-galactosides, that is distributed throughout both the cytoplasm and the nucleus. ß-galactose-containing glycoproteins are localized only on the cell surface and in the lumen of endocytic compartments, therefore they interact with Gal-3 only as a result of endosomal membrane rupture. Recent data have demonstrated that this phenomenon may occur, as in our case, following lysosomal damage and may sequester damaged organelles into autophagosomes [130].

Moving from the above described observations, the activation of TFEB was investigated. This latter, in fact, promotes the clearance of lysosomes, favoring their fusion with plasma membrane, in order to remove their toxic content by exocytosis [61]. Consistently with gene expression profile data, we demonstrated that the amount of nuclear active TFEB is significantly lower in E-CSC, that are consequently less effective in cutting out their dysfunctional lysosomes.

As a natural consequence of all the previous results just discussed, the mTOR pathway was examined because of its functional interconnection with senescence, TFEB [88] and ALP [131]. Indeed, mTOR activation may provoke stem cell exhaustion and aging [125], inhibition of autophagy, reduction of lysosome functionality [131] and the inactivation of TFEB. In line with miRNA expression profiling, E-CSC show an intensified activation of mTOR or, to be more precise, of mTORC1 as supported by a trend toward increased phosphorylation of its downstream target S6K in Threonine^{389}, and a reduced phosphorylation of Akt in Ser^{473}. Consistently the expression of E-CSC Autophagic markers showed incoherence between higher levels of autophagosome generation marker (Atg3, Atg7, LC3BII) and higher levels of p62/SQSTM1 (i.e. a ubiquitin-binding protein, selectively incorporated into autophagosomes, whose levels inversely correlate with autophagic activity) [126]. As a whole, these data demonstrated that, in E-CSC, the autophagosomes are not degraded and suggest that in these cells the autophagic flux is blocked, providing the last and final demonstration that ALP is ineffective in CSCs isolated from patients with HF.

Our second aim was, therefore, to develop a drug-based strategy able to reactivate ALP and contrast E-CSC senescence by targeting mTOR. Given its ability to inhibit mTOR [132], the drug chosen for the E-CSC treatment was Rapamycin.

First of all, a pilot titration study was conducted. This study with ascending drug concentrations allowed us to identify in 10nM the optimal dose that was used in a three-day treatment.

This therapy was able to reduce both the fraction of CD49a/α1 integrin and p16INK^{4A} E-CSC positive cells without further modifying the cell surface immunophenotype, nor prejudicing the differentiation, proliferation and migration ability. The demonstration that these effects were not recognized in D-CSC treated with Rapamycin, confirms that in these cells, mTORC1 is already inactive, possibly as a result of the post-transcriptional activity of hsa-miR-10b-5p, hsa-miR-146b-5p, hsa-miR-155-5p, hsa-miR-199b-5p and hsa-miR-299-5p.

Amazingly, the effectiveness of our strategy in restoring the function of the lysosomal compartment of explanted cells was underlined by: the restoration of the acidity of lysosomes, the decreased load of lipofuscin in lysosomes, and the amplified amount of active nuclear TFEB. The latter result suggests that the observed trend toward a reduction of the lysosomal compartment size may be due to an increase in lysosomal exocytosis. This suggestion is in line with recent data obtained by *Settembre* and colleagues, who demonstrated that mTORC1 inactivates TFEB by a transient interaction on lysosomal membrane [88].

As expected, protein level determinations confirmed the successful inhibition of mTORC1 by Rapamycin. Interestingly our pharmacologic strategy was able to reestablish the autophagic flux.

In conclusion, our results draw for the first time a complex scenario in which TFEB, senescence, and mTORC1 play the roles of *the Good, the Bad* and *the Ugly,* respectively. Specifically, chronic stress and inflammatory conditions, to which CSCs resident in failing hearts have to respond, push the cells towards a senescent phenotype, that is characterized by a hyperactivation of mTORC1 [52]. This latter, in addition to directly inhibit autophagy, also prevents the nuclear translocation of TFEB, thus switching off its ability to orchestrate and promote the degradation activity of the cell. As a consequence, both the biogenesis of new lysosomes and the disposal of toxic substances by lysosomal exocytosis are impaired. Because of this, waste materials accumulate within the lysosome, generating lipofuscin that jeopardize its digestive potential and inhibit its fusion with autophagosomes. As a result, ALP and the cellular clearance mechanisms diminish, thus threatening protein homeostasis, and leading to new stress, inflammatory conditions and, as a consequence, to cell senescence and aging [133]. It's established in this manner a vicious circle that feed senescence as schematized in **Figure 5.1**.

Noteworthy, Rapamycin treatment interrupts upstream this vicious circle by inhibiting mTORC1 and is effective in awakening ALP and in counteracting senescence.

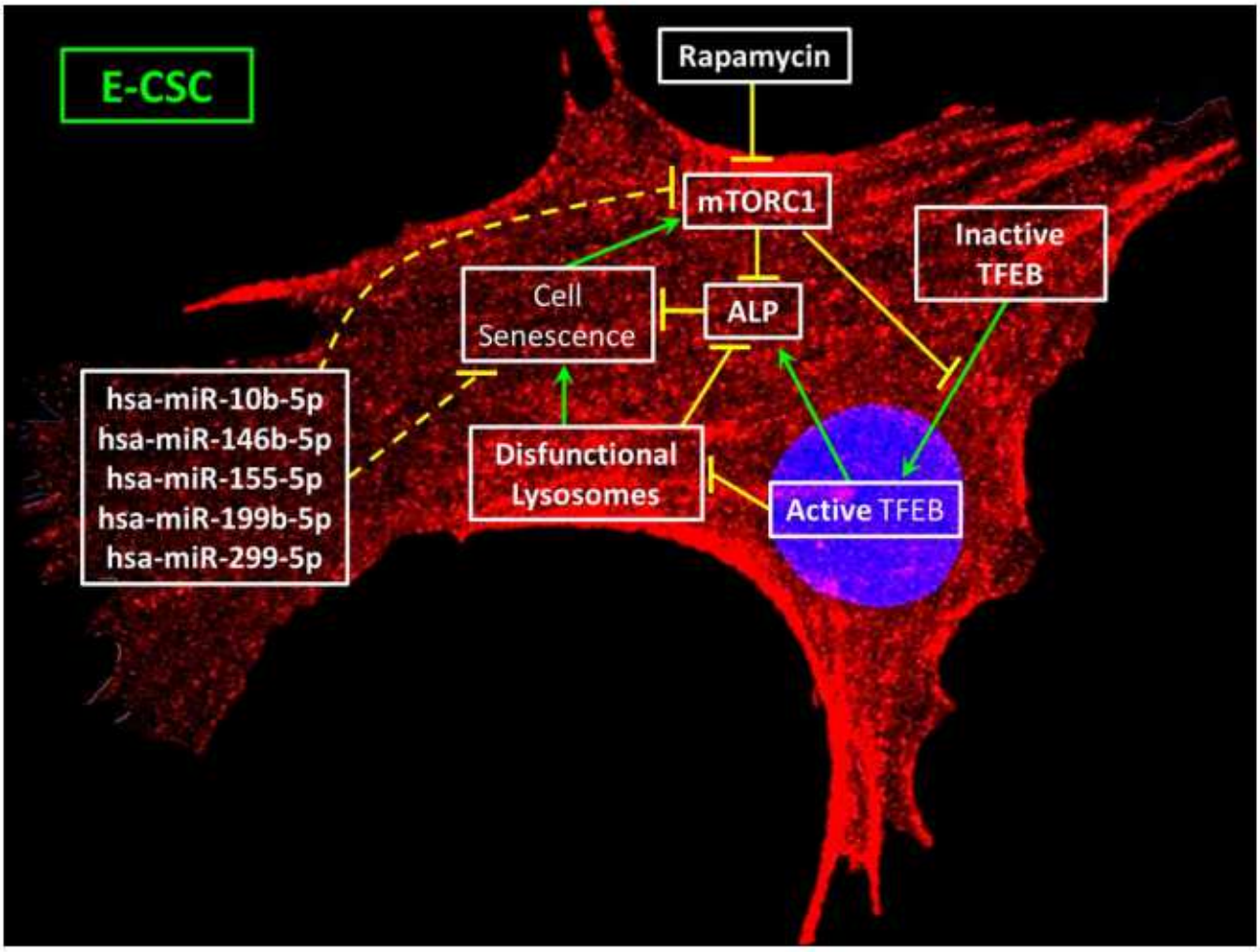

Figure 5.1. Concluding Model of a Feed-Forward Loop That Enhances Cell Senescence by mTORC1 Activation in ECSC. Green sharp end arrows indicate activation; yellow blunt end arrows indicate repression; yellow dotted blunt end arrows indicate ineffective repression.

6. CONCLUDING REMARKS

With our work we demonstrate that ALP dysfunction can be reverted rejuvenating senescent E-CSC. Specifically Rapamycin is able to reactivate ALP, eventually contrasting cell senescence in CSCs.

The impact of our results has been proven by the fact that this study led to a larger project in which 10nM Rapamycin was coupled with 0.5μM Resveratrol. The synergic action of two coupled drugs reduced E-CSC senescence, reestablishing their *in vitro* protective activity on cardiomyocytes. Moreover three-day long *ex vivo* treatment with Rapamycin and Resveratrol improved E-CSC capacity to induce cardiac repair upon injection in the mouse infarcted heart, leading to reduced cardiomyocyte senescence and apoptosis and increased abundance of endogenous c-Kit positive CSCs in the periinfarct area. This finding opens promising avenues for optimal regenerative treatments with autologous CSCs, without the need of prolonged therapy or gene manipulation. The work has been published last September and can be found in attached Appendix A [52].

BIBLIOGRAPHY

1. Go, A.S., et al., *Heart disease and stroke statistics--2014 update: a report from the American Heart Association.* Circulation, 2014. **129**(3): p. e28-e292.
2. Dickstein, K., et al., *ESC Guidelines for the diagnosis and treatment of acute and chronic heart failure 2008.* European Heart Journal, 2008. **29**(19): p. 2388-2442.
3. Bleumink, G.S., et al., *Quantifying the heart failure epidemic: prevalence, incidence rate, lifetime risk and prognosis of heart failure.* European Heart Journal, 2004. **25**(18): p. 1614-1619.
4. Stewart, S., et al., *The current cost of heart failure to the National Health Service in the UK.* European Journal of Heart Failure, 2002. **4**(3): p. 361-371.
5. Cannon, C.P., et al., *2013 ACCF/AHA Key Data Elements and Definitions for Measuring the Clinical Management and Outcomes of Patients With Acute Coronary Syndromes and Coronary Artery Disease: A Report of the American College of Cardiology Foundation/American Heart Association Task Force on Clinical Data Standards (Writing Committee to Develop Acute Coronary Syndromes and Coronary Artery Disease Clinical Data Standards).* Critical Pathways in Cardiology, 2013. **12**(2): p. 65-105 10.1097/HPC.0b013e3182846e16.
6. McMurray, J.J., et al., *ESC Guidelines for the diagnosis and treatment of acute and chronic heart failure 2012: The Task Force for the Diagnosis and Treatment of Acute and Chronic Heart Failure 2012 of the European Society of Cardiology. Developed in collaboration with the Heart Failure Association (HFA) of the ESC.* Eur Heart J, 2012. **33**(14): p. 1787-847.
7. Watson, R.D.S., C.R. Gibbs, and G.Y.H. Lip, *Clinical features and complications.* BMJ : British Medical Journal, 2000. **320**(7229): p. 236-239.
8. *The Criteria Committee of the New York Heart Association . Nomenclature and Criteria for Diagnosis of Diseases of the Heart and Great Vessels.* 9th ed Little, Brown & Co; Boston, Mass, 1994: p. 253–256.
9. TR, H., *Principles of Internal Medicine.* New York, NY: The Blakiston Company, 1950.
10. Allan, R., et al., *Cellular transplantation: future therapeutic options.* Curr Opin Cardiol, 2007. **22**(2): p. 104-10.
11. Rose, E.A., et al., *Long-Term Use of a Left Ventricular Assist Device for End-Stage Heart Failure.* New England Journal of Medicine, 2001. **345**(20): p. 1435-1443.
12. Braunwald, E., *The Management of Heart Failure: The Past, the Present, and the Future.* Circulation: Heart Failure, 2008. **1**(1): p. 58-62.
13. Ma, H., *The Discovery of Stem Cell.* Stem Cell, 2013. **4**(1): p. 4-6.
14. Smith, A., *A glossary for stem-cell biology.* Nature, 2006. **441**(7097): p. 1060-1060.
15. Verfaillie, C.M., M.F. Pera, and P.M. Lansdorp, *Stem cells: hype and reality.* Hematology Am Soc Hematol Educ Program, 2002: p. 369-91.
16. Kolios, G. and Y. Moodley, *Introduction to Stem Cells and Regenerative Medicine.* Respiration, 2013. **85**(1): p. 3-10.
17. Leri, A., J. Kajstura, and P. Anversa, *Cardiac Stem Cells and Mechanisms of Myocardial Regeneration.* Vol. 85. 2005. 1373-1416.
18. Beltrami, A.P., et al., *Evidence That Human Cardiac Myocytes Divide after Myocardial Infarction.* New England Journal of Medicine, 2001. **344**(23): p. 1750-1757.
19. Kajstura, J., et al., *Myocyte proliferation in end-stage cardiac failure in humans.* Proceedings of the National Academy of Sciences, 1998. **95**(15): p. 8801-8805.
20. Anversa, P., et al., *Hypertensive cardiomyopathy. Myocyte nuclei hyperplasia in the mammalian rat heart.* The Journal of Clinical Investigation, 1990. **85**(4): p. 994-997.
21. Urbanek, K., et al., *Intense myocyte formation from cardiac stem cells in human cardiac hypertrophy.* Proceedings of the National Academy of Sciences, 2003. **100**(18): p. 10440-10445.
22. Bollini, S., N. Smart, and P.R. Riley, *Resident cardiac progenitor cells: At the heart of regeneration.* Journal of Molecular and Cellular Cardiology. **50**(2): p. 296-303.
23. Beltrami, A., *Multiple sources for cardiac stem cells and their cardiogenic potential.* Regenerating the Heart (eds. Cohen, I.S. & Gaudette, G.R.), 2011: p. 149–171.
24. Bearzi, C., et al., *Human cardiac stem cells.* Proceedings of the National Academy of Sciences, 2007. **104**(35): p. 14068-14073.
25. Beltrami, A.P., et al., *Adult cardiac stem cells are multipotent and support myocardial regeneration.* Cell, 2003. **114**(6): p. 763-76.
26. Urbanek, K., et al., *Myocardial regeneration by activation of multipotent cardiac stem cells in ischemic heart failure.* Proceedings of the National Academy of Sciences of the United States of America, 2005. **102**(24): p. 8692-8697.

27. Smart, N., et al., *Thymosin [bgr]4 induces adult epicardial progenitor mobilization and neovascularization.* Nature, 2007. **445**(7124): p. 177-182.
28. Castaldo, C., et al., *CD117-Positive Cells in Adult Human Heart Are Localized in the Subepicardium, and Their Activation Is Associated with Laminin-1 and α 6 Integrin Expression.* STEM CELLS, 2008. **26**(7): p. 1723-1731.
29. Quaini, F., et al., *Chimerism of the transplanted heart.* N Engl J Med, 2002. **346**(1): p. 5-15.
30. Deb, A., et al., *Bone marrow-derived cardiomyocytes are present in adult human heart: A study of gender-mismatched bone marrow transplantation patients.* Circulation, 2003. **107**(9): p. 1247-9.
31. Verardo, R., et al., *Specific mesothelial signature marks the heterogeneity of mesenchymal stem cells from high-grade serous ovarian cancer.* Stem Cells, 2014. **32**(11): p. 2998-3011.
32. Mouquet, F., et al., *Restoration of cardiac progenitor cells after myocardial infarction by self-proliferation and selective homing of bone marrow-derived stem cells.* Circ Res, 2005. **97**(11): p. 1090-2.
33. Nakanishi, C., et al., *Activation of cardiac progenitor cells through paracrine effects of mesenchymal stem cells.* Biochem Biophys Res Commun, 2008. **374**(1): p. 11-6.
34. Messina, E., et al., *Isolation and expansion of adult cardiac stem cells from human and murine heart.* Circ Res, 2004. **95**(9): p. 911-21.
35. Bolli, R., et al., *Cardiac stem cells in patients with ischaemic cardiomyopathy (SCIPIO): initial results of a randomised phase 1 trial.* Lancet, 2011. **378**(9806): p. 1847-57.
36. Chugh, A.R., et al., *Administration of cardiac stem cells in patients with ischemic cardiomyopathy: the SCIPIO trial: surgical aspects and interim analysis of myocardial function and viability by magnetic resonance.* Circulation, 2012. **126**(11 Suppl 1): p. S54-64.
37. Matar, A.A. and J.J. Chong, *Stem cell therapy for cardiac dysfunction.* Springerplus, 2014. **3**: p. 440.
38. Makkar, R.R., et al., *Intracoronary cardiosphere-derived cells for heart regeneration after myocardial infarction (CADUCEUS): a prospective, randomised phase 1 trial.* Lancet, 2012. **379**(9819): p. 895-904.
39. Lopez-Otin, C., et al., *The hallmarks of aging.* Cell, 2013. **153**(6): p. 1194-217.
40. Hayflick, L. and P.S. Moorhead, *The serial cultivation of human diploid cell strains.* Exp Cell Res, 1961. **25**: p. 585-621.
41. Beltrami, A.P., D. Cesselli, and C.A. Beltrami, *At the stem of youth and health.* Pharmacol Ther, 2011. **129**(1): p. 3-20.
42. Gorgoulis, V.G. and T.D. Halazonetis, *Oncogene-induced senescence: the bright and dark side of the response.* Curr Opin Cell Biol, 2010. **22**(6): p. 816-27.
43. Ressler, S., et al., *p16INK4A is a robust in vivo biomarker of cellular aging in human skin.* Aging Cell, 2006. **5**(5): p. 379-89.
44. Kosar, M., et al., *Senescence-associated heterochromatin foci are dispensable for cellular senescence, occur in a cell type- and insult-dependent manner and follow expression of p16(ink4a).* Cell Cycle, 2011. **10**(3): p. 457-68.
45. Acosta, J.C., et al., *A complex secretory program orchestrated by the inflammasome controls paracrine senescence.* Nat Cell Biol, 2013. **15**(8): p. 978-90.
46. Cesselli, D., et al., *Effects of age and heart failure on human cardiac stem cell function.* Am J Pathol, 2011. **179**(1): p. 349-66.
47. Chimenti, C., et al., *Senescence and death of primitive cells and myocytes lead to premature cardiac aging and heart failure.* Circ Res, 2003. **93**(7): p. 604-13.
48. Beltrami, A.P., D. Cesselli, and C.A. Beltrami, *Stem cell senescence and regenerative paradigms.* Clin Pharmacol Ther, 2012. **91**(1): p. 21-9.
49. De Angelis, A., et al., *Anthracycline cardiomyopathy is mediated by depletion of the cardiac stem cell pool and is rescued by restoration of progenitor cell function.* Circulation, 2010. **121**(2): p. 276-92.
50. Bearzi, C., et al., *Human cardiac stem cells.* Proc Natl Acad Sci U S A, 2007. **104**(35): p. 14068-73.
51. Vasile, E., et al., *Differential expression of thymosin beta-10 by early passage and senescent vascular endothelium is modulated by VPF/VEGF: evidence for senescent endothelial cells in vivo at sites of atherosclerosis.* FASEB J, 2001. **15**(2): p. 458-66.
52. Avolio, E., et al., *Ex vivo molecular rejuvenation improves the therapeutic activity of senescent human cardiac stem cells in a mouse model of myocardial infarction.* Stem Cells, 2014. **32**(9): p. 2373-85.
53. Olanow, C.W., M.B. Stern, and K. Sethi, *The scientific and clinical basis for the treatment of Parkinson disease (2009).* Neurology, 2009. **72**(21 Suppl 4): p. S1-136.
54. De Duve, C., et al., *Tissue fractionation studies. 6. Intracellular distribution patterns of enzymes in rat-liver tissue.* Biochem J, 1955. **60**(4): p. 604-17.
55. Novikoff, A.B., H. Beaufay, and C. De Duve, *Electron microscopy of lysosomerich fractions from rat liver.* J Biophys Biochem Cytol, 1956. **2**(4 Suppl): p. 179-84.
56. Duve, C., *Exploring cells with a centrifuge.* Science, 1975. **189**(4198): p. 186-94.
57. Luzio, J.P., P.R. Pryor, and N.A. Bright, *Lysosomes: fusion and function.* Nat Rev Mol Cell Biol, 2007. **8**(8): p. 622-32.
58. Fehrenbacher, N., et al., *Sensitization to the lysosomal cell death pathway by oncogene-induced down-regulation of lysosome-associated membrane proteins 1 and 2.* Cancer Res, 2008. **68**(16): p. 6623-33.

59. Saftig, P. and J. Klumperman, *Lysosome biogenesis and lysosomal membrane proteins: trafficking meets function.* Nat Rev Mol Cell Biol, 2009. **10**(9): p. 623-35.
60. Rajawat, Y.S., Z. Hilioti, and I. Bossis, *Aging: central role for autophagy and the lysosomal degradative system.* Ageing Res Rev, 2009. **8**(3): p. 199-213.
61. Medina, Diego L., et al., *Transcriptional Activation of Lysosomal Exocytosis Promotes Cellular Clearance.* Developmental Cell, 2011. **21**(3): p. 421-430.
62. Ge, W., et al., *The Roles of Lysosomes in Inflammation and Autoimmune Diseases.* Int Rev Immunol, 2014.
63. Appelqvist, H., et al., *The lysosome: from waste bag to potential therapeutic target.* J Mol Cell Biol, 2013. **5**(4): p. 214-26.
64. Boya, P. and G. Kroemer, *Lysosomal membrane permeabilization in cell death.* Oncogene, 2008. **27**(50): p. 6434-51.
65. Boya, P., *Lysosomal function and dysfunction: mechanism and disease.* Antioxid Redox Signal, 2012. **17**(5): p. 766-74.
66. Levine, B. and D.J. Klionsky, *Development by self-digestion: molecular mechanisms and biological functions of autophagy.* Dev Cell, 2004. **6**(4): p. 463-77.
67. Rezzani, R., A. Stacchiotti, and L.F. Rodella, *Morphological and biochemical studies on aging and autophagy.* Ageing Res Rev, 2012. **11**(1): p. 10-31.
68. Kundu, M. and C.B. Thompson, *Autophagy: basic principles and relevance to disease.* Annu Rev Pathol, 2008. **3**: p. 427-55.
69. Ichimura, Y. and M. Komatsu, *Selective degradation of p62 by autophagy.* Semin Immunopathol, 2010. **32**(4): p. 431-6.
70. Ge, L., et al., *The protein-vesicle network of autophagy.* Curr Opin Cell Biol, 2014. **29**: p. 18-24.
71. Tanida, I., T. Ueno, and E. Kominami, *LC3 conjugation system in mammalian autophagy.* Int J Biochem Cell Biol, 2004. **36**(12): p. 2503-18.
72. Armstrong, A., et al., *Lysosomal network proteins as potential novel CSF biomarkers for Alzheimer's disease.* Neuromolecular Med, 2014. **16**(1): p. 150-60.
73. Johnson, S.C., P.S. Rabinovitch, and M. Kaeberlein, *mTOR is a key modulator of ageing and age-related disease.* Nature, 2013. **493**(7432): p. 338-45.
74. Thoreen, C.C., et al., *An ATP-competitive mammalian target of rapamycin inhibitor reveals rapamycin-resistant functions of mTORC1.* J Biol Chem, 2009. **284**(12): p. 8023-32.
75. Guertin, D.A. and D.M. Sabatini, *Defining the role of mTOR in cancer.* Cancer Cell, 2007. **12**(1): p. 9-22.
76. Manning, B.D. and L.C. Cantley, *AKT/PKB signaling: navigating downstream.* Cell, 2007. **129**(7): p. 1261-74.
77. Richter, J.D. and N. Sonenberg, *Regulation of cap-dependent translation by eIF4E inhibitory proteins.* Nature, 2005. **433**(7025): p. 477-80.
78. Barbet, N.C., et al., *TOR controls translation initiation and early G1 progression in yeast.* Mol Biol Cell, 1996. **7**(1): p. 25-42.
79. Noda, T. and Y. Ohsumi, *Tor, a phosphatidylinositol kinase homologue, controls autophagy in yeast.* J Biol Chem, 1998. **273**(7): p. 3963-6.
80. Neshat, M.S., et al., *Enhanced sensitivity of PTEN-deficient tumors to inhibition of FRAP/mTOR.* Proc Natl Acad Sci U S A, 2001. **98**(18): p. 10314-9.
81. Pedersen, S., et al., *Distinct repression of translation by wortmannin and rapamycin.* Eur J Biochem, 1997. **247**(1): p. 449-56.
82. Taneike, M., et al., *Inhibition of autophagy in the heart induces age-related cardiomyopathy.* Autophagy, 2010. **6**(5): p. 600-606.
83. Sancak, Y., et al., *Ragulator-Rag complex targets mTORC1 to the lysosomal surface and is necessary for its activation by amino acids.* Cell, 2010. **141**(2): p. 290-303.
84. Korolchuk, V.I., et al., *Lysosomal positioning coordinates cellular nutrient responses.* Nat Cell Biol, 2011. **13**(4): p. 453-60.
85. Yu, L., et al., *Termination of autophagy and reformation of lysosomes regulated by mTOR.* Nature, 2010. **465**(7300): p. 942-6.
86. Sardiello, M., et al., *A gene network regulating lysosomal biogenesis and function.* Science, 2009. **325**(5939): p. 473-7.
87. Settembre, C., et al., *TFEB links autophagy to lysosomal biogenesis.* Science, 2011. **332**(6036): p. 1429-33.
88. Settembre, C., et al., *A lysosome-to-nucleus signalling mechanism senses and regulates the lysosome via mTOR and TFEB.* EMBO J, 2012. **31**(5): p. 1095-108.
89. Palmieri, M., et al., *Characterization of the CLEAR network reveals an integrated control of cellular clearance pathways.* Human Molecular Genetics, 2011. **20**(19): p. 3852-3866.
90. Dehay, B., et al., *Pathogenic lysosomal depletion in Parkinson's disease.* J Neurosci, 2010. **30**(37): p. 12535-44.
91. Willis, M.S. and C. Patterson, *Proteotoxicity and cardiac dysfunction--Alzheimer's disease of the heart?* N Engl J Med, 2013. **368**(5): p. 455-64.

92. Ulbricht, A., V. Arndt, and J. Hohfeld, *Chaperone-assisted proteostasis is essential for mechanotransduction in mammalian cells.* Commun Integr Biol, 2013. **6**(4): p. e24925.
93. Terman, A. and U.T. Brunk, *Lipofuscin.* Int J Biochem Cell Biol, 2004. **36**(8): p. 1400-4.
94. Terman, A., et al., *The involvement of lysosomes in myocardial aging and disease.* Curr Cardiol Rev, 2008. **4**(2): p. 107-15.
95. Shimomura, H., et al., *Autophagic degeneration as a possible mechanism of myocardial cell death in dilated cardiomyopathy.* Jpn Circ J, 2001. **65**(11): p. 965-8.
96. De Meyer, G.R., G.W. De Keulenaer, and W. Martinet, *Role of autophagy in heart failure associated with aging.* Heart Fail Rev, 2010. **15**(5): p. 423-30.
97. Jones, D.S., S.H. Podolsky, and J.A. Greene, *The Burden of Disease and the Changing Task of Medicine.* New England Journal of Medicine, 2012. **366**(25): p. 2333-2338.
98. Neubauer, S., *The Failing Heart — An Engine Out of Fuel.* New England Journal of Medicine, 2007. **356**(11): p. 1140-1151.
99. Hunt, S.A., et al., *2009 Focused Update Incorporated Into the ACC/AHA 2005 Guidelines for the Diagnosis and Management of Heart Failure in Adults: A Report of the American College of Cardiology Foundation/American Heart Association Task Force on Practice Guidelines Developed in Collaboration With the International Society for Heart and Lung Transplantation.* Journal of the American College of Cardiology, 2009. **53**(15): p. e1-e90.
100. Koga, H., S. Kaushik, and A.M. Cuervo, *Protein Homeostasis and Aging: the importance of exquisite quality control.* Ageing research reviews, 2011. **10**(2): p. 205-215.
101. Levine, B. and G. Kroemer, *Autophagy in the Pathogenesis of Disease.* Cell, 2008. **132**(1): p. 27-42.
102. Ravikumar, B., et al., *Regulation of Mammalian Autophagy in Physiology and Pathophysiology.* Vol. 90. 2010. 1383-1435.
103. Beltrami, C.A., et al., *Structural basis of end-stage failure in ischemic cardiomyopathy in humans.* Circulation, 1994. **89**(1): p. 151-63.
104. Beltrami, A.P., et al., *Multipotent cells can be generated in vitro from several adult human organs (heart, liver, and bone marrow).* Blood, 2007. **110**(9): p. 3438-46.
105. Cesselli, D., et al., *Cardiac stem cell senescence.* Methods Mol Biol, 2013. **976**: p. 81-97.
106. Baker, D.J. and J.M. Sedivy, *Probing the depths of cellular senescence.* The Journal of Cell Biology, 2013. **202**(1): p. 11-13.
107. Schneider, C.A., W.S. Rasband, and K.W. Eliceiri, *NIH Image to ImageJ: 25 years of image analysis.* Nat Methods, 2012. **9**(7): p. 671-5.
108. Yu, G., et al., *clusterProfiler: an R Package for Comparing Biological Themes Among Gene Clusters.* OMICS : a Journal of Integrative Biology, 2012. **16**(5): p. 284-287.
109. Yu, G., *DOSE: an R/Bioconductor package for Disease Ontology Semantic and Enrichment analysis.* Bioinformatics.
110. The Gene Ontology, C., et al., *Gene Ontology: tool for the unification of biology.* Nature genetics, 2000. **25**(1): p. 25-29.
111. Kanehisa, M., et al., *KEGG for representation and analysis of molecular networks involving diseases and drugs.* Nucleic Acids Research, 2010. **38**(Database issue): p. D355-D360.
112. Haw, R., et al., *Reactome pathway analysis to enrich biological discovery in proteomics data sets.* PROTEOMICS, 2011. **11**(18): p. 3598-3613.
113. Osborne, J.D., et al., *Annotating the human genome with Disease Ontology.* BMC Genomics, 2009. **10**(Suppl 1): p. S6-S6.
114. Luo, W. and C. Brouwer, *Pathview: an R/Bioconductor package for pathway-based data integration and visualization.* Bioinformatics, 2013. **29**(14): p. 1830-1831.
115. Jegga, A.G., et al., *Systems biology of the autophagy-lysosomal pathway.* Autophagy, 2011. **7**(5): p. 477-489.
116. Livak, K.J. and T.D. Schmittgen, *Analysis of Relative Gene Expression Data Using Real-Time Quantitative PCR and the 2− Δ Δ CT Method.* Methods, 2001. **25**(4): p. 402-408.
117. Sethupathy, P., B. Corda, and A.G. Hatzigeorgiou, *TarBase: A comprehensive database of experimentally supported animal microRNA targets.* RNA, 2006. **12**(2): p. 192-197.
118. Papadopoulos, G.L., et al., *The database of experimentally supported targets: a functional update of TarBase.* Nucleic Acids Research, 2009. **37**(Database issue): p. D155-D158.
119. Burgess, M.L., J.C. McCrea, and H.L. Hedrick, *Age-associated changes in cardiac matrix and integrins.* Mechanisms of Ageing and Development, 2001. **122**(15): p. 1739-1756.
120. Lawless, C., et al., *Quantitative assessment of markers for cell senescence.* Experimental Gerontology, 2010. **45**(10): p. 772-778.
121. Olsson, M., I. Rundquist, and U. Brunk, *FLOW CYTOFLUOROMETRY OF LYSOSOMAL ACRIDINE ORANGE UPTAKE BY LIVING CULTURED CELLS Effect of Trypsinization and Starvation.* Acta Pathologica Microbiologica Scandinavica Series A : Pathology, 1987. **95A**(1-6): p. 159-165.
122. Paz, I., et al., *Galectin-3, a marker for vacuole lysis by invasive pathogens.* Cell Microbiol, 2010. **12**(4): p. 530-44.

123. Korotchkina, L.G., et al., *The choice between p53-induced senescence and quiescence is determined in part by the mTOR pathway.* Aging (Albany NY), 2010. **2**(6): p. 344-352.
124. Gan, B. and R.A. DePinho, *mTORC1 signaling governs hematopoietic stem cell quiescence.* Cell cycle (Georgetown, Tex.), 2009. **8**(7): p. 1003-1006.
125. Huang, J. and B.D. Manning, *A complex interplay between Akt, TSC2, and the two mTOR complexes.* Biochemical Society transactions, 2009. **37**(Pt 1): p. 217-222.
126. Mizushima, N., T. Yoshimorim, and B. Levine, *Methods in Mammalian Autophagy Research.* Cell, 2010. **140**(3): p. 313-326.
127. Tannous, P., et al., *Intracellular protein aggregation is a proximal trigger of cardiomyocyte autophagy.* Circulation, 2008. **117**(24): p. 3070-8.
128. Vecellio, M., et al., *The histone acetylase activator pentadecylidenemalonate 1b rescues proliferation and differentiation in the human cardiac mesenchymal cells of type 2 diabetic patients.* Diabetes, 2014. **63**(6): p. 2132-47.
129. Settembre, C. and A. Ballabio, *TFEB regulates autophagy: an integrated coordination of cellular degradation and recycling processes.* Autophagy, 2011. **7**(11): p. 1379-81.
130. Maejima, I., et al., *Autophagy sequesters damaged lysosomes to control lysosomal biogenesis and kidney injury.* EMBO J, 2013. **32**(17): p. 2336-47.
131. Zhou, J., et al., *Activation of lysosomal function in the course of autophagy via mTORC1 suppression and autophagosome-lysosome fusion.* Cell Res, 2013. **23**(4): p. 508-23.
132. Heitman, J., N.R. Movva, and M.N. Hall, *Targets for cell cycle arrest by the immunosuppressant rapamycin in yeast.* Science, 1991. **253**(5022): p. 905-9.
133. Morimoto, R.I. and A.M. Cuervo, *Proteostasis and the aging proteome in health and disease.* J Gerontol A Biol Sci Med Sci, 2014. **69 Suppl 1**: p. S33-8.

ADDITIONAL INFORMATION

CONFERENCE PROCEEDINGS

Invited Speaker

"Human Cardiac Stem Cells obtained from failing hearts are characterized by a pharmacologically reversible dysfunction in the Autophagy-Lysosome Pathway".
Gianfranceschi, G; Athanasakis, E; Mazzega, E; Caragnano, A; Cesselli, D; Finato, N; Scoles, G; Beltrami CA; Beltrami, AP.
III Monalisa Quidproquo Midsummer Festival,
(Udine, Italy; 09.07.2014)

"Human Cardiac Stem Cells obtained from failing hearts are characterized by a pharmacologically reversible dysfunction in the Autophagy-Lysosome Pathway".
Gianfranceschi, G; Athanasakis, E; Mazzega, E; Caragnano, A; Cesselli, D; Finato, N; Scoles, G; Beltrami CA; Beltrami, AP.
Adriatic Society of Patology, "23th International Meeting",
(Ancona, Italy; 29.06.2014)

"hLGDB: a database on human lysosomal genes and their regulation".
Gianfranceschi, G; Brozzi A; Cesselli, D; Scoles, G; Beltrami CA; Beltrami, AP.
I Monalisa Quidproquo Midsummer Meeting,
(Udine, Italy; 30.07.2012)

Abstract in Journal

1. "*Pharmacologic rejuvenation of senescent human cardiac stem cells enhances myocardial repair*".
Avolio, E; Gianfranceschi, G; Caragnano, A; Athanasakis, E; Katare, R; Meloni, M; C; Beltrami, CA; Cesselli, D; Madeddu, P; Beltrami, AP.
Cardiovascular Research Supplements (2014) 103, S52–S53,
doi: 10.1093/CVR/CVU087.
Frontiers in CardioVascular Biology 2014
(Barcelona, Spain; 04-06/07/2014)

Abstract in Act of Congress

1. *"Human Cardiac Stem Cells obtained from failing hearts are characterized by a pharmacologically reversible dysfunction in the Autophagy-Lysosome Pathway".*
Gianfranceschi, G; Avolio, E; Athanasakis, E; Mazzega, E; Caragnano, A; Cesselli, D; Finato, N; Scoles, G; Madeddu, P; Beltrami, AP.
European Society of Cardiology Congress 2014,
(Barcelona, Spain; 30.08-03.09/2014)

2. *"Fighting senescence in the heart: a novel intervention protocol is able to revert human Cardiac Stem Cells senescence in vitro enhancing their regenerative potential in vivo".*
Avolio, E; Gianfranceschi, G; Caragnano, A; Athanasakis, E; Katare, R; Meloni, M; Palma, A; Barchiesi, A; Vascotto, C; Toffoletto, B; Mazzega, E; Finato, N; Aresu, G; Livi, U; Emanueli, C; Beltrami, CA; Madeddu, P; Cesselli D; Beltrami, AP.
Cell Senescence in Cancer and Ageing.

(Cambridge, UK; 20-23/07/2013).

3. *"Ex vivo inhibition of TORC1 improves the therapeutic activity of senescent human cardiac stem cells in a mouse model of myocardial infarction"*.
Gianfranceschi, G; Avolio, E; Caragnano, A; Athanasakis, E; Katare, R; Meloni, M; Barchiesi, A; Vascotto, C; Toffoletto, B; Palma, A; Finato, N; Aresu, G; Livi, U; Emanueli, C; Beltrami, CA; Madeddu, P; Cesselli, D; Beltrami, AP , Scoles, G.
The European CLINAM & ETPN Summit.
(Basel, Switzerand; 23-26/06/13)

4. **"***Rapamycin and Resveratrol attenuate human Cardiac Stem Cell senescence in vitro and ameliorate their regenerative potential in vivo*".
Caragnano, A; Avolio, E; Gianfranceschi, G; Zanon, V; Katare, R; Bergamin, N; Sorrentino, M; Finato, N; Livi, U; Madeddu, P; Cesselli, D; Beltrami, AP; Beltrami, CA.
3rd Meeting Stem Cell Research Italy Society.
(Ferrara, Italy; 20-22/06/2012)

5. "An in vitro, image-based platform to evaluate human stem cell senescence".
Avolio, E; Caragnano, A; Gianfranceschi, G; Cesselli, D; Beltrami, AP; Livi, U; Beltrami, CA.
11thEuropean Congress on Telepathology and 5th International Congress on Virtual Microscopy.
(Venice, Italy; 6-9/06/12)

6. "Circulating exosomes: an integrated flow-cytometric- and Atomic Force Microscopy-based analysis".
Toffoletto. B; Parisse, P; Mangoni, D; Gianfranceschi, G; Cesselli, D; Beltrami, AP; Ius, T; Skrap, M; Beltrami, CA.
11thEuropean Congress on Telepathology and 5th International Congress on Virtual Microscopy,
(Venice, Italy; 6-9/06/12)

7. "*Pharmacological attenuation of Cardiac Stem Cell senescence in vitro increases their reparative ability in vivo*".
Avolio, E; Caragnano, A; Vascotto, C; Gianfranceschi, G; Livi, U; Katare, R; Madeddu, P; Cesselli, D; Beltrami, CA; Beltrami, AP.
Frontiers in Cardiac and Vascular Regeneration.
(ICGEB-Trieste, Italy; 30/05/2012-03/06/2012)

PUBBLICATIONS

Publications Deriving from the Present Study

1. "*Ex vivo molecular rejuvenation improves the therapeutic activity of senescent human cardiac stem cells in a mouse model of myocardial infarction*".
   Avolio, E[1]; **Gianfranceschi, G**[1]; Cesselli, D; Caragnano, A; Athanasakis, E; Katare, R; Meloni, M; Palma, A; Barchiesi, A; Vascotto, C; Toffoletto, B; Mazzega E; Finato, N; Aresu, G; Livi, U; Emanueli, C; Scoles, G; Beltrami, CA; Madeddu, P; Beltrami, AP.
   Stem Cells 2014. doi: 10.1002/stem.1728[§]

Other Pubblications

1. "*Stem Cell Senescence as the Memory of Past Injuries*".
   Gianfranceschi, G; Gri, G; Cesselli, D; Beltrami, AP.
   Current Pathobiology Reports 2015. DOI 10.1007/840139-015-0071-5[§]

2. *"The Redox Function of APE1 Is Involved in the Differentiation Process of Stem Cells toward a Neuronal Cell Fate".*
   Domenis, R[1]; Bergamin, N[1]; **Gianfranceschi, G**; Vascotto, C; Romanello, M; Rigo, S; Vagnarelli, G; Faggiani, M; Parodi, P; Kelley, MR; Beltrami, CA; Cesselli, D; Tell, G; Beltrami, AP.
   PloS ONE 2014. 9(2) e89232[§]

[1]: These authors contributed equally to the work.
[§]: Available in Appendix A

SUPPLEMENTARY CONTENTS

TABLE S.1. LIST OF GENES UP-REGULATED IN E-CSC RESPECT TO AGE- AND SEX-MATCHED D-CSC.
Fold-change <-1.7; p<0.05.

ENTREZ GENE ID	GENE SYMBOL	FOLD CHANGE	P VALUE
84312	BRMS1L	1,742222291	0,002455564
2597	GAPDH	15,35100465	2,42E-05
3176	HNMT	14,40661001	1,27E-05
51012	SLMO2	13,80867295	0,000168136
3569	IL6	11,54419823	0,000243279
10476	ATP5H	8,311962019	0,000335859
3553	IL1B	8,230355028	0,00011028
2919	CXCL1	8,221692389	0,008195695
3690	ITGB3	7,945632168	0,000138267
79651	RHBDF2	7,507919318	0,000232009
4074	M6PR	7,224844461	2,58E-06
84942	WDR73	6,916317356	0,002255068
81578	COL21A1	6,669901022	4,56E-05
384	ARG2	5,03483154	0,000109679
5672	PSG4	4,951029944	5,29E-06
5617	PRL	4,854917525	0,010394856
9653	HS2ST1	4,756215044	0,001768715
7874	USP7	4,717505844	0,000551384
1643	DDB2	4,693554391	0,001010292
2547	XRCC6	4,683454011	0,001523376
55273	TMEM100	4,631265007	8,60E-05
51024	FIS1	4,563833016	0,000366028
84343	HPS3	4,447960233	0,005397499
8406	SRPX	4,444615758	0,000817943
25975	EGFL6	4,309082976	0,000156134
23024	PDZRN3	4,304062116	9,24E-06
7980	TFPI2	4,287780944	0,001827877
1521	CTSW	4,231116955	0,002907659
4236	MFAP1	4,17427492	7,36E-05
11282	MGAT4B	3,991404411	1,56E-05
3371	TNC	3,979531577	0,028143059
8871	SYNJ2	3,91875806	0,000333939
8870	IER3	3,873229537	0,001005519
5743	PTGS2	3,802111694	0,003929584

ENTREZ GENE ID	GENE SYMBOL	FOLD CHANGE	P VALUE
7057	THBS1	3,766794661	0,012305489
51706	CYB5R1	3,696116946	6,14E-05
4016	LOXL1	3,671731221	0,028955101
6146	RPL22	3,646153182	7,58E-05
6741	SSB	3,566852393	0,002268206
9168	TMSB10	3,513434242	0,001401778
7296	TXNRD1	3,457645017	0,000265517
8828	NRP2	3,40406563	6,25E-05
729238	SFTPA2	3,359552711	0,000299299
7022	TFAP2C	3,305136746	0,000943526
3021	H3F3B	3,217376433	0,005901923
7327	UBE2G2	3,157907529	0,007549411
1230	CCR1	3,000965818	0,000436537
4486	MST1R	2,963742241	0,001314611
1465	CSRP1	2,9431525	0,000130349
6175	RPLP0	2,910266273	0,006153096
6786	STIM1	2,892162395	0,00105458
27344	PCSK1N	2,873698819	0,003464782
79627	OGFRL1	2,873409138	0,004238783
7329	UBE2I	2,86615691	6,27E-05
283459	GATC	2,766419472	0,000290554
5069	PAPPA	2,733719811	0,010973974
23429	RYBP	2,706729021	0,000365533
23424	TDRD7	2,690587842	0,000102329
4905	NSF	2,688302714	0,001998371
5054	SERPINE1	2,678455822	0,001119251
10631	POSTN	2,67547622	0,000832224
10525	HYOU1	2,665778249	0,005872358
972	CD74	2,663092684	0,000327764
57410	SCYL1	2,660198642	0,032022534
9601	PDIA4	2,656321593	0,006413038
4123	MAN2C1	2,654148094	0,000333133
51021	MRPS16	2,634350596	2,05E-05
2791	GNG11	2,625707381	0,001293449
9382	COG1	2,622789835	0,024247485
56892	C8orf4	2,614702067	0,000192762
65084	TMEM135	2,609557498	2,65E-05
3490	IGFBP7	2,606845331	0,000379816
6130	RPL7A	2,598313681	0,002286198
5546	PRCC	2,571143913	0,000408121
1843	DUSP1	2,540706721	0,002598378
6303	SAT1	2,532787765	0,001953832
7052	TGM2	2,526135206	0,007331229
63827	BCAN	2,524342358	4,40E-05

ENTREZ GENE ID	GENE SYMBOL	FOLD CHANGE	P VALUE
4357	MPST	2,52003101	0,000245818
80153	EDC3	2,51268258	0,00040234
6594	SMARCA1	2,501162394	0,002399006
23193	GANAB	2,475454936	0,039480539
3783	KCNN4	2,452192437	0,000460728
29123	ANKRD11	2,445242724	0,008024281
84321	THOC3	2,422197271	0,008242698
84066	TEX35	2,412614042	0,000609822
8802	SUCLG1	2,405358303	6,10E-05
80011	FAM192A	2,403077406	0,015071885
1933	EEF1B2	2,400966725	9,02E-05
5552	SRGN	2,395010698	0,004528124
6372	CXCL6	2,38885157	0,000483966
9500	MAGED1	2,383852921	0,000204054
10126	DNAL4	2,383363561	0,000965249
2669	GEM	2,361709732	0,001313785
81610	FAM83D	2,352620715	0,000441749
26470	SEZ6L2	2,329584946	0,009939535
84872	ZC3H10	2,326455458	0,005800407
8076	MFAP5	2,322130938	0,040420194
7873	MANF	2,309842505	0,010882382
8624	PSMG1	2,285670869	0,011955392
7168	TPM1	2,267739589	5,62E-05
55709	KBTBD4	2,260741196	0,006664834
6288	SAA1	2,250121115	0,002137379
348235	SKA2	2,245042291	0,004028893
55968	NSFL1C	2,241892059	0,001631166
124565	SLC38A10	2,241050574	0,010385292
7414	VCL	2,236822184	0,000591264
22913	RALY	2,235408537	0,010466931
11176	BAZ2A	2,234169227	0,000646332
7043	TGFB3	2,225639148	0,000196971
3301	DNAJA1	2,22159432	0,001575658
5704	PSMC4	2,219111338	0,01070893
5464	PPA1	2,214869924	0,000115627
6376	CX3CL1	2,21402651	0,000637466
2707	GJB3	2,212680135	0,000312921
2561	GABRB2	2,212477356	0,000186657
55355	HJURP	2,212250895	0,012417064
6509	SLC1A4	2,207538551	0,005471412
80381	CD276	2,193684967	0,003389523
65108	MARCKSL1	2,190326428	0,000120783
2192	FBLN1	2,185200942	0,002875697
4135	MAP6	2,18084207	0,011315742

ENTREZ GENE ID	GENE SYMBOL	FOLD CHANGE	P VALUE
5898	RALA	2,167576632	0,002178796
2114	ETS2	2,163666721	0,000101325
54973	CPSF3L	2,156520579	0,003601415
857	CAV1	2,147978346	0,00514628
8451	CUL4A	2,140252893	0,000913473
5358	PLS3	2,13892149	0,005377184
7415	VCP	2,115400104	0,000107806
5977	DPF2	2,114341937	0,001045582
5869	RAB5B	2,105136186	0,001500334
6304	SATB1	2,104454387	0,006489343
6897	TARS	2,099285935	0,002012251
23645	PPP1R15A	2,093584316	0,006583739
64949	MRPS26	2,092177534	0,000611002
8818	DPM2	2,08500282	0,000758602
3636	INPPL1	2,079816453	0,000357713
6520	SLC3A2	2,068661158	0,052254731
6782	HSPA13	2,068454749	0,013476556
51421	AMOTL2	2,066228186	0,000535195
79572	ATP13A3	2,061208304	0,000531545
27316	RBMX	2,055549664	0,002654182
3398	ID2	2,054834943	0,013784833
1839	HBEGF	2,051308139	0,002361327
9518	GDF15	2,050086167	0,019564423
5880	RAC2	2,046349704	0,000291505
3326	HSP90AB1	2,046274236	0,007530896
9401	RECQL4	2,045218194	0,0012712
10772	SRSF10	2,044800523	0,004221108
9890	LPPR4	2,043732965	0,014044838
57035	RSRP1	2,041146094	0,001005745
55207	ARL8B	2,040588706	0,001167473
5189	PEX1	2,034637857	0,001372712
4162	MCAM	2,03444043	0,012031026
112939	NACC1	2,033898743	0,005753537
1915	EEF1A1	2,033620907	0,004297737
8479	HIRIP3	2,029698367	0,001511762
4211	MEIS1	2,028220722	0,000616365
9260	PDLIM7	2,025393628	0,000129465
10199	MPHOSPH10	2,015661741	0,002275597
11211	FZD10	2,014825251	0,025839343
2316	FLNA	2,013142375	0,000383609
5049	PAFAH1B2	2,012578852	0,019847571
7013	TERF1	2,006710538	0,004888777
5528	PPP2R5D	2,00660993	0,008347453
308	ANXA5	2,005254462	0,010574629

ENTREZ GENE ID	GENE SYMBOL	FOLD CHANGE	P VALUE
3006	HIST1H1C	2,001117967	0,002045502
337	APOA4	2,000491556	0,000271022
55502	HES6	1,999757974	0,00171151
4478	MSN	1,998224749	0,005692465
55701	ARHGEF40	1,997012584	0,000150129
5351	PLOD1	1,99208862	0,000173755
6352	CCL5	1,990194805	0,042320746
8877	SPHK1	1,989423165	0,001120049
1457	CSNK2A1	1,989040279	0,022426541
9097	USP14	1,98732794	0,015279104
79109	MAPKAP1	1,985621688	0,001188278
123096	SLC25A29	1,98398048	0,002283341
2232	FDXR	1,983541209	0,004092873
5432	POLR2C	1,981185053	0,004696371
633	BGN	1,97949686	0,010121176
355	FAS	1,978545241	0,000201235
5892	RAD51D	1,976174915	0,006390391
6890	TAP1	1,97421784	0,000974208
57146	TMEM159	1,973659919	0,004262713
81671	VMP1	1,968427204	0,007293135
79581	SLC52A2	1,965132701	0,036509742
2317	FLNB	1,963418528	0,001272424
8498	RANBP3	1,962384666	0,036979404
81556	VWA9	1,959096609	0,015332455
2319	FLOT2	1,957046402	0,003603905
25804	LSM4	1,956249811	0,001405799
6232	RPS27	1,953308454	0,001707958
5525	PPP2R5A	1,950946699	0,001258791
51330	TNFRSF12A	1,947910166	0,002134892
114990	VASN	1,946910869	0,001852856
7162	TPBG	1,94653055	0,000555833
8237	USP11	1,945848407	0,00464268
54496	PRMT7	1,944768045	0,016769558
23166	STAB1	1,943667777	0,001263796
800	CALD1	1,94164033	0,04427662
5708	PSMD2	1,941558383	0,002202406
8330	HIST1H2AK	1,940867433	0,016894359
83989	FAM172A	1,94043767	0,004271928
51386	EIF3L	1,940104456	0,000451501
286530	P2RY8	1,936446942	0,000109768
3491	CYR61	1,933222613	0,026132739
1068	CETN1	1,930945715	0,000262551
4861	NPAS1	1,930777771	0,002965861
6545	SLC7A4	1,930721894	0,000374297

ENTREZ GENE ID	GENE SYMBOL	FOLD CHANGE	P VALUE
10147	SUGP2	1,928268208	0,001349262
10133	OPTN	1,928024853	0,004360988
54995	OXSM	1,927422119	0,000568511
8621	CDK13	1,927098102	0,001712679
8715	NOL4	1,926366412	0,003538265
801	CALM1	1,923927862	0,001331254
7328	UBE2H	1,922308961	0,001200301
84866	TMEM25	1,921764797	0,006344066
2782	GNB1	1,920729136	0,003189428
6650	CAPN15	1,915208284	0,017754363
10602	CDC42EP3	1,913425054	0,017816762
10236	HNRNPR	1,912889075	0,002122314
4602	MYB	1,912392825	0,001729665
65263	PYCRL	1,910855343	0,017907309
7265	TTC1	1,907487386	0,00184736
81555	YIPF5	1,906606723	0,01805866
5601	MAPK9	1,906038547	0,002511446
23180	RFTN1	1,905311061	0,000680373
57326	PBXIP1	1,905147622	0,011366774
25937	WWTR1	1,90188083	0,009874474
5918	RARRES1	1,900648111	0,005956588
9703	KIAA0100	1,900548662	0,000163896
1611	DAP	1,897622937	0,001469457
788	SLC25A20	1,895426853	0,001668374
3976	LIF	1,894207269	0,016075945
6426	SRSF1	1,894063417	0,001783027
124222	PAQR4	1,893232313	0,000286705
1267	CNP	1,889965284	0,001698156
56904	SH3GLB2	1,889619455	0,018685009
10383	TUBB4B	1,88954212	0,014963369
11285	B4GALT7	1,88953879	0,000235754
140465	MYL6B	1,889164486	0,005258079
6626	SNRPA	1,884893061	0,002489519
6139	RPL17	1,88332914	0,000125375
11335	CBX3	1,881901032	0,000332534
55691	FRMD4A	1,877195376	0,014797711
64788	LMF1	1,875793579	0,023424742
5074	PAWR	1,870585559	0,001563676
124402	UBALD1	1,868941786	0,000336018
4082	MARCKS	1,867201777	0,019566933
7249	TSC2	1,865823946	0,006054461
3831	KLC1	1,864485733	0,000381613
81037	CLPTM1L	1,860168685	0,002133622
84516	DCTN5	1,85989294	0,000140275

ENTREZ GENE ID	GENE SYMBOL	FOLD CHANGE	P VALUE
7048	TGFBR2	1,85938749	0,002640679
9855	FARP2	1,859053607	0,037403537
5660	PSAP	1,858416352	0,000181353
2767	GNA11	1,857287914	0,019978546
10432	RBM14	1,855798583	0,001980594
9255	AIMP1	1,854663073	0,020089862
55041	PLEKHB2	1,854445308	0,002157904
10367	MICU1	1,852464323	0,001756105
54332	GDAP1	1,850390054	0,003427588
84966	IGSF21	1,85031709	0,020276375
29956	CERS2	1,847449709	0,021845657
54965	PIGX	1,846763977	0,000400748
6046	BRD2	1,84618399	0,000148666
79571	GCC1	1,843448969	0,000484789
6142	RPL18A	1,841655179	0,001029629
7280	TUBB2A	1,841604138	0,000409714
865	CBFB	1,841016339	0,027808845
4147	MATN2	1,839800751	0,000633885
1687	DFNA5	1,839130823	0,002388137
207	AKT1	1,836841934	0,006124456
27020	NPTN	1,835945677	0,018246609
125950	RAVER1	1,834220545	0,003003598
57827	C6orf47	1,833151381	0,000995981
56655	POLE4	1,83266001	0,004645451
9056	SLC7A7	1,832583268	0,004835307
55055	ZWILCH	1,83224846	0,000189414
79596	RNF219	1,831257873	0,011698167
10493	VAT1	1,831015093	0,003213618
2580	GAK	1,826675205	0,000178251
6184	RPN1	1,826629096	0,017847652
9397	NMT2	1,82457871	0,00321147
29803	REPIN1	1,824129897	0,015671697
7536	SF1	1,823164886	0,002090204
89792	GAL3ST3	1,822791441	0,001804204
81631	MAP1LC3B	1,82274545	0,021527217
7130	TNFAIP6	1,821700584	0,021534605
5585	PKN1	1,820981212	0,00027393
414236	C10orf55	1,819398012	0,021687473
4232	MEST	1,819294187	0,002801076
9879	DDX46	1,816997165	0,000764712
7126	TNFAIP1	1,816522373	0,000439139
25988	HINFP	1,814756821	0,006725703
60313	GPBP1L1	1,81443109	0,00942337
64332	NFKBIZ	1,812366238	0,002186941

ENTREZ GENE ID	GENE SYMBOL	FOLD CHANGE	P VALUE
2923	PDIA3	1,812120218	0,006840727
84287	ZDHHC16	1,811854518	0,000903101
3777	KCNK3	1,809730714	0,01019804
56265	CPXM1	1,809566491	0,002659502
9887	SMG7	1,809288221	0,003604135
292	SLC25A5	1,806808823	0,00246207
87	ACTN1	1,806795457	0,006687169
5790	PTPRCAP	1,806223792	0,006255236
10471	PFDN6	1,804893822	0,005569431
10160	FARP1	1,796832114	0,001170998
5798	PTPRN	1,796517239	0,022835816
9367	RAB9A	1,79634141	0,005308802
4897	NRCAM	1,796266677	0,005429018
10076	PTPRU	1,796120203	0,001163037
26173	INTS1	1,795211396	0,001701158
6747	SSR3	1,794619122	0,002613602
6427	SRSF2	1,794610145	0,002913495
23761	PISD	1,792759424	0,000209395
1981	EIF4G1	1,791955697	0,001627884
27233	SULT1C4	1,791493919	0,015345998
29083	GTPBP8	1,789906906	0,010137806
51524	TMEM138	1,789707459	0,015074635
7323	UBE2D3	1,787626108	0,000821923
4152	MBD1	1,787355958	0,006033162
78987	CRELD1	1,786941713	0,006523835
55012	PPP2R3C	1,785879753	0,000842031
23401	FRAT2	1,785612788	0,004033478
283768	GOLGA8G	1,785109484	0,023445008
6513	SLC2A1	1,784334158	0,001720738
51340	CRNKL1	1,781691814	0,000682567
8510	MMP23B	1,780882635	0,054082488
23400	ATP13A2	1,78082459	0,001098453
23277	CLUH	1,779774119	0,000308848
166	AES	1,779255316	0,001107183
2686	GGT7	1,77768807	0,007877779
25934	NIPSNAP3A	1,775575277	0,000223202
6176	RPLP1	1,774649589	0,002179545
2783	GNB2	1,773906711	0,001034417
220972	MARCH8	1,773793213	0,002117776
51138	COPS4	1,773419957	0,009410769
306	ANXA3	1,773054166	0,005412867
400	ARL1	1,770971217	0,018880164
201931	TMEM192	1,769182221	0,00480181
22920	KIFAP3	1,768542813	0,007758726

ENTREZ GENE ID	GENE SYMBOL	FOLD CHANGE	P VALUE
1849	DUSP7	1,767114479	0,024459945
57473	ZNF512B	1,76697068	0,024468335
5281	PIGF	1,766763984	0,006385234
25917	THUMPD3	1,763605889	0,042541544
5652	PRSS8	1,762925661	0,000205829
80727	TTYH3	1,762425009	0,000953603
57580	PREX1	1,76223983	0,001321596
9933	KIAA0020	1,760315314	0,002207356
2030	SLC29A1	1,760177289	0,004747151
2487	FRZB	1,75954299	0,000202263
6838	SURF6	1,756813119	0,000490093
8394	PIP5K1A	1,755312591	0,000280015
51537	MTFP1	1,755135912	0,000316848
8220	DGCR14	1,75447235	0,0022466
56903	PAPOLB	1,753077373	0,003017333
57584	ARHGAP21	1,751492711	0,000200737
6464	SHC1	1,750528095	0,01124704
4705	NDUFA10	1,749935497	0,002668915
7922	SLC39A7	1,749602746	0,001538317
6542	SLC7A2	1,748705229	0,000732216
23406	COTL1	1,747970899	0,004777645
5327	PLAT	1,747573143	0,000253382
9789	SPCS2	1,746113977	0,002054018
56935	SMCO4	1,744957442	0,00399228
6936	GCFC2	1,744945061	0,025809314
57801	HES4	1,744770119	0,002515081
6558	SLC12A2	1,743933526	0,012596108
4345	CD200	1,743770616	0,013054886
26502	NARF	1,743573536	0,030224452
84312	BRMS1L	1,742222291	0,002455564

TABLE S2. LIST OF GENES DOWN-REGULATED IN E-CSC RESPECT TO AGE- AND SEX-MATCHED D-CSC. Fold-change <-1.7; p<0.05.

ENTREZ GENE ID	GENE SYMBOL	FOLD CHANGE	P VALUE
6482	ST3GAL1	-15,16827598	0,004606309
50632	CALY	-7,395529977	0,000670908
2192	FBLN1	-6,779128624	0,006838258
4123	MAN2C1	-6,19907124	0,001799374
55255	WDR41	-6,171036088	0,002741347
5476	CTSA	-6,057549414	0,001303558
1513	CTSK	-5,826886008	0,008955134
3486	IGFBP3	-5,569876883	0,003642089
1191	CLU	-5,556881094	0,001194381
10095	ARPC1B	-5,200352891	0,00010522
126393	HSPB6	-5,181180723	0,000380172
3985	LIMK2	-4,503116201	0,000575103
2983	GUCY1B3	-4,427166224	0,004349841
10423	CDIPT	-4,301086912	0,000156304
51124	IER3IP1	-4,188772518	0,000681537
23475	QPRT	-4,072116225	0,000149526
3489	IGFBP6	-4,013875251	0,001874553
9506	PAGE4	-3,904686324	0,016658056
6352	CCL5	-3,641414634	0,006223143
2644	GCHFR	-3,586364354	0,003564003
92906	HNRNPLL	-3,488981961	0,00461891
115703	ARHGAP33	-3,479192521	0,001319293
79961	DENND2D	-3,448253075	0,001286389
93611	FBXO44	-3,436791046	0,003527977
23295	MGRN1	-3,401938614	0,000287195
259173	ALS2CL	-3,235822334	0,001742427
197370	NSMCE1	-3,227065195	0,001364435
857	CAV1	-3,200866468	0,004361961
1514	CTSL	-3,178730849	0,000429377
25970	SH2B1	-3,148177886	0,001352259
379	ARL4D	-3,119058072	0,01964812
1831	TSC22D3	-3,101226796	0,027267538
5327	PLAT	-3,075418016	0,01895865
57124	CD248	-3,062029337	0,00183376
6523	SLC5A1	-3,036831902	0,024483239
6281	S100A10	-3,027274925	0,000993894
84231	TRAF7	-3,005974535	0,003630099
90576	ZNF799	-2,995531054	2,47E-05
54517	PUS7	-2,960597496	1,17E-05
90019	SYT8	-2,917952272	0,003067737
84302	TMEM246	-2,883270384	0,000122817
8078	USP5	-2,863673029	0,023098055

ENTREZ GENE ID	GENE SYMBOL	FOLD CHANGE	P VALUE
90203	SNX21	-2,863210648	0,006137555
29103	DNAJC15	-2,854074742	0,008895265
29978	UBQLN2	-2,849141303	0,004451294
2214	FCGR3A	-2,838191773	0,005427872
4741	NEFM	-2,833122307	0,000223559
9675	TTI1	-2,827360972	0,00059667
7528	YY1	-2,827061035	7,04E-05
7070	THY1	-2,819926552	0,026485559
9741	LAPTM4A	-2,788078701	0,026194973
9122	SLC16A4	-2,767671439	0,000428862
8449	DHX16	-2,762312025	7,35E-05
4853	NOTCH2	-2,760278099	0,000202249
10457	GPNMB	-2,741469386	0,000408625
2264	FGFR4	-2,736280932	0,018488374
1551	CYP3A7	-2,726089691	0,024903723
10607	TBL3	-2,682140267	0,001006253
213	ALB	-2,672816887	0,000647848
3303	HSPA1A	-2,669316015	0,023235579
6674	SPAG1	-2,66196271	0,033132062
23164	MPRIP	-2,651759124	0,000221697
60	ACTB	-2,639448663	0,006520421
2252	FGF7	-2,621426009	0,001348544
1487	CTBP1	-2,613283026	0,033357123
55922	NKRF	-2,595274716	0,029255343
8535	CBX4	-2,580029204	0,005657352
5528	PPP2R5D	-2,534562961	0,043798474
94107	TMEM203	-2,531260911	9,15E-05
8862	APLN	-2,520737899	0,000703775
5740	PTGIS	-2,514320362	0,007037136
2199	FBLN2	-2,507885046	0,015945714
5118	PCOLCE	-2,48526959	0,004672942
1674	DES	-2,479186539	0,00050385
29126	CD274	-2,471050929	0,008146674
337867	UBAC2	-2,465070298	0,039169806
8517	IKBKG	-2,452157599	0,004481533
9590	AKAP12	-2,448961985	0,045374671
27173	SLC39A1	-2,438217069	0,000232772
221937	FOXK1	-2,434364043	0,000967185
1525	CXADR	-2,432650183	0,000535254
10773	ZBTB6	-2,43205742	0,012888546
8717	TRADD	-2,429848597	0,029087904
9053	MAP7	-2,4240957	0,027738817
10522	DEAF1	-2,4051388	7,47E-05
6202	RPS8	-2,403933886	0,021630384

ENTREZ GENE ID	GENE SYMBOL	FOLD CHANGE	P VALUE
125	ADH1B	-2,380791072	0,027794124
4835	NQO2	-2,377612409	0,000408028
254122	SNX32	-2,362624907	0,00134272
10668	CGRRF1	-2,361803277	0,028034561
991	CDC20	-2,357495899	0,007088549
6455	SH3GL1	-2,353374739	0,000555474
9140	ATG12	-2,350349454	0,000725274
8660	IRS2	-2,34664301	0,006374805
2315	MLANA	-2,346480605	7,96E-05
4060	LUM	-2,34605348	0,008527563
6152	RPL24	-2,344748805	0,012702048
8284	KDM5D	-2,34066185	0,049079187
1635	DCTD	-2,339555307	0,005584771
84445	LZTS2	-2,335933874	0,001848469
1436	CSF1R	-2,334591579	0,036342389
5763	PTMS	-2,324939317	0,015277266
27005	USP21	-2,324111836	0,003713234
2896	GRN	-2,3187447	0,025472873
10208	USPL1	-2,317534174	0,038340448
4779	NFE2L1	-2,311066121	0,02106761
23395	LARS2	-2,309819655	0,002068554
23048	FNBP1	-2,303326326	0,042786191
5333	PLCD1	-2,300445448	0,000208148
8532	CPZ	-2,297782845	3,67E-05
9673	SLC25A44	-2,287635658	0,00951319
57599	WDR48	-2,286867179	0,005245007
51703	ACSL5	-2,281594253	0,001109597
5644	PRSS1	-2,278999265	0,030639828
28960	DCPS	-2,266570624	1,00E-04
57178	ZMIZ1	-2,259417907	4,66E-05
2289	FKBP5	-2,257234193	0,006141917
287	ANK2	-2,256139656	0,019046563
80005	DOCK5	-2,251325992	0,005253612
1979	EIF4EBP2	-2,241768572	0,000921152
7107	GPR137B	-2,238036694	0,000140101
2321	FLT1	-2,236797612	0,04328012
55111	PLEKHJ1	-2,226855009	0,005197322
100130531	LOC100130531	-2,226771832	0,000212756
5270	SERPINE2	-2,22594041	0,003093468
5168	ENPP2	-2,218382075	0,0124241
51592	TRIM33	-2,214962458	0,008671035
2063	NR2F6	-2,213117151	0,030727443
84034	EMILIN2	-2,208110005	0,001645555
26227	PHGDH	-2,207724677	0,000352363

ENTREZ GENE ID	GENE SYMBOL	FOLD CHANGE	P VALUE
10513	APPBP2	-2,205206278	0,007249735
56925	LXN	-2,200223847	0,027671154
3606	IL18	-2,199827747	0,001820909
9584	RBM39	-2,199526413	0,03038753
10518	CIB2	-2,1949405	0,005878597
2882	GPX7	-2,194872093	0,010208645
3105	HLA-A	-2,189857536	0,004564518
2551	GABPA	-2,189185166	0,013966191
10370	CITED2	-2,188383155	0,000525179
3978	LIG1	-2,180551787	0,000917341
10914	PAPOLA	-2,179337383	0,014289979
8189	SYMPK	-2,177160522	0,002457056
1364	CLDN4	-2,170093201	0,007331069
116138	KLHDC3	-2,169889896	0,001543855
7052	TGM2	-2,169178211	0,000340581
23032	USP33	-2,167668583	0,001030632
100133941	CD24	-2,166177642	0,00097882
10105	PPIF	-2,160999012	0,02431387
90379	DCAF15	-2,159188437	0,003924087
1645	AKR1C1	-2,158236355	0,001644648
27316	RBMX	-2,155811194	0,030392175
29959	NRBP1	-2,150544649	0,003527612
549	AUH	-2,150411388	0,006169138
5700	PSMC1	-2,149924522	0,032068131
1601	DAB2	-2,145115773	0,000295593
1915	EEF1A1	-2,14345672	0,000756783
27285	TEKT2	-2,143352864	0,047378904
221037	JMJD1C	-2,142934404	0,044400895
375	ARF1	-2,138812612	0,034914865
6228	RPS23	-2,138082408	0,033141351
5879	RAC1	-2,136997765	0,019955533
1959	EGR2	-2,135835409	0,001250029
9747	FAM115A	-2,133103657	0,020009777
728340	GTF2H2C	-2,131865558	0,036570269
996	CDC27	-2,130418962	0,003636428
10127	ZNF263	-2,129358916	0,040422663
28965	SLC27A6	-2,128633381	0,023044377
57017	COQ9	-2,128014835	0,006605589
4681	NBL1	-2,125386247	0,000673465
51061	TXNDC11	-2,123894803	0,016801291
4665	NAB2	-2,122365776	0,017658133
51148	CERCAM	-2,11149134	0,029184865
64005	MYO1G	-2,110496581	0,00026659
4784	NFIX	-2,109704809	0,000829159

ENTREZ GENE ID	GENE SYMBOL	FOLD CHANGE	P VALUE
8608	RDH16	-2,108852614	0,038137258
2947	GSTM3	-2,104716386	0,001539695
187	APLNR	-2,094274192	0,003221196
7341	SUMO1	-2,090649205	0,0026872
3691	ITGB4	-2,087779113	9,17E-05
23647	ARFIP2	-2,087446103	0,001931463
9214	FAIM3	-2,085658054	0,00145953
91689	SMDT1	-2,084820181	0,022088415
4528	MTIF2	-2,07975942	0,003337423
203	AK1	-2,079358728	0,025276594
7512	XPNPEP2	-2,076913916	0,001286559
23549	DNPEP	-2,073523352	0,001523881
4948	OCA2	-2,071033562	0,002665013
54681	P4HTM	-2,06880936	0,000302199
405	ARNT	-2,065025113	0,032310823
252839	TMEM9	-2,064797156	0,021300589
63877	FAM204A	-2,06246334	0,010328973
163059	ZNF433	-2,060945342	0,010679528
1298	COL9A2	-2,060787219	0,000108932
3785	KCNQ2	-2,055934167	0,009970382
3669	ISG20	-2,055051482	0,023630009
9123	SLC16A3	-2,055001852	0,001926378
2213	FCGR2B	-2,051406747	0,024791178
23640	HSPBP1	-2,05061061	0,007193167
100	ADA	-2,0503481	0,030173349
1277	COL1A1	-2,047178452	0,000132916
1503	CTPS1	-2,043756714	0,042505497
6015	RING1	-2,042986902	0,005023385
3741	KCNA5	-2,0422952	0,028764738
51604	PIGT	-2,040439494	0,001190657
27237	ARHGEF16	-2,038323621	0,000422729
51230	PHF20	-2,035949597	0,050916535
54913	RPP25	-2,030897016	0,009922515
10440	TIMM17A	-2,030841259	0,042298986
23175	LPIN1	-2,029888501	0,000342846
29960	FTSJ2	-2,02901332	0,001789434
7409	VAV1	-2,024877205	0,014505387
26608	TBL2	-2,024611996	0,03270748
3155	HMGCL	-2,024053823	0,014348883
2992	GYG1	-2,023288313	0,000159879
6470	SHMT1	-2,022983472	0,009298858
200316	APOBEC3F	-2,022298796	0,003001833
805	CALM2	-2,021455178	0,015691433
126129	CPT1C	-2,020435627	0,002061217

ENTREZ GENE ID	GENE SYMBOL	FOLD CHANGE	P VALUE
1290	COL5A2	-2,01974339	0,014635099
5630	PRPH	-2,009394938	0,032444951
1123	CHN1	-2,008707452	0,001986096
1781	DYNC1I2	-2,004951627	0,000803415
65010	SLC26A6	-2,004789338	0,001834714
390	RND3	-2,002034355	0,047487229
84259	DCUN1D5	-1,998653818	0,034384462
2335	FN1	-1,997864809	0,026202025
8446	DUSP11	-1,997676177	0,015214985
10398	MYL9	-1,995584831	0,010381175
85315	PAQR8	-1,994883714	0,022230901
27289	RND1	-1,994834211	0,037588926
23511	NUP188	-1,993571237	0,034843566
90990	KIFC2	-1,993561459	0,007148152
427	ASAH1	-1,993224877	0,015336534
84256	FLYWCH1	-1,991562087	0,003864068
10026	PIGK	-1,990035706	0,0154246
5927	KDM5A	-1,989079435	0,035594505
291	SLC25A4	-1,986830889	0,02240707
7431	VIM	-1,984974906	0,008331521
23024	PDZRN3	-1,984827879	0,000337135
10079	ATP9A	-1,984468745	0,001241656
2035	EPB41	-1,983420229	0,009263937
6346	CCL1	-1,983407874	0,04060765
5045	FURIN	-1,976531547	0,013751378
2339	FNTA	-1,976489562	0,015148244
10284	SAP18	-1,970889278	0,038263612
320	APBA1	-1,969638384	0,00844275
80256	FAM214B	-1,968291504	0,001261596
2170	FABP3	-1,966361098	0,002861605
11235	PDCD10	-1,961928977	0,000498477
1020	CDK5	-1,96104166	0,025860506
23207	PLEKHM2	-1,958493407	0,005338217
847	CAT	-1,956096256	0,036422614
84861	KLHL22	-1,954826736	0,001333005
56270	WDR45B	-1,952719124	0,001266935
124402	UBALD1	-1,949792581	0,012297832
1901	S1PR1	-1,949276013	0,00260158
79096	C11orf49	-1,94891069	0,005125887
9276	COPB2	-1,947275618	0,016401714
4697	NDUFA4	-1,941980865	0,000452089
10728	PTGES3	-1,939990161	0,007406095
84894	LINGO1	-1,939897342	0,005975903
2173	FABP7	-1,93748626	0,000126243

ENTREZ GENE ID	GENE SYMBOL	FOLD CHANGE	P VALUE
6595	SMARCA2	-1,935315461	0,000380245
1066	CES1	-1,935089604	0,01492737
7416	VDAC1	-1,932602664	0,000362681
5055	SERPINB2	-1,931480481	0,000950019
1482	NKX2-5	-1,929773324	0,017514906
26086	GPSM1	-1,928911904	0,008093855
9002	F2RL3	-1,927637217	0,000424734
442578	STAG3L3	-1,927124265	0,008963661
131583	FAM43A	-1,926190134	0,014749986
54498	SMOX	-1,925031244	0,001868312
55929	DMAP1	-1,92469687	0,001896798
6415	SEPW1	-1,923211961	0,017478614
7005	TEAD3	-1,921709246	0,017529855
84939	MUM1	-1,92166941	0,016696281
64219	PJA1	-1,919821362	0,020892101
9526	MPDU1	-1,919529303	0,001818517
148304	C1orf74	-1,918312331	0,000743743
23162	MAPK8IP3	-1,918210352	0,001013216
6443	SGCB	-1,916701965	0,002067324
800	CALD1	-1,916344263	0,002078244
51529	ANAPC11	-1,914263917	0,025711828
4724	NDUFS4	-1,913556443	0,000130451
64112	MOAP1	-1,913265054	0,001566173
51700	CYB5R2	-1,911901264	0,050612171
3005	H1F0	-1,911258453	0,000656864
64432	MRPS25	-1,910033529	0,007442489
998	CDC42	-1,908953796	0,00315614
65258	MPPE1	-1,907939466	0,013782803
6895	TARBP2	-1,907289985	0,002504953
55379	LRRC59	-1,906031173	0,00327228
3242	HPD	-1,904418794	0,009867244
4172	MCM3	-1,903129072	0,00048653
9404	LPXN	-1,898436809	0,016043515
3620	IDO1	-1,896722411	0,000193252
23209	MLC1	-1,893157792	0,015058224
4843	NOS2	-1,892103993	0,030797367
153527	ZMAT2	-1,890184339	0,001254768
6134	RPL10	-1,887024119	0,000655231
4947	OAZ2	-1,885860285	0,000687366
10534	SSSCA1	-1,885636587	0,033280039
4673	NAP1L1	-1,884417937	0,007177872
60676	PAPPA2	-1,881697883	0,000144256
55658	RNF126	-1,878646624	0,028896037
3840	KPNA4	-1,87557799	0,010509931

ENTREZ GENE ID	GENE SYMBOL	FOLD CHANGE	P VALUE
567	B2M	-1,875447343	0,026985439
10634	GAS2L1	-1,874148544	0,001838354
7072	TIA1	-1,873804056	0,003879112
829	CAPZA1	-1,872652157	0,036962905
4957	ODF2	-1,871474212	0,047315878
383	ARG1	-1,869777256	0,003157939
1488	CTBP2	-1,869452842	0,002166112
3554	IL1R1	-1,869428458	0,000166583
2180	ACSL1	-1,868135724	0,013070198
6636	SNRPF	-1,868089925	0,016884486
10499	NCOA2	-1,868085788	0,008720197
400	ARL1	-1,866614017	0,012869431
5434	POLR2E	-1,865327789	0,003623176
51776	ZAK	-1,864310079	0,000209733
5316	PKNOX1	-1,862811232	0,000926096
2202	EFEMP1	-1,861108019	0,000663765
393	ARHGAP4	-1,859106414	0,003644688
8890	EIF2B4	-1,858977574	0,000465648
4583	MUC2	-1,856701993	0,042685988
10581	IFITM2	-1,854562764	0,010211089
64231	MS4A6A	-1,851149811	0,001611721
6747	SSR3	-1,850100221	0,000399932
54849	DEF8	-1,849004267	0,002860043
54471	MIEF1	-1,847494298	0,011163176
116150	NUS1	-1,845983387	0,021197861
201627	DENND6A	-1,845275496	0,010336328
7857	SCG2	-1,843585917	0,005647078
116984	ARAP2	-1,843547032	0,001572907
4907	NT5E	-1,842109428	0,000290941
83940	TATDN1	-1,841249713	0,0050601
7851	MALL	-1,841147269	0,022787792
8273	SLC10A3	-1,840180707	0,001915506
3992	FADS1	-1,838405422	0,004191254
9468	PCYT1B	-1,838293575	0,002888402
26033	ATRNL1	-1,838129756	0,000619337
159013	CXorf38	-1,837786184	0,00404226
966	CD59	-1,836303495	0,020897125
2020	EN2	-1,83368797	0,033239278
54441	STAG3L1	-1,832973853	0,025328199
381	ARF5	-1,832092803	0,015063428
2688	GH1	-1,830980288	0,00036595
201595	STT3B	-1,830906131	0,000572879
4091	SMAD6	-1,830100665	0,00100348
222183	SRRM3	-1,828922308	0,002240131

ENTREZ GENE ID	GENE SYMBOL	FOLD CHANGE	P VALUE
28511	NKIRAS2	-1,828250023	0,005405651
2939	GSTA2	-1,826648672	0,02227846
1442	CSH1	-1,826640905	0,019756207
54014	BRWD1	-1,821741503	0,000713077
9277	WDR46	-1,821086888	0,002422222
23060	ZNF609	-1,820597999	0,030833963
1973	EIF4A1	-1,81940774	0,004714656
780	DDR1	-1,819182879	0,000194682
84886	C1orf198	-1,816652173	0,003843061
1942	EFNA1	-1,816402978	0,039188417
5052	PRDX1	-1,816366415	0,02823405
56997	ADCK3	-1,81631265	0,001187593
9202	ZMYM4	-1,81131153	0,033190232
6840	SVIL	-1,807720392	0,027079364
6124	RPL4	-1,805814429	0,003274845
51150	SDF4	-1,805367543	0,008387119
6059	ABCE1	-1,80375034	0,007216058
10123	ARL4C	-1,803254111	0,000973687
10949	HNRNPA0	-1,800833275	0,017460018
6810	STX4	-1,800368421	0,008115249
537	ATP6AP1	-1,800105528	0,011090197
5054	SERPINE1	-1,799459702	0,001704774
23287	AGTPBP1	-1,798894386	0,001685143
323	APBB2	-1,797995381	0,018584924
6218	RPS17	-1,797862805	0,003317329
84717	HDGFRP2	-1,797254817	0,003409917
64427	TTC31	-1,796541127	0,001698719
64598	MOSPD3	-1,795432105	0,00399924
23213	SULF1	-1,794706044	0,017362776
400506	KNOP1	-1,794360937	0,001583956
26092	TOR1AIP1	-1,793685861	0,028916284
5176	SERPINF1	-1,793062093	0,011855185
6948	TCN2	-1,792717239	0,012562915
84254	CAMKK1	-1,792541417	0,000172122
51170	HSD17B11	-1,792350241	0,000398501
7280	TUBB2A	-1,790310131	0,003563784
93185	IGSF8	-1,789663852	0,002665635
29952	DPP7	-1,789222315	0,000470659
8237	USP11	-1,788873729	0,006342473
55075	UACA	-1,788835027	0,012701899
26234	FBXL5	-1,788270064	0,014796026
26259	FBXW8	-1,786779723	0,00549708
8725	URI1	-1,786110462	0,015704676
163126	EID2	-1,785866924	0,023403762

ENTREZ GENE ID	GENE SYMBOL	FOLD CHANGE	P VALUE
10036	CHAF1A	-1,785756998	0,000513117
127281	FAM213B	-1,780835447	0,000300743
5226	PGD	-1,780589144	0,002110131
220	ALDH1A3	-1,780330411	0,049460477
29923	HILPDA	-1,779641005	0,000994555
11124	FAF1	-1,778571898	0,025150322
3782	KCNN3	-1,77816615	0,017404256
29763	PACSIN3	-1,775706024	0,01643973
22820	COPG1	-1,775396396	0,003605084
3638	INSIG1	-1,774850281	0,031734177
54587	MXRA8	-1,774281979	0,021607287
2266	FGG	-1,773859607	0,037163421
25873	RPL36	-1,77325881	0,000244286
4692	NDN	-1,772523426	0,008882118
57472	CNOT6	-1,771900984	0,001205612
5717	PSMD11	-1,768129782	0,005423029
191	AHCY	-1,767850738	0,000227445
7123	CLEC3B	-1,767284903	0,00195525
28988	DBNL	-1,763299021	0,003181619
4256	MGP	-1,762945519	0,02505173
10101	NUBP2	-1,761708512	0,003406558
51290	ERGIC2	-1,761497186	0,004693641
126133	ALDH16A1	-1,761161274	0,003045295
1318	SLC31A2	-1,761086824	0,007400815
5567	PRKACB	-1,760397297	0,005593967
3730	KAL1	-1,759745141	0,046244506
57045	TWSG1	-1,758211807	0,000385246
1511	CTSG	-1,757029374	0,004149704
113146	AHNAK2	-1,75658583	0,004571239

TABLE S.3 LIST OF BIOLOGICAL PROCESSESS (BP) ONTOLOGYS ENRICHED IN GENES UP-REGULATED IN E-CSC. p.adjust<0.01.

BPID	DESCRIPTION	P.VALUE	P.ADJUST	GENE NUMBER
GO:0008150	biological_process	2,2E-29	2,1E-26	329
GO:0009987	cellular process	5,1E-20	2,4E-17	305
GO:0044699	single-organism process	1,3E-14	4,1E-12	264
GO:0044763	single-organism cellular process	3,6E-14	8,4E-12	246
GO:0016043	cellular component organization	4,0E-13	7,6E-11	140
GO:0071840	cellular component organization or biogenesis	5,7E-13	9,1E-11	142
GO:0006950	response to stress	6,4E-11	8,7E-09	105
GO:0009611	response to wounding	4,9E-10	5,8E-08	52
GO:0051649	establishment of localization in cell	1,0E-09	1,1E-07	73
GO:0016482	cytoplasmic transport	3,2E-09	3,0E-07	40
GO:0051641	cellular localization	5,8E-09	5,0E-07	77
GO:0072594	establishment of protein localization to organelle	1,7E-08	1,3E-06	28
GO:0033365	protein localization to organelle	2,8E-08	2,1E-06	31
GO:0046907	intracellular transport	3,4E-08	2,2E-06	53
GO:0006605	protein targeting	3,4E-08	2,2E-06	29
GO:0008152	metabolic process	3,7E-08	2,2E-06	224
GO:0042060	wound healing	4,5E-08	2,5E-06	33
GO:0071704	organic substance metabolic process	7,4E-08	3,9E-06	215
GO:0044237	cellular metabolic process	7,9E-08	3,9E-06	207
GO:0016071	mRNA metabolic process	1,4E-07	6,5E-06	32
GO:0019538	protein metabolic process	2,9E-07	1,3E-05	113
GO:0006809	nitric oxide biosynthetic process	3,6E-07	1,5E-05	9
GO:0007275	multicellular organismal development	4,3E-07	1,8E-05	114
GO:0033036	macromolecule localization	4,6E-07	1,8E-05	66
GO:0032502	developmental process	5,2E-07	2,0E-05	125
GO:0051179	localization	6,2E-07	2,2E-05	120
GO:0050896	response to stimulus	6,2E-07	2,2E-05	167
GO:0007596	blood coagulation	6,4E-07	2,2E-05	27
GO:0050817	coagulation	7,1E-07	2,3E-05	27
GO:0007599	hemostasis	7,4E-07	2,3E-05	27
GO:0044238	primary metabolic process	7,7E-07	2,3E-05	206
GO:0050878	regulation of body fluid levels	7,7E-07	2,3E-05	30
GO:0042127	regulation of cell proliferation	8,9E-07	2,6E-05	47
GO:0071702	organic substance transport	1,4E-06	3,8E-05	66
GO:0001525	angiogenesis	1,4E-06	3,8E-05	22
GO:0065007	biological regulation	1,5E-06	4,0E-05	205
GO:0048856	anatomical structure development	2,3E-06	5,9E-05	111
GO:0046209	nitric oxide metabolic process	2,5E-06	6,3E-05	9
GO:0001775	cell activation	2,9E-06	6,8E-05	34
GO:0044267	cellular protein metabolic process	3,0E-06	6,8E-05	95
GO:0007155	cell adhesion	3,0E-06	6,8E-05	39
GO:0008283	cell proliferation	3,1E-06	6,8E-05	55
GO:0032501	multicellular organismal process	3,2E-06	6,8E-05	146

BPID	DESCRIPTION	P.VALUE	P.ADJUST	GENE NUMBER
GO:0022610	biological adhesion	3,2E-06	6,8E-05	39
GO:0006412	translation	3,2E-06	6,8E-05	25
GO:0034613	cellular protein localization	3,7E-06	7,5E-05	40
GO:0051234	establishment of localization	3,8E-06	7,7E-05	100
GO:0006886	intracellular protein transport	4,0E-06	7,8E-05	32
GO:0030168	platelet activation	4,0E-06	7,8E-05	16
GO:0070727	cellular macromolecule localization	4,1E-06	7,8E-05	40
GO:0044085	cellular component biogenesis	4,5E-06	8,3E-05	60
GO:0044707	single-multicellular organism process	5,1E-06	9,3E-05	141
GO:0048731	system development	5,2E-06	9,3E-05	98
GO:0033554	cellular response to stress	5,7E-06	9,8E-05	46
GO:0048661	positive regulation of smooth muscle cell proliferation	5,7E-06	9,8E-05	7
GO:0006915	apoptotic process	5,8E-06	9,8E-05	53
GO:0006810	transport	6,1E-06	1,0E-04	98
GO:0001944	vasculature development	6,9E-06	1,1E-04	26
GO:0044765	single-organism transport	7,3E-06	1,2E-04	85
GO:0012501	programmed cell death	7,5E-06	1,2E-04	53
GO:0050789	regulation of biological process	7,6E-06	1,2E-04	192
GO:0042221	response to chemical stimulus	8,0E-06	1,2E-04	85
GO:0045428	regulation of nitric oxide biosynthetic process	9,6E-06	1,4E-04	7
GO:0071453	cellular response to oxygen levels	9,7E-06	1,4E-04	10
GO:0000375	RNA splicing, via transesterification reactions	1,1E-05	1,6E-04	15
GO:0043933	macromolecular complex subunit organization	1,1E-05	1,6E-04	49
GO:0008380	RNA splicing	1,1E-05	1,6E-04	19
GO:0050794	regulation of cellular process	1,2E-05	1,6E-04	183
GO:0008104	protein localization	1,3E-05	1,8E-04	55
GO:0070972	protein localization to endoplasmic reticulum	1,4E-05	1,9E-04	11
GO:0045429	positive regulation of nitric oxide biosynthetic process	1,4E-05	1,9E-04	6
GO:0022607	cellular component assembly	1,5E-05	1,9E-04	55
GO:0009605	response to external stimulus	1,5E-05	2,0E-04	47
GO:0043170	macromolecule metabolic process	1,8E-05	2,3E-04	174
GO:0008219	cell death	1,9E-05	2,5E-04	56
GO:0030198	extracellular matrix organization	2,0E-05	2,5E-04	18
GO:0016265	death	2,0E-05	2,5E-04	56
GO:0043062	extracellular structure organization	2,1E-05	2,5E-04	18
GO:0006614	SRP-dependent cotranslational protein targeting to membrane	2,1E-05	2,6E-04	10
GO:0006807	nitrogen compound metabolic process	2,2E-05	2,6E-04	146
GO:0010634	positive regulation of epithelial cell migration	2,2E-05	2,6E-04	8
GO:0002576	platelet degranulation	2,4E-05	2,7E-04	9
GO:0008285	negative regulation of cell proliferation	2,4E-05	2,8E-04	25
GO:0044260	cellular macromolecule metabolic process	2,5E-05	2,8E-04	160
GO:0006414	translational elongation	2,5E-05	2,8E-04	10
GO:0006613	cotranslational protein targeting to membrane	2,5E-05	2,8E-04	10
GO:0010605	negative regulation of macromolecule metabolic process	2,7E-05	2,9E-04	48

BPID	DESCRIPTION	P.VALUE	P.ADJUST	GENE NUMBER
GO:0045047	protein targeting to ER	2,7E-05	3,0E-04	10
GO:0002376	immune system process	2,9E-05	3,1E-04	62
GO:0072599	establishment of protein localization to endoplasmic reticulum	3,0E-05	3,1E-04	10
GO:0006928	cellular component movement	3,1E-05	3,2E-04	48
GO:0045184	establishment of protein localization	3,1E-05	3,2E-04	46
GO:0048514	blood vessel morphogenesis	3,2E-05	3,2E-04	22
GO:0016477	cell migration	3,2E-05	3,2E-04	34
GO:0030335	positive regulation of cell migration	3,2E-05	3,2E-04	15
GO:0050900	leukocyte migration	3,2E-05	3,2E-04	16
GO:0048523	negative regulation of cellular process	3,5E-05	3,3E-04	83
GO:0000377	RNA splicing, via transesterification reactions with bulged adenosine as nucleophile	3,5E-05	3,3E-04	14
GO:0000398	mRNA splicing, via spliceosome	3,5E-05	3,3E-04	14
GO:0070482	response to oxygen levels	3,5E-05	3,3E-04	15
GO:0048519	negative regulation of biological process	3,8E-05	3,6E-04	89
GO:2000147	positive regulation of cell motility	3,9E-05	3,6E-04	15
GO:0051704	multi-organism process	4,4E-05	4,1E-04	46
GO:0032101	regulation of response to external stimulus	4,6E-05	4,2E-04	21
GO:0015031	protein transport	4,7E-05	4,2E-04	44
GO:0090150	establishment of protein localization to membrane	5,0E-05	4,4E-04	14
GO:0040011	locomotion	5,0E-05	4,4E-04	44
GO:0032879	regulation of localization	5,1E-05	4,4E-04	48
GO:0051272	positive regulation of cellular component movement	5,1E-05	4,5E-04	15
GO:0065008	regulation of biological quality	5,2E-05	4,5E-04	81
GO:0044767	single-organism developmental process	5,8E-05	4,9E-04	95
GO:0007566	embryo implantation	5,8E-05	4,9E-04	6
GO:0040017	positive regulation of locomotion	5,9E-05	4,9E-04	15
GO:0046903	secretion	6,3E-05	5,2E-04	32
GO:0065009	regulation of molecular function	6,9E-05	5,6E-04	57
GO:0072358	cardiovascular system development	6,9E-05	5,6E-04	31
GO:0072359	circulatory system development	6,9E-05	5,6E-04	31
GO:0001568	blood vessel development	7,1E-05	5,7E-04	23
GO:0048870	cell motility	7,3E-05	5,8E-04	35
GO:0051674	localization of cell	7,3E-05	5,8E-04	35
GO:0006996	organelle organization	7,8E-05	6,0E-04	68
GO:0016032	viral process	7,8E-05	6,0E-04	27
GO:0044764	multi-organism cellular process	8,2E-05	6,3E-04	27
GO:0009892	negative regulation of metabolic process	8,4E-05	6,4E-04	49
GO:0051716	cellular response to stimulus	8,6E-05	6,5E-04	128
GO:0010942	positive regulation of cell death	8,7E-05	6,6E-04	18
GO:0009628	response to abiotic stimulus	9,2E-05	6,8E-04	32
GO:0010033	response to organic substance	9,2E-05	6,8E-04	61
GO:0006913	nucleocytoplasmic transport	1,0E-04	7,4E-04	18
GO:0052547	regulation of peptidase activity	1,1E-04	7,9E-04	15
GO:0043065	positive regulation of apoptotic process	1,1E-04	8,1E-04	17

BPID	DESCRIPTION	P.VALUE	P.ADJUST	GENE NUMBER
GO:0009058	biosynthetic process	1,1E-04	8,2E-04	128
GO:0051169	nuclear transport	1,2E-04	8,5E-04	18
GO:0032103	positive regulation of response to external stimulus	1,3E-04	9,0E-04	11
GO:0043068	positive regulation of programmed cell death	1,4E-04	9,8E-04	17
GO:0030879	mammary gland development	1,4E-04	9,8E-04	10
GO:0016192	vesicle-mediated transport	1,4E-04	9,8E-04	35
GO:0007565	female pregnancy	1,4E-04	9,8E-04	11
GO:0070887	cellular response to chemical stimulus	1,5E-04	1,0E-03	57
GO:0006935	chemotaxis	1,5E-04	1,0E-03	25
GO:0042330	taxis	1,5E-04	1,0E-03	25
GO:0006612	protein targeting to membrane	1,5E-04	1,0E-03	11
GO:0010627	regulation of intracellular protein kinase cascade	1,6E-04	1,1E-03	28
GO:0000165	MAPK cascade	1,6E-04	1,1E-03	23
GO:2000145	regulation of cell motility	1,6E-04	1,1E-03	20
GO:0072657	protein localization to membrane	1,6E-04	1,1E-03	15
GO:0040012	regulation of locomotion	1,7E-04	1,1E-03	21
GO:0045785	positive regulation of cell adhesion	1,7E-04	1,1E-03	10
GO:0044248	cellular catabolic process	1,8E-04	1,1E-03	53
GO:0043408	regulation of MAPK cascade	1,8E-04	1,1E-03	21
GO:0051246	regulation of protein metabolic process	1,9E-04	1,2E-03	48
GO:0010595	positive regulation of endothelial cell migration	2,0E-04	1,2E-03	6
GO:0006954	inflammatory response	2,0E-04	1,3E-03	22
GO:0034641	cellular nitrogen compound metabolic process	2,0E-04	1,3E-03	134
GO:0044092	negative regulation of molecular function	2,1E-04	1,3E-03	27
GO:0048660	regulation of smooth muscle cell proliferation	2,1E-04	1,3E-03	7
GO:0022612	gland morphogenesis	2,2E-04	1,3E-03	9
GO:1901576	organic substance biosynthetic process	2,3E-04	1,3E-03	125
GO:0030334	regulation of cell migration	2,3E-04	1,3E-03	19
GO:0009966	regulation of signal transduction	2,3E-04	1,4E-03	57
GO:0006397	mRNA processing	2,3E-04	1,4E-03	19
GO:0043491	protein kinase B signaling cascade	2,4E-04	1,4E-03	9
GO:0009059	macromolecule biosynthetic process	2,4E-04	1,4E-03	107
GO:0044249	cellular biosynthetic process	2,4E-04	1,4E-03	123
GO:2001233	regulation of apoptotic signaling pathway	2,4E-04	1,4E-03	12
GO:0050790	regulation of catalytic activity	2,5E-04	1,4E-03	46
GO:0001666	response to hypoxia	2,5E-04	1,4E-03	13
GO:0006887	exocytosis	2,6E-04	1,5E-03	15
GO:0043405	regulation of MAP kinase activity	2,6E-04	1,5E-03	14
GO:0052548	regulation of endopeptidase activity	2,7E-04	1,5E-03	14
GO:0036293	response to decreased oxygen levels	2,8E-04	1,5E-03	13
GO:0048659	smooth muscle cell proliferation	2,8E-04	1,5E-03	7
GO:0023052	signaling	2,8E-04	1,5E-03	117
GO:0044700	single organism signaling	2,8E-04	1,5E-03	117
GO:0071310	cellular response to organic substance	2,8E-04	1,5E-03	47

BPID	DESCRIPTION	P.VALUE	P.ADJUST	GENE NUMBER
GO:0006457	protein folding	2,8E-04	1,5E-03	12
GO:0048522	positive regulation of cellular process	2,8E-04	1,5E-03	84
GO:0000184	nuclear-transcribed mRNA catabolic process, nonsense-mediated decay	3,1E-04	1,6E-03	9
GO:0023051	regulation of signaling	3,1E-04	1,6E-03	62
GO:0044403	symbiosis, encompassing mutualism through parasitism	3,1E-04	1,6E-03	27
GO:0044419	interspecies interaction between organisms	3,1E-04	1,6E-03	27
GO:0007154	cell communication	3,1E-04	1,6E-03	119
GO:0006952	defense response	3,2E-04	1,7E-03	43
GO:0044093	positive regulation of molecular function	3,3E-04	1,7E-03	37
GO:0051270	regulation of cellular component movement	3,3E-04	1,7E-03	21
GO:0010646	regulation of cell communication	3,3E-04	1,7E-03	62
GO:0002690	positive regulation of leukocyte chemotaxis	3,5E-04	1,8E-03	6
GO:0042981	regulation of apoptotic process	3,5E-04	1,8E-03	37
GO:0008284	positive regulation of cell proliferation	3,7E-04	1,8E-03	26
GO:0051094	positive regulation of developmental process	3,7E-04	1,8E-03	27
GO:0043281	regulation of cysteine-type endopeptidase activity involved in apoptotic process	3,9E-04	1,9E-03	11
GO:0043086	negative regulation of catalytic activity	3,9E-04	1,9E-03	22
GO:0043085	positive regulation of catalytic activity	3,9E-04	1,9E-03	32
GO:0010941	regulation of cell death	4,0E-04	2,0E-03	38
GO:0006464	cellular protein modification process	4,1E-04	2,0E-03	69
GO:0036211	protein modification process	4,1E-04	2,0E-03	69
GO:0010467	gene expression	4,1E-04	2,0E-03	109
GO:0032940	secretion by cell	4,2E-04	2,0E-03	27
GO:0000956	nuclear-transcribed mRNA catabolic process	4,2E-04	2,0E-03	11
GO:0043067	regulation of programmed cell death	4,3E-04	2,0E-03	37
GO:0071705	nitrogen compound transport	4,3E-04	2,0E-03	23
GO:0009057	macromolecule catabolic process	4,8E-04	2,2E-03	32
GO:0071822	protein complex subunit organization	4,8E-04	2,2E-03	37
GO:0048583	regulation of response to stimulus	5,1E-04	2,4E-03	70
GO:0051248	negative regulation of protein metabolic process	5,2E-04	2,4E-03	21
GO:0006413	translational initiation	5,2E-04	2,4E-03	10
GO:0048513	organ development	5,2E-04	2,4E-03	68
GO:0048646	anatomical structure formation involved in morphogenesis	5,3E-04	2,4E-03	30
GO:0034645	cellular macromolecule biosynthetic process	5,3E-04	2,4E-03	103
GO:0043412	macromolecule modification	5,5E-04	2,5E-03	71
GO:0010632	regulation of epithelial cell migration	5,8E-04	2,6E-03	8
GO:0051348	negative regulation of transferase activity	5,9E-04	2,6E-03	11
GO:0065003	macromolecular complex assembly	5,9E-04	2,6E-03	36
GO:0006139	nucleobase-containing compound metabolic process	6,0E-04	2,7E-03	124
GO:0048732	gland development	6,2E-04	2,7E-03	14
GO:0030595	leukocyte chemotaxis	6,2E-04	2,7E-03	9
GO:0048771	tissue remodeling	6,2E-04	2,7E-03	9
GO:2000116	regulation of cysteine-type endopeptidase activity	6,4E-04	2,8E-03	11
GO:0051049	regulation of transport	6,6E-04	2,8E-03	35

BPID	DESCRIPTION	P.VALUE	P.ADJUST	GENE NUMBER
GO:0031324	negative regulation of cellular metabolic process	6,6E-04	2,8E-03	43
GO:0048518	positive regulation of biological process	6,6E-04	2,8E-03	91
GO:0019216	regulation of lipid metabolic process	6,7E-04	2,8E-03	12
GO:0071363	cellular response to growth factor stimulus	7,0E-04	3,0E-03	23
GO:0060326	cell chemotaxis	7,0E-04	3,0E-03	10
GO:0007167	enzyme linked receptor protein signaling pathway	7,1E-04	3,0E-03	31
GO:0017038	protein import	7,1E-04	3,0E-03	13
GO:0006606	protein import into nucleus	7,2E-04	3,0E-03	12
GO:0044744	protein targeting to nucleus	7,2E-04	3,0E-03	12
GO:0006402	mRNA catabolic process	7,3E-04	3,0E-03	11
GO:0051338	regulation of transferase activity	7,3E-04	3,0E-03	25
GO:0019080	viral genome expression	7,8E-04	3,2E-03	10
GO:0008610	lipid biosynthetic process	7,8E-04	3,2E-03	22
GO:0051170	nuclear import	8,1E-04	3,3E-03	12
GO:0002688	regulation of leukocyte chemotaxis	8,2E-04	3,3E-03	6
GO:0051247	positive regulation of protein metabolic process	8,3E-04	3,3E-03	31
GO:0043409	negative regulation of MAPK cascade	8,5E-04	3,4E-03	8
GO:0034504	protein localization to nucleus	8,6E-04	3,4E-03	13
GO:0044706	multi-multicellular organism process	8,7E-04	3,5E-03	11
GO:0007165	signal transduction	8,9E-04	3,5E-03	104
GO:0001503	ossification	9,0E-04	3,5E-03	14
GO:2001235	positive regulation of apoptotic signaling pathway	9,0E-04	3,5E-03	6
GO:0070848	response to growth factor stimulus	9,3E-04	3,6E-03	23
GO:0016044	cellular membrane organization	9,4E-04	3,7E-03	25
GO:0061024	membrane organization	9,8E-04	3,8E-03	25
GO:1900180	regulation of protein localization to nucleus	1,1E-03	4,1E-03	9
GO:0043549	regulation of kinase activity	1,1E-03	4,1E-03	24
GO:0044703	multi-organism reproductive process	1,1E-03	4,1E-03	11
GO:0009056	catabolic process	1,1E-03	4,1E-03	58
GO:0050870	positive regulation of T cell activation	1,1E-03	4,3E-03	10
GO:0007243	intracellular protein kinase cascade	1,1E-03	4,3E-03	30
GO:0045598	regulation of fat cell differentiation	1,2E-03	4,4E-03	6
GO:0002685	regulation of leukocyte migration	1,2E-03	4,4E-03	7
GO:0036294	cellular response to decreased oxygen levels	1,2E-03	4,4E-03	7
GO:0071456	cellular response to hypoxia	1,2E-03	4,4E-03	7
GO:0023056	positive regulation of signaling	1,2E-03	4,5E-03	30
GO:0097190	apoptotic signaling pathway	1,2E-03	4,5E-03	17
GO:0045859	regulation of protein kinase activity	1,2E-03	4,5E-03	23
GO:0002687	positive regulation of leukocyte migration	1,3E-03	4,6E-03	6
GO:0043407	negative regulation of MAP kinase activity	1,3E-03	4,6E-03	6
GO:0033993	response to lipid	1,3E-03	4,6E-03	21
GO:2001236	regulation of extrinsic apoptotic signaling pathway	1,3E-03	4,6E-03	7
GO:0010647	positive regulation of cell communication	1,3E-03	4,6E-03	30
GO:0051336	regulation of hydrolase activity	1,3E-03	4,7E-03	27

BPID	DESCRIPTION	P.VALUE	P.ADJUST	GENE NUMBER
GO:0044265	cellular macromolecule catabolic process	1,3E-03	4,7E-03	26
GO:0033673	negative regulation of kinase activity	1,3E-03	4,8E-03	10
GO:0006415	translational termination	1,3E-03	4,8E-03	7
GO:0032368	regulation of lipid transport	1,4E-03	4,8E-03	6
GO:0031401	positive regulation of protein modification process	1,4E-03	5,0E-03	26
GO:0045597	positive regulation of cell differentiation	1,4E-03	5,0E-03	20
GO:0018279	protein N-linked glycosylation via asparagine	1,4E-03	5,0E-03	7
GO:0045766	positive regulation of angiogenesis	1,4E-03	5,0E-03	7
GO:0046483	heterocycle metabolic process	1,5E-03	5,1E-03	125
GO:0042307	positive regulation of protein import into nucleus	1,5E-03	5,1E-03	6
GO:0050727	regulation of inflammatory response	1,5E-03	5,3E-03	11
GO:0018196	peptidyl-asparagine modification	1,5E-03	5,3E-03	7
GO:0015711	organic anion transport	1,5E-03	5,3E-03	14
GO:0010631	epithelial cell migration	1,6E-03	5,3E-03	9
GO:0090132	epithelium migration	1,6E-03	5,3E-03	9
GO:0001701	in utero embryonic development	1,6E-03	5,4E-03	15
GO:0071621	granulocyte chemotaxis	1,7E-03	5,7E-03	6
GO:0010876	lipid localization	1,7E-03	5,7E-03	12
GO:0071900	regulation of protein serine/threonine kinase activity	1,7E-03	5,8E-03	16
GO:0090304	nucleic acid metabolic process	1,8E-03	5,9E-03	106
GO:0051128	regulation of cellular component organization	1,8E-03	6,1E-03	40
GO:0050729	positive regulation of inflammatory response	1,8E-03	6,1E-03	6
GO:1901575	organic substance catabolic process	1,9E-03	6,2E-03	52
GO:0019083	viral transcription	1,9E-03	6,2E-03	9
GO:0002694	regulation of leukocyte activation	1,9E-03	6,2E-03	15
GO:0090130	tissue migration	2,0E-03	6,4E-03	9
GO:0006839	mitochondrial transport	2,0E-03	6,7E-03	9
GO:0046467	membrane lipid biosynthetic process	2,1E-03	6,7E-03	7
GO:0045321	leukocyte activation	2,1E-03	6,8E-03	21
GO:0006487	protein N-linked glycosylation	2,2E-03	7,1E-03	7
GO:0009653	anatomical structure morphogenesis	2,2E-03	7,2E-03	56
GO:0072593	reactive oxygen species metabolic process	2,3E-03	7,2E-03	8
GO:1901360	organic cyclic compound metabolic process	2,3E-03	7,2E-03	128
GO:0006401	RNA catabolic process	2,3E-03	7,3E-03	11
GO:0006725	cellular aromatic compound metabolic process	2,3E-03	7,3E-03	124
GO:0048584	positive regulation of response to stimulus	2,3E-03	7,3E-03	38
GO:0009967	positive regulation of signal transduction	2,3E-03	7,3E-03	28
GO:0010951	negative regulation of endopeptidase activity	2,4E-03	7,4E-03	8
GO:0009725	response to hormone stimulus	2,4E-03	7,6E-03	23
GO:0006820	anion transport	2,4E-03	7,6E-03	15
GO:0010558	negative regulation of macromolecule biosynthetic process	2,4E-03	7,6E-03	31
GO:1902107	positive regulation of leukocyte differentiation	2,5E-03	7,6E-03	7
GO:0009101	glycoprotein biosynthetic process	2,5E-03	7,6E-03	14
GO:0001934	positive regulation of protein phosphorylation	2,5E-03	7,6E-03	21

BPID	DESCRIPTION	P.VALUE	P.ADJUST	GENE NUMBER
GO:0009888	tissue development	2,6E-03	7,9E-03	42
GO:0046890	regulation of lipid biosynthetic process	2,6E-03	8,0E-03	7
GO:0015849	organic acid transport	2,6E-03	8,0E-03	11
GO:0046942	carboxylic acid transport	2,6E-03	8,0E-03	11
GO:0030278	regulation of ossification	2,7E-03	8,1E-03	9
GO:0034655	nucleobase-containing compound catabolic process	2,7E-03	8,1E-03	26
GO:0010038	response to metal ion	2,7E-03	8,2E-03	11
GO:0010466	negative regulation of peptidase activity	2,7E-03	8,2E-03	8
GO:0019222	regulation of metabolic process	2,7E-03	8,2E-03	114
GO:0007166	cell surface receptor signaling pathway	2,7E-03	8,2E-03	64
GO:0090316	positive regulation of intracellular protein transport	2,7E-03	8,2E-03	7
GO:0044270	cellular nitrogen compound catabolic process	2,8E-03	8,2E-03	27
GO:0030036	actin cytoskeleton organization	2,8E-03	8,2E-03	17
GO:0050921	positive regulation of chemotaxis	2,9E-03	8,7E-03	6
GO:0048545	response to steroid hormone stimulus	3,0E-03	8,7E-03	12
GO:0032268	regulation of cellular protein metabolic process	3,0E-03	8,7E-03	39
GO:0006469	negative regulation of protein kinase activity	3,0E-03	8,8E-03	9
GO:0042327	positive regulation of phosphorylation	3,2E-03	9,3E-03	21
GO:0050920	regulation of chemotaxis	3,2E-03	9,4E-03	7
GO:0045765	regulation of angiogenesis	3,3E-03	9,4E-03	9
GO:0010594	regulation of endothelial cell migration	3,3E-03	9,7E-03	6
GO:0042306	regulation of protein import into nucleus	3,4E-03	9,9E-03	8
GO:0032270	positive regulation of cellular protein metabolic process	3,5E-03	9,9E-03	27

TABLE S.4. LIST OF BIOLOGICAL PROCESSESS (BP) ONTOLOGYS ENRICHED IN GENES DOWN-REGULATED IN E-CSC. p.adjust<0.01.

BPID	DESCRIPTION	P.VALUE	P.ADJUST	GENE NUMBER
GO:0008150	biological_process	5,7E-34	5,4E-31	381
GO:0009987	cellular process	3,5E-22	1,7E-19	352
GO:0044763	single-organism cellular process	4,3E-20	1,4E-17	294
GO:0044699	single-organism process	4,4E-19	1,1E-16	311
GO:0071840	cellular component organization or biogenesis	3,2E-13	6,0E-11	160
GO:0016043	cellular component organization	3,8E-13	6,0E-11	157
GO:0008152	metabolic process	3,8E-12	5,1E-10	269
GO:0065007	biological regulation	5,4E-12	6,4E-10	254
GO:0071704	organic substance metabolic process	1,4E-10	1,5E-08	255
GO:0050896	response to stimulus	2,3E-10	2,2E-08	203
GO:0009056	catabolic process	2,9E-10	2,5E-08	88
GO:0050789	regulation of biological process	5,4E-10	4,3E-08	236
GO:0042221	response to chemical stimulus	6,0E-10	4,4E-08	110
GO:0044237	cellular metabolic process	1,8E-09	1,2E-07	242
GO:0007154	cell communication	3,6E-09	2,3E-07	157
GO:0044238	primary metabolic process	4,2E-09	2,5E-07	244
GO:0044248	cellular catabolic process	5,5E-09	3,0E-07	74
GO:1901575	organic substance catabolic process	5,6E-09	3,0E-07	78
GO:0050794	regulation of cellular process	9,9E-09	5,0E-07	222
GO:0051716	cellular response to stimulus	2,8E-08	1,2E-06	161
GO:0023052	signaling	2,8E-08	1,2E-06	151
GO:0044700	single organism signaling	2,8E-08	1,2E-06	151
GO:0044403	symbiosis, encompassing mutualism through parasitism	6,5E-08	2,6E-06	39
GO:0044419	interspecies interaction between organisms	6,5E-08	2,6E-06	39
GO:0008283	cell proliferation	8,6E-08	3,3E-06	66
GO:0010033	response to organic substance	9,4E-08	3,4E-06	79
GO:0006928	cellular component movement	1,1E-07	3,8E-06	61
GO:0016032	viral process	1,9E-07	6,2E-06	36
GO:0048518	positive regulation of biological process	1,9E-07	6,2E-06	119
GO:0044710	single-organism metabolic process	2,0E-07	6,2E-06	106
GO:0044764	multi-organism cellular process	2,0E-07	6,2E-06	36
GO:0022411	cellular component disassembly	3,3E-07	9,9E-06	26
GO:0009605	response to external stimulus	4,3E-07	1,2E-05	57
GO:0007165	signal transduction	4,5E-07	1,3E-05	134
GO:0019538	protein metabolic process	6,6E-07	1,8E-05	126
GO:0048519	negative regulation of biological process	1,0E-06	2,7E-05	107
GO:0043170	macromolecule metabolic process	1,2E-06	3,1E-05	204
GO:0006996	organelle organization	1,6E-06	4,0E-05	83
GO:0032501	multicellular organismal process	1,6E-06	4,0E-05	167
GO:0070887	cellular response to chemical stimulus	1,8E-06	4,4E-05	71
GO:0042127	regulation of cell proliferation	2,2E-06	5,2E-05	51
GO:1901361	organic cyclic compound catabolic process	3,0E-06	6,7E-05	40
GO:0044707	single-multicellular organism process	3,1E-06	6,9E-05	161

BPID	DESCRIPTION	P.VALUE	P.ADJUST	GENE NUMBER
GO:0051179	localization	4,2E-06	8,9E-05	132
GO:0006950	response to stress	4,2E-06	8,9E-05	101
GO:0035556	intracellular signal transduction	5,3E-06	1,1E-04	71
GO:0050878	regulation of body fluid levels	5,6E-06	1,1E-04	31
GO:0046700	heterocycle catabolic process	6,6E-06	1,3E-04	38
GO:0051704	multi-organism process	6,7E-06	1,3E-04	54
GO:0044270	cellular nitrogen compound catabolic process	6,7E-06	1,3E-04	38
GO:0019439	aromatic compound catabolic process	7,1E-06	1,3E-04	38
GO:0030155	regulation of cell adhesion	7,3E-06	1,3E-04	19
GO:0048583	regulation of response to stimulus	7,5E-06	1,3E-04	87
GO:0009057	macromolecule catabolic process	7,8E-06	1,4E-04	41
GO:0048522	positive regulation of cellular process	8,3E-06	1,4E-04	102
GO:0006810	transport	8,3E-06	1,4E-04	110
GO:0071822	protein complex subunit organization	8,4E-06	1,4E-04	47
GO:0071310	cellular response to organic substance	8,8E-06	1,4E-04	58
GO:0044281	small molecule metabolic process	9,0E-06	1,5E-04	86
GO:0044267	cellular protein metabolic process	9,2E-06	1,5E-04	105
GO:0051234	establishment of localization	1,0E-05	1,6E-04	111
GO:0034655	nucleobase-containing compound catabolic process	1,2E-05	1,9E-04	36
GO:0009611	response to wounding	1,3E-05	1,9E-04	46
GO:0022617	extracellular matrix disassembly	1,4E-05	2,1E-04	10
GO:0048731	system development	2,0E-05	3,0E-04	108
GO:0065008	regulation of biological quality	2,2E-05	3,1E-04	93
GO:0048523	negative regulation of cellular process	2,8E-05	3,9E-04	94
GO:0007596	blood coagulation	2,8E-05	3,9E-04	26
GO:0050817	coagulation	3,1E-05	4,3E-04	26
GO:0044765	single-organism transport	3,2E-05	4,3E-04	93
GO:0007599	hemostasis	3,2E-05	4,3E-04	26
GO:0043067	regulation of programmed cell death	3,3E-05	4,4E-04	45
GO:0043933	macromolecular complex subunit organization	3,4E-05	4,4E-04	53
GO:0010941	regulation of cell death	3,5E-05	4,5E-04	46
GO:0002376	immune system process	4,0E-05	5,1E-04	69
GO:0030198	extracellular matrix organization	4,2E-05	5,2E-04	19
GO:0043062	extracellular structure organization	4,4E-05	5,4E-04	19
GO:0048584	positive regulation of response to stimulus	4,4E-05	5,4E-04	49
GO:1901565	organonitrogen compound catabolic process	4,7E-05	5,7E-04	33
GO:0070848	response to growth factor stimulus	4,8E-05	5,8E-04	29
GO:0044093	positive regulation of molecular function	5,0E-05	5,9E-04	44
GO:0040011	locomotion	5,4E-05	6,2E-04	49
GO:0042981	regulation of apoptotic process	5,4E-05	6,2E-04	44
GO:0012501	programmed cell death	6,2E-05	7,0E-04	56
GO:0044260	cellular macromolecule metabolic process	6,4E-05	7,2E-04	180
GO:0019058	viral infectious cycle	7,0E-05	7,7E-04	16
GO:0051129	negative regulation of cellular component organization	8,0E-05	8,8E-04	20

BPID	DESCRIPTION	P.VALUE	P.ADJUST	GENE NUMBER
GO:0071363	cellular response to growth factor stimulus	8,3E-05	9,0E-04	28
GO:0051246	regulation of protein metabolic process	8,9E-05	9,6E-04	55
GO:0006915	apoptotic process	9,3E-05	9,8E-04	55
GO:0060255	regulation of macromolecule metabolic process	9,6E-05	1,0E-03	123
GO:0023051	regulation of signaling	9,7E-05	1,0E-03	72
GO:0006952	defense response	9,8E-05	1,0E-03	50
GO:0008219	cell death	1,0E-04	1,0E-03	60
GO:0006413	translational initiation	1,0E-04	1,0E-03	12
GO:0010646	regulation of cell communication	1,0E-04	1,0E-03	72
GO:0016265	death	1,1E-04	1,1E-03	60
GO:0032270	positive regulation of cellular protein metabolic process	1,2E-04	1,1E-03	35
GO:0080134	regulation of response to stress	1,2E-04	1,2E-03	34
GO:0007167	enzyme linked receptor protein signaling pathway	1,2E-04	1,2E-03	37
GO:0007166	cell surface receptor signaling pathway	1,2E-04	1,2E-03	79
GO:0019222	regulation of metabolic process	1,2E-04	1,2E-03	138
GO:0044265	cellular macromolecule catabolic process	1,3E-04	1,2E-03	32
GO:0043085	positive regulation of catalytic activity	1,5E-04	1,3E-03	37
GO:0019752	carboxylic acid metabolic process	1,5E-04	1,3E-03	36
GO:0045862	positive regulation of proteolysis	1,6E-04	1,4E-03	8
GO:0007275	multicellular organismal development	1,6E-04	1,4E-03	117
GO:0006461	protein complex assembly	1,7E-04	1,5E-03	35
GO:0043436	oxoacid metabolic process	1,8E-04	1,5E-03	39
GO:0070271	protein complex biogenesis	1,8E-04	1,6E-03	35
GO:0065003	macromolecular complex assembly	1,8E-04	1,6E-03	42
GO:0050790	regulation of catalytic activity	1,9E-04	1,6E-03	52
GO:0033628	regulation of cell adhesion mediated by integrin	2,0E-04	1,7E-03	6
GO:1901700	response to oxygen-containing compound	2,1E-04	1,7E-03	40
GO:0065009	regulation of molecular function	2,1E-04	1,8E-03	62
GO:0006082	organic acid metabolic process	2,4E-04	2,0E-03	39
GO:0030154	cell differentiation	2,5E-04	2,0E-03	86
GO:0006935	chemotaxis	2,6E-04	2,1E-03	27
GO:0042330	taxis	2,6E-04	2,1E-03	27
GO:0009892	negative regulation of metabolic process	2,6E-04	2,1E-03	53
GO:0032268	regulation of cellular protein metabolic process	2,7E-04	2,1E-03	48
GO:0044767	single-organism developmental process	2,9E-04	2,2E-03	104
GO:0006508	proteolysis	2,9E-04	2,3E-03	38
GO:0048732	gland development	3,0E-04	2,3E-03	16
GO:0006900	membrane budding	3,0E-04	2,3E-03	6
GO:0051128	regulation of cellular component organization	3,0E-04	2,3E-03	48
GO:0051247	positive regulation of protein metabolic process	3,1E-04	2,3E-03	36
GO:0032787	monocarboxylic acid metabolic process	3,2E-04	2,4E-03	22
GO:0051649	establishment of localization in cell	3,2E-04	2,4E-03	63
GO:0032502	developmental process	3,3E-04	2,4E-03	128
GO:0051641	cellular localization	3,5E-04	2,5E-03	69

BPID	DESCRIPTION	P.VALUE	P.ADJUST	GENE NUMBER
GO:0048856	anatomical structure development	3,5E-04	2,5E-03	115
GO:0009653	anatomical structure morphogenesis	3,6E-04	2,5E-03	67
GO:0030162	regulation of proteolysis	3,6E-04	2,5E-03	12
GO:0042060	wound healing	3,6E-04	2,5E-03	27
GO:0070647	protein modification by small protein conjugation or removal	3,7E-04	2,6E-03	28
GO:0034641	cellular nitrogen compound metabolic process	3,8E-04	2,6E-03	151
GO:0009966	regulation of signal transduction	4,2E-04	2,9E-03	63
GO:0015718	monocarboxylic acid transport	4,3E-04	2,9E-03	9
GO:0042542	response to hydrogen peroxide	4,5E-04	3,1E-03	8
GO:0040012	regulation of locomotion	4,8E-04	3,2E-03	22
GO:0009058	biosynthetic process	4,8E-04	3,2E-03	142
GO:0080090	regulation of primary metabolic process	4,8E-04	3,2E-03	123
GO:0010604	positive regulation of macromolecule metabolic process	5,0E-04	3,3E-03	62
GO:0010605	negative regulation of macromolecule metabolic process	5,0E-04	3,3E-03	49
GO:0001944	vasculature development	5,1E-04	3,3E-03	24
GO:0010942	positive regulation of cell death	5,2E-04	3,4E-03	18
GO:0030334	regulation of cell migration	5,4E-04	3,4E-03	20
GO:1901576	organic substance biosynthetic process	5,4E-04	3,4E-03	140
GO:0033627	cell adhesion mediated by integrin	5,4E-04	3,4E-03	6
GO:0019079	viral genome replication	5,6E-04	3,5E-03	7
GO:0016050	vesicle organization	5,6E-04	3,5E-03	9
GO:0001568	blood vessel development	5,9E-04	3,7E-03	23
GO:0006807	nitrogen compound metabolic process	6,1E-04	3,7E-03	158
GO:1901606	alpha-amino acid catabolic process	6,2E-04	3,8E-03	8
GO:0043065	positive regulation of apoptotic process	6,2E-04	3,8E-03	17
GO:0022612	gland morphogenesis	6,4E-04	3,9E-03	9
GO:0019080	viral genome expression	6,5E-04	3,9E-03	11
GO:0035821	modification of morphology or physiology of other organism	6,7E-04	4,0E-03	19
GO:0031401	positive regulation of protein modification process	6,7E-04	4,0E-03	30
GO:0033993	response to lipid	7,0E-04	4,1E-03	24
GO:0031331	positive regulation of cellular catabolic process	7,3E-04	4,3E-03	9
GO:0048869	cellular developmental process	7,6E-04	4,4E-03	88
GO:0043068	positive regulation of programmed cell death	7,6E-04	4,4E-03	17
GO:0006401	RNA catabolic process	7,8E-04	4,5E-03	13
GO:0016044	cellular membrane organization	8,0E-04	4,6E-03	28
GO:0061024	membrane organization	8,4E-04	4,8E-03	28
GO:0031325	positive regulation of cellular metabolic process	8,9E-04	5,0E-03	62
GO:0051270	regulation of cellular component movement	9,2E-04	5,2E-03	22
GO:0042454	ribonucleoside catabolic process	9,3E-04	5,2E-03	20
GO:0006725	cellular aromatic compound metabolic process	9,5E-04	5,3E-03	144
GO:0031589	cell-substrate adhesion	9,6E-04	5,3E-03	13
GO:0006955	immune response	9,8E-04	5,4E-03	44
GO:0009719	response to endogenous stimulus	1,0E-03	5,5E-03	40
GO:0042176	regulation of protein catabolic process	1,0E-03	5,5E-03	11

BPID	DESCRIPTION	P.VALUE	P.ADJUST	GENE NUMBER
GO:0044085	cellular component biogenesis	1,0E-03	5,5E-03	58
GO:2000145	regulation of cell motility	1,0E-03	5,6E-03	20
GO:0051817	modification of morphology or physiology of other organism involved in symbiotic interaction	1,1E-03	5,6E-03	18
GO:0030163	protein catabolic process	1,1E-03	5,6E-03	24
GO:0016477	cell migration	1,1E-03	5,6E-03	33
GO:0031347	regulation of defense response	1,1E-03	5,6E-03	21
GO:0016192	vesicle-mediated transport	1,1E-03	5,7E-03	36
GO:0070972	protein localization to endoplasmic reticulum	1,1E-03	5,8E-03	9
GO:0043900	regulation of multi-organism process	1,1E-03	5,8E-03	13
GO:0048870	cell motility	1,2E-03	5,9E-03	35
GO:0051674	localization of cell	1,2E-03	5,9E-03	35
GO:1901360	organic cyclic compound metabolic process	1,2E-03	6,0E-03	148
GO:0048812	neuron projection morphogenesis	1,2E-03	6,2E-03	24
GO:0032388	positive regulation of intracellular transport	1,2E-03	6,2E-03	10
GO:0009893	positive regulation of metabolic process	1,2E-03	6,2E-03	64
GO:0006793	phosphorus metabolic process	1,3E-03	6,3E-03	74
GO:0022607	cellular component assembly	1,3E-03	6,3E-03	54
GO:0009164	nucleoside catabolic process	1,3E-03	6,4E-03	20
GO:0016054	organic acid catabolic process	1,3E-03	6,5E-03	12
GO:0046395	carboxylic acid catabolic process	1,3E-03	6,5E-03	12
GO:1901657	glycosyl compound metabolic process	1,3E-03	6,5E-03	25
GO:0014070	response to organic cyclic compound	1,4E-03	6,7E-03	23
GO:0071702	organic substance transport	1,4E-03	6,8E-03	62
GO:0007155	cell adhesion	1,4E-03	6,8E-03	35
GO:0019083	viral transcription	1,4E-03	6,8E-03	10
GO:0072523	purine-containing compound catabolic process	1,5E-03	6,9E-03	21
GO:0022610	biological adhesion	1,5E-03	6,9E-03	35
GO:1901658	glycosyl compound catabolic process	1,5E-03	6,9E-03	20
GO:0008284	positive regulation of cell proliferation	1,5E-03	6,9E-03	27
GO:0007169	transmembrane receptor protein tyrosine kinase signaling pathway	1,5E-03	7,0E-03	26
GO:0043412	macromolecule modification	1,5E-03	7,1E-03	78
GO:0045087	innate immune response	1,5E-03	7,1E-03	30
GO:0048514	blood vessel morphogenesis	1,6E-03	7,3E-03	20
GO:0043161	proteasomal ubiquitin-dependent protein catabolic process	1,7E-03	7,6E-03	13
GO:0006614	SRP-dependent cotranslational protein targeting to membrane	1,7E-03	7,7E-03	8
GO:0001676	long-chain fatty acid metabolic process	1,7E-03	7,7E-03	7
GO:0006152	purine nucleoside catabolic process	1,8E-03	7,9E-03	19
GO:0046130	purine ribonucleoside catabolic process	1,8E-03	7,9E-03	19
GO:0032963	collagen metabolic process	1,8E-03	8,0E-03	8
GO:0051701	interaction with host	1,9E-03	8,3E-03	18
GO:0006796	phosphate-containing compound metabolic process	1,9E-03	8,3E-03	72
GO:0048513	organ development	1,9E-03	8,3E-03	74
GO:0006414	translational elongation	1,9E-03	8,3E-03	8
GO:0006613	cotranslational protein targeting to membrane	1,9E-03	8,3E-03	8

BPID	DESCRIPTION	P.VALUE	P.ADJUST	GENE NUMBER
GO:0006612	protein targeting to membrane	1,9E-03	8,3E-03	10
GO:0002682	regulation of immune system process	2,0E-03	8,4E-03	37
GO:0006139	nucleobase-containing compound metabolic process	2,0E-03	8,4E-03	138
GO:1901564	organonitrogen compound metabolic process	2,0E-03	8,5E-03	54
GO:0045047	protein targeting to ER	2,0E-03	8,6E-03	8
GO:0009116	nucleoside metabolic process	2,0E-03	8,7E-03	24
GO:0009615	response to virus	2,1E-03	8,8E-03	14
GO:0032101	regulation of response to external stimulus	2,1E-03	8,9E-03	19
GO:0072599	establishment of protein localization to endoplasmic reticulum	2,1E-03	8,9E-03	8
GO:0006629	lipid metabolic process	2,2E-03	9,2E-03	40
GO:0045732	positive regulation of protein catabolic process	2,2E-03	9,2E-03	7
GO:0044249	cellular biosynthetic process	2,2E-03	9,2E-03	134
GO:0031324	negative regulation of cellular metabolic process	2,3E-03	9,4E-03	46
GO:0071345	cellular response to cytokine stimulus	2,3E-03	9,6E-03	19
GO:0006402	mRNA catabolic process	2,4E-03	9,6E-03	11
GO:0060548	negative regulation of cell death	2,4E-03	9,6E-03	26
GO:0031323	regulation of cellular metabolic process	2,4E-03	9,7E-03	120
GO:0006464	cellular protein modification process	2,4E-03	9,7E-03	74
GO:0036211	protein modification process	2,4E-03	9,7E-03	74
GO:0001525	angiogenesis	2,5E-03	9,8E-03	17
GO:0046483	heterocycle metabolic process	2,5E-03	9,9E-03	141
GO:0009063	cellular amino acid catabolic process	2,5E-03	1,0E-02	8
GO:0044259	multicellular organismal macromolecule metabolic process	2,5E-03	1,0E-02	8

TABLE S.5. LIST OF CELLULAR COMPONENT (CC) ONTOLOGYS ENRICHED IN GENES UP-REGULATED IN E-CSC. p.adjust<0.01.

CCID	DESCRIPTION	P.VALUE	P.ADJUST	GENE NUMBER
GO:0044444	cytoplasmic part	2,9E-10	1,3E-08	192
GO:0044424	intracellular part	3,0E-10	1,3E-08	294
GO:0044446	intracellular organelle part	3,4E-10	1,3E-08	180
GO:0005737	cytoplasm	4,2E-10	1,3E-08	239
GO:0005575	cellular_component	4,7E-10	1,3E-08	353
GO:0044422	organelle part	8,1E-10	1,8E-08	181
GO:0005622	intracellular	8,8E-10	1,8E-08	295
GO:0043226	organelle	3,4E-09	6,0E-08	264
GO:0043229	intracellular organelle	4,6E-09	7,3E-08	263
GO:0032991	macromolecular complex	7,4E-09	1,0E-07	126
GO:0043227	membrane-bounded organelle	3,5E-07	4,3E-06	239
GO:0009986	cell surface	3,7E-07	4,3E-06	29
GO:0043231	intracellular membrane-bounded organelle	4,4E-07	4,3E-06	238
GO:0044464	cell part	4,6E-07	4,3E-06	321
GO:0005623	cell	4,6E-07	4,3E-06	321
GO:0031988	membrane-bounded vesicle	5,1E-07	4,5E-06	43
GO:0031982	vesicle	9,0E-07	7,5E-06	45
GO:0042470	melanosome	2,4E-06	1,8E-05	11
GO:0048770	pigment granule	2,4E-06	1,8E-05	11
GO:0044421	extracellular region part	5,9E-06	4,2E-05	45
GO:0031410	cytoplasmic vesicle	8,8E-06	5,9E-05	40
GO:0016023	cytoplasmic membrane-bounded vesicle	9,3E-06	5,9E-05	38
GO:0043234	protein complex	6,7E-05	4,1E-04	97
GO:0005829	cytosol	8,6E-05	5,1E-04	76
GO:0030529	ribonucleoprotein complex	1,5E-04	8,7E-04	26
GO:0043228	non-membrane-bounded organelle	2,6E-04	1,4E-03	89
GO:0043232	intracellular non-membrane-bounded organelle	2,6E-04	1,4E-03	89
GO:0043233	organelle lumen	3,1E-04	1,6E-03	77
GO:0022625	cytosolic large ribosomal subunit	5,0E-04	2,4E-03	6
GO:0031974	membrane-enclosed lumen	5,4E-04	2,5E-03	77
GO:0070062	extracellular vesicular exosome	6,4E-04	2,8E-03	7
GO:0005615	extracellular space	6,5E-04	2,8E-03	31
GO:0043230	extracellular organelle	7,5E-04	3,1E-03	7
GO:0065010	extracellular membrane-bounded organelle	7,5E-04	3,1E-03	7
GO:0031983	vesicle lumen	8,8E-04	3,4E-03	7
GO:0060205	cytoplasmic membrane-bounded vesicle lumen	8,8E-04	3,4E-03	7
GO:0005681	spliceosomal complex	9,4E-04	3,6E-03	10
GO:0005694	chromosome	9,7E-04	3,6E-03	25
GO:0031091	platelet alpha granule	1,2E-03	4,2E-03	6
GO:0044427	chromosomal part	1,2E-03	4,2E-03	22
GO:0044391	ribosomal subunit	1,3E-03	4,4E-03	9
GO:0005783	endoplasmic reticulum	1,4E-03	4,7E-03	42
GO:0022626	cytosolic ribosome	2,0E-03	6,6E-03	7
GO:0031090	organelle membrane	2,2E-03	7,0E-03	68
GO:0009897	external side of plasma membrane	2,5E-03	7,7E-03	11
GO:0030141	secretory granule	2,6E-03	7,9E-03	13
GO:0070013	intracellular organelle lumen	2,7E-03	8,2E-03	71

TABLE S.6. LIST OF CELLULAR COMPONENT (CC) ONTOLOGYS ENRICHED IN GENES DOWN-REGULATED IN E-CSC. p.adjust<0.01.

CCID	DESCRIPTION	P.VALUE	P.ADJUST	GENE NUMBER
GO:0005737	cytoplasm	8,3E-20	1,2E-17	293
GO:0044444	cytoplasmic part	7,9E-16	5,6E-14	230
GO:0044424	intracellular part	1,2E-15	5,6E-14	342
GO:0005622	intracellular	5,2E-15	1,9E-13	343
GO:0005575	cellular_component	3,0E-11	6,6E-10	398
GO:0044464	cell part	3,1E-11	6,6E-10	370
GO:0005623	cell	3,2E-11	6,6E-10	370
GO:0043226	organelle	2,1E-09	3,8E-08	295
GO:0005829	cytosol	5,9E-09	9,6E-08	99
GO:0043229	intracellular organelle	9,8E-09	1,4E-07	292
GO:0043227	membrane-bounded organelle	4,7E-08	6,3E-07	270
GO:0031988	membrane-bounded vesicle	5,9E-08	7,1E-07	49
GO:0044421	extracellular region part	9,4E-08	1,1E-06	54
GO:0031982	vesicle	1,4E-07	1,5E-06	51
GO:0043231	intracellular membrane-bounded organelle	1,7E-07	1,7E-06	267
GO:0044422	organelle part	8,9E-07	8,1E-06	188
GO:0044446	intracellular organelle part	1,1E-06	9,7E-06	185
GO:0016023	cytoplasmic membrane-bounded vesicle	2,2E-06	1,8E-05	43
GO:0005615	extracellular space	5,2E-06	4,0E-05	40
GO:0031410	cytoplasmic vesicle	6,0E-06	4,4E-05	44
GO:0032991	macromolecular complex	1,8E-05	1,3E-04	125
GO:0043234	protein complex	7,7E-05	5,1E-04	107
GO:0005576	extracellular region	1,0E-04	6,3E-04	74
GO:0031012	extracellular matrix	1,8E-04	1,1E-03	22
GO:0042470	melanosome	2,4E-04	1,4E-03	9
GO:0048770	pigment granule	2,4E-04	1,4E-03	9
GO:0031594	neuromuscular junction	2,5E-04	1,4E-03	6
GO:0043233	organelle lumen	3,2E-04	1,7E-03	85
GO:0031974	membrane-enclosed lumen	5,8E-04	2,8E-03	85
GO:0012505	endomembrane system	5,9E-04	2,8E-03	56
GO:0005783	endoplasmic reticulum	8,9E-04	4,2E-03	47
GO:0044432	endoplasmic reticulum part	9,4E-04	4,2E-03	36
GO:0030141	secretory granule	9,8E-04	4,3E-03	15
GO:0048471	perinuclear region of cytoplasm	1,3E-03	5,4E-03	22
GO:0070062	extracellular vesicular exosome	1,3E-03	5,4E-03	7
GO:0043230	extracellular organelle	1,5E-03	5,9E-03	7
GO:0065010	extracellular membrane-bounded organelle	1,5E-03	5,9E-03	7
GO:0000323	lytic vacuole	2,0E-03	7,5E-03	17
GO:0005764	lysosome	2,0E-03	7,5E-03	17
GO:0031091	platelet alpha granule	2,2E-03	7,9E-03	6
GO:0005773	vacuole	2,3E-03	8,2E-03	19
GO:0070013	intracellular organelle lumen	2,4E-03	8,3E-03	79
GO:0044445	cytosolic part	2,6E-03	8,7E-03	11
GO:0000151	ubiquitin ligase complex	2,8E-03	9,1E-03	10

TABLE S.7. LIST OF MOLECULAR FUNCTION (MF) ONTOLOGYS ENRICHED IN GENES UP-REGULATED IN E-CSC. p.adjust<0.01.

MFID	DESCRIPTION	P.VALUE	P.ADJUST	GENE NUMBER
GO:0003674	molecular_function	7,0E-24	9,1E-22	319
GO:0005515	protein binding	6,6E-21	4,3E-19	215
GO:0005488	binding	9,7E-19	4,2E-17	279
GO:0003723	RNA binding	1,9E-06	6,0E-05	36
GO:0017111	nucleoside-triphosphatase activity	1,2E-05	2,2E-04	31
GO:0016462	pyrophosphatase activity	1,2E-05	2,2E-04	32
GO:0016818	hydrolase activity, acting on acid anhydrides, in phosphorus-containing anhydrides	1,2E-05	2,2E-04	32
GO:0016817	hydrolase activity, acting on acid anhydrides	1,4E-05	2,2E-04	32
GO:0005102	receptor binding	1,5E-05	2,2E-04	42
GO:0000166	nucleotide binding	2,0E-05	2,4E-04	67
GO:1901265	nucleoside phosphate binding	2,0E-05	2,4E-04	67
GO:0036094	small molecule binding	2,2E-05	2,4E-04	70
GO:0005539	glycosaminoglycan binding	5,9E-05	5,7E-04	12
GO:0003924	GTPase activity	6,1E-05	5,7E-04	14
GO:0008092	cytoskeletal protein binding	7,4E-05	6,4E-04	27
GO:0043168	anion binding	1,1E-04	9,1E-04	73
GO:0019899	enzyme binding	1,2E-04	9,1E-04	38
GO:0097367	carbohydrate derivative binding	1,6E-04	1,1E-03	12
GO:0003824	catalytic activity	1,8E-04	1,3E-03	124
GO:0016787	hydrolase activity	4,1E-04	2,7E-03	63
GO:0005126	cytokine receptor binding	4,7E-04	2,9E-03	12
GO:0032550	purine ribonucleoside binding	5,1E-04	2,9E-03	51
GO:0001883	purine nucleoside binding	5,3E-04	2,9E-03	51
GO:0032549	ribonucleoside binding	5,3E-04	2,9E-03	51
GO:0001882	nucleoside binding	6,1E-04	3,1E-03	51
GO:0032555	purine ribonucleotide binding	7,3E-04	3,6E-03	51
GO:0035639	purine ribonucleoside triphosphate binding	8,1E-04	3,9E-03	50
GO:0032553	ribonucleotide binding	8,7E-04	3,9E-03	51
GO:0019955	cytokine binding	9,1E-04	3,9E-03	6
GO:0017076	purine nucleotide binding	9,1E-04	3,9E-03	51
GO:0016887	ATPase activity	1,7E-03	7,0E-03	15
GO:0042802	identical protein binding	2,2E-03	8,8E-03	28
GO:0005525	GTP binding	2,3E-03	9,0E-03	15

TABLE S.8. LIST OF MOLECULAR FUNCTION (MF) ONTOLOGYS ENRICHED IN GENES DOWN-REGULATED IN E-CSC. p.adjust<0.01.

MFID	DESCRIPTION	P.VALUE	P.ADJUST	GENE NUMBER
GO:0003674	molecular_function	5,4E-28	8,4E-26	375
GO:0005488	binding	1,2E-17	9,5E-16	320
GO:0005515	protein binding	5,2E-16	2,7E-14	233
GO:0005198	structural molecule activity	3,6E-08	1,4E-06	36
GO:0003824	catalytic activity	9,1E-07	2,8E-05	154
GO:0043167	ion binding	3,8E-06	9,8E-05	167
GO:0005201	extracellular matrix structural constituent	5,8E-06	1,3E-04	10
GO:0043168	anion binding	4,6E-05	8,9E-04	85
GO:0005102	receptor binding	3,0E-04	5,1E-03	43
GO:0016491	oxidoreductase activity	3,5E-04	5,4E-03	29
GO:0008201	heparin binding	4,0E-04	5,5E-03	10
GO:0008289	lipid binding	4,3E-04	5,5E-03	30
GO:0035091	phosphatidylinositol binding	5,1E-04	6,1E-03	11
GO:0016616	oxidoreductase activity, acting on the CH-OH group of donors, NAD or NADP as acceptor	6,5E-04	7,2E-03	9
GO:0030234	enzyme regulator activity	7,6E-04	7,8E-03	36
GO:1901681	sulfur compound binding	8,5E-04	8,2E-03	11
GO:0016787	hydrolase activity	1,0E-03	9,1E-03	70
GO:0003924	GTPase activity	1,1E-03	9,1E-03	13

TABLE S.9. LIST OF KEGG PATHWAYS ENRICHED IN GENES DOWN-REGULATED IN D-CSC. p.adjust<0.01.

KEGGID	DESCRIPTION	P.VALUE	P.ADJUST	GENE NUMBER
hsa04141	Protein processing in endoplasmic reticulum	0,001	0,012	14
hsa05142	Chagas disease (American trypanosomiasis)	0,001	0,013	10
hsa05146	Amoebiasis	0,005	0,036	9

TABLE S10. LIST OF REACTOME PATHWAYS ENRICHED IN GENES DOWN-REGULATED IN D-CSC. p.adjust<0.01.

ID	DESCRIPTION	P.VALUE	P.ADJUST	GENE NUMBER
109582	Hemostasis	3,2E-05	2,8E-03	30
76002	Platelet activation, signaling and aggregation	6,7E-05	2,8E-03	17
114608	Platelet degranulation	9,2E-05	2,8E-03	10
76005	Response to elevated platelet cytosolic Ca2+	1,5E-04	3,4E-03	10
1566948	Elastic fibre formation	1,3E-03	2,4E-02	6

TABLE S.11. LIST OF KEGG PATHWAYS ENRICHED IN GENE TARGET OF MICRORNAS UNDEREXPRESSED IN E-CSC. p.adjust<0.05.

ID	DESCRIPTION	P.VALUE	P.ADJUST	GENE NUMBER
hsa05210	Colorectal cancer	1,7E-07	1,5E-05	17
hsa05212	Pancreatic cancer	1,1E-06	3,4E-05	17
hsa05200	Pathways in cancer	1,2E-06	3,4E-05	44
hsa05213	Endometrial cancer	1,5E-05	3,3E-04	13
hsa05219	Bladder cancer	4,3E-05	7,5E-04	11
hsa04520	Adherens junction	1,6E-04	2,4E-03	14
hsa03013	RNA transport	2,2E-04	2,7E-03	22
hsa05144	Malaria	2,8E-04	3,0E-03	11
hsa05160	Hepatitis C	3,0E-04	3,0E-03	20
hsa05218	Melanoma	4,5E-04	3,8E-03	13
hsa05223	Non-small cell lung cancer	4,8E-04	3,8E-03	11
hsa05220	Chronic myeloid leukemia	5,9E-04	4,4E-03	13
hsa04510	Focal adhesion	8,1E-04	5,5E-03	25
hsa05142	Chagas disease (American trypanosomiasis)	2,2E-03	1,4E-02	15
hsa04662	B cell receptor signaling pathway	2,5E-03	1,4E-02	12
hsa05222	Small cell lung cancer	2,5E-03	1,4E-02	13
hsa04310	Wnt signaling pathway	3,1E-03	1,6E-02	19
hsa04660	T cell receptor signaling pathway	3,2E-03	1,6E-02	15
hsa04210	Apoptosis	3,8E-03	1,7E-02	13
hsa05215	Prostate cancer	3,8E-03	1,7E-02	13
hsa04620	Toll-like receptor signaling pathway	4,9E-03	2,0E-02	14
hsa04910	Insulin signaling pathway	6,3E-03	2,4E-02	17
hsa04722	Neurotrophin signaling pathway	6,4E-03	2,4E-02	16
hsa04512	ECM-receptor interaction	7,1E-03	2,6E-02	12
hsa05214	Glioma	7,4E-03	2,6E-02	10
hsa04530	Tight junction	9,8E-03	3,2E-02	16
hsa05120	Epithelial cell signaling in Helicobacter pylori infection	1,0E-02	3,2E-02	10
hsa05221	Acute myeloid leukemia	1,0E-02	3,2E-02	9
hsa04115	p53 signaling pathway	1,1E-02	3,4E-02	10
hsa04110	Cell cycle	1,5E-02	4,5E-02	15
hsa04150	mTOR signaling pathway	1,6E-02	4,5E-02	8
hsa05412	Arrhythmogenic right ventricular cardiomyopathy (ARVC)	1,8E-02	4,9E-02	10

TABLE S.12. LIST OF REACTOME PATHWAYS ENRICHED IN GENE TARGET OF MICRORNAS UNDEREXPRESSED IN E-CSC. p.adjust<0.05.

ID	DESCRIPTION	P.VALUE	P.ADJUST	NUMBER GENES
2454202	Fc epsilon receptor (FCERI) signaling	5,0E-05	6,2E-03	25
379716	Cytosolic tRNA aminoacylation	5,0E-05	6,2E-03	8
1912408	Pre-NOTCH Transcription and Translation	1,0E-04	8,8E-03	7
1912422	Pre-NOTCH Expression and Processing	2,9E-04	1,2E-02	8
2559585	Oncogene Induced Senescence	2,9E-04	1,2E-02	8
535734	Fatty acid, triacylglycerol, and ketone body metabolism	2,9E-04	1,2E-02	20
452723	Transcriptional regulation of pluripotent stem cells	4,5E-04	1,6E-02	6
3000171	Non-integrin membrane-ECM interactions	6,6E-04	1,8E-02	11
379724	tRNA Aminoacylation	7,1E-04	1,8E-02	9
166520	Signalling by NGF	7,3E-04	1,8E-02	31
198203	PI3K/AKT activation	9,4E-04	2,1E-02	15
1266738	Developmental Biology	1,1E-03	2,1E-02	41
186797	Signaling by PDGF	1,2E-03	2,1E-02	22
1433557	Signaling by SCF-KIT	1,3E-03	2,1E-02	18
2173795	Downregulation of SMAD2/3:SMAD4 transcriptional activity	1,5E-03	2,1E-02	6
2730905	Role of LAT2/NTAL/LAB on calcium mobilization	1,7E-03	2,1E-02	15
201451	Signaling by BMP	1,9E-03	2,1E-02	6
446728	Cell junction organization	1,9E-03	2,1E-02	13
1250342	PI3K events in ERBB4 signaling	2,0E-03	2,1E-02	14
1257604	PIP3 activates AKT signaling	2,0E-03	2,1E-02	14
190926	PI-3K cascade	2,0E-03	2,1E-02	14
1963642	PI3K events in ERBB2 signaling	2,0E-03	2,1E-02	14
2219528	PI3K/AKT Signaling in Cancer	2,0E-03	2,1E-02	14
1280218	Adaptive Immune System	2,0E-03	2,1E-02	55
1168372	Downstream signaling events of B Cell Receptor (BCR)	2,1E-03	2,2E-02	20
418990	Adherens junctions interactions	2,4E-03	2,3E-02	7
2424491	DAP12 signaling	2,6E-03	2,3E-02	19
1226099	Signaling by FGFR in disease	2,7E-03	2,3E-02	20
180292	GAB1 signalosome	2,7E-03	2,3E-02	14
2262752	Cellular responses to stress	2,8E-03	2,3E-02	28
157118	Signaling by NOTCH	2,9E-03	2,4E-02	14
421270	Cell-cell junction organization	3,1E-03	2,5E-02	10
2426168	Activation of gene expression by SREBF (SREBP)	3,7E-03	2,8E-02	6
432722	Golgi Associated Vesicle Biogenesis	5,0E-03	3,5E-02	9
166054	Activated TLR4 signalling	5,1E-03	3,5E-02	13
190333	Downstream signaling of activated FGFR	5,2E-03	3,5E-02	17
186763	Downstream signal transduction	5,2E-03	3,5E-02	18
1227986	Signaling by ERBB2	5,6E-03	3,7E-02	18
983705	Signaling by the B Cell Receptor (BCR)	5,7E-03	3,7E-02	21
166016	Toll Like Receptor 4 (TLR4) Cascade	6,5E-03	4,1E-02	13
177929	Signaling by EGFR	6,7E-03	4,1E-02	19
1643713	Signaling by EGFR in Cancer	7,6E-03	4,4E-02	19
2172127	DAP12 interactions	7,6E-03	4,4E-02	19
1655829	Regulation of cholesterol biosynthesis by SREBP (SREBF)	7,7E-03	4,4E-02	7
3769402	deactivation of the beta-catenin transactivating complex	7,8E-03	4,4E-02	6
187037	NGF signalling via TRKA from the plasma membrane	8,5E-03	4,7E-02	21
2559583	Cellular Senescence	8,8E-03	4,7E-02	20

TABLE S.13. LIST OF DISEASE ONTOLOGY PATHWAYS ENRICHED IN GENE TARGET OF MICRORNAS UNDEREXPRESSED IN E-CSC. p.adjust<0.05.

ID	DESCRIPTION	P.VALUE	P.ADJUST	GENE NUMBER
DOLite:100	Cancer	6,2E-09	3,8E-07	83
DOLite:411	Pancreatitis	1,6E-04	4,8E-03	10
DOLite:33	Adenovirus infection	9,0E-04	1,8E-02	11
DOLite:31	Adenoma	4,4E-03	4,8E-02	7
DOLite:230	Hamman-Rich syndrome	5,5E-03	4,8E-02	6
DOLite:257	Hypercholesterolemia	5,5E-03	4,8E-02	6
DOLite:260	Hyperinsulinism	5,5E-03	4,8E-02	6

APPENDIX A

Volume 32, Number 9, September 2014

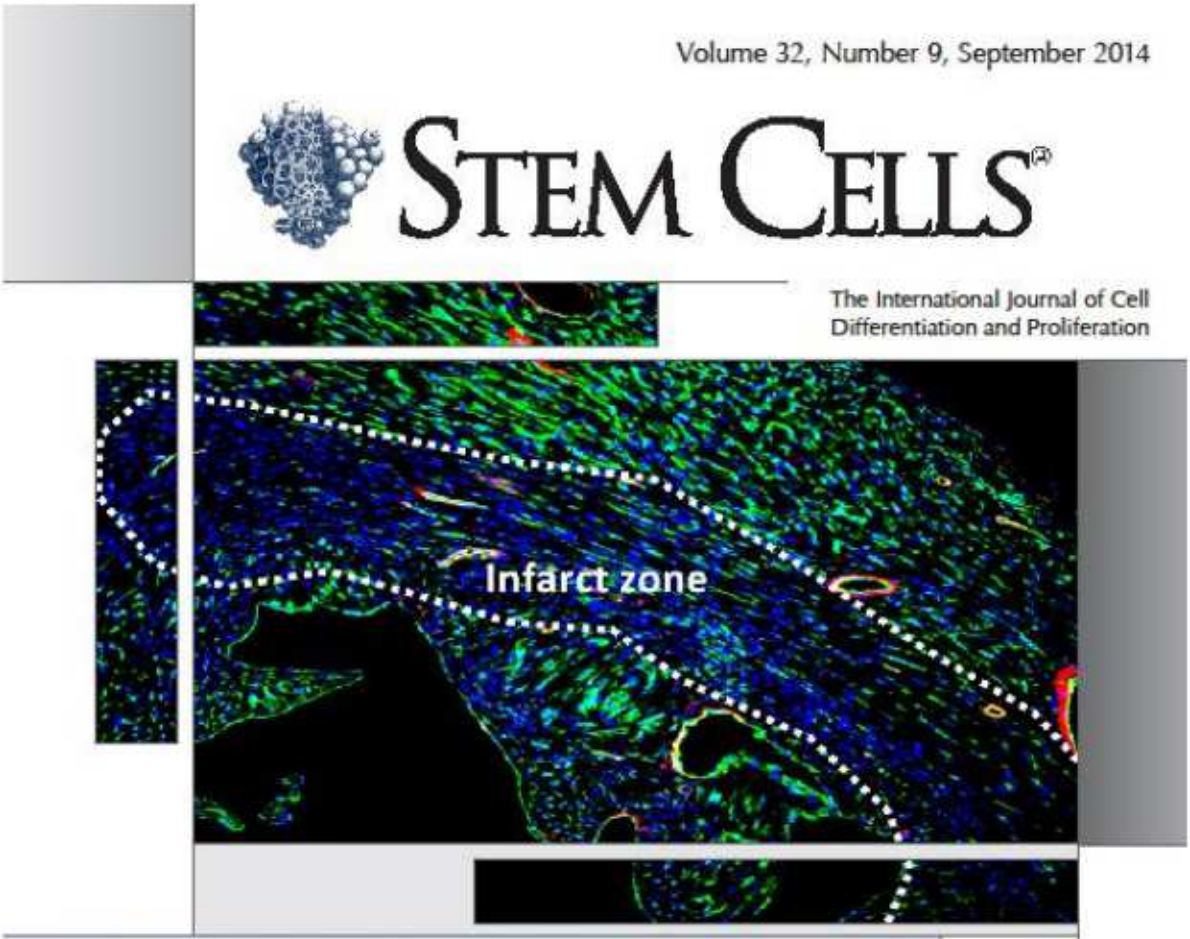

INSIDE THIS ISSUE

See Complete Table of Contents Inside

Sister Journal of STEM CELLS TRANSLATIONAL MEDICINE www.StemCellsTM.com

AlphaMed Press
WILEY-BLACKWELL
www.StemCells.com

STEM CELLS®

REGENERATIVE MEDICINE

Ex Vivo Molecular Rejuvenation Improves the Therapeutic Activity of Senescent Human Cardiac Stem Cells in a Mouse Model of Myocardial Infarction

ELISA AVOLIO, MSc[1*]; GIUSEPPE GIANFRANCESCHI, MSc[1*]; DANIELA CESSELLI, MD, PHD[1]; ANGELA CARAGNANO, MSc[1]; EMMANOUIL ATHANASAKIS, MSc[1]; RAJESH KATARE, PHD[2]; MARCO MELONI, PHD[3]; ANITA PALMA, PHD[1]; ARIANNA BARCHIESI, MSc[1]; CARLO VASCOTTO, PHD[1]; BARBARA TOFFOLETTO, MSc[1]; ELISA MAZZEGA, MSc[1]; NICOLETTA FINATO, MD[1]; GIUSEPPE ARESU, MD[4]; UGOLINO LIVI, MD[4]; COSTANZA EMANUELI, PHD[3]; GIACINTO SCOLES, PHD[1]; CARLO ALBERTO BELTRAMI, MD[1]; PAOLO MADEDDU, MD[2] & ANTONIO PAOLO BELTRAMI, MD, PHD§[1]

[1] Department of Medical and Biological Sciences, University of Udine, Udine, Italy; [2] Experimental Cardiovascular Medicine and [3] Vascular Pathology and Regeneration, Bristol Heart Institute, School of Clinical Sciences, University of Bristol, Bristol, United Kingdom; [4] Department of Experimental Medical and Clinical Sciences, University of Udine, Udine, Italy

§ Corresponding Author: Antonio Paolo Beltrami, MD, PhD; Istituto di Anatomia Patologica, Università degli Studi di Udine, C.S.L., Azienda Ospedaliero Universitaria di Udine, 33100 Udine, Italy; tel: +390432559477; fax: +390432559420; email: antonio.beltrami@uniud.it; * These authors contributed equally to the work.; Non-standard Abbreviations and Acronyms: CSC, cardiac stem cells; D-CSC, cardiac stem cells isolated from donor hearts; E-CSC, cardiac stem cells isolated from explanted, failing hearts; TR-E-CSC, E-CSC treated with rapamycin and resveratrol; SI/RO, simulated ischemia/reoxygenation injury; DDR, DNA-damage response

Received December 12, 2013; accepted for publication April 17, 2014

1066-5099/2014/$30.00/0

This article has been accepted for publication and undergone full peer review but has not been through the copyediting, typesetting, pagination and proofreading process which may lead to differences between this version and the Version of Record. Please cite this article as doi: 10.1002/stem.1728

Key words. stem cells • myocardial infarction • cellular senescence • heart failure.

ABSTRACT

Cardiac Stem Cells (CSC) from explanted decompensated hearts (E-CSC) are, with respect to those obtained from healthy donors (D-CSC), senescent and functionally impaired.

Objective. We aimed to identify alterations in signaling pathways that are associated with CSC senescence. Additionally, we investigated if pharmacological modulation of altered pathways can reduce CSC senescence in vitro and enhance their reparative ability in vivo.

Methods and results. Measurement of secreted factors showed that E-CSC release larger amounts of proinflammatory cytokine IL1ß compared with D-CSC. Using blocking antibodies, we verified that IL1ß hampers the paracrine protective action of E-CSC on cardiomyocyte viability. IL1ß acts intracrinally inducing IKKß signaling, a mechanism that via NF-κB upregulates the expression of IL1ß itself. Moreover, E-CSC show reduced levels of AMP protein kinase (AMPK) activating phosphorylation. This latter event, together with enhanced IKKß signaling, increases TORC1 activity, thereby impairing the autophagic flux and inhibiting the phosphorylation of Akt and cAMP response element–binding protein (CREB). The combined use of rapamycin and resveratrol enhanced AMPK, thereby restoring downstream signaling and reducing IL1ß secretion. These molecular corrections reduced E-CSC senescence, reestablishing their protective activity on cardiomyocytes. Moreover ex vivo treatment with rapamycin and resveratrol improved E-CSC capacity to induce cardiac repair upon injection in the mouse infarcted heart, leading to reduced cardiomyocyte senescence and apoptosis and increased abundance of endogenous c-Kit$^+$ CSC in the peri-infarct area.

Conclusion. Molecular rejuvenation of patient-derived CSC by short pharmacologic conditioning boosts their in vivo reparative abilities. This ap-

proach might prove useful for refinement of CSC-based therapies. STEM CELLS *2014; 00:000–000*

INTRODUCTION

Cellular senescence, a specialized form of permanent growth arrest caused by stressful stimuli, is a more dynamic process than we previously thought [1, 2]. Stem cells senesce too; their ageing is accelerated by cardiovascular risk factors and contributes to disruption of tissue homeostasis and repair [3, 4]. This is also true for stem cells harboured within the human heart. Cardiac Stem Cells (CSC) isolated from failing explanted hearts (E-CSC) display, with respect to those isolated from healthy donor hearts (D-CSC), a significant accumulation of senescent cells *in vitro* [5]. However, the impact that cellular senescence exerts on CSC's *in vivo* reparative abilities is still undetermined. This issue is particularly relevant, given the encouraging results of autologous CSC-based clinical trials, which showed preliminary evidence of therapeutic efficacy [6, 7]. We have previously documented that the availability of endogenous CSC is increased by stabilization of prosurvival signaling with Pim-1 genetic engineering [8] or by controlling redox state with an activator of the pentose phosphate pathway [9]. However, to the best of our knowledge, no previous study has targeted key molecular networks implicated in stem cell dysfunction.

To gain insights into ageing mechanisms, we first investigated if the secretome of E-CSC is enriched in soluble factors able both to strengthen senescence in an autocrine fashion and to induce it paracrinally on neighboring cardiac cells (i.e. senescence associated secretory phenotype -SASP-) [10]. We specifically focused on IL1ß, given the role of this interleukin in inflammation. The secretion of IL1ß is highly regulated both transcriptionally and post-transcriptionally. NF-κB binds to the IL1ß promoter stimulating the expression of the 35-kd pro-IL1ß, which is inactive and remains within the cell [11]. To be secreted, IL1ß needs to be processed by the inflammasome, a molecular platform able to activate caspase 1 (previously known as Interleukin-1 Converting Enzyme, ICE) [11]. Since impaired AMPK activation and autophagy are involved in the activation of the inflammasome and IL1ß secretion in myeloid cells [12], we compared the activation status of this pathway in D- and E-CSC. Next, we studied the molecular networks interconnected with AMPK signaling that have been involved in cell senescence [13]. Among the most prominent ones, we focused on the mTOR-signaling pathway. Intriguingly, this latter is inhibited by AMPK [13] but may be activated by IKKß in response to IL1ß stimulation [14, 15]. mTOR plays a central role in cell senescence since its inactivation converts cellular senescence (a permanent exit from the cell cycle) into quiescence (a reversible cell cycle withdrawal) [16], while its activation may determine stem cell exhaustion and aging [17]. mTOR is required for the activity of two multiprotein complexes (i.e. TORC1 and TORC2) [18]. TORC1 is rapamycin sensitive, regulates both ribosomal biogenesis, (phosphorylating the 4E-binding proteins, 4E-BPs), and protein synthesis (phosphorylating the ribosomal S6 kinase, S6K), and inhibits autophagy [19]. TORC2 is rapamycin insensitive and activates Akt *via* phosphorylation at Ser [473]. Importantly, TORC1 antagonizes TORC2, inhibiting the PI3K-Akt pathway [18]. Finally, we analyzed CREB, a transcription factor that can be phosphorylated by AMPK [20] and is involved in age-related diseases [21, 22] and in the regulation of several organism activities, ranging from metabolism -*via* Sirt1- [23] to the circadian rhythm -regulating miRNA-132- [24].

To identify a pharmacological treatment able to reverse the above-described molecular alterations and, eventually, E-CSC senescence *in vitro*, we tested rapamycin and resveratrol. The first drug was employed for its reported ability to inhibit TORC1, thus converting cellular senescence into quiescence [25]. Resveratrol was chosen both for its well-established positive effects on the cardiovascular system [26] and for its ability to suppress cell senescence, possibly reducing, either directly or indirectly, TORC1 activation [27-30].

In conclusion, we identified a drug treatment that, combining rapamycin and resveratrol, activates AMPK, reduces IL1ß secretion, and is able to attenuate E-CSC senescence in vitro. Additionally, we demonstrated that E-CSC are characterized by a reduced ability to repair myocardial infarction in vivo. Importantly, we newly show that a combined ex vivo drug-treatment with rapamycin and resveratrol restores the reparative ability of senescent CSC to control levels.

MATERIALS AND METHODS

Detailed supplemental methods are available online.

Human Cardiac Stem Cell (CSC) isolation and culture

Atrial samples were collected both from donor hearts (n=14) and from explanted hearts (n=20) of patients undergoing cardiac transplantation at the University Hospital of Udine (Supplementary Table1). The study was approved by the Ethics Committee of Udine (reference number 47831) and written consent was obtained from each patient.

Atrial fragments were first disaggregated mechanically with scalpels and then enzymatically dissociated, in a 0.25% Collagenase type II solution (Worthington, Lakewood, NJ) for 15-20 minutes at 37°C. The cell suspension was first centrifuged at 100g for 1 minute to remove myocytes and subsequently at 500g for 10 minutes and filtered through a sieve whose pore size is 40 µm (BD Falcon). Isolated cells ($1.5 \cdot 10^6$) were then plated in 100-mm dishes and cultured as in [31].

Mouse model of Myocardial Infarction (MI)

8-week-old female SCID/beige mice were used for in vivo experiments. MI was induced by occlusion of the left anterior descending coronary artery, followed by injection of CSC ($3{\cdot}10^5$ cells per heart) or vehicle at 3 different sites along the infarct border zone, as in [32]. Two weeks later, MI animals were sacrificed, hearts were arrested in diastole with $CdCl_2$ and perfusion-fixed with 10% (vol/vol) formalin. Dimensional and functional parameters were measured with a high-frequency, high-resolution echocardiography system (Vevo 770, VisualSonics, Toronto, Canada) both before coronary artery ligation (Supplementary Figure 1), and 2 weeks post-MI. Left ventricular (LV) pressure was measured with a 1.4F Millar catheter (Millar Instruments, Houston, TX) before animals were euthanized.

Histological studies

Formalin-fixed, paraffin embedded 4 µm sections were used. Scar size was evaluated on Azan-Mallory stained sections. See Supplementary Table 2 and Expanded Methods.

Western Blot and ELISA analyses

Total lysates and cell culture supernatants from D-CSC, untreated- and drug-treated- E-CSC were used for western blotting and ELISA, respectively. See Supplementary Table 2 and Expanded Methods.

Ischemia/Reperfusion injury in isolated cardiomyocytes

Cardiomyocytes isolated from 4 adult male Wistar rat hearts were subjected to Simulated Ischemia (SI) for 40 min followed by 17 hours of ReOxygenation (RO) in myocyte culture medium conditioned or not by CSC. See Expanded Methods.

Statistical analyses

Characteristics of the study population are described using means±SEM. Data were analyzed for normal distribution by Kolmogorov-Smirnov test. T-test or Mann-Whitney test, as appropriate, was used to compare continuous variables between two groups. Drug-treatment assays were analyzed by repeated measurements one-way Anova followed by Bonferroni post-test or by Kruskal-Wallis followed by Dunn's post-test, as appropriate. In order to distinguish the effects of age and pathology on CSC senescence parameters (dependent variables), a univariate general linear model was employed in which pathology was considered as fixed factor and age as covariate.

Probability values (p) less than 0.05 were considered significant. Results are shown as means±SEM.

Analyses were conducted with Prism, version 4.0c and SPSS20 for Macintosh software.

RESULTS

CSC isolated from failing hearts are senescent

CSC, dissociated from atrial fragments of both normal and pathologic human hearts, can be expanded *in vitro* as proliferating cultures of undifferentiated c-Kit positive cells (Figure 1A), cloned, and differentiated towards myocyte (Figure 1B), smooth muscle (Figure 1C), and endothelial (Figure 1D) lineages [5, 31].

Undifferentiated D- and E-CSC share a similar surface immunophenotype, with the only exception of CD49a which was more expressed by E-CSC (Figure 1E, Supplementary Figure 2) [5]. As expected, cultures of undifferentiated E-CSC are significantly enriched in cells displaying typical senescence features, such as the expression of the cyclin dependent kinase inhibitor $p16^{INK4a}$ (Figure 1F-H) or the persistence of an activated DNA damage response -DDR- (Figure 1I-K) [1]. Furthermore, E-CSC are less proliferating (Figure 1L-N, Supplementary Figure 3) and more apoptotic (Figure 1O-Q) as compared with D-CSC. Although both age and pathology may play a role in the senescence process [5], univariate linear model analysis showed that the pathological status is, in the present case study, the only independent predictor for $p16^{INK4a}$ ($p<0.0001$), DDR ($p=0.004$), Ki67 ($p<0.0001$) and TUNEL ($p=0.02$) levels in CSCs.

E-CSC release an IL1ß-rich secretome that fails to protect cardiomyocytes from ischemia reperfusion injury

In order to determine whether a SASP characterizes E-CSC, we measured, in their culture supernatants, 14 senescence-associated cytokines and growth factors. Both D- and E-CSC secrete similar levels of bFGF, HGF, VEGF, IL6, and IL8. However, IL1ß was more abundant in E-CSC culture supernatants (Figure 2A). Next, we evaluated the biological effect of the CSC secretome on the apoptosis and senescence of adult rat cardiomyocytes exposed in vitro to SI/RO, according to the protocol illustrated in Figure 2B. Post-conditioning cardiomyocytes with the D-CSC culture supernatant significantly reduced both these processes, as assessed by measurements of caspase 3/7 activity (Figure 2C) and frequency of p16 positive cells (Figure 2D, E). In contrast, the conditioned medium of E-CSC did not exert any protective effect. The addition of an anti-IL1ß antibody did not modify the anti-senescence and anti-apoptotic action of D-CSC medium (Supplementary Figure 4), but restored these properties when added to the E-CSC medium prior to incubation with cardiomyocytes (Figure 2F, G).

Altogether these results indicate that the secretion of IL1ß by E-CSC abrogates the protective effect of CSC's secretome on cardiomyocyte apoptosis and senescence.

Molecular pathways associated with E-CSC senescence and secretory phenotype: (NF)-κB, AMPK, mTOR and autophagy

Next, we evaluated the transcriptional and post-transcriptional regulation of IL1ß release. The engagement of IL1ß with its receptor (IL1R) may induce IL1ß transcription, by activating the canonical Nuclear Factor (NF)-κB signaling pathway, which involves mostly IKKß- and NEMO-dependent degradation of IκBs [15, 33] (Figure 3A). Consistently, we observed that: the levels of IKKß phosphorylated on Ser^{177} were significantly higher in patient-derived E-CSC (Figure 3B), and the addition of an anti-IL1ß antibody to E-CSC culture medium reduced IKKß phosphorylation (Figure 3C). Additionally, E-CSC expressed significantly higher levels of both pro-IL1ß and microRNA-146a, another validated NF-κB transcriptional target that may be induced by the same IL1ß [34, 35] (Figure 3D).

The post-translational level of regulation involves the activation of the inflammasome. In line, E-CSC were enriched in cleaved Caspase 1 (Figure 3E), while the addition of an inhibitor of Caspase 1 activity to E-CSC reduced the release of IL1ß (Figure 3F). E-CSC showed also a significant reduction in the levels of activated AMPK (Figure 4A). This was coupled with an enhanced activity of TORC1, as suggested by three lines of evidence: first, S6K, one TORC1 downstream target, tended to be more phosphorylated in E-CSC (Figure 4B); second, Akt, which is negatively regulated by TORC1 [18], showed decreased Ser^{473} phosphorylation in E-CSC (Figure 4C); third, autophagy, which is repressed by TORC1 [19], is consistently altered in E-CSC. In support of the last assumption, although enriched in Atg3, Atg7 and LC3BII, E-CSC showed significantly increased levels of p62, a ubiquitin-binding scaffold protein also called sequestosome 1 (SQSTM1), whose accumulation is suggestive of a block in the autophagic degradation (Figure 4D). Altogether these results indicate that the increased release of IL1ß derives from the concomitant increase in NF-κB-driven pro-IL1ß gene transcription and inflammasome activation. This latter event is likely to be related to reduced AMPK activation, increased TORC1 activity, associated with an arrest in the autophagic flux.

Besides their effects on autophagy and inflammasome activation, both AMPK and Akt can phosphorylate CREB on $Serine^{133}$, thereby activating downstream effectors [36]. Consistently, $phospho\text{-}CREB^{Ser133}$ was higher in D-CSC as compared to E-CSC (Figure 4E). While Sirt1, a downstream target of CREB signaling [23], did not differ between the two cell types, micro-RNA132 (Figure 4F, G), a transcriptional target of CREB, was significantly more abundant in D-CSC, supporting a secondary involvement of CREB signaling in E-CSC senescence.

Rapamycin and resveratrol cooperatively reduce E-CSC senescence

Subsequently, we tried both to revert E-CSC senescence and to restore the in vitro protective effects of CSC by a short *ex vivo* pharmacological treatment. To this aim, first we performed a pilot titration study, testing the acute effect of 1nM-, 10nM-, 100nM- and 1μM-rapamycin and 100nM-, 0.5μM-, 1μM- and 100μM-resveratrol on CSC death, senescence, and proliferation (Supplementary Figure 5). Based on these results, we focused on dosages of rapamycin (10nM) and resveratrol (0.5μM) that reduce the fraction of senescent E-CSC and are below the threshold of cytotoxicity (Supplementary Figure 5). Both drugs reduce the frequency of p16 positive E-CSC with no supplemental effect with drug combination (Supplementary Figure 6Ai), while the latter was required to reduce DNA damage as assessed by measurement of γH2AX in Ki67 negative cells (Supplementary Figure 6Aii). Moreover, rapamycin induced a slight increase in the fraction of apoptotic E-CSC while resveratrol produced the opposite effect; hence, the two drugs nullified each other with regard to apoptosis, when tested in combination (Supplementary Figure 6Aiii). Cell migration was seemingly improved by resveratrol only (Supplementary Figure 6Av), with no additive effect by combined treatment. This latter significantly increased the fraction of cycling cells, although a significant increase in growth speed was induced only by resveratrol (Supplementary Figure 6Aiv, B). Intriguingly, drug treatment had a minimal effect on D-CSC, mainly increasing cell proliferation (data not shown).

Concerning molecular mechanisms, the combined drug treatment resulted in a significant increase in AMPK phosphorylation (Figure 5A, B), a result that was not obtained treating CSC with the single drugs. When looking at other molecular nodes of the network, rapamycin was responsible for most of the observed effects. Specifically, it attenuated TORC1 signaling activation, as supported by the significant decrease in the phosphorylation of S6K on Thr^{389} (Figure 5A, C) and it significantly increased the phosphorylation of Akt on Ser^{473} (Figure 5A, D). In addition, although none of these two drugs modified the expression of Beclin1, Atg3, Atg7 or LC3BII (Supplementary Figure 7), rapamycin significantly reduced p62/SQSTM1 levels (Figure 5A, E), suggesting an improvement in the autophagic flux. Additionally, drug treatment, especially resveratrol, increased CREB phosphorylation on Ser^{133} (Figure 5A, F) and its downstream targets Sirt1 (Figure 5A, G) and microRNA-132 (Figure 5A, H). Last, although drug treatment did not modify either IKKß phosphorylation (Figure 5A, I) or IL1ß and micro-RNA 146a transcript levels (data not shown), it significantly reduced the levels of activated Caspase 1 (Figure 5A, J). Importantly, preconditioning of E-CSC with resveratrol and rapamycin modified the secretory profile of these cells, remarkably decreasing the release of IL1ß (Supplementary Figure 8A). As a consequence, drug treatment partly restored the

ability of E-CSC's secretome to protect cardiomyocytes exposed to SI/RO injury from senescence and apoptosis (Supplementary Figure 8B). In contrast, drug treatment had no effect on the biological activity of D-CSC's secretome (Supplementary Figure 9).

Altogether these results indicate that a three-day long pharmacologic treatment of E-CSC with a combination of rapamycin and resveratrol reduces the fraction of cells affected by cell senescence and increases their proliferative rate. These improvements are associated with increased AMPK phosphorylation. Most importantly, drug treatment reduced IL1ß secretion and restored the protective effects of E-CSC secretome.

In vitro pharmacologic pre-treatment of senescent CSC improves their in vivo reparative potential

Last we verified if CSC obtained from end-stage failing hearts favor myocardial repair as efficiently as those obtained from normal hearts. Additionally, we investigated if rescuing the senescent traits of E-CSC *ex vivo* would translate into improved outcomes of cell therapy. To this aim, infarcted, immunodeficient mice (n=70) were injected with either vehicle (n=17 mice), CSC obtained from 8 healthy human hearts (n=18 mice), or CSC obtained from 7 explanted human hearts (n=17 mice). Additionally, 5 different E-CSC lines were exposed for 3 days to resveratrol and rapamycin and 2 days later implanted in the infarct border zone, in the same animal model (n=18) described above.

Cell therapy with any of the three cell types improved cardiac output; however, D-CSC outperformed E-CSC with respect to both cardiac dimensional parameters, including LVAW and LVESV, and functional indexes, including LVESV, LVEF, LVFS and dP/dt (Figure 6A). Importantly, animals implanted with *ex vivo* conditioned E-CSC (TR-E-CSC) showed an improvement in cardiac dimensional and functional parameters compared with animals given non-conditioned media, thus matching the results obtained in animals implanted with D-CSC (Figure 6A).

Moreover, we observed a reduction in scar size only if D-CSC or drug-treated E-CSC were employed for cell therapy (Figure 6B). These results were coupled with an angiogenic boost, where D-CSC increased the tissue density of capillaries and small arterioles, while TR-E-CSC incremented the density of larger arterioles (Figure 6C). Treatment with D-CSC protected cardiomyocytes residing in the peri-infarct region (border-zone) from cell apoptosis (Figure 7A, D) and senescence (Figure 7B, I). E-CSC treatment not only lacked such a protective effect, but was also associated with an increase in myocyte apoptosis and senescence in the remote myocardium (Figure 7D, I). Importantly, rapamycin and resveratrol partially restored the positive impact of this cell type. Similar effects were also observed on the frequency of cycling myocytes residing in the border-zone (Figure 7C, E).

Cell therapy may favor myocardial repair by recruiting endogenous CSC to the site of myocardial damage [37]. Consistently, we observed a significant increase in the frequency of cardiac primitive/progenitor cells in D-CSC and TR-E-CSC injected animals, while E-CSC treatment failed in recruiting primitive cells (Figure 7F-H, J).

Altogether these data indicate that, although E-CSC show a blunted in vivo reparative ability, pharmacologic preconditioning with rapamycin and resveratrol restores the capacity of these cells to facilitate myocardial healing and to improve cardiac performance.

DISCUSSION

Previously, we have shown that a large fraction of CSC isolated from failing hearts is affected by cell senescence processes [5]. In this study, we newly identify key molecular mechanisms of this accrued senescence. This could be traced back to an altered secretome, which is remarkably enriched with IL1ß, a potent pro-inflammatory cytokine that plays a primary role in the pathophysiology of cardiovascular disease and heart failure [38]. Consistently, we provide evidence that IL1ß weakens the protective effect of E-CSC's on the apoptosis and senescence of adult cardiomyocytes exposed to SI/RO in vitro, In fact, the secretome released by senescent cells (SASP) plays a crucial role in aging and age-related pathologies, since it may reinforce senescence autocrinally or induce senescence paracrinally [39]. Importantly, recent data have demonstrated that the entire SASP process is orchestrated by IL1 secretion that follows inflammasome activation [10]. This latter is a crucial event that may be triggered by danger signals (e.g. ATP, high-mobility group protein B1, free fatty acids, islet amyloid polypeptide, and mono- sodium uric acid crystals) or by reactive oxygen species (ROS) [40]. Importantly, the accumulation of these latter has been associated, in myeloid cells, with an impairment of the autophagic flux that follows a decrease in AMPK activity [12].. Therefore, we decided to compare the status of this pathway in D- and E-CSC.

Noteworthy, we found that AMPK is less phosphorylated in E-CSC than in control D-CSC, in analogy to what observed both in cardiomyocytes isolated from spontaneously hypertensive rats or in cardiac tissue of doxorubicin-treated rats [41, 42]. Given the central role played by AMPK in regulating cell metabolism, this result is corroborated by our previous gene expression findings [5], which showed a different expression of gene sets associated with lipid-, carbohydrate-, and amino acid- metabolism between D- and E-CSC. We further demonstrate that the activation status of several molecular pathways interconnected with AMPK signaling is significantly perturbed in E-CSC. Among the most prominent ones, we show that E-CSC have an enhanced TORC1 activity, as supported by: a trend towards increased phospho-S6K^{Thr389} levels, a block in the autophagic flux (i.e. an accumulation of autophagic markers in the absence of reduced p62/SQSTM1 levels)

and a reduction in Akt activation [18]. Although several lines of evidence indicate that mTOR plays a prominent role in cellular senescence and organismal aging [43], the exact mechanism leading to the activation of TORC1 is less clear. Our results indicate that, in senescent E-CSC, AMPK may cooperate with autocrine/paracrine inflammatory signals to activate mTOR in a PI3K/Akt-independent fashion. These data are consistent with the proven ability of IL1ß to stimulate TORC1 activity via IKKß [15].

In addition, the reduced activation of Akt, observed in E-CSC, may be responsible, at least in part, for the decreased activating phosphorylation of CREB on Ser^{133} that attenuates this signaling pathway in E-CSC [36]. Our observations are consistent with the impaired CREB signaling characterizing senescent fibroblasts [44]. In senescent cells, a defective activation of CREB pathway is reportedly coupled with the altered circadian expression of clock genes, possibly *via* a mechanism that involves microRNA-132 [24, 44, 45].

Moving from these observations, we decided to use: 1) rapamycin, a TORC1 inhibitor, that may also activate AMPK [46], and 2) resveratrol for its ability to activate AMPK and possibly CREB, elevating intracellular cAMP levels [47]. We demonstrate here for the first time that rapamycin and resveratrol cooperate to activate AMPK. Rapamycin acted mostly inhibiting $S6K^{Thr389}$ phosphorylation, increasing Akt^{Ser473} phosphorylation, and reversing the autophagic arrest, thus suggesting that TORC1 was required for these events [18]. Resveratrol given at a very low dose (0.5µM) acted mainly potentiating CREB phosphorylation which, in turn, incremented microRNA-132 and Sirt1 expression. However, drug treatment did not modify IKKß phosphorylation or NF-κB signaling. This result is consistent with the observed activation of Akt upon exposure to rapamycin and resveratrol, since a complex cross-talk between these two pathways is well established [48].

Importantly, we demonstrated that rapamycin and resveratrol reduce by approximately 80% IL1ß secretion, thus restoring the ability of E-CSC's secretome to prevent cardiomyocyte death and senescence. Since NF-κB signaling was not significantly modified by drug treatment, our data suggest that rapamycin and resveratrol act reducing the activation of Caspase 1. In line with our findings, recent pilot clinical trials have started to experiment the use of IL1ß blockade (with Anakira, a recombinant human IL1Ra) both in acute myocardial infarction [49, 50] and chronic heart failure [51]. In this latter group, Anakira reduced the levels of plasmatic IL1 by nearly 90%, supporting the notion that IL1 follows a positive feedback loop in heart failure [38].

Last, we newly demonstrated that microRNA-132, a critical mediator of the beneficial effects of cell therapy that was recently described by our groups [32], although constitutively expressed by CSC, is reduced in senescent cells. Importantly, drug treatment reversed this alteration.

Although cellular senescence is strongly associated with age-related pathologies [3, 4], this cellular process plays an uncertain role in tissue repair in vivo, since it could be transiently required for proper healing of injuries by releasing paracrine factors [52]. This hypothesis has never been tested in acute MI. The present work newly documents that senescent CSC repair cardiac injury in vivo less effectively than non-senescent ones. The implantation of senescent CSC in the border zone of infarcted murine hearts does not enhance either angiogenesis or cardiomyocyte proliferation, while it increases myocyte senescence and apoptosis, suggesting that E-CSC may exert a negative paracrine effect. These results are in line with recent data obtained by Naftali-Shani and colleagues, who showed the proinflammatory properties of human Cardiac Mesenchymal Stem Cells obtained from failing hearts [53]. Strikingly, the same, IL1-based, mechanism for stem cell dysfunction was shown to impair the ability of bone marrow cells, obtained from donor infarcted mice, to repair myocardial infarction in syngeneic animals [54].

Finally, we demonstrated that the ex vivo pretreatment of E-CSC with rapamycin and resveratrol was able to restore their reparative potential to levels observed with D-CSC. This effect consisted of: an enhanced arteriolar density, decreased cardiomyocyte senescence and apoptosis, and increased recruitment of host CSC, which were anatomically mirrored by reduced infarct size and functionally corresponded by improvement of contractility indexes. However, our animal study has been possibly limited by the lack of post-MI echocardiographic baseline data and the short (2 weeks) follow-up.

The wide range of effects exerted by ex vivo preconditioning suggests that rejuvenated E-CSC act through direct and indirect means probably *via* paracrine influence on various cellular components of the infarcted heart [55]. These results indicate for the first time that the moderate effect of cell therapy using senescent CSCs can be strikingly enhanced by *ex vivo* preconditioning with anti-aging drugs. The therapeutic effect of drug-rejuvenated CSC is twofold relevant: it invigorates the use of autologous cell treatment (as results were superimposable with that of D-CSC) and represents a less risky approach with respect of genetic modification strategies.

Recently a work by Cheng and colleagues has suggested that cardiosphere-derived cells (CDC) obtained from advanced heart failure patients exhibit higher reparative potential than CDC obtained from donated hearts [56]. The observed discrepancy between our results and this work may be related to a series of technical differences. Specifically, Cheng obtained CDC from the septum, while we obtained CSC from atrial tissue, the richest source of cardiac stem cells [57]. Additionally, as normal control, we grew D-CSC from discarded atrial fragments of donated hearts collected at time of transplantation, while Cheng expanded Normal-CDC from endomyocardial biopsies of donated hearts after

their implantation in recipient, failing patients under immunosuppressive regimens.

Conclusion

Our data indicate that senescent CSC obtained from end-stage failing hearts show an impaired reparative ability in vivo. AMPK, Akt/mTOR/S6K and CREB pathways play a central role in this process. Importantly, the pathologic phenotype is not irreversible. The translational relevance of our work is supported by the fact that recently autologous CSC-based clinical trials showed preliminary evidence of therapeutic efficacy [6, 7]. Based on the present work, we provide evidence that E-CSC based cell therapy may be suboptimal. Moreover, we demonstrate that a very short pharmacologic conditioning could rejuvenate, without the requirement for the genetic manipulation of cells [58], patient-derived cells, boosting in vivo cardiac regeneration. This finding opens new avenues for optimal regenerative treatments with autologous CSC.

Acknowledgement of grants

Italian Ministry of Health, G.R.-2007-683407 (D.C.). Project ERC- 7FP SP 2 IDEAS QUIDPROQUO G.A. n. 269051. Title: "Molecular nanotechnology for life science applications: quantitative interactomics for diagnostics, proteomics and quantitative oncology" (D.C., A.P.B.). Human pericyte progenitor cells and cardiac progenitor cells for specialized stimulation of neovascularisation and cardiomyogenesis of the infarcted heart. BHF Project Grant (P.M.). National Health Research Institute, BRU grant (P.M.).

Conflict of interests

Nothing to disclose.

Author Contributions

E.A.: planned experiments, performed experiments, analysed data; G.G.: planned experiments, performed experiments, analysed data; D.C.: planned experiments, performed experiments, analysed data, wrote the article; A.C.: planned experiments, performed experiments, analysed data; E.A.: performed experiments, analysed data; R.K.: performed experiments, analysed data; M.M.: performed experiments, analysed data; A.P.: performed experiments, analysed data; A.B.: performed experiments, analysed data; C.V.: performed experiments, analysed data; B.T.: performed experiments, analysed data; E.M.: performed experiments, analysed data; N.F.: recruited patients, collected samples; G.A.: recruited patients, collected samples; U.L.: recruited patients, collected samples; C.E.: critically evaluated article draft; G.S.: critically evaluated article draft; C.A.B.: wrote article, critically evaluated article draft; P.M.: planned experiments, wrote article, critically evaluated article draft; A.P.B.: planned experiments, analysed data, wrote article.

References

1 Lawless C, Wang C, Jurk D, et al. Quantitative assessment of markers for cell senescence. Exp Gerontol 2010;45(10):772-8.

2 Baker DJ, Sedivy JM. Probing the depths of cellular senescence. J Cell Biol 2013;**202**(1):11-3.

3 Beltrami AP, Cesselli D, Beltrami CA. At the stem of youth and health. Pharmacol Ther 2011;**129**(1):3-20.

4 Beltrami AP, Cesselli D, Beltrami CA. Stem Cell Senescence and Regenerative Paradigms. Clinical Pharmacology & Therapeutics 2012;**91**(1):21-29.

5 Cesselli D, Beltrami AP, D'Aurizio F, *et al.* Effects of Age and Heart Failure on Human Cardiac Stem Cell Function. Am J Pathol 2011;**179**(1):349-366.

6 Bolli R, Chugh AR, D'Amario D, *et al.* Cardiac stem cells in patients with ischaemic cardiomyopathy (SCIPIO): initial results of a randomised phase 1 trial. Lancet 2011;**378**(9806):1847-57.

7 Makkar RR, Smith RR, Cheng K, *et al.* Intracoronary cardiosphere-derived cells for heart regeneration after myocardial infarction (CADUCEUS): a prospective, randomised phase 1 trial. Lancet 2012;**379**(9819):895-904.

8 Cottage CT, Bailey B, Fischer KM, *et al.* Cardiac progenitor cell cycling stimulated by pim-1 kinase. Circ Res 2010;**106**(5):891-901.

9 Katare R, Oikawa A, Cesselli D, *et al.* Boosting the pentose phosphate pathway restores cardiac progenitor cell availability in diabetes. Cardiovasc Res 2013;**97**(1):55-65.

10 Acosta JC, Banito A, Wuestefeld T, *et al.* A complex secretory program orchestrated by the inflammasome controls paracrine senescence. Nat Cell Biol 2013;**15**(8):978-90.

11 Pope RM, Tschopp J. The role of interleukin-1 and the inflammasome in gout: implications for therapy. Arthritis Rheum 2007;**56**(10):3183-8.

12 Wen H, Gris D, Lei Y, *et al.* Fatty acid-induced NLRP3-ASC inflammasome activation interferes with insulin signaling. Nat Immunol 2011;**12**(5):408-15.

13 Salminen A, Kaarniranta K. AMP-activated protein kinase (AMPK) controls the aging process via an integrated signaling network. Ageing Res Rev 2012;**11**(2):230-41.

14 Laplante M, Sabatini DM. mTOR signaling in growth control and disease. Cell 2012;**149**(2):274-93.

15 Lee DF, Kuo HP, Chen CT, *et al.* IKK beta suppression of TSC1 links inflammation and tumor angiogenesis via the mTOR pathway. Cell 2007;**130**(3):440-55.

16 Korotchkina LG, Leontieva OV, Bukreeva EI, *et al.* The choice between p53-induced senescence and quiescence is determined in part by the mTOR pathway. Aging (Albany NY) 2010;**2**(6):344-52.

17 Gan B, DePinho RA. mTORC1 signaling governs hematopoietic stem cell quiescence. Cell Cycle 2009;**8**(7):1003-6.

18 Huang J, Manning BD. A complex interplay between Akt, TSC2 and the two mTOR complexes. Biochem Soc Trans 2009;**37**(Pt 1):217-22.

19 Zoncu R, Efeyan A, Sabatini DM. mTOR: from growth signal integration to cancer, diabetes and ageing. Nat Rev Mol Cell Biol 2011;**12**(1):21-35.

20 Thomson DM, Herway ST, Fillmore N, *et al.* AMP-activated protein kinase phosphorylates transcription factors of the CREB family. J Appl Physiol (1985) 2008;**104**(2):429-38.

21 Hansen RT, 3rd, Zhang HT. Senescent-induced dysregulation of cAMP/CREB signaling and correlations with cognitive decline. Brain Res 2013;**1516**:93-109.

22 Fusco S, Ripoli C, Podda MV, *et al.* A role for neuronal cAMP responsive-element binding (CREB)-1 in brain responses to calorie restriction. Proc Natl Acad Sci U S A 2012;**109**(2):621-6.

23 Noriega LG, Feige JN, Canto C, *et al.* CREB and ChREBP oppositely regulate SIRT1 expression in response to energy availability. EMBO Rep 2011;**12**(10):1069-76.

24 Alvarez-Saavedra M, Antoun G, Yanagiya A, *et al.* miRNA-132 orchestrates chromatin remodeling and translational control of the circadian clock. Hum Mol Genet 2011;**20**(4):731-51.

25 Blagosklonny MV. Cell cycle arrest is not yet senescence, which is not just cell cycle arrest: terminology for TOR-driven aging. Aging (Albany NY) 2012;**4**(3):159-65.

26 Li H, Xia N, Forstermann U. Cardiovascular effects and molecular targets of resveratrol. Nitric Oxide 2012;**26**(2):102-10.

27 Demidenko ZN, Blagosklonny MV. At concentrations that inhibit mTOR, resveratrol suppresses cellular senescence. Cell Cycle 2009;**8**(12):1901-4.

28 Xia L, Wang XX, Hu XS, *et al.* Resveratrol reduces endothelial progenitor cells senescence through augmentation of telomerase activity by Akt-dependent mechanisms. Br J Pharmacol 2008;**155**(3):387-94.

29 Penumathsa SV, Thirunavukkarasu M, Zhan L, *et al.* Resveratrol enhances GLUT-4 translocation to the caveolar lipid raft fractions through AMPK/Akt/eNOS signalling pathway in diabetic myocardium. J Cell Mol Med 2008;**12**(6A):2350-61.

30 Dasgupta B, Milbrandt J. Resveratrol stimulates AMP kinase activity in neurons. Proc Natl Acad Sci U S A 2007;**104**(17):7217-22.

31 Cesselli D, D'Aurizio F, Marcon P, *et al.* Cardiac stem cell senescence. Methods Mol Biol 2013;**976**:81-97.

32 Katare R, Riu F, Mitchell K, *et al.* Transplantation of Human Pericyte Progenitor Cells Improves the Repair of Infarcted Heart Through Activation of an Angiogenic Program Involving Micro-RNA-132. Circ Res 2011;**109**(8):894-906.

33 Scheidereit C. IkappaB kinase complexes: gateways to NF-kappaB activation and transcription. Oncogene 2006;**25**(51):6685-705.

34 McMillan DH, Woeller CF, Thatcher TH, *et al.* Attenuation of inflammatory mediator production by the NF-kappaB member RelB is mediated by microRNA-146a in lung fibroblasts. Am J Physiol Lung Cell Mol Physiol 2013;**304**(11):L774-81.

35 Halkein J, Tabruyn SP, Ricke-Hoch M, *et al.* MicroRNA-146a is a therapeutic target and biomarker for peripartum cardiomyopathy. J Clin Invest 2013;**123**(5):2143-54.

36 Du K, Montminy M. CREB is a regulatory target for the protein kinase Akt/PKB. J Biol Chem 1998;**273**(49):32377-9.

37 Hatzistergos KE, Quevedo H, Oskouei BN, *et al.* Bone marrow mesenchymal stem cells stimulate cardiac stem cell proliferation and differentiation. Circ Res 2010;**107**(7):913-22.

38 Van Tassell BW, Toldo S, Mezzaroma E, *et al.* Targeting interleukin-1 in heart disease. Circulation 2013;**128**(17):1910-23.

39 Coppe JP, Desprez PY, Krtolica A, *et al.* The senescence-associated secretory phenotype: the dark side of tumor suppression. Annu Rev Pathol 2010;**5**:99-118.

40 Lee HM, Kim JJ, Kim HJ, *et al.* Upregulated NLRP3 inflammasome activation in patients with type 2 diabetes. Diabetes 2013;**62**(1):194-204.

41 Gratia S, Kay L, Potenza L, *et al.* Inhibition of AMPK signalling by doxorubicin: at the crossroads of the cardiac responses to energetic, oxidative, and genotoxic stress. Cardiovasc Res 2012;**95**(3):290-9.

42 Dolinsky VW, Chan AY, Robillard Frayne I, *et al.* Resveratrol prevents the prohypertrophic effects of oxidative stress on LKB1. Circulation 2009;**119**(12):1643-52.

43 Johnson SC, Rabinovitch PS, Kaeberlein M. mTOR is a key modulator of ageing and age-related disease. Nature 2013;**493**(7432):338-45.

44 Chin JH, Okazaki M, Frazier JS, *et al.* Impaired cAMP-mediated gene expression and decreased cAMP response element binding protein in senescent cells. Am J Physiol 1996;**271**(1 Pt 1):C362-71.

45 Kunieda T, Minamino T, Katsuno T, *et al.* Cellular senescence impairs circadian expression of clock genes in vitro and in vivo. Circ Res 2006;**98**(4):532-9.

46 Habib SL. Mechanism of activation of AMPK and upregulation of OGG1 by rapamycin in cancer cells. Oncotarget 2011;**2**(12):958-9.

47 Park SJ, Ahmad F, Philp A, *et al.* Resveratrol ameliorates aging-related metabolic phenotypes by inhibiting cAMP phosphodiesterases. Cell 2012;**148**(3):421-33.

48 Vaughan S, Jat PS. Deciphering the role of nuclear factor-kappaB in cellular senescence. Aging (Albany NY) 2011;**3**(10):913-9.

49 Abbate A, Kontos MC, Grizzard JD, *et al.* Interleukin-1 blockade with anakinra to prevent adverse cardiac remodeling after acute myocardial infarction (Virginia Commonwealth University Anakinra Remodeling Trial [VCU-ART] Pilot study). Am J Cardiol 2010;**105**(10):1371-1377 e1.

50 Abbate A, Van Tassell BW, Biondi-Zoccai G, *et al.* Effects of interleukin-1 blockade with anakinra on adverse cardiac remodeling and heart failure after acute myocardial infarction [from the Virginia Commonwealth University-Anakinra Remodeling Trial (2) (VCU-ART2) pilot study]. Am J Cardiol 2013;**111**(10):1394-400.

51 Van Tassell BW, Arena RA, Toldo S, *et al.* Enhanced interleukin-1 activity contributes to exercise intolerance in patients with systolic heart failure. PLoS One 2012;**7**(3):e33438.

52 Rodier F, Campisi J. Four faces of cellular senescence. J Cell Biol 2011;**192**(4):547-56.

53 Naftali-Shani N, Itzhaki-Alfia A, Landa-Rouben N, *et al.* The origin of human mesenchymal stromal cells dictates their reparative properties. J Am Heart Assoc 2013;**2**(5):e000253.

54 Wang X, Takagawa J, Lam VC, *et al.* Donor myocardial infarction impairs the therapeutic potential of bone marrow cells by an interleukin-1-mediated inflammatory response. Sci Transl Med 2011;**3**(100):100ra90.

55 Barile L, Lionetti V. Prometheus's heart: what lies beneath. J Cell Mol Med 2012;**16**(2):228-36.

56 Cheng K, Malliaras K, Smith RR, *et al.* Human Cardiosphere-Derived Cells From Advanced Heart Failure Patients Exhibit Augmented Functional Potency in Myocardial Repair. JACC Heart Fail 2014;**2**(1):49-61.

57 Itzhaki-Alfia A, Leor J, Raanani E, *et al.* Patient characteristics and cell source determine the number of isolated human cardiac progenitor cells. Circulation 2009;**120**(25):2559-66.

58 Mohsin S, Khan M, Nguyen J, *et al.* Rejuvenation of human cardiac progenitor cells with Pim-1 kinase. Circ Res 2013;**113**(10):1169-79.

See www.StemCells.com for supporting information available online. STEM CELLS *; 00:000–000*

Figure 1. CSC Characterization. Undifferentiated CSC express cKit (**A**, yellow) and can differentiate into cardiac myosin positive (**B**, white), smooth muscle positive (**C**, green), and CD31 positive (**D**, purple) cells. Representative Flow-Cytometry histograms of cultured D- and E-CSC (**E**) analyzed after three passages *in vitro*. Isotype control IgG-staining profiles (red histogram) are shown superimposed to specific antibody staining profiles (green histogram). Confocal images of cultured D-CSC (F, I, **L**, O) and E-CSC (G, J, M, P) illustrating: the nuclear expression of the senescence marker $p16^{INK4A}$ (arrows, red) both in D-CSC (F) and E-CSC (**G**); the presence of cells showing a persistent DDR (i.e. expressing the □H2AX histone variant -arrows, red-, in the absence of Ki67 -green-) both in D-CSC (I) and E-CSC (J); the presence of D-CSC (L) and E-CSC (M) cycling cells (Ki67, arrows, green); the presence of apoptotic D-CSC (O) and E-CSC (**P**) (TUNEL, arrows, green). Nuclei are shown by the blue fluorescence of 4', 6-diamidino-2-phenylindole (DAPI). Split channel images of the cells comprised in the squares are shown at a higher magnification in the right portion of each figure. Histograms (H, K, N, Q) represent the fraction of cells (%) positive to the above-described immuno-stainings. * $p<0.05$ vs D-CSC.

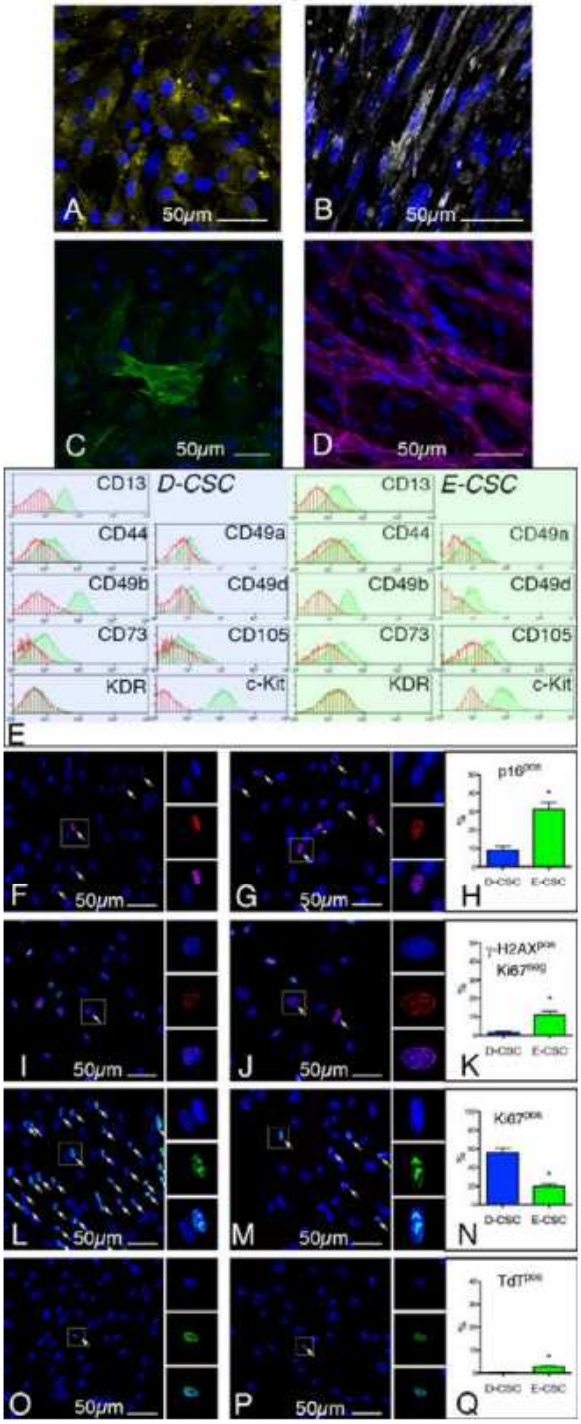
A
50μm
B
50μm
C
50μm
D
50μm
CD13
D-CSC
CD44
CD49a
CD49b
CD49d
CD73
CD105
KDR
c-Kit
CD13
E-CSC
CD44
CD49a
CD49b
CD49d
CD73
CD105
KDR
c-Kit
E
F
50μm
G
50μm
H
I
50μm
J
50μm
K
L
50μm
M
50μm
N
O
50μm
P
50μm
Q
D-CSC
E-CSC

Figure 2. E-CSC release the detrimental cytokine IL1ß. Histograms representing the quantity of pro-angiogenic growth factors (VEGF, HGF, and bFGF) and inflammatory (IL6, IL8, IL1ß) cytokines released by D-CSC and E-CSC in the culture supernatant (A). Quantities of secreted factors were normalized for the volume of the collected supernatant, CSC number and hours of incubation. (B-G) Effects of CSC culture supernatant on isolated adult rat cardiomyocytes exposed to a SI/RO protocol (B). Caspase activity was dosed by a luminescent assay and normalized with the activity of myocytes exposed to vehicle (**C**), while $p16^{pos}$ (arrows, green, D) cardiomyocytes were identified by immunofluorescence. Myocyte cytoplasm and nuclei were labeled by alpha-sarcomeric actin antibody (red) and DAPI (blue), respectively. Histograms (C, E, F, G) summarize quantitative data of the effect exerted by the culture supernatant of: D- vs E-CSC (C, E) or E-CSC added or not with anti-IL1ß antibody (F, G) on myocyte apoptosis and senescence. *, ** p<0.05 vs I, and II bar, respectively.

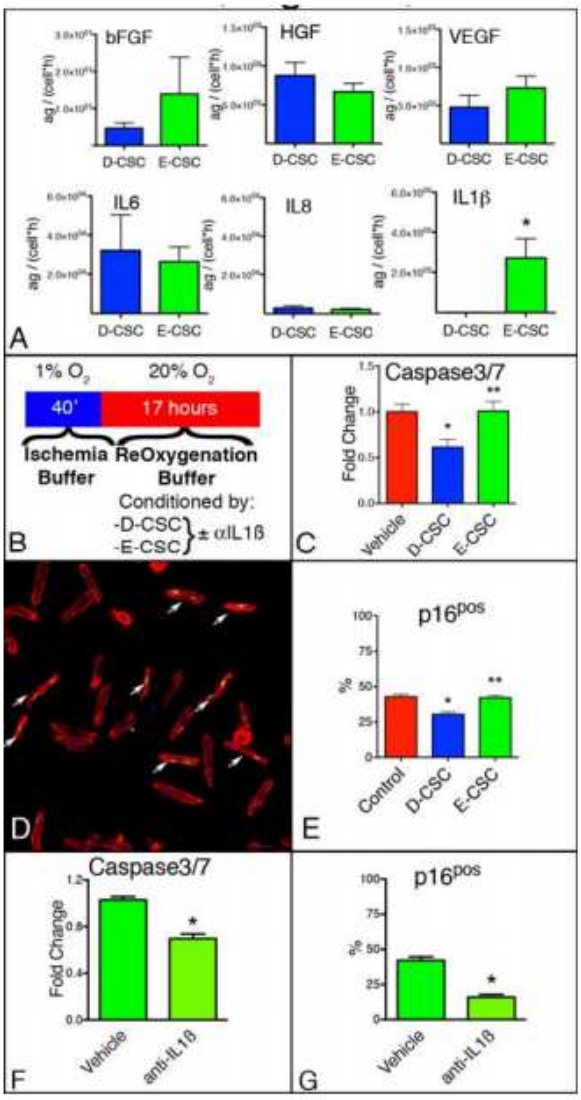

Figure 3. IL1ß secretion is associated with an autocrine/paracrine loop that requires Caspase1 activity. Described interconnections between molecular pathways that have been associated both with paracrine (IL1ß) and intrinsic cellular senescence are depicted in cartoon (**A**). Sharp end arrows indicate activation, while blunt end arrows indicate repression. (B, C, E) Representative Western Blots of cell extracts obtained from: 3 D-CSC and 3 E-CSC (**B**, **E**), and 3 E-CSC either treated or not with an anti-IL1ß antibody (**C**). Blotted proteins were incubated with antibodies directed against IKKß, phospho-IKKß^{Ser177} (**B**, **C**), and Caspase1 (**E**). Histograms (**B**, **C**, **E**) show the results of the densitometric analyses. Histograms in (**D**) show the expression levels of IL1ß mRNA and microRNA-146a in D- and E-CSC. Histograms in (**F**) show the quantity of IL1ß secreted by E-CSC either in the absence (Vehicle) or presence (Casp 1 inh) of the caspase 1 inhibitor Z-YVAD-FMK. * p<0.05 vs I bar.

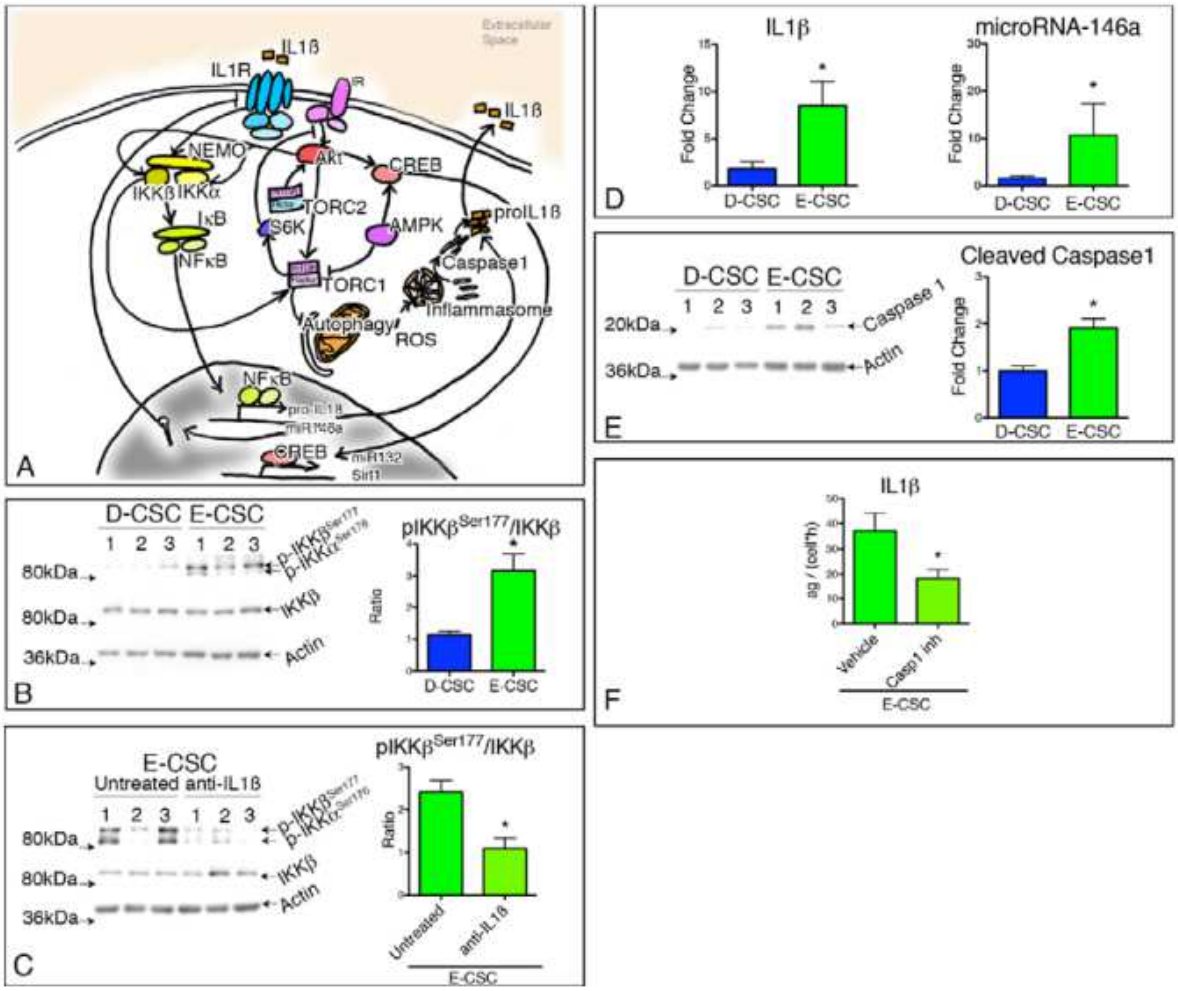

Figure 4. Senescent E-CSC show reduced AMPK, Akt, and CREB activating phosphorylation levels and increased TORC1 activity. (A-D, E, G) Representative Western Blots of cell extracts obtained from 3 D-CSC and 3 E-CSC. Blotted proteins were incubated with antibodies directed against AMPK, phospho-AMPK^{Thr172} (A), S6K, phospho-S6K^{Thr389} (B), Akt, phospho-Akt^{Ser473} (C), Atg7, p62/SQSTM1, Atg3, and LC3B (D), CREB, phospho-CREB^{Ser133} (E), and Sirt1 (G). Histograms in (A-D, E, G) show the results of the densitometric analyses. Bar graphs in (**F**) show the expression of micro-RNA 132 in D- and E-CSC. * p<0.05 vs D-CSC.

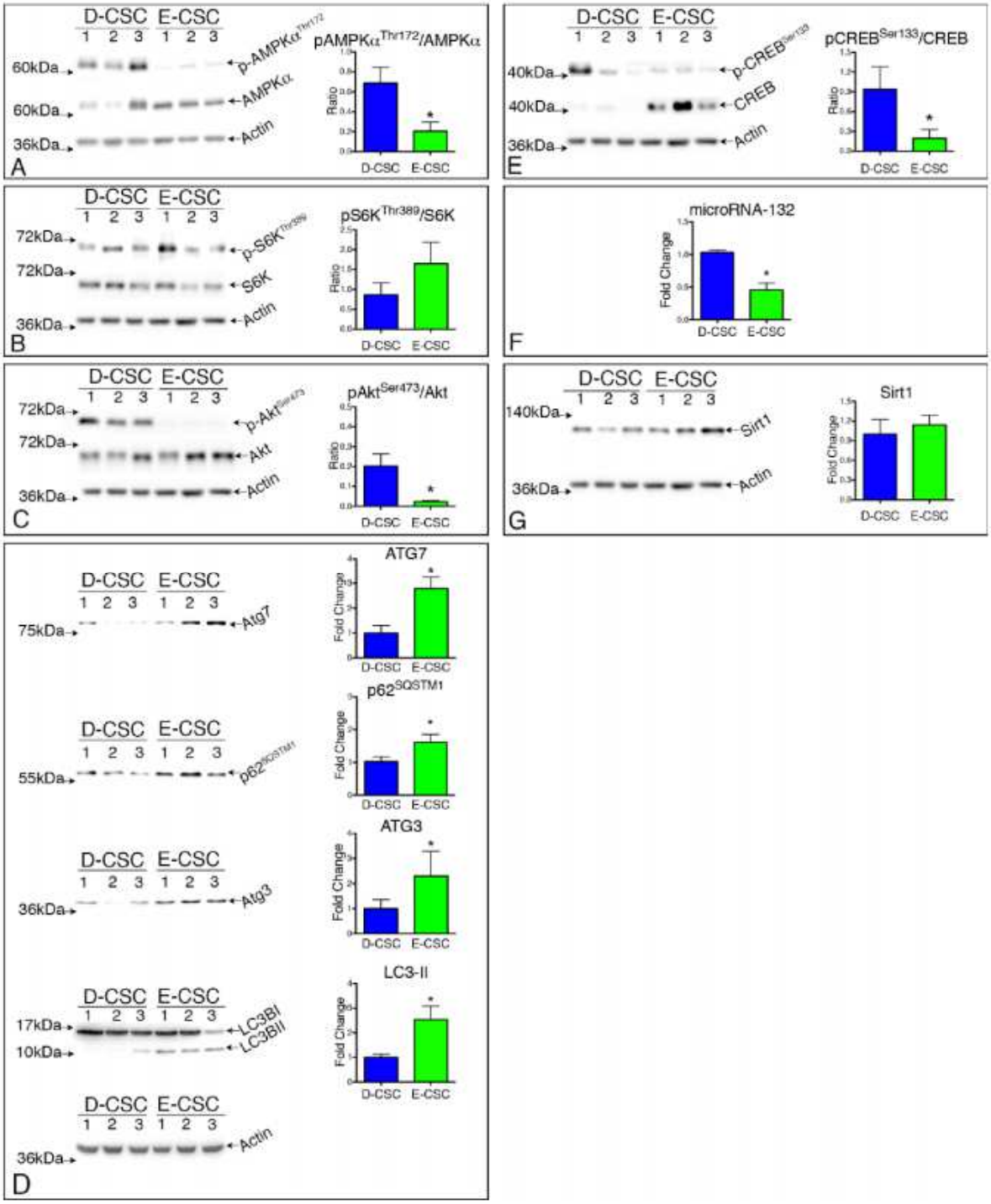

Figure 5. Effects of rapamycin and resveratrol treatment on E-CSC. Western blot of cell extracts obtained from 2 E-CSC (E-CSC #1, and E-CSC#2) showing the effect of drug treatment on AMPK, phospho-AMK^{Thr172}, S6K, phospho-S6K^{Thr389}, Akt, phospho-Akt^{Ser473}, p62/SQSTM1, CREB, phospho-CREB^{Ser133}, Sirt1, IKKß, phospho-IKKß^{Ser177}, and cleaved Caspase 1 levels (**A**). Densitometric analysis of WB and relative expression of microRNA-132 are shown in histograms (B-J). *, **, *** p<0.05 vs Vehicle, Rapamycin, and Resveratrol, respectively.

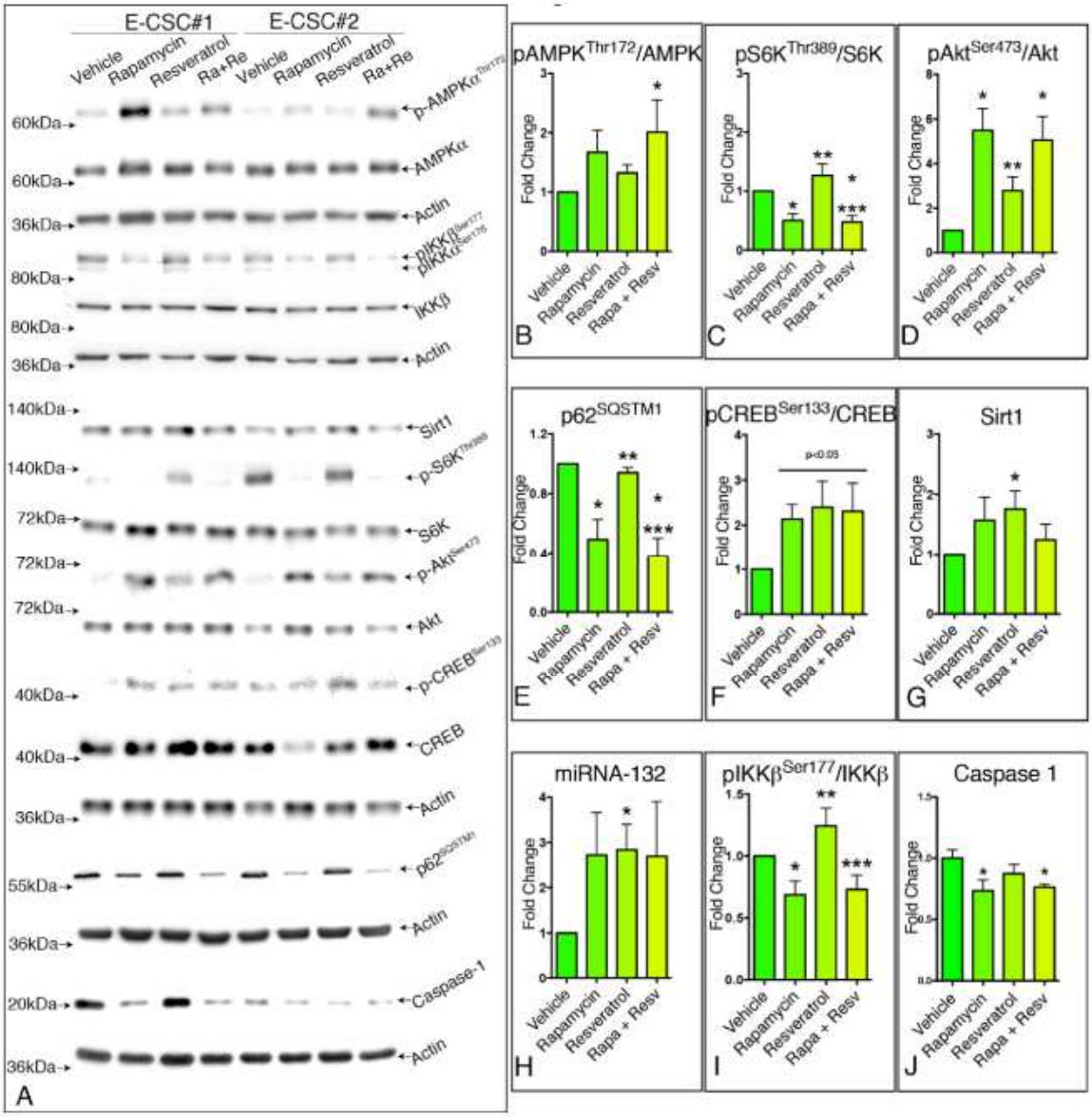

Figure 6. Pretreatment of E-CSC with rapamycin and resveratrol restores their ability to repair infarcted murine hearts. Bar graphs showing anatomic and hemodynamic parameters (A) of infarcted mouse hearts injected either with Vehicle (n=17), D-CSC (n=18), E-CSC (n=17), or drug treated (TR) E-CSC (n=18) 14 days post-MI. Trichrome staining of transverse sections of infarcted mouse hearts injected with Vehicle, D-CSC, E-CSC or TR-E-CSC (B). Bar graphs show the volume fraction of myocardium occupied by the scar. Epifluorescence images of Isolectin B4 (green), α-smooth muscle actin (red) and nuclear (blue) staining of infarcted mouse hearts injected with either Vehicle, D-CSC or E-CSC (C, upper panels). Bar graphs in the lower panels show the measured density of capillaries, small (<20μm in diameter) and large (>20μm in diameter) arterioles. Values are means±SEM. *, **, *** p<0.05 vs Vehicle, D-CSC, and E-CSC respectively. LVAW: left ventricle anterior wall thickness; LVPW: left ventricle posterior wall thickness; LVESD: left ventricle end systolic diameter; LVEDD: left ventricle end diastolic diameter; LVESV: left ventricle end systolic volume; LVEDV: left ventricle end diastolic volume; LVSV: left ventricle stroke volume; LVEF: left ventricle ejection fraction; LVFS: left ventricle fractional shortening; CO: cardiac output; s: systole; d: diastole.

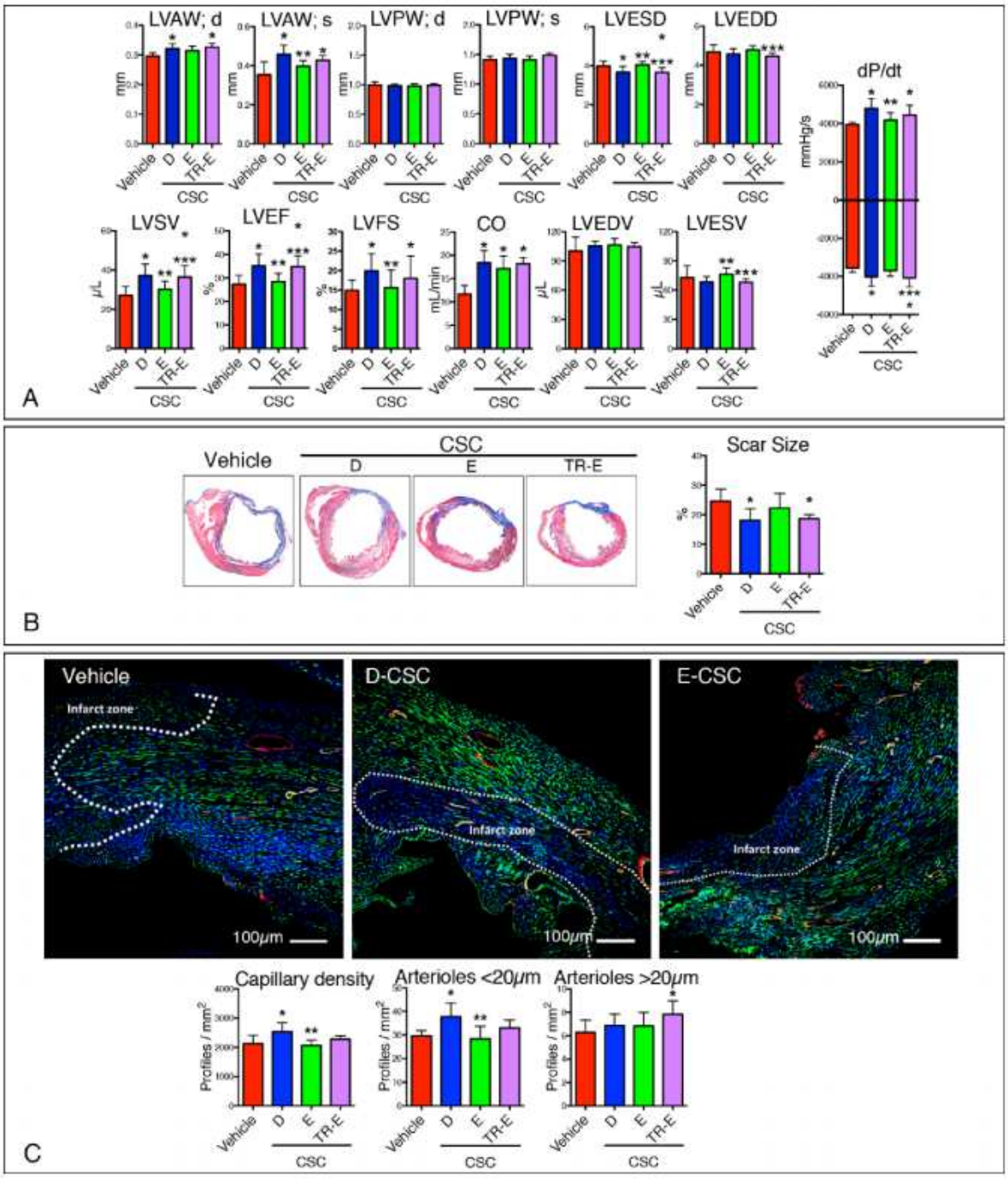

Figure 7. Rapamycin and resveratrol restore the ability of E-CSC to repair infarcted murine hearts. Confocal images of TUNEL positive (green nuclear positivity) apoptotic cardiomyocytes (**A**), senescent myocytes (H2AX nuclear positivity in Ki67 negative cells) (**B**), and cycling cardiomyocytes (Ki67 nuclear positivity, green) (C). Myocyte cytoplasm is labeled by α-sarcomeric actin (α-SA, white), while DAPI labels nuclei in blue. Histograms (**D**, **E**, **I**) summarize quantitative data. Confocal images of a representative mastocyte ($cKit^+$/mast-cell $tryptase^+$ cell, **F**), cardiac stem/progenitor cell ($cKit^+$/α-SA^- cell, **G**), and myocyte precursor ($cKit^+$/ α-SA^+ cell, **H**). cKit is depicted in red, tryptase in green, α-SA in white, nuclei in blue. Histograms summarizing quantitative data on the density of total $cKit^+$/$Tryptase^-$ cells, stem/progenitor cells and precursors in the left ventricle (**J**). *, **, *** $p<0.05$ vs Vehicle, D-CSC and E-CSC respectively.

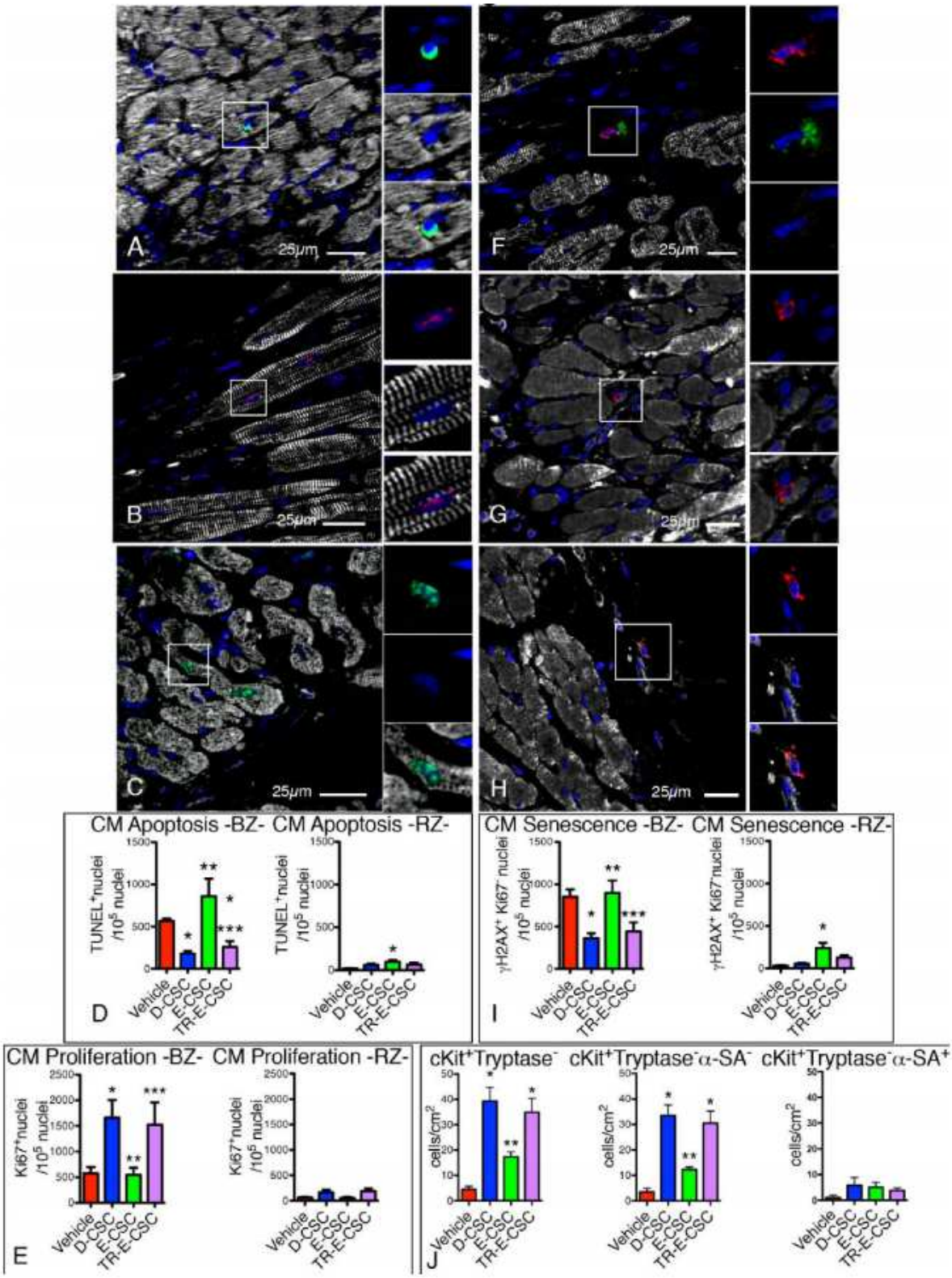
A
25μm
F
25μm
B
25μm
G
25μm
C
25μm
H
25μm
CM Apoptosis -BZ-
CM Apoptosis -RZ-
TUNEL+nuclei /10^5 nuclei
D
CM Senescence -BZ-
CM Senescence -RZ-
γH2AX+ Ki67- nuclei /10^5 nuclei
I
CM Proliferation -BZ-
CM Proliferation -RZ-
Ki67+nuclei /10^5 nuclei
E
cKit+Tryptase-
cKit+Tryptase-α-SA-
cKit+Tryptase-α-SA+
cells/cm2
J
Vehicle
D-CSC
E-CSC
TR-E-CSC

Curr Pathobiol Rep
DOI 10.1007/s40139-015-0071-5

TISSUE ENGINEERING AND REGENERATION, (BRYAN BROWN AND CHRISTOPHER DEARTH, SECTION EDITORS)

Stem Cell Senescence as the Memory of Past Injuries

Giuseppe Gianfranceschi · Giorgia Gri · Daniela Cesselli · Antonio Paolo Beltrami

Abstract Stem cell senescence may play a central role in both aging and age-related pathologies, being associated with a functional impairment of both homeostasis and the regenerative properties of tissues. The possibility to interfere with this detrimental phenomenon requires a careful elucidation of the mechanisms that initiate and maintain this cellular response. In this review, we will discuss the hypothesis that cellular senescence could be considered the biological memory of the action of different types of stressors on the organism, leading to a complex phenotype that includes both intrinsic (e.g., gene expression, chromatin organization, and cell metabolism) and extrinsic (e.g., secretome) changes. Finally, it will be shown that cell senescence blunts the regenerative ability of human cardiac stem cells and that the pharmacological inhibition of this detrimental cell process restores the functional properties of primitive cells in vivo.

This article is part of the Topical Collection on *Tissue Engineering and Regeneration*.

G. Gianfranceschi · G. Gri · D. Cesselli · A. P. Beltrami (✉)
Department of Medical and Biological Sciences, University of Udine, Udine, Italy
e-mail: antonio.beltrami@uniud.it

G. Gianfranceschi
e-mail: giuseppe.gianfranceschi@uniud.it

G. Gri
e-mail: giorgia.gri@uniud.it

D. Cesselli
e-mail: daniela.cesselli@uniud.it

A. P. Beltrami
Istituto di Anatomia Patologica, C.S.L (P01S0360), Azienda Ospedaliero Universitaria "S. Maria della Misericordia", 33100 Udine, Italy

Keywords Aging · Stem cell · Cell senescence · Cardiac stem cell · Regeneration

Introduction

In the first decade of the 2000s, a number of reports from many laboratories have demonstrated that tissue resident stem cells could be identified in almost every tissue of an organism, including those that are characterized by a low level of cell turnover, such as the heart [1]. Given that stem cell-based therapies have been successfully employed since decades to regenerate the hematopoietic system, as well as burned skin, and, more recently, the corneal epithelium [2], different stem cell types were tested for their ability to help healing injured tissues. Specifically, great expectations were pinned on the ability of stem cells to repair injuries that were considered thus far irreparable, such as myocardial infarction [3]. As a result, several clinical trials have experimented over the last years the feasibility, safety, and, in part, the efficacy of stem cell therapy for the treatment of ischemic heart disease [4]. However, this latter, that may be considered to be an age-related pathology, is associated with stem cell senescence and dysfunction and may impair the reparative abilities of primitive cells [5]. Therefore, we need to understand, at a molecular level, the relationship linking organism aging with stem cell senescence. Once identified the key pathways that lead to stem cell dysfunction, rejuvenation strategies may be tested to restore the reparative properties of aged stem cells.

The term senescence (i.e., biological aging) defines the complex, paraphysiological changes occurring in most living organisms, leading to a progressive deterioration of their ability to adequately maintain tissue homeostasis or to repair tissues after injury [6]. This decline is associated

Published online: 25 January 2015

with the occurrence of age-related diseases and, eventually, with the vulnerability to sudden health deterioration triggered by minor stressor events (i.e., frailty) [7]. In an attempt to understand why and how do we age, both evolutionary theorists and biologists have elaborated several hundred of theories [8]. Nonetheless, the dispute on whether aging is an active or passive process is still open, and a universally accepted theoretical model has not been elaborated yet [9]. However, an agreement has been reached on some commonalities among the different theories: the selection pressure decreases with age, thus limiting the counter-selection of genes that lead to senescence in late ages (mutation accumulation theory); a gene that may grant increased fitness early in life and be deleterious in advanced ages is likely to be selected (antagonistic pleiotropy theory); and multiple trade-offs exist, in organisms, between the repair and maintenance of soma and reproduction (disposable soma theory) [9]. In line, a recent study on mortality and fertility of 46 multicellular species revealed that there is a great variability of patterns among species [10••], thus prompting new, more complex models that evolve from the core of the disposable soma theory [11]. Altogether, these theories highlight the importance of the interaction between environmental stressors and costly, somatic, error-preventing, and error-correcting systems. Removal of stressors, rather than an increased organism resistance, is suspected to be responsible for the dramatic reduction in mortality that has characterized the last few generations of the humankind [11].

In order to explain senescence, we need also to uncover the biological mechanisms that lead to organism deterioration only in advanced years. Specifically, senescence is a continuous process that is not dictated by age-specific genes that are meant to be activated only in late ages but rather by the action of early acting genes (or past injuries) that may progressively alter the cell's biochemical environment, thus activating potentially noxious genetic programs [12]. Intriguingly, these processes may be cumulative and translate into a non linear increase in mortality [12].

Although a major effort was done in a recent paper to pinpoint the major hallmarks of aging [6], we will discuss here the hypothesis that cellular senescence may be considered the biological memory of the action of stressors on the organism, thus embodying many hallmarks of aging and be responsible for weakening stem cell function, debilitating both their ability to maintain tissue integrity and their capacity to regenerate damaged tissues.

Cell Senescence and Biological Aging

The term cellular senescence was first used to describe the irreversible growth arrest that characterizes diploid fibroblasts expanded in culture above a fixed number of population doublings [13]. The original intuition of these authors was that organism aging was possibly to be related to the phenomenon they detected in vitro, that was therefore named replicative senescence. Two observations corroborated this hypothesis: firstly, the end-replication problem, which determines, in human cells, the loss of 30–150 bp per round of replication [14] and secondly, the correlation between the replicative capacity of cultured cells and their average telomeric length, together with the finding that telomere erosion to the critical length of 4 kb provides a strong signal for cell cycle exit [15].

However, the relationship linking telomere length with cell proliferation and organism aging is not always a straightforward one. In fact, animals with very long telomeres (i.e., laboratory mice) develop age-related morbidities and die at a younger age than humans [16]. However, recent studies demonstrate that, in mice, telomeres shorten 100 times faster than in humans and that the assessment of the rate of telomere erosion correlates with mouse lifespan [17••]. Telomeres may also shorten independently from cell proliferation, as a consequence of mild levels of intracellular reactive oxygen species (ROS) [15]. Furthermore, when DNA damage is localized to telomeres, it cannot be repaired and locks the cells into a permanently maintained DNA damage response (DDR) [18••].

Since the first description of replicative senescence, a number of studies have demonstrated that cell senescence is a common, but rather complex, cell response to a variety of stressors, ranging from activated oncogenes to advanced glycation end-products (AGE), many of which related to aging (Fig. 1). From an evolutionary standpoint, cell senescence may have been selected to prevent the occurrence of tumors in young animals, preserving fitness, but may have a causal role in organism senescence (see below). In line, the selective ablation of senescent cells from BubR1 deficient mice reduces the age-related phenotype in several tissues of this progeroid animal [19••].

Cell Senescence as a Complex and Dynamic Phenotype

Although the essential feature of cell senescence is an irreversible withdrawal of potentially damaged cells from the cell cycle, this phenotype is composite and associated with changes in chromatin organization, gene expression, cell metabolism, and the repertoire of secreted molecules [5]. Furthermore, recent data indicate that cell senescence is a dynamic phenomenon that progresses, extends, and deepens over time [20].

Effector Mechanisms of Permanent Growth Arrest

The permanent growth arrest that characterizes senescent cells is established and maintained by at least two potent

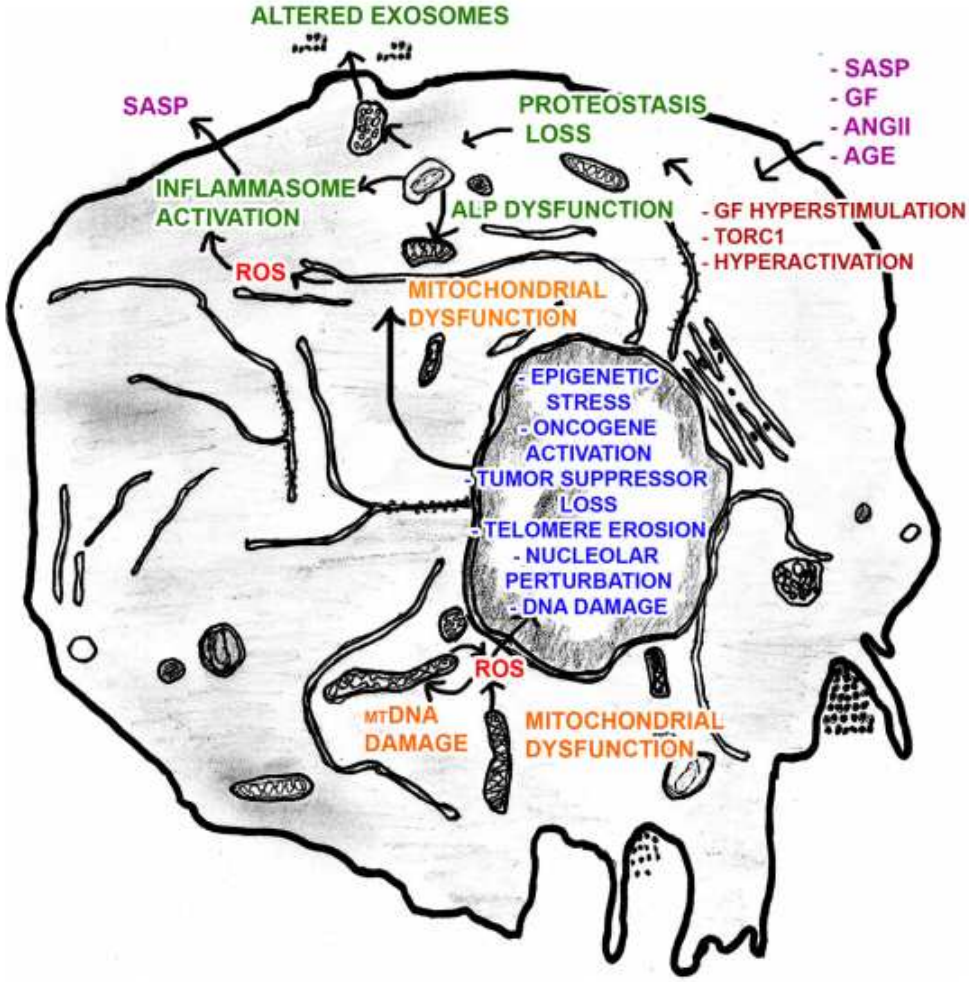

Fig. 1 Cartoon depicting cell stressors responsible for cell senescence and their respective mechanism of action (see text for details). *SASP* senescence associated secretory phenotype, *GF* growth factors, *ANGII* angiotensin II, *AGE* advanced glycation end-products, *ALP* autophagy lysosome pathway, *ROS* reactive oxygen species, *mtDNA* mitochondrial DNA

and interconnected tumor suppressor pathways, namely p53/p21^{Cip1} and p16^{INK4A}/pRb [21].

Many senescence-inducing stimuli, such as dysfunctional telomeres, DNA damage, and activated oncogenes, generate a persistent DDR, similar to that associated with double-strand DNA breaks, which is essential to establish and maintain the senescent phenotype. In fact, loss of DDR checkpoint kinases ATM or CHK2, which are able to activate p53, prevents p53/p21^{Cip1} dependent cell senescence [22]. The main features of these persistent DDR foci, also named "DNA segments with chromatin alterations reinforcing senescence" or DNA-SCARS, are their association with PML nuclear bodies, and with the activated forms of both CHK2 and p53, in the absence of the DNA repair proteins RPA and RAD51, single-stranded DNA, and DNA synthesis [23].

Senescence-inducing stimuli may also act by de-repressing the *INK4-ARF* locus. This latter encodes three potent tumor suppressors [p16^{INK4A}, p15^{INK4B}, and ARF (p14^{ARF} in humans, p19^{ARF} in mice)] that are frequently co-deleted in cancers [24]. p16^{INK4A} and p15^{INK4B} are cyclin-dependent kinase inhibitors (CDKI) that prevent the activation of Retinoblastoma (RB) family members [RB, RBL1 (p107) and RBL2 (p130)], critical regulators of DNA replication and cell cycle progression, genomic stability, apoptosis, and differentiation [25]. ARF, instead, interacts with Mdm2, promoting its degradation, thus stabilizing p53 [26]. In normal conditions, the *INK4-ARF* locus is not very expressed either in undifferentiated stem cells or in young animals, but it is induced with injury or aging [24]. Epigenetic mechanisms play a key role in maintaining the locus in a repressed state and in de-repressing it under stress conditions (see below).

Epigenetic Changes in Senescent Cells

A detailed description of the impact of epigenetics in cell senescence is beyond the scope of this review (see [27] for review). Here, we will pinpoint key epigenetic alterations (i.e., DNA methylation, histone modifications, and nuclear compartmentalization of chromatin) linked to cell senescence.

One of the main roles of DNA methylation is to silence mobile genomic elements (ME) that compose 50–75 % of human genome [28]. Intriguingly, aging, cancer, and cellular senescence are characterized by a global hypermethylation of CGIs (i.e., CpG rich sequences or CpG islands) associated with a hypo-methylation of the CpG poor areas [29, 30]. Recent data indicate that, in senescent cells, the chromatin of ME (i.e., *Alu*, SVA, and L1) is relatively more open and is associated with increased ME transcription and transposition [31•, 32•]. This phenomenon seems to be associated with a loss of stem cell self-renewal, while the stable suppression of *Alu* transcription was able to reverse the senescent phenotype [31•]. Conversely, the inactivation of MeCP2 (methyl CpG binding protein 2), a repressor of L1 expression and retrotransposition, induces cell senescence and DNA damage in Mesenchymal Stem Cells and is associated with the neurodevelopmental disorder Rett syndrome [33].

Cellular senescence is associated with profound chromatin alterations. One of the best-described ones occurs in response to telomeric shortening. Functional telomeres are characterized by epigenetic marks typical of heterochromatin and by the ability to repress natural or artificially inserted neighboring genes (effect known as telomeric position effect, TPE) [34]. The Sir2 family member SIRT6 plays a key role in TPE, maintaining transcriptional repression, while its depletion in human cells leads to telomere dysfunction with end-to-end chromosome fusions and cell senescence [35]. Last, telomere shortening is associated with loss of heterochromatin marks and a more permissive chromatin state [36]. In close proximity to telomeres are located CpG islands promoters that drive the transcription of telomeric-repeat containing RNA (TERRA), whose expression is repressed by telomere elongation [34]. Once transcribed, TERRAs are localized at telomeres, where they play important roles for the maintenance of telomere structure and integrity, DNA replication, and the regulation of both telomerase activity and the process of heterochromatinization [37].

Other examples of the primary role played by epigenetics in cell senescence are the mechanism of activation of the INK4-ARF locus, the profound chromatin modifications occurring in senescent cells that lead to the heterochromatinization of E2F target genes, and their subsequent permanent repression even in promitogenic environments [38].

Last, recent data support the existence of spatial chromatin compartments where genes are differentially regulated [39]. CTCF, a master regulator of chromatin assembly, is involved in the transcriptional regulation of genes that exert a crucial role in cellular senescence (e.g., hTERT, Rb, INK4-ARF, and p53, reviewed in [40]). Additionally, lamin B1, a component of the filamentous protein network linking the inner nuclear membrane with repressive chromatin environments, declines to undetectable levels during cell senescence [41]. This feature of senescent cells is associated with the alteration of large, contiguous stretches of chromatin, and with the modulation of senescence genes [42].

Deepening Cell Senescence and Keeping Memory of Past Injuries

Accumulating evidence reveals that senescent cells may enter a deeper stage of senescence with time. In line, the inducible ectopic expression of $p21^{Cip1}$ determines a reversible cell cycle arrest if the gene is turned off after 1 day and a senescence program that cannot be reverted if $p21^{Cip1}$ expression is abolished after 3 days [43]. Although cell senescence has been defined a persistently maintained DDR, DNA damage foci diminish in cells that have been kept in culture for 3 months after the onset of senescence. In spite of this observation, deeply senescent cells preserve their ability to activate DNA checkpoint and repair machinery in response to oxidative stress [44]. In this regard, several factors (e.g., mitochondrial dysfunction and ROS [45], senescence associated secretory phenotype (SASP, see below) [46••], HES1 [43], retrotransposition [31•, 32•], and nuclear integrity [47]) have been considered to be crucial to sustain and deepen the senescent phenotype.

The hypothesis that free radicals, mitochondrial function, and aging are strictly related processes has been postulated almost 60 years ago [48]. However, conflicting results obtained with animal models with either increased or depressed antioxidant defenses leave, at least, a certain degree of uncertainty [49, 50]. Although ROS are involved in the aging process, the cause–effect relationship between ROS production and aging is still controversial [51]. Nonetheless, ROS are very likely involved in establishing and stabilizing cell senescence, as both replicative [52] and oncogene-induced senescence [53] are associated with increased ROS production. Specifically, cell senescence, induced either by ionizing radiations or telomere uncapping, determines a loss of the mitochondrial membrane potential, a reduced ability to maintain $[Ca^{2+}]_i$ levels, and increased intracellular ROS levels that eventually lead to the constant induction of DNA damage foci containing γH2A.X [45]. Authors identified a paracrine pathway involving $p21^{Cip1}$, GADD5A, p38MAPK, and TGFβ as critical for these events [45].

A major effort has been recently devoted to the identification of molecular pathways that distinguish a reversible cell cycle exit (i.e., quiescence) from the irreversible loss of the proliferative potential that characterizes cell senescence. Rather than being a passive state, cell quiescence is actively maintained by specific molecular mechanisms,

some of which are determined by the initiating signal, while others are universally characteristic of quiescence [54]. Among these latter, the expression of HES-1 (a transcriptional repressor acting downstream of both Notch and Hedgehog signaling) is required to protect quiescent cells from differentiation and senescence [43].

Finally, cellular senescence involves, as described above, an extensive chromatin remodeling, which is characterized by an increased demethylation, transcription, and transposition of genomic ME. This event is associated with the formation of persistently activated DNA damage foci and with the loss of DNA repair efficiency in pericentric chromatin [31•]. Additionally, senescent cells display reduced histone and lamin B1 levels, loss of the integrity of the nuclear envelope, herniation of the nuclear envelope, and dispersal of chromatin fragments from nucleus to the cytoplasm, where they are delivered to and processed by the lysosomes [47].

Altogether, the emerging picture is much more dynamic than previously thought, and the demonstration that senescent cells may lose their genomic integrity with time challenges the current view of the long-term stability and viability of senescent cells.

Spreading Senescence

During the progression of cell senescence, soluble factors released by senescent cells profoundly modify the surrounding environment-inducing senescence on neighboring cells. Several cytokines, such as CXCR2 ligands, IL-6, IGFBP7, and PAI-1 have been considered to be responsible for these events [46••]. In this context, a central role for NF-κB signaling has been evoked [55], but the entire picture was clarified only recently, demonstrating that paracrine senescence is a full senescence process that relies on the activation of $p16^{INK4A}$, $p21^{Cip1}$, and p53 and that can be partially abolished employing VEGF/Flt3, TGFB1R, and CCR2 inhibitors [46••]. Moreover, authors identified IL1R activation as the most potent inducer of autocrine senescence and as the coordinator of the expression of SASP [46••].

Inflammation and Aging

Age-related disorders such as cancer, diabetes, atherosclerosis, and osteoarthritis are always associated with low-level chronic inflammation. This latter is a feature that characterizes *nfkb1* null mice and is associated with the premature aging and reduced regeneration properties of these animals [56•]. Experimental models of age-related pathologies have helped introducing the concept of "inflammaging," a terminology used to describe the age-related increase in systemic proinflammatory status in mammalians in the absence of detectable pathogens [57]. The multiple cooperating mechanisms driving inflammaging are overlapping with those inducing cell senescence: the accumulation of proinflammatory DNA damage [58]; the occurrence of a defective autophagic response [59]; the enhanced activation of NF-κB signaling [55, 60]; the systemic release of microRNAs capable of modulating the inflammatory status (inflamma-miRs) [61]; and the capability of senescent cells to secrete proinflammatory cytokines by means of SASP [46••, 62]. Danger signals deriving from some, if not all, of these events result in ROS production and oxidative stress, which in turn could stimulate intracellular danger sensing multiprotein platforms, namely inflammasome, leading to increased production of IL-1β, IL-18, TNF, and interferons [6, 59].

Focusing on the effect of SASP on the immune system, the repertoire of molecules released by senescent cells is enriched in inflammatory cytokines and other immune modulators that could potentially attract innate and acquired immune cells (reviewed in [57]). However, it has not yet being fully characterized if different senescent cells and tissues are able to produce the same inflammatory compounds in vivo. Indeed, in vitro expression of inflammatory genes by senescent human cells varies significantly according to the cell types [63]. For example, as opposed to the retinal pigment epithelial cells, senescent dermal fibroblasts upregulate the expression of transcripts for inflammatory chemokines and cytokines, that are capable of recruiting macrophages, neutrophils, dendritic cells, and memory T cells to the sites of inflammation [63]. This gene expression profile seems to overlap with that of fibroblasts activated during wound healing [64]. Moreover, the SASP composition could depend on type of mechanism triggering the senescence process and may vary with time [65, 66]. Vascular smooth muscle cell (VSMC) senescence, that is associated with atherosclerosis and may be induced by activated *Ras*, results in the upregulation of inflammatory chemokines in vitro. Similarly, when overexpressed in VSMC in vivo, *Ras* induces cell senescence and causes accumulation of macrophages in the intima, indicating a causal relationship between *Ras* activation, senescence, and vascular inflammation [67]. Nonetheless, the first description of a functional interaction between senescent cells and cells of the immune system comes from Xue et al. [68]. These researchers showed that reactivation of endogenous p53 in p53-deficient murine liver carcinoma can induce a cellular senescence program associated with the upregulation of inflammatory chemokines and adhesion molecules, including ICAM1 and VCAM1, indicating a mechanism by which senescent cells could facilitate tumor immune recognition and paving the way for studies on "senescence immunosurveillance" [69]. Senescent human myeloma cell lines express natural killer (NK) cell-

activating ligands on their surface in response to activation of the DDR; as a consequence, NK-cell degranulation against these cells is enhanced in vitro [70]. Thus, it is conceivable that NK cells represent an immunosurveillance mechanism toward cells undergoing stress-induced cell senescence programs, such as those triggered by DNA damage. $CD4^+$ acquired immune cells too are attracted, together with macrophages, by premalignant senescent cells expressing oncogenic N-Ras [71] and are involved in their clearance, representing an efficient immune surveillance system of the liver [72].

Changes in gene networks and signaling pathways in aged lymphocytes and innate cells of the immune system that could affect their efficiency should be considered when dealing with functional studies on the mutual influences of immune cells and senescent tissues. For instance, with aging, T cells increase the expression of the inhibitory molecule CTLA-4 and decrease the CD28 activator [73, 74], furthermore both $CD4^+$ and $CD8^+$ T cells acquire the expression of NK-specific KIR genes [75], and, finally, $CD4^+$ T cells can acquire cytotoxic activity through the expression of perforin and granzymes [76]. Thus, it would be interesting to study the effect of SASP directly on these senescent T cells that are under the control of NK-related regulatory molecules and can be found in several autoimmune age-related diseases including diabetes mellitus, rheumatoid arthritis, multiple sclerosis, and ankylosing spondylitis [75].

Stress Resistance, Longevity, and Loss of Proteostasis

Recent data point to the commonalities between aging and stress biology, being the rate of senescence the result of the interaction between the environment and the ability of the organism to respond to stress. While acute stressors (i.e., hormetic stress) may be beneficial, activating resistance mechanisms, chronic stressors have been associated with aging and disease [77]. Conversely, interventions able to increase animal lifespan do so by increasing the resistance of cells to a multitude of stressors [78]. In line, a significant association between multi-stress resistance and animal lifespan has been demonstrated [79]. Importantly, stress resistance has been strongly linked to the maintenance of normal proteostasis [80], consisting in keeping the balance among protein synthesis, folding, and turnover [81]. The loss of proteostasis is an event that occurs early in aging, and is catastrophic for cell viability [82••]. Furthermore, when experimentally mimicked, loss of proteostasis reduces cell viability, impairs the ability of cells to mount a stress response, and depletes cells of key proteins involved in a broad range of functions, including chromatin regulation [83]. Several mechanisms are in place in order to control proteostasis, which include molecular mechanisms (i.e., chaperones, ubiquitin–proteasome-system), intracellular- (e.g., autophagy), intercellular-, and interorgan-proteostatic networks (poorly characterized, but equally important) [84••]. Loss of the proteostatic control results in the accumulation of proteinaceous aggregates characterized by altered conformation and post-translational modifications, as those observed in Senile Amyloidosis, a pathologic condition that affects up to 25 % of subjects older than 80 years [85], or those that compose the pigment lipofuscin [86]. The accumulation of proteinaceous aggregates in the lysosomal compartment may exert several deleterious effects. Specifically, it may impair the autophagic flux [87] which, in turn, leads to the accumulation of dysfunctional mitochondria, enhancing intracellular ROS levels, eventually triggering cell senescence [88]. Furthermore, lipofuscin accumulation is associated with lysosomal iron overload, sensitization of lysosomes to ROS, destabilization of the lysosomal permeability [89], and activation of the inflammasome [59]. Finally, misfolded proteins may be transferred intercellularly, similarly to what occurs in transmissible prion disease and neurodegenerative disorders, by means of exosomes [90].

Last, the importance of protein homeostasis in cell longevity is manifest by primitive species, such as Hydras and other Cnidarians, that appear to be able to escape aging and death, the final destination of all the multicellular organisms. The secret of the prevention of senescence and consequent potential immortality seems to be hidden in a constant mitotic activity that thwarts the accumulation of damaged macromolecules and organelles diluted by repetitive divisions [91].

Stem Cell Senescence Impairs Regeneration

A wide consensus has been reached on the notion that primitive, undifferentiated cells reside in most animal tissues and replace cells lost as a result of the normal wear and tear processes or following injuries. However, senescent, dysfunctional stem cells accumulate in tissues, as a consequence of organism aging or following the exposure to pathologic stressors [5], and may become progressively impaired in their ability to replace lost cells or to repair tissue damage. In line, a progressive alteration of several stem cell types (including hematopoietic, skin, and neural ones) is known to occur with aging [21]. Importantly, age-related pathologies such as diabetes [92] and cardiac disease [93] reduce the ability of progenitor cells to repair infarcted myocardium or injured vessels.

However, it is still debated whether the observed stem cell dysfunction has to be related to either cell-intrinsic pathways or to alterations of the environment (i.e., the

niche or other soluble factors). Both these mechanisms seem to be important [5], being the second one responsible for the age-related decline in muscle and cardiac function observed in parabiosis experiments [94].

We addressed this issue, evaluating whether stem cell senescence typically characterizes failing human hearts. In line, ischemic cardiomyopathy depletes atria of primitive cells [95•], while leading to the accumulation of senescent stem cells in the ventricles [96]. Functionally, both age and pathology exert a negative impact on cardiac stem cells, decreasing their telomerase activity, increasing the frequency of cells showing telomere associated dysfunction foci, and blunting their proliferative and migratory capabilities [95•]. Furthermore, cell senescence is characterized by the secretion of factors that impair the protective effect usually exerted by the secretome of primitive cells on cardiomyocyte ischemia reperfusion injury, being IL-1β the major responsible of this detrimental effect [97••]. This latter, coupled with the hyperactivation of mTOR signaling, an arrest in the autophagic flux and the resulting activation of the inflammasome, creates a vicious autocrine and paracrine cycle, where senescence induces and "spreads" more senescence [97••]. In line, primitive cells isolated from failing hearts may impact negatively in the healing process of myocardial infarction in mice. However, rapamycin, an inhibitor of the TORC1 complex of mTOR, is able to reverse these alterations, reducing IL-1β secretion, decreasing the frequency of senescent cells and eventually restoring the regenerative ability of primitive cardiac cells [97••]. The ability of rapamycin to revert stem cell senescence was further enhanced by adding resveratrol, able to activate AMPK, thus contributing to mTOR inhibition [97••]. In conclusion, a pharmacological reversion of intrinsic alterations affecting senescent stem cells attenuates paracrine senescence and restores their regenerative properties in vivo [97••].

Conclusion

Stem cells are responsible for replenishing cells lost either as a result of the normal turnover or following injury. However, these cells are not immune from stress and may retain memory of sub-lethal damage in the form of epigenetic alterations, loss of proteostatic mechanisms, or production of proinflammatory cytokines. Consequently, both their capacity to replace cells lost for the normal wear and tear mechanisms and their regenerative abilities diminish with time. In fact, it is well established that aging per se impairs the ability of hematopoietic stem cells to repopulate recipient animals in vivo [98]. However, the impact that aging exerts on the in vivo regenerative ability of other stem cell types has been investigated less extensively. A notable exception is a recent work that studied the effect of aging on skeletal muscle derived stem cells (MuSC) regenerative properties. Specifically, although the regenerative ability of MuSC declines as a function of donor age, aged stem cells may be rejuvenated providing proper biophysical and biochemical cues [99]. Finally, the same age-related pathologies (e.g., ischemic heart disease or diabetes) that could benefit from stem cell-based therapies exert a detrimental impact on both tissue resident stem cells [97••, 100] and hematopoietic stem cells [93]. As a consequence, the in vivo regenerative abilities of both cardiac stem cells and bone marrow cells isolated from pathologic organisms are severely impaired. Therefore, a deeper understanding of the common mechanisms that lead to stem cell dysfunction, both during chronological aging and in age-related pathologies, holds the promise both to pharmacologically rejuvenate aged stem cells for regenerative purposes and to slow the degenerative changes that occur in vivo.

Compliance with Ethics Guidelines

Conflict of Interest Giuseppe Gianfranceschi, Giorgia Gri, Daniela Cesselli, and Antonio Paolo Beltrami declare that they have no conflict of interest.

Human and Animal Rights and Informed Consent This article refers to studies with human or animal subjects performed by the authors that were approved by the Ethics Committee of Udine. Written consent was obtained from each patient.

References

Papers of particular interest, published recently, have been highlighted as:

- • Of importance
- •• Of major importance

1. Beltrami AP, Barlucchi L, Torella D et al (2003) Adult cardiac stem cells are multipotent and support myocardial regeneration. Cell 114(6):763–776
2. Pellegrini G, Rama P, Mavilio F et al (2009) Epithelial stem cells in corneal regeneration and epidermal gene therapy. J Pathol 217(2):217–228
3. Beltrami A, Cesselli D, Beltrami C (2012) Cardiac resident stem cells: work (still) in progress. J Stem Cell Res Ther S9:001
4. Tongers J, Losordo DW, Landmesser U (2011) Stem and progenitor cell-based therapy in ischaemic heart disease: promise, uncertainties, and challenges. Eur Heart J 32(10):1197–1206
5. Beltrami AP, Cesselli D, Beltrami CA (2012) Stem cell senescence and regenerative paradigms. Clin Pharmacol Ther 91(1):21–29
6. Lopez-Otin C, Blasco MA, Partridge L et al (2013) The hallmarks of aging. Cell 153(6):1194–1217
7. Clegg A, Young J, Iliffe S et al (2013) Frailty in elderly people. Lancet 381(9868):752–762
8. Rando TA (2006) Stem cells, ageing and the quest for immortality. Nature 441(7097):1080–1086

9. Trindade LS, Aigaki T, Peixoto AA et al (2013) A novel classification system for evolutionary aging theories. Front Genet 4:25
10. •• Jones OR, Scheuerlein A, Salguero-Gomez R et al (2014) Diversity of ageing across the tree of life. Nature 505(7482): 169–173. *Study showing that patterns of mortality and fertility differ profoundly among species.*
11. Le Cunff Y, Baudisch A, Pakdaman K (2014) Evolution of aging: individual life history trade-offs and population heterogeneity account for mortality patterns across species. J Evol Biol 27(8):1706–1720
12. Wensink M (2013) Age-specificity and the evolution of senescence: a discussion. Biogerontology 14(1):99–105
13. Hayflick L, Moorhead PS (1961) The serial cultivation of human diploid cell strains. Exp Cell Res 25:585–621
14. Harley CB, Futcher AB, Greider CW (1990) Telomeres shorten during ageing of human fibroblasts. Nature 345(6274):458–460
15. von Zglinicki T, Saretzki G, Docke W et al (1995) Mild hyperoxia shortens telomeres and inhibits proliferation of fibroblasts: a model for senescence? Exp Cell Res 220(1):186–193
16. Rudolph KL, Chang S, Lee HW et al (1999) Longevity, stress response, and cancer in aging telomerase-deficient mice. Cell 96(5):701–712
17. •• Vera E, Bernardes de Jesus B, Foronda M et al (2012) The rate of increase of short telomeres predicts longevity in mammals. Cell Rep 2(4):732–737. *Study demonstrating that the rate of formation of short telomeres predicts longevity.*
18. •• Hewitt G, Jurk D, Marques FD et al (2012) Telomeres are favoured targets of a persistent DNA damage response in ageing and stress-induced senescence. Nat Commun 3:708. *In this study, authors show that telomeric DNA damage cannot be repaired and may be responsible for the permanently mantained DDR.*
19. •• Baker DJ, Wijshake T, Tchkonia T et al (2011) Clearance of p16Ink4a-positive senescent cells delays ageing-associated disorders. Nature 479:232–236. *This study demonstrates that removal of senescent cells may result in a reduction of age related tissue changes.*
20. Baker DJ, Sedivy JM (2013) Probing the depths of cellular senescence. J Cell Biol 202(1):11–13
21. Beltrami AP, Cesselli D, Beltrami CA (2011) At the stem of youth and health. Pharmacol Ther 129(1):3–20
22. van Deursen JM (2014) The role of senescent cells in ageing. Nature 509(7501):439–446
23. Rodier F, Munoz DP, Teachenor R et al (2011) DNA-SCARS: distinct nuclear structures that sustain damage-induced senescence growth arrest and inflammatory cytokine secretion. J Cell Sci 124(Pt 1):68–81
24. Sherr CJ (2012) Ink4-Arf locus in cancer and aging. Wiley Interdiscip Rev Dev Biol 1(5):731–741
25. Sage J, Straight AF (2010) RB's original CIN? Genes Dev 24(13):1329–1333
26. Zhang Y, Xiong Y, Yarbrough WG (1998) ARF promotes MDM2 degradation and stabilizes p53: ARF-INK4a locus deletion impairs both the Rb and p53 tumor suppression pathways. Cell 92(6):725–734
27. Decottignies A, d'Adda di Fagagna F (2011) Epigenetic alterations associated with cellular senescence: a barrier against tumorigenesis or a red carpet for cancer? Semin Cancer Biol 21(6):360–366
28. de Koning AP, Gu W, Castoe TA et al (2011) Repetitive elements may comprise over two-thirds of the human genome. PLoS Genet 7(12):e1002384
29. Huidobro C, Fernandez AF, Fraga MF (2013) Aging epigenetics: causes and consequences. Mol Aspects Med 34(4):765–781
30. Shen H, Laird PW (2013) Interplay between the cancer genome and epigenome. Cell 153(1):38–55
31. • Wang J, Geesman GJ, Hostikka SL et al (2011) Inhibition of activated pericentromeric SINE/Alu repeat transcription in senescent human adult stem cells reinstates self-renewal. Cell Cycle 10(17):3016–3030. *This study shows the importance of ME activation in stem cell senescence and dysfunction.*
32. • De Cecco M, Criscione SW, Peckham EJ et al (2013) Genomes of replicatively senescent cells undergo global epigenetic changes leading to gene silencing and activation of transposable elements. Aging Cell 12(2):247–256. *This study shows the importance of ME activation in stem cell senescence and dysfunction.*
33. Squillaro T, Alessio N, Cipollaro M et al (2010) Partial silencing of methyl cytosine protein binding 2 (MECP2) in mesenchymal stem cells induces senescence with an increase in damaged DNA. FASEB J 24(5):1593–1603
34. Arnoult N, Van Beneden A, Decottignies A (2012) Telomere length regulates TERRA levels through increased trimethylation of telomeric H3K9 and HP1alpha. Nat Struct Mol Biol 19(9):948–956
35. Michishita E, McCord RA, Boxer LD et al (2009) Cell cycle-dependent deacetylation of telomeric histone H3 lysine K56 by human SIRT6. Cell Cycle 8(16):2664–2666
36. Benetti R, Garcia-Cao M, Blasco MA (2007) Telomere length regulates the epigenetic status of mammalian telomeres and subtelomeres. Nat Genet 39(2):243–250
37. Pfeiffer V, Lingner J (2012) TERRA promotes telomere shortening through exonuclease 1-mediated resection of chromosome ends. PLoS Genet 8(6):e1002747
38. O'Sullivan RJ, Karlseder J (2012) The great unravelling: chromatin as a modulator of the aging process. Trends Biochem Sci 37(11):466–476
39. Dixon JR, Selvaraj S, Yue F et al (2012) Topological domains in mammalian genomes identified by analysis of chromatin interactions. Nature 485(7398):376–380
40. Fiorentino FP, Giordano A (2012) The tumor suppressor role of CTCF. J Cell Physiol 227(2):479–492
41. Dreesen O, Chojnowski A, Ong PF et al (2013) Lamin B1 fluctuations have differential effects on cellular proliferation and senescence. J Cell Biol 200(5):605–617
42. Shah PP, Donahue G, Otte GL et al (2013) Lamin B1 depletion in senescent cells triggers large-scale changes in gene expression and the chromatin landscape. Genes Dev 27(16):1787–1799
43. Sang L, Coller HA, Roberts JM (2008) Control of the reversibility of cellular quiescence by the transcriptional repressor HES1. Science 321(5892):1095–1100
44. Chen JH, Ozanne SE (2006) Deep senescent human fibroblasts show diminished DNA damage foci but retain checkpoint capacity to oxidative stress. FEBS Lett 580(28–29):6669–6673
45. Passos JF, Nelson G, Wang C et al (2010) Feedback between p21 and reactive oxygen production is necessary for cell senescence. Mol Syst Biol 6:347
46. •• Acosta JC, Banito A, Wuestefeld T et al (2013) A complex secretory program orchestrated by the inflammasome controls paracrine senescence. Nat Cell Biol 15(8):978–990. *This study demonstrates the pivotal role of inflammasome activation and IL-1 secretion in regulating the SASP.*
47. Ivanov A, Pawlikowski J, Manoharan I et al (2013) Lysosome-mediated processing of chromatin in senescence. J Cell Biol 202(1):129–143
48. Harman D (1956) Aging: a theory based on free radical and radiation chemistry. J Gerontol 11(3):298–300
49. Zhang Y, Ikeno Y, Qi W et al (2009) Mice deficient in both Mn superoxide dismutase and glutathione peroxidase-1 have increased oxidative damage and a greater incidence of pathology but no reduction in longevity. J Gerontol A 64(12):1212–1220
50. Schriner SE, Linford NJ, Martin GM et al (2005) Extension of murine life span by overexpression of catalase targeted to mitochondria. Science 308(5730):1909–1911

51. Blagosklonny MV (2008) Aging: ROS or TOR. Cell Cycle 7(21):3344–3354
52. Passos JF, Saretzki G, Ahmed S et al (2007) Mitochondrial dysfunction accounts for the stochastic heterogeneity in telomere-dependent senescence. PLoS Biol 5(5):e110
53. Takahashi A, Ohtani N, Yamakoshi K et al (2006) Mitogenic signalling and the p16INK4a-Rb pathway cooperate to enforce irreversible cellular senescence. Nat Cell Biol 8(11):1291–1297
54. Coller HA, Sang L, Roberts JM (2006) A new description of cellular quiescence. PLoS Biol 4(3):e83
55. Chien Y, Scuoppo C, Wang X et al (2011) Control of the senescence-associated secretory phenotype by NF-kappaB promotes senescence and enhances chemosensitivity. Genes Dev 25(20):2125–2136
56. • Jurk D, Wilson C, Passos JF et al (2014) Chronic inflammation induces telomere dysfunction and accelerates ageing in mice. Nat Commun 2:4172. *Study showing the role of inflammation in impairing tissue regeneration and aging.*
57. Freund A, Orjalo AV, Desprez PY et al (2010) Inflammatory networks during cellular senescence: causes and consequences. Trends Mol Med 16(5):238–246
58. Bonafe M, Storci G, Franceschi C (2012) Inflamm-aging of the stem cell niche: breast cancer as a paradigmatic example: breakdown of the multi-shell cytokine network fuels cancer in aged people. BioEssays 34(1):40–49
59. Salminen A, Kaarniranta K, Kauppinen A (2012) Inflammaging: disturbed interplay between autophagy and inflammasomes. Aging (Albany NY) 4(3):166–175
60. Salminen A, Huuskonen J, Ojala J et al (2008) Activation of innate immunity system during aging: NF-kB signaling is the molecular culprit of inflamm-aging. [Research Support, Non-U.S. Gov't Review]. Ageing Res Rev 7(2):83–105
61. Olivieri F, Rippo MR, Procopio AD et al (2013) Circulating inflamma-miRs in aging and age-related diseases. Front Genet 4:121
62. Coppe JP, Desprez PY, Krtolica A et al (2010) The senescence-associated secretory phenotype: the dark side of tumor suppression. Annu Rev Pathol 5:99–118
63. Shelton DN, Chang E, Whittier PS et al (1999) Microarray analysis of replicative senescence. Curr Biol 9(17):939–945
64. Martin P (1997) Wound healing–aiming for perfect skin regeneration. Science 276(5309):75–81
65. Coppe JP, Patil CK, Rodier F et al (2008) Senescence-associated secretory phenotypes reveal cell-nonautonomous functions of oncogenic RAS and the p53 tumor suppressor. PLoS Biol 6(12):2853–2868
66. Coppe JP, Rodier F, Patil CK et al (2011) Tumor suppressor and aging biomarker p16(INK4a) induces cellular senescence without the associated inflammatory secretory phenotype. J Biol Chem 286(42):36396–36403
67. Minamino T, Yoshida T, Tateno K et al (2003) Ras induces vascular smooth muscle cell senescence and inflammation in human atherosclerosis. Circulation 108(18):2264–2269
68. Xue W, Zender L, Miething C et al (2007) Senescence and tumour clearance is triggered by p53 restoration in murine liver carcinomas. Nature 445(7128):656–660
69. Serrano M (2011) Cancer: final act of senescence. Nature 479(7374):481–482
70. Soriani A, Zingoni A, Cerboni C et al (2009) ATM-ATR-dependent up-regulation of DNAM-1 and NKG2D ligands on multiple myeloma cells by therapeutic agents results in enhanced NK-cell susceptibility and is associated with a senescent phenotype. Blood 113(15):3503–3511
71. Kang TW, Yevsa T, Woller N et al (2011) Senescence surveillance of pre-malignant hepatocytes limits liver cancer development. Nature 479(7374):547–551
72. Hoenicke L, Zender L (2012) Immune surveillance of senescent cells—biological significance in cancer- and non-cancer pathologies. Carcinogenesis 33(6):1123–1126
73. Effros RB, Boucher N, Porter V et al (1994) Decline in CD28+ T cells in centenarians and in long-term T cell cultures: a possible cause for both in vivo and in vitro immunosenescence. Exp Gerontol 29(6):601–609
74. Leng Q, Bentwich Z, Borkow G (2002) CTLA-4 upregulation during aging. Mech Ageing Dev 123(10):1419–1421
75. Goronzy JJ, Weyand CM (2003) Aging, autoimmunity and arthritis: T-cell senescence and contraction of T-cell repertoire diversity—catalysts of autoimmunity and chronic inflammation. Arthritis Res Ther 5(5):225–234
76. Appay V, Zaunders JJ, Papagno L et al (2002) Characterization of CD4(+) CTLs ex vivo. J Immunol 168(11):5954–5958
77. Epel ES, Lithgow GJ (2014) Stress biology and aging mechanisms: toward understanding the deep connection between adaptation to stress and longevity. J Gerontol A 69(Suppl 1):S10–S16
78. Murakami S (2006) Stress resistance in long-lived mouse models. Exp Gerontol 41(10):1014–1019
79. Harper JM, Salmon AB, Leiser SF et al (2007) Skin-derived fibroblasts from long-lived species are resistant to some, but not all, lethal stresses and to the mitochondrial inhibitor rotenone. Aging Cell 6(1):1–13
80. Morimoto RI, Cuervo AM (2014) Proteostasis and the aging proteome in health and disease. J Gerontol A 69(Suppl 1):S33–S38
81. Balch WE, Morimoto RI, Dillin A et al (2008) Adapting proteostasis for disease intervention. Science 319(5865):916–919
82. •• Ben-Zvi A, Miller EA, Morimoto RI (2009) Collapse of proteostasis represents an early molecular event in Caenorhabditis elegans aging. Proc Natl Acad Sci USA 106(35): 14914–14919. *Study showing that loss of proteostasis is one of the earliest events in aging.*
83. Olzscha H, Schermann SM, Woerner AC et al (2011) Amyloid-like aggregates sequester numerous metastable proteins with essential cellular functions. Cell 144(1):67–78
84. •• Taylor RC, Dillin A (2013) XBP-1 is a cell-nonautonomous regulator of stress resistance and longevity. Cell 153(7):1435–1447. *Study showing that proteostasis may be enhanced paracrinally through the release of microvesicles.*
85. Tanskanen M, Peuralinna T, Polvikoski T et al (2008) Senile systemic amyloidosis affects 25% of the very aged and associates with genetic variation in alpha2-macroglobulin and tau: a population-based autopsy study. Ann Med 40(3):232–239
86. Hohn A, Grune T (2013) Lipofuscin: formation, effects and role of macroautophagy. Redox Biol 1(1):140–144
87. Krohne TU, Stratmann NK, Kopitz J et al (2010) Effects of lipid peroxidation products on lipofuscinogenesis and autophagy in human retinal pigment epithelial cells. Exp Eye Res 90(3): 465–471
88. Dalle Pezze P, Nelson G, Otten EG et al (2014) Dynamic modelling of pathways to cellular senescence reveals strategies for targeted interventions. PLoS Comput Biol 10(8):e1003728
89. Kurz T, Terman A, Gustafsson B et al (2008) Lysosomes and oxidative stress in aging and apoptosis. Biochim Biophys Acta 1780(11):1291–1303
90. Schneider A, Simons M (2013) Exosomes: vesicular carriers for intercellular communication in neurodegenerative disorders. Cell Tissue Res 352(1):33–47
91. Terman A, Brunk UT (2005) Is aging the price for memory? Biogerontology 6(3):205–210
92. Sorrentino SA, Bahlmann FH, Besler C et al (2007) Oxidant stress impairs in vivo reendothelialization capacity of endothelial progenitor cells from patients with type 2 diabetes mellitus:

restoration by the peroxisome proliferator-activated receptor-gamma agonist rosiglitazone. Circulation 116(2):163–173
93. Wang X, Takagawa J, Lam VC et al (2011) Donor myocardial infarction impairs the therapeutic potential of bone marrow cells by an interleukin-1-mediated inflammatory response. Sci Transl Med 3(100):100ra190
94. Loffredo FS, Steinhauser ML, Jay SM et al (2013) Growth differentiation factor 11 is a circulating factor that reverses age-related cardiac hypertrophy. Cell 153(4):828–839
95. • Cesselli D, Beltrami AP, D'Aurizio F et al (2011) Effects of age and heart failure on human cardiac stem cell function. Am J Pathol 179(1):349–366. *Study showing that age and pathology increase the rate of cardiac stem cell senescence and dysfunction*.
96. Urbanek K, Torella D, Sheikh F et al (2005) Myocardial regeneration by activation of multipotent cardiac stem cells in ischemic heart failure. Proc Natl Acad Sci USA 102(24):8692–8697
97. •• Avolio E, Gianfranceschi G, Cesselli D et al (2014) Ex vivo molecular rejuvenation improves the therapeutic activity of senescent human cardiac stem cells in a mouse model of myocardial infarction. Stem Cells 32(9):2373–2385. *Study showing that the pharmacologic attenuation of stem cell senescence may enhance the reparative properties of cardiac progenitor cells*.
98. Janzen V, Forkert R, Fleming HE et al (2006) Stem-cell ageing modified by the cyclin-dependent kinase inhibitor p16INK4a. Nature 443(7110):421–426
99. Cosgrove BD, Gilbert PM, Porpiglia E et al (2014) Rejuvenation of the muscle stem cell population restores strength to injured aged muscles. Nat Med 20(3):255–264
100. Vecellio M, Spallotta F, Nanni S et al (2014) The histone acetylase activator pentadecylidenemalonate 1b rescues proliferation and differentiation in the human cardiac mesenchymal cells of type 2 diabetic patients. Diabetes 63(6): 2132–2147

OPEN ACCESS Freely available online

PLOS ONE

The Redox Function of APE1 Is Involved in the Differentiation Process of Stem Cells toward a Neuronal Cell Fate

Rossana Domenis[1☯], Natascha Bergamin[1☯], Giuseppe Gianfranceschi[1], Carlo Vascotto[1], Milena Romanello[1], Silvia Rigo[1], Giovanna Vagnarelli[1], Massimo Faggiani[1], Piercamillo Parodi[2], Mark R. Kelley[3], Carlo Alberto Beltrami[1], Daniela Cesselli[1], Gianluca Tell[1]*, Antonio Paolo Beltrami[1]*

1 Department of Medical and Biological Sciences, University of Udine, Udine, Italy, **2** Department of Experimental and Clinical Medical Sciences, University of Udine, Udine, Italy, **3** Department of Pediatrics (Section of Hematology/Oncology), Herman B. Wells Center for Pediatric Research, Indiana University School of Medicine, Indianapolis, Indiana, United States of America

Abstract

Low-to-moderate levels of reactive oxygen species (ROS) govern different steps of neurogenesis *via* molecular pathways that have been decrypted only partially. Although it has been postulated that redox-sensitive molecules are involved in neuronal differentiation, the molecular bases for this process have not been elucidated yet. The aim of this work was therefore to study the role played by the redox-sensitive, multifunctional protein APE1/Ref-1 (APE1) in the differentiation process of human adipose tissue-derived multipotent adult stem cells (hAT-MASC) and embryonic carcinoma stem cells (EC) towards a neuronal phenotype. Methods and results: Applying a definite protocol, hAT-MASC can adopt a neural fate. During this maturation process, differentiating cells significantly increase their intracellular Reactive Oxygen Species (ROS) levels and increase the APE1 nuclear fraction bound to chromatin. This latter event is paralleled by the increase of nuclear NF-κB, a transcription factor regulated by APE1 in a redox-dependent fashion. Importantly, the addition of the antioxidant N-acetyl cysteine (NAC) to the differentiation medium partially prevents the nuclear accumulation of APE1, increasing the neuronal differentiation of hAT-MASC. To investigate the involvement of APE1 in the differentiation process, we employed E3330, a specific inhibitor of the APE1 redox function. The addition of E3330, either to the neurogenic embryonic carcinoma cell line NT2-D1or to hAT-MASC, increases the differentiation of stem cells towards a neural phenotype, biasing the differentiation towards specific subtypes, such as dopaminergic cells. In conclusion, during the differentiation process of stem cells towards a neuroectodermic phenotype, APE1 is recruited, in a ROS-dependent manner, to the chromatin. This event is associated with an inhibitory effect of APE1 on neurogenesis that may be reversed by E3330. Therefore, E3330 may be employed both to boost neural differentiation and to bias the differentiation potential of stem cells towards specific neuronal subtypes. These findings provide a molecular basis for the redox-mediated hypothesis of neuronal differentiation program.

Citation: Domenis R, Bergamin N, Gianfranceschi G, Vascotto C, Romanello M, et al. (2014) The Redox Function of APE1 Is Involved in the Differentiation Process of Stem Cells toward a Neuronal Cell Fate. PLoS ONE 9(2): e89232. doi:10.1371/journal.pone.0089232

Editor: Manlio Vinciguerra, University College London, United Kingdom

Received October 18, 2013; **Accepted** January 16, 2014; **Published** February 19, 2014

Funding: The authors declare that the research leading to these results has received funding from the European Union Seventh Framework Programme (FP7/2007–2013) under grant agreement Health-F2-2009-241762, for the project FLIP and by grants from Associazione Italiana per la Ricerca sul Cancro (AIRC) (IG10269), Ministero dell'Istruzione, dell'Università e della Ricerca (MIUR) (FIRB_RBRN07BMCT); the Regione Friulia Venezia Giulia for the Project 'MINA' under the program entitled: "Programma per la Cooperazione Transfrontaliera Italia-Slovenia 2007–2013" to GT; Italian Ministry of Health, G.R.-2007-683407 (D.C.); and Project ERC- 7FP SP 2 IDEAS QUIDPROQUO G.A. n. 269051 (D.C., A.P.B., G.G.). Financial support for this work was provided by the National Institutes of Health (NCICA121168, CA167291), and the Riley Children's Foundation to MRK. The funders had no role in study design, data collection and analysis, decision to publish, or preparation of the manuscript.

Competing Interests: The authors have read the journal's policy and declare that they have no conflict of interest, with the exception of Dr. Mark R. Kelley, who is the Chief Scientific Founder and consultant for ApeX Therapeutics, a company that has licensed IP from his work. Dr. Beltrami is a PLoS ONE Editorial Board member, but this does not alter the authors' adherence to all the PLOS ONE policies on sharing data and materials.

* E-mail: gianluca.tell@uniud.it (GT); antonio.beltrami@uniud.it (APB)

☯ These authors contributed equally to this work.

Introduction

APE1/Ref-1 (Apurinic apyrimidinic Endonuclease/Redox effector factor 1, also called APEX1 or Ref-1 and here referred to as APE1) the mammalian ortholog of *E. coli* Xth (Exo III), is a master regulator of cellular response to oxidative stress and plays a central role in the maintenance of genome stability and transcriptional regulation. Upon removal of the damaged base, APE1 cleaves the abasic site to facilitate DNA repair. The vital effects of APE1 appear to depend on its role in the base excision repair pathways of DNA lesions [1]. However, APE1 also has another major cellular function, since it works as a reduction-oxidation (redox) factor and stimulates the DNA binding activity of several transcription factors that are involved in cell proliferation and differentiation. This function is accounted for by the redox sensitive Cys65. This effect is obtained as a redox co-activation of different transcription factors both involved in cellular response to

oxidative stress, such as Nuclear Factor-kappaB (NF-kB), Early growth response protein-1 (Egr-1), p53, Hypoxia-inducible factor 1-alpha (HIF-1α), cAMP response element-binding protein (CREB), activator protein 1 (AP-1) and in differentiation programs such as Paired box containing proteins (Pax) in different cell systems [2]. Recent *in vitro* studies showed that APE1 adopts different unfolded conformations depending on the redox state of its Cys residues, in particular C65 and C93 [3]; moreover, the APE1 redox inhibitor (E)-3-(2-(5,6-dimethoxy-3-methyl-1,4-benzoquinonyl))-2-nonyl propenoic acid (E3330) was shown to decrease the amount of the redox-active protein by driving C65 into disulfide bonds. E3330 holds clinical potential as a specific inhibitor of APE1 redox function, without interfering with its endonuclease activity (for reviews see [4,5]). The importance of this function is highlighted by results demonstrating that NF-kB-mediated gene expression is regulated by APE1 redox activity, without effects on IκBα degradation [6,7]. E3330 was also found to selectively inhibit growth/migration of human pancreatic cancer cells [8], suggesting that the APE1 redox function could represent a good candidate for inhibition of tumor invasion and metastasis. We recently demonstrated that E3330-treatment inhibits the TNFα-induced IL8 production driven by NF-κB, in hepatic cancer cell lines [9]. However, knowledge on the detailed molecular mechanisms responsible for the C65-mediated APE1 redox function and for the effects of E3330 inhibition on APE1 *in vivo* are only at its beginning. We recently provided evidence that this redox regulation of APE1 may impact on protein subcellular mitochondrial trafficking [10]. In this regard, the specific block of APE1 redox activity on NF-kB with E3330 impairs hemangioblast development *in vitro* [*11*], thus confirming the leading role of APE1 redox function in affecting the cell differentiation programs. A third non-canonical and poorly characterized APE1 function is represented by its transcriptional activity mediated by direct binding of APE1 to the negative calcium response elements (nCaRE) [12,13] present on different promoters, including parathormone (PTH), APE1, Bcl-2-associated X protein (Bax) and sirtuin 1 (SIRT1)[10, 11 (Antoniali et al., MBoC in Press)]. The two major functions of APE1, redox and base-excision repair, are completely independent. In fact, the N-terminus, which contains the nuclear localization signal sequence (NLS), is principally devoted to redox-mediated transcriptional co-activation activity and promotes, through its lysine residues, the ability of APE1 to interact both with nucleic acids and with nucleophosmin [14], while the C-terminus exerts the enzymatic activity on the abasic sites of DNA mainly through the residue H309 in the catalytic site [15]. Furthermore, a new unsuspected function of APE1 in RNA metabolism, which is controlled by the N-terminal domain of the protein, has been recently discovered. In particular, it has been demonstrated that APE1 acts as a cleansing factor of abasic rRNA and is able to bind hairpin structures of RNA molecules [16,17].

APE1 is essential for cell viability [18] and therefore a detailed comprehension of the molecular targets of APE1 functions has been very difficult. Conditional knock-out and knock-down strategies [1,19] confirmed the essentiality of this protein and allowed establishment of cell models to inspect and characterize, in better detail, the major functions of APE1. However, knowledge of the molecular effectors regulated by APE1 in determining its biological essentiality is still scanty.

Concerning the role played by APE1 on neuronal cells, it seems to be essential both in protecting cells toward oxidative stress and in controlling the differentiation program. In fact, it has been demonstrated that APE1 promotes NF-kB-driven glial cell-derived neurotrophic factor (GDNF) receptor α1 expression, thus inducing GDNF responsiveness, which subsequently both stimulates neurite outgrowth and protects cells from amyloid peptide and oxidative stress [20]. GDNF was originally characterized as a potent neurotrophic factor, specific for the survival and differentiation of the midbrain dopaminergic neurons [21]. Interestingly, APE1 is highly expressed, *in vivo*, in selected regions of the central nervous system [22,23] supporting its pivotal role for neuronal cells. In pathological settings, a reduction in APE1 expression has been shown to occur: in the hippocampus after hypoxic/ischemic injury [24], in the cortex after compression injury [25], and in the spinal cord after ischemia [26], while increased nuclear levels have been described in Alzheimer's disease cerebral cortex, corroborating the view that the cellular adaptive response to the oxidative stress condition is involved in the pathogenesis of this disease [27].

However, the role played by APE1 in the differentiation of either embryonic or adult stem cells towards the neural and glial lineages has not been investigated thus far. To this aim, we employed two distinct cell systems: 1) a human Embryonic Carcinoma cell line (hEC) that possesses a well-established ability to differentiate towards a neural fate (NTERA2 cl.D1 -NT2-D1-) [28] and 2) non-immortalized human adult stem cells. Specifically, we isolated and cultured Multipotent Adult Stem Cells (MASC) from adipose tissue, modifying a culture protocol that we already used to isolate similar cells from adult human bone marrow, heart, liver and skin biopsies [29–31]. MASC display clonogenicity, self-renewal ability, and multipotency, express pluripotent state specific transcription factors (i.e. OCT4, Nanog, Sox2, and Rex1), display high levels of telomerase activity, and a gene expression profile highly similar, irrespectively from the tissue of origin [29]. Most importantly, MASC can differentiate into neuron-like cells that display, on top of markers of cell differentiation, functional properties of neuronal cells [29].

The goal of the present study was to evaluate the potential role played by the APE1 redox function in the differentiation process of stem cells towards a neuronal fate.

Materials and Methods

Tissue Donors and Ethical Approval

Human adipose tissue samples of healthy donors ($n = 31$) undergoing plastic surgery were collected after informed consent. The study was approved by the Ethics Committee of Udine (reference number 47831) and a written consent was obtained from each enrolled subject.

Culture and Differentiation of NT2-D1

NTERA-2 cl.D1 (NT2-D1) cells were purchased from Istituto Zooprofilattico di Lombardia ed Emilia (IZSLER) cultured in Dulbecco's modified Eagle's medium (high glucose) containing 10% fetal bovine serum (FBS), 4 mM glutamine and 1% Penicillin/Streptomycin. For neuronal differentiation, NT2-D1 cells were cultured for four weeks in Opti-MEM containing 4% FBS, 4 mM glutamine, 56 μM β-mercapto-ethanol, 1% Penicillin/Streptomycin and 100 mM all-trans retinoic acid (ATRA). Following ATRA treatment cells were split 1:6. After 1–2 days cultures were mechanically shaken to dislodge cells and these free-floating cells were plated onto Matrigel (50 μg/ml) coated growth surface and treated for two weeks with 10 μM fluorodeoxyuridine, 10 μM uridine and 1 μM cytosine arabinoside. For the inhibition of APE1, E3330 [20 μM] was added to the culture medium starting from the third week of differentiation.

Human Adipose Tissue Derived MASCs (hAT-MASCs)

After tumescent liposuction, lipoaspirates were centrifuged at 3×10^3 *g* for 3 minutes and the stromal vascular fraction was collected in a sterile container. The samples were enzymatically dissociated in a 0.05% Collagenase type II solution (Sigma-Aldrich) in Joklik modified Eagle's Medium (Sigma-Aldrich) for 20 minutes at 37°C. Collagenase activity was stopped by the addition of 0.1% BSA (Sigma-Aldrich) solution in Joklik modified Eagle's Medium (Sigma-Aldrich). Cell suspension was centrifuged at 1×10^3 *g* for 10 minutes. Samples collected from different subjects were kept distinct and used to obtain distinct hAT-MASC cell lines.

2.0×10^6 freshly isolated human cells were plated onto 100 mm human fibronectin (Sigma-Aldrich) coated dishes (BD Falcon) in an expansion medium composed as follows: 60% low glucose DMEM (Invitrogen), 40% MCDB-201, 1 mg/mL linoleic acid-BSA, 10^{-9} M dexamethasone, 10^{-4} M ascorbic acid-2 phosphate, 1X insulin-transferrin-sodium selenite (all from Sigma-Aldrich), 2% fetal bovine serum (StemCell Technologies), 10 ng/ml human or murine PDGF-BB, 10 ng/ml human or murine EGF (both from Peprotech EC). Medium was replaced with fresh one every 4 days. Once cells reached 70–80% of confluence, they were detached with 0.25% trypsin-EDTA (Sigma-Aldrich) and re-plated at a density of $1–2\times10^3/cm^2$.

Flow Cytometry

At passage 3 (P3), cells grown in expansion medium were detached with 0.25% trypsin-EDTA (Sigma-Aldrich) and, after a 20 minutes recovery phase, were incubated with the following properly conjugated primary antibodies: CD10, CD13, CD29, CD49a, CD49b, CD49d, CD90, CD73, CD44, CD59, CD45, HLA-DR, CD117, CD34, CD 271 (BD Biosciences), CD105, CD66e, KDR (Serotech), CD133 (Miltenyi Biotec), CXCR4 (R&D), ABCG-2 (Chemicon International).

Single Cell Cloning

P2 cells were individually deposited onto the wells of a 96wells Terasaki plate with an automated cell sorter (MoFlo, DakoCytomation) and cultured in expansion medium, as in [29]. About 700 wells were seeded for each analyzed cell line.

Multilineage Differentiation of hAT-MASC

Multilineage differentiation was induced as in Beltrami et al. 2007.

For neural differentiation, hAT-MASCs were plated at a density of $3\times10^3/cm^2$ in DMEM-HG, 10% FBS, N1. After 24 hours, medium was replaced with a medium added with 1% B27 (Invitrogen), 10 ng/ml EGF (Peprotech) and 20 ng/ml bFGF (Peprotech), N2. After 5 days, cells were washed and incubated for 9 days with DMEM containing 5 µg/ml insulin, 200 µM indomethacin and 0.5 mM IBMX (all from Sigma-Aldrich) in the absence of FBS, N3. For experiments involving the use of antioxidants, 10 mM N-acetyl cysteine was added to the culture medium, while for experiments requiring the inhibition of APE1 redox function, the specific inhibitor E3330 was employed (kindly provided by Prof. M.R. Kelley) [4]. Specifically, in hAT-MASC cultures E3330 was either added at a concentration of 20 µM during the last step of the differentiation protocol (N3) or at a concentration of 40 µM and 20 µM during the last two steps of the differentiation protocol (N2 and N3, respectively).

Measurement of Intracellular Reactive Oxygen Species (ROS) Generation

Following the manufacturer's protocol, cells were loaded with 5 µM 5–[and -6]-chloromethyl–2′,7′-dichlorodihydrofluorescein diacetate acetyl ester (CM-H_2DCFDA, Molecular Probe, Eugene, OR, USA) for 15 minutes, protected from light, in Opti-MEM (Invitrogen). Then, 1 mM H_20_2 was added for 30 minutes as positive control. The cells were washed once with PBS and the production of ROS was visualized by inverted fluorescence microscope and images were quantified by ImageJ software.

Protein Extraction

To prepare the total protein extracts, 2×10^6 cells were lysed in 50 mM Tris-HCl pH 7.5; 150 mM NaCl; 1 mM EDTA, 1% Triton X-100 containing a cocktail of protease inhibitor (Sigma-Aldrich), 0.5 mM PMSF, 1 mM NaF, 1 mM Na_3VO_4 and 0.1 mM DTT). The suspension was then incubated at 4°C for 30 minutes, sonicated and then subjected to centrifugation for 20 minutes at 12000×g. The supernatant was collected as total extract and stored at −80°C for biochemical assays.

To separate the soluble (S1) and insoluble (P1) fractions cells pellets (3×10^6cells) were incubated for 10 min at 4°C under orbital rotation in 200 ml ice-cold CSK buffer (100 mM NaCl, 300 mM sucrose, 10 mM PIPES, pH 6.8, 3 mM $MgCl_2$, 1 mM DTT, 1 mM EGTA) containing 0.5% Triton X-100 and protease inhibitors. After centrifugation at 5000×g for 5 min, the supernatant (soluble proteins) was recovered (S1 fraction). Pellets were washed three times with 1 ml ice-cold CSK and centrifuged at 5,000×g for 5 min. The resulting pellets (P1, chromatin fraction) were resuspended in 30 ml of 20 mM Tris-HCl buffer, pH 8, 150 mM NaCl, 0.1% NP40, 1 mM EDTA and protease inhibitors. The suspension was sonicated and centrifuged for 30 min at 13,000×g at 4°C and the supernatant was recovered. Protein content was measured using a colorimetric Bradford assay (Bio-Rad Laboratories, Richmond, CA) with bovine serum albumin as a standard.

Western-blot Analysis

Loading of the extracts was normalized by protein content. Aliquots from the cell extracts were denatured by heating at 95°C for 5 min. Samples were electophoresed on 10% SDS-PAGE and then transferred to nitrocellulose membranes as previously described [32]. To confirm the amounts of protein in each lane, membranes were stained with Ponceau rouge, and a second gel was run in parallel and stained with Comassie. Blots were incubated with the following antibodies: mouse monoclonal anti-APE1 antibody (kindly provided by Prof. M.R. Kelley), and rabbit antibody anti-actin (Sigma) to normalize the protein content in the total extracts; then with the corresponding peroxidase–conjugated anti-serum (Sigma). The bands were visualized and analyzed using a ChemiDoc XRS (Bio-Rad, Milano, Italy) and associated software.

Immunofluorescence Confocal Analysis

Cells fixed in 4% (wt/vol) paraformaldehyde for 20 min at room temperature were permeabilized for 5 min with PBS–0.25% (wt/vol) Triton X-100 and incubated for 30 min with 5% normal donkey serum in PBS–0.1% (wt/vol) Triton X-100 (blocking solution) to block unspecific binding of the antibodies. Cells were then incubated with the following antibodies: OCT-4, Sox2 and Nanog to evaluate primitive cell transcriptional settings; GATA4, cytokeratin 8-18-19, smooth muscle actin (SMA), connexin43, alfa-sarcomeric actin (ASA), glial fibrillary acidic protein (GFAP),

β3 tubulin, Microtubule Associate Protein2 (MAP2), and Basic Myelin Protein to evaluate multilineage differentiation (Table S1). To evaluate the role of APE1 in neuronal differentiation, cells were incubated for 3 h with a mouse monoclonal antibody [32], previously labeled by using the Zenon Mouse IgG Labeling Kit (Molecular Probes), utilizing the Alexa Fluor 488-labeled Fab fragment directed against the Fc portion of the IgG primary anti-APE antibody, in accordance to instructions, diluted 1:2 in blocking solution alone, or together with anti NFkB p65 rabbit polyclonal antibody 1:100 (Santa Cruz Biotechnology, CA, USA). In this case, after washing cells were incubated for 90 min with secondary Alexa Fluor 546 conjugated goat anti rabbit antibody. Nuclei were then counterstained by DAPI (Sigma), and the microscope slides mounted and visualized through a Leica TCS SP laser-scanning confocal microscope (Leica Microsystems, Wetzlar, Germany) equipped with a 488-nm argon laser, a 543-nmHeNe laser, and a 63x oil fluorescence objective.

Quantitative Analysis of Immunofluorescence

To obtain quantitative data of the nuclear levels of APE1, images of immunofluorescently labeled cells were acquired with a fully automated dedicated imaging system (DMI6000B, Leica Microsystems or BD Pathway 850, Becton Dickinson). Scrupulous care was taken to keep constant both the exposure time and gain of the camera, and to set these parameters in order to avoid image saturation. Images of APE1 were taken before acquiring DAPI images and an internal shutter was employed to avoid unnecessary exposure of the specimen to light, thus minimizing photobleaching effects. A quantitation of the total fluorescence of nuclear APE1 staining was obtained employing ImageJ software [33]. A threshold was applied to DAPI images both to measure nuclear areas and to create a mask to measure the average intensity of APE1 fluorescence. APE1 Integrated Fluorescence Intensity (IFI) was computed for each nucleus multiplying each nuclear area for the respective mean grey value of APE1.

Real-Time RT-PCR

Total RNA was extracted from both non-confluent cultures of undifferentiated and differentiated cells at P3 using the TRIzol Reagent (Invitrogen). After treatment with DNase I (Ambion), first strand cDNA synthesis was performed with 1 μg total RNA using random hexanucleotides and MMLV reverse transcriptase (Invitrogen). Primers were designed from available human sequences using the primer analysis software Primer3 (Table S2). Quantitative RT-PCR was performed using Roche LightCycler 480 Real-Time PCR System and the LightCycler 480 SYBR Green I Master (Roche), following manufacturer's instructions. HPRT was used as internal control for normalization. LightCycler 480 Basic software (Roche) utilized the second derivative maximum method to identify the crossing point (Cp).

Statistics

Characteristics of the study population are described using means±SEM. Data were analyzed for normal distribution by Kolmogorov-Smirnov test. T-test or Mann-Whitney test, as appropriate, was used to compare continuous variables between two groups. Drug-treatment assays were analyzed by repeated measurements one-way Anova followed by Bonferroni post-test or by Friedman test followed by Dunn's post-test, as appropriate. Probability values (p) less than 0.05 were considered significant. Analyses were conducted with Prism, version 4.0c and SPSS20 for Macintosh software.

Results

Neuronal Differentiation of EC and Adult Stem Cells

To dissect the role played by APE1 on neuronal differentiation, we first used NT2-D1, a human teratocarcinoma cell line that can generate central nervous system neurons [28]. To induce their differentiation towards a neural fate, we adopted a protocol that involved the use of retinoic acid (ATRA) treatment for four consecutive weeks, followed by the incubation of the cells for two additional weeks in retinoic acid-free medium (Figure 1A). To verify the level of differentiation reached by NT2-D1, cells were characterized at the gene and protein expression levels. After one week of exposure to ATRA, NT2-D1 cells significantly down-regulated Nanog, Nestin and Sox2, representing markers of an undifferentiated state. This latter transcription factor, however, was still expressed at low levels by a large fraction of cells, being typically expressed by neuronal progenitors (Figure S1). Neuronal commitment and differentiation was evaluated by immunofluorescence and by realtime PCR, through which we analyzed transcripts of genes typically expressed by specific cell subtypes (Figure S2). Quantitatively, differentiated cells showed a significant increase in transcripts for glutamate decarboxylase (GAD1, a marker of GABAergic neurons), acetylcholinesterase (ACHE, a marker of cholinergic neurons), dopamine transporter (DAT, expressed by dopaminergic neurons), vesicular glutamate transporter1 (VGLUT1, marker of glutamatergic neurons) and Glutamate receptor subunit epsilon-1 (GRIN2a) (Figure 1B). Concomitantly, NT2-D1 cells significantly increased their positivity to MAP2 and GFAP, known markers of neural and glial cells, respectively. These proteins became organized showing a filamentous pattern starting from the third week of differentiation (Figure 1C).

As a second cellular model, we employed primary human Multipotent Adult Stem Cells isolated from adipose tissue (hAT) samples [31], adapting to this tissue the method that we previously used to generate these cells from human liver, heart, bone marrow, and skin biopsies [29,30]. Briefly, we generated 31 plastic adherent, proliferating cell lines from adipose tissue samples with very high efficiency. After three passages in culture, hAT-derived cell lines were characterized to check the acquisition of MASC features. Adipose-tissue derived cell lines showed a mesenchymal cell surface immunophenotype (Figure 2A), expressed the transcription factors Oct-4, NANOG and SOX2, were clonogenic and multipotent (Figure 2B). In order to induce hAT-MASC differentiation towards a neuronal fate, a three-step protocol was employed. hAT-MASC were first exposed to a high serum culture medium (N1) for one day, and subsequently to EGF and bFGF for 5 days (N2). At the end of this commitment period, cells were maintained in a serum-free medium containing insulin, indomethacin, and IBMX for 2–5 days (N3). During this last step cells displayed a remarkable morphological change: starting from a flattened and polygonal shape, their cytoplasm retracted towards the nucleus, leaving long cellular processes peripherally (Figure 2C). Quantitatively, differentiated cells showed, with respect to undifferentiated hAT-MASCs (n = 6), a significant increase in transcripts for myelin basic protein (MBP), glial fibrillary acidic protein (GFAP), Grin2A, choline acetyltransferase (CHAT), acetylcholinesterase (ACHE), and dopamine transporter (DAT), suggesting a stochastic maturation of primitive cells towards different neuronal and glial phenotypes (Figure 2D).

Altogether these results demonstrated that we could obtain cells with similar neuronal properties from both adult and EC stem cells.

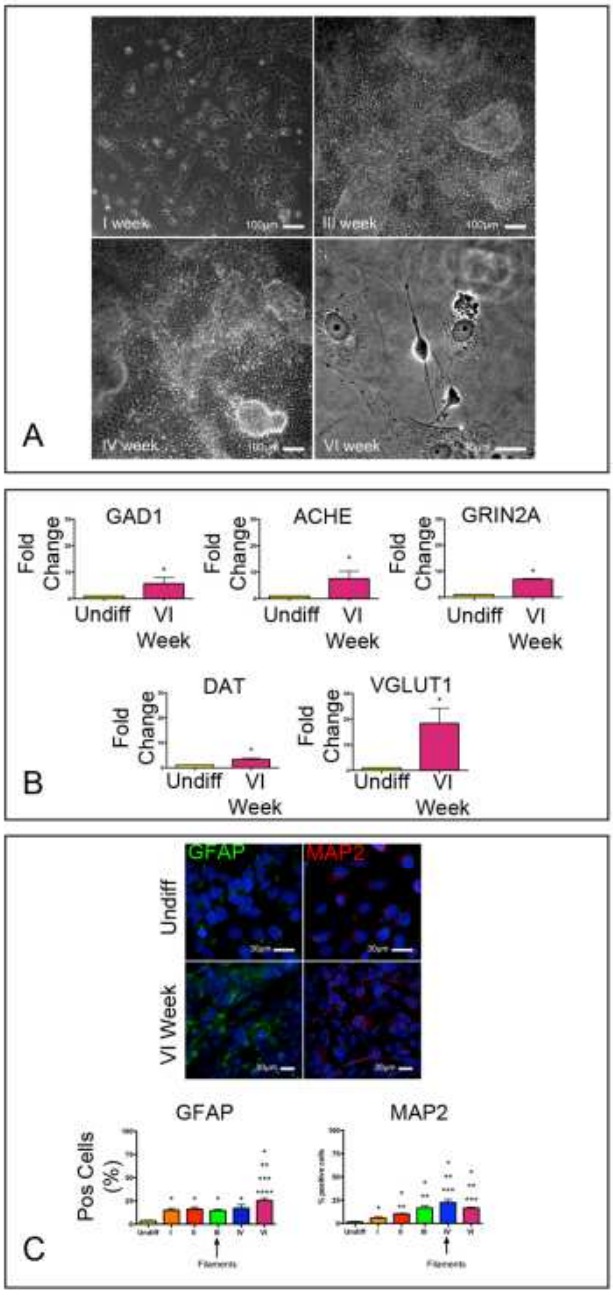

Figure 1. All-Trans Retinoic Acid (ATRA) induces neuronal differentiation of NT2-D1 cells. (**A**) Phase contrast images of NT2-D1 cells exposed to ATRA taken during the 1st, 3rd, 4th and 6th week of differentiation. (**B**) Histograms showing the relative expression of transcripts of markers of specific neuronal subtypes in differentiated NT2-D1 cells (VI week) versus undifferentiated cells. (**C**) Immunofluorescence images of undifferentiated (upper panels) and NT2-D1 cells exposed to the differentiation protocol for 6 weeks (VI week). GFAP and MAP2 were tested as markers of neural and glial lineages. Histograms represent the fraction (%) of cells positive to the tested markers during the differentiation period. Nuclei are stained in blue by 4′,6-diamidino-2-phenylindole (DAPI). Arrows indicate when, during the differentiation protocol, immunoreactive filaments were first observed. *, **, ***, **** $p<0.05$ vs I, II, III, and IV column, respectively.
doi:10.1371/journal.pone.0089232.g001

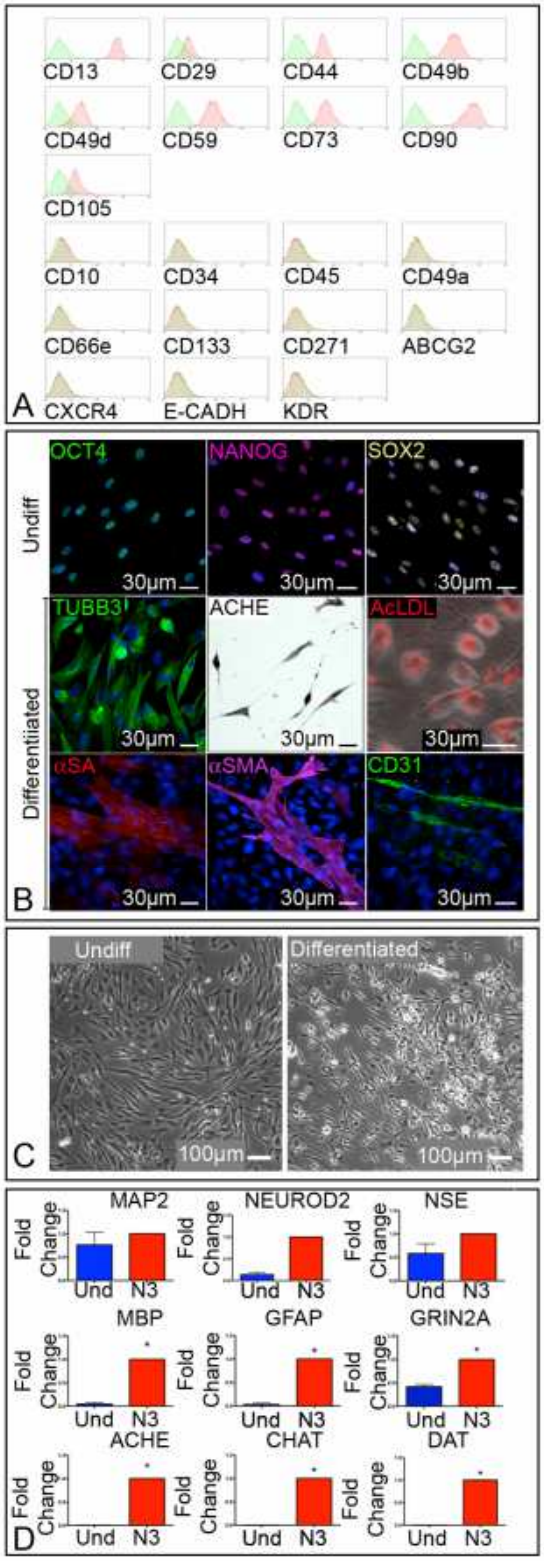

Figure 2. Characterization and neuronal differentiation of human adipose-tissue derived Multipotent Adult Stem Cells (hAT-MASC). (**A**) Representative flow cytometry histograms of a hAT-derived multipotent stem cell population. Plots show isotype control IgG-staining profile (green histogram) versus specific antibody staining profile (red histogram). hAT-MASCs express high levels of mesenchymal

stem cell markers (CD90, CD73, CD44, while they are negative for hematopoietic markers CD45 and CD34). (**B**) Immunofluorescence images of undifferentiated and differentiated hAT-MASC. Undifferentiated cells express the pluripotent state specific transcription factors Oct4 (green), Nanog (purple) and Sox2 (yellow). When exposed to neural differentiation medium these cells express the neural markers ß3 tubulin (TUBB3, green) and acetylcholinesterase (ACHE, brown). Once induced to differentiate into hepatocytes, hAT-MASC uptake acetylated LDL (AcLDL, red). Once exposed to myogenic or endothelial media, these cells express either alpha-sarcomeric actin (ASA, red), smooth muscle actin (SMA, purple) or PE-CAM (CD31, green). Nuclei are stained by DAPI (blue). (**C**) Phase contrast images of undifferentiated and differentiated hAT-MASC. (**D**) Histograms showing the relative expression of transcripts of neuronal and glial markers in differentiated hAT-MASC cells (N3, red histogram) versus undifferentiated cells (blue histogram).
doi:10.1371/journal.pone.0089232.g002

Reactive Oxygen Species (ROS)-dependent Nuclear Translocation of APE1 during Neuronal Differentiation

With the aim of exploring the involvement of ROS and APE1 in the differentiation of stem cells towards a neuronal fate, we first exposed hAT-MASC to the differentiation protocol and analyzed intracellular ROS levels. As shown in figures 3A–D, intracellular ROS significantly increased upon differentiation. This effect was abrogated, at least in part, by the addition of the ROS scavenger N-acetyl cysteine (NAC) to the culture medium. Quantitative immunofluorescence analysis of APE1 showed a similar trend (Figure 3E–K). Specifically, in non-differentiated cells (from undifferentiated to N2), APE1 was predominantly localized to the nucleus, while there was a significant increase in the nuclear content of the protein in N3, the most differentiated stage. The addition of NAC during the differentiation stage partially abolished this latter event (Figure 3K).

We then tested whether the observed nuclear increase was accompanied by a parallel increase in protein expression. As shown in (Figure 3L), testing APE1 expression in total protein extracts, we were not able to demonstrate the occurrence of any significant increase in total expression concomitant to the proceeding of differentiation. This was confirmed by RT-PCR experiments (data not shown), suggesting that the increase of APE1 in the nucleus was dependent on a nuclear accumulation of the protein rather than on a mere change in the expression levels.

We then analyzed the amount of APE1 bound to insoluble chromatin fraction, by performing a biochemical extraction protocol. The soluble protein fraction (S1) was recovered by extracting cells with CSK buffer. The resulting cell pellet (P1) corresponded to the proteins bound to DNA. Using these extraction conditions, we demonstrated a two fold increase in the expression of APE1 bound to DNA in the N2 and N3 stages compared to the non-differentiated (Control) or proliferating cells (N1) (Figure 3M).

The increase of APE1 bound to chromatin suggested the existence of a correlation with an increase of its DNA-related functions (i.e. both repair and/or transcriptional activities). Therefore, we tested whether this observation could correlate with the functional activity of NF-kB, a well-known transcriptional factor regulated by APE1. As expected, we observed a nuclear accumulation of p65-NF-kB, which correlated with the increase in the intensity of APE1 nuclear fluorescence (Figure 3N, O).

APE1 Redox Function Drives the Neuronal Fate of Differentiating Stem Cells

Last, we studied the involvement of APE1 in the neuronal differentiation of both adult and EC stem cells.

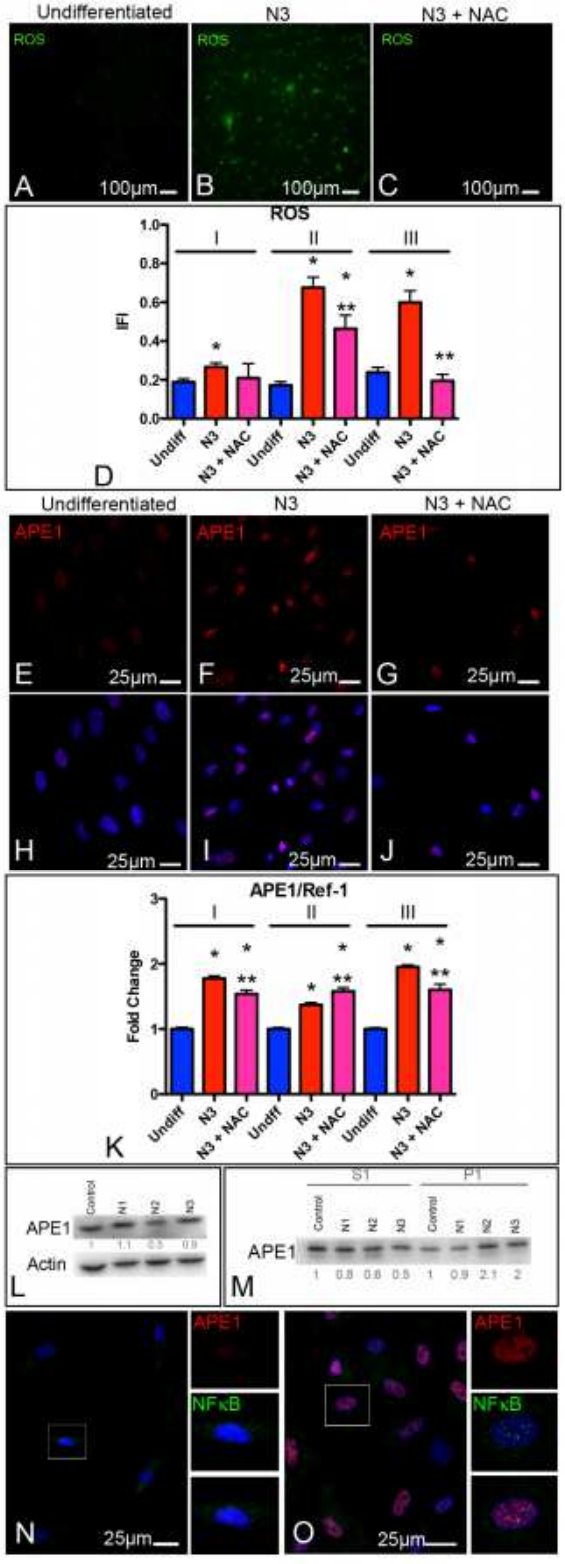

Figure 3. Differentiation towards a neuronal fate increases both intracellular ROS levels and the nuclear localization of APE1. (**A–D**) Epifluorescence images of undifferentiated (undiff, **A**), and differentiated hAT-MASC cultured either in the absence (N3, **B**) or in the presence (N3+NAC, **C**) of NAC. The ROS sensitive, green fluorescent dye CM-H_2DCFDA was used to quantitate intracellular ROS levels. Histograms (**D**) show the quantification of the Integrated Fluorescence

Intensity (IFI) of the above-described groups in 3 (I–III) independent hAT-MASC lines. (**E–G**) Immunofluorescence images of APE1 (red) in undifferentiated, N3, and N3+NAC groups. (**H–J**) Nuclear localization of APE1 is shown superimposing to the above images, the blue fluorescence of DAPI staining. APE1 expression was quantified in the three groups by analyzing the IFI of APE1 nuclear fluorescence. Histograms (**K**) summarizing data for APE1 nuclear quantitative fluorescence. (**L**) Representative Western blot of APE1. 10 μg of total protein extracts were loaded onto a 10% SDS-PAGE, blotted and incubated with the APE1 primary antibody and horseradish peroxidase-conjugated secondary antibody. Numbers at the bottom were obtained from densitometric analysis of three independent experiments, normalized versus actin. (**M**) Cells in the different stages of differentiation were separated into fractions S1 (soluble proteins) and P1 (proteins bound to DNA). Equivalent amounts were analyzed by western blot with antibody against APE1. Numbers at the bottom were obtained from densitometric analysis of three independent experiments, normalized versus a gel run in parallel and stained with Comassie. (**N, O**) Immunofluorescence images showing colocalization of APE1 (red) with the p65 subunit of NFkB (green) obtained both in undifferentiated and differentiated (N3) hAT-MASC. Cells comprised in the square are shown at higher magnification in the panels localized at the right side of each picture, where the contribution of APE1 and NFkB are shown as separate images. *, ** $p<0.05$ vs Undifferentiated or N3 cells, respectively.

doi:10.1371/journal.pone.0089232.g003

For this purpose, we first evaluated the impact exerted by the addition of NAC to the neural differentiation media of hAT-MASC. As shown in figure 4A-B, the morphology of cells reaching the end of the differentiation period was dramatically affected by the antioxidant treatment. Additionally, NAC significantly increased the fraction of differentiated cells expressing the neuronal marker MAP2, without affecting the expression of the glial marker MBP (Figure 4C–J).

Based on these data, we investigated the role of APE1 redox function on neuronal differentiation using an APE1 specific redox inhibitor E3330. For this purpose, we first assessed the toxicity of E3330 on hAT-MASCs, exposing these cells either during the last step (N3) or during the last two steps of the differentiation protocol (N2 and N3). E3330, at a dose ranging from 10–100 μM, had no apparent effect on undifferentiated hAT-MASC viability, as assessed by MTT assay (Figure 5A), while its addition to differentiating cells significantly affected cell yield (Figure 5B). Therefore, for subsequent studies, we employed a dose and administration scheme that balanced E3330 toxicity with its effects on APE1. Interestingly, the addition of E3330 during the first day of incubation with N3 medium significantly increased nuclear levels of APE1, as detected by quantitative fluorescence imaging (Figure 5C, D). On the contrary, when E3330 was added during the entire differentiation period, we observed a significant decrease in APE1 nuclear levels (Figure 5C, D).

The addition of E3330 during the differentiation protocol, significantly increased transcripts associated with neuronal differentiation; specifically, with respect to differentiated hAT-MASCs not exposed to E3330, the exposed ones up-regulated the transcripts for the neuronal markers NeuroD2 and MAP2 (Figure 6A). Furthermore, E3330-treatment increased the expression of markers of cholinergic (CHAT), and dopaminergic (DAT) neurons (Figure 6A). Last, cells exposed to E3330 showed an increase in immunoreactivity against both MAP2 and MBP (Figure 6B).

Similar results were also obtained exposing the cell line NT2-D1 to E3330 starting from the 3rd week of differentiation. Specifically, with respect to the non-treated ones, E3330-treated cells expressed significantly higher levels of GAD1, ACHE, and DAT. On the contrary, Vesicular glutamate transporter 1, and Grin2A were not up-regulated by the inhibition of APE1 redox function (Figure 7A).

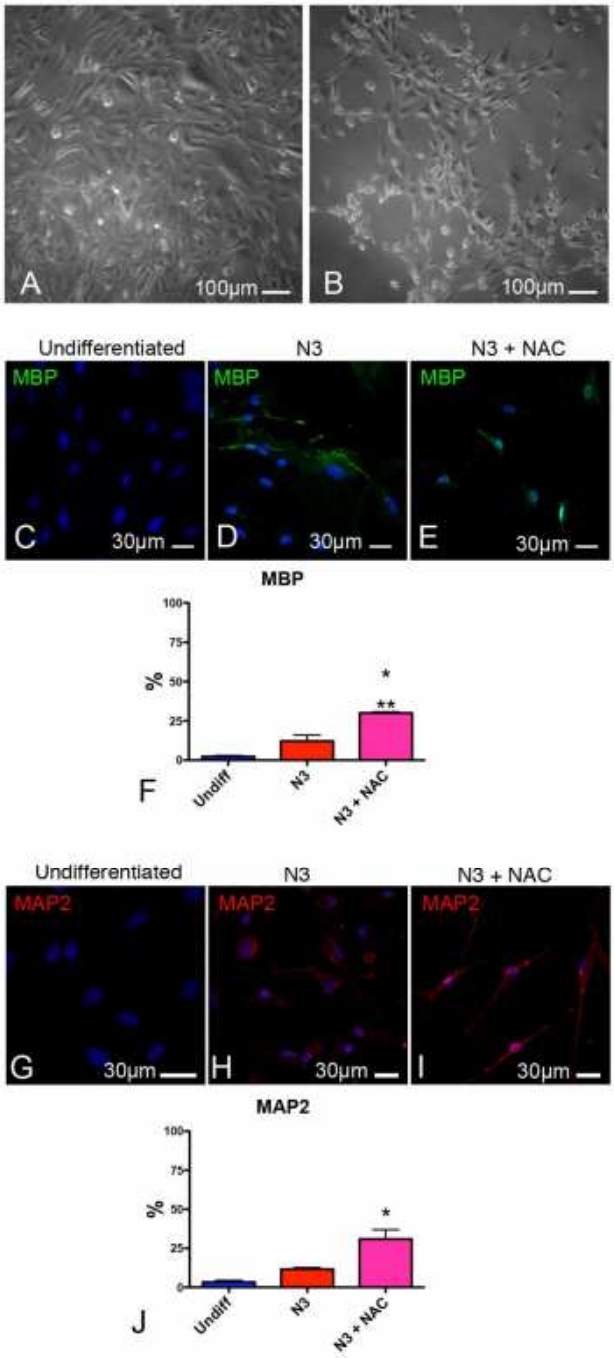

Figure 4. Impact exerted by ROS on the differentiation of adult stem cell towards a neural fate. (**A**, **B**) Contrast phase images of hAT-MASC differentiated in the absence (**A**) or in the presence (**B**) of NAC. Fluorescence images showing MBP (**C**, green) and MAP2 (**G**, red) expression in undifferentiated hAT-MASC and in hAT-MASC differentiated either in the absence (**D**, **H**) or presence of NAC (**E**, **I**). Histograms (**F**, **J**) represent the fraction of cells positive for MBP or MAP2. n = 3 distinct hAT-MASC lines; *, ** $p<0.05$ vs Undifferentiated or N3 cells, respectively.

doi:10.1371/journal.pone.0089232.g004

Last, E3330-treatment significantly increased the immunoreactivity of differentiated cells against MAP2, while it had no effect on GFAP (Figure 7B, C).

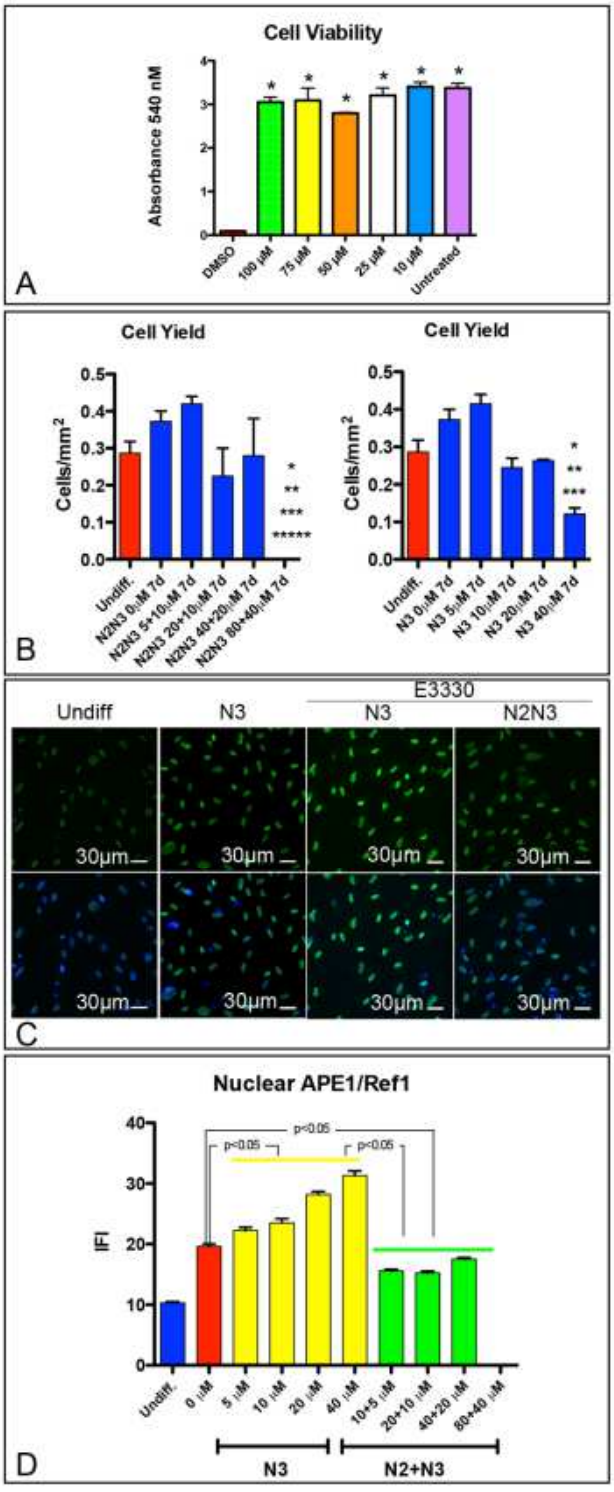

Figure 5. Effects of E3330 on cell viability, proliferation and APE1 expression. (**A**) Histograms summarizing the results of a viability assay (MTT) performed following the exposure of undifferentiated hAT-MASC to either positive control (DMSO), negative control (untreated), or 10 µM, 25 µM, 50 µM, 75 µM, and 100 µM of E3330. (**B**) Histograms summarizing the effects of the exposure of hAT-MASC to E3330 -during either the last step (N3) or the last two steps (N2N3) of differentiation- on the yield of cells at the end of the differentiation protocol. (**C**) Immunofluorescence images showing the effects the exposure of hAT-MASC to E3330–during either N3 or N2N3- on APE1 expression (green). Nuclei are blue labeled by DAPI. (**D**) Quantification of Ape1 nuclear expression (IFI) is summarized in histograms. *, **, ***, ***** p<0.05 vs I, II, III, and V column, respectively.
doi:10.1371/journal.pone.0089232.g005

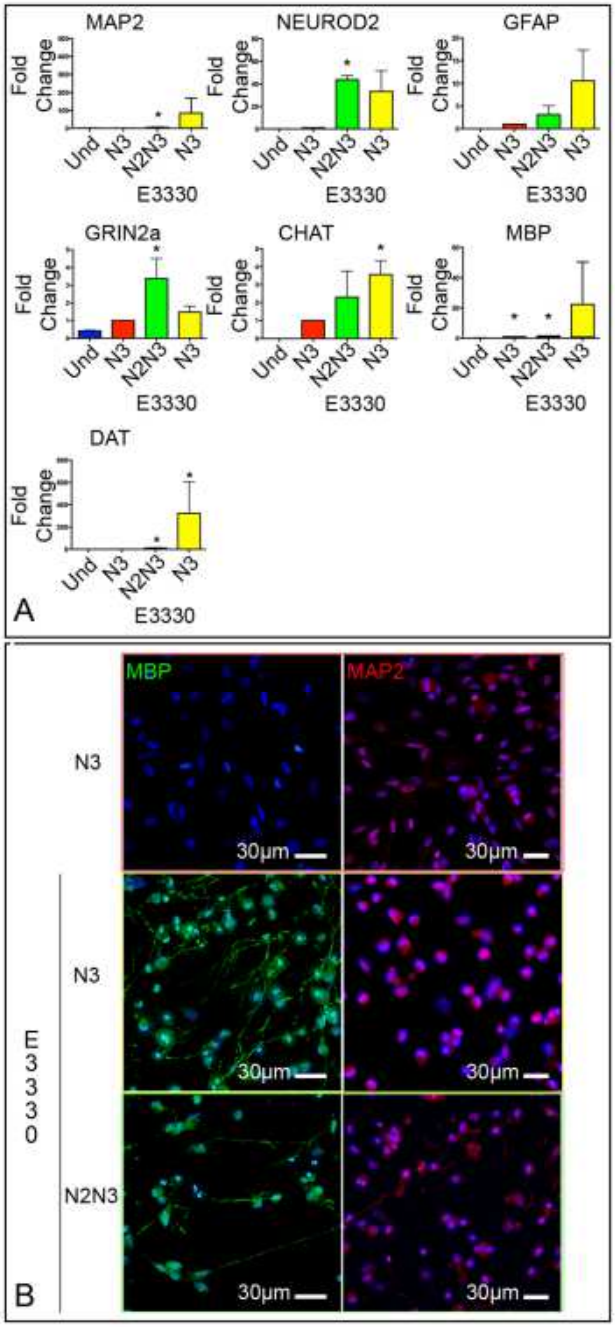

Figure 6. E3330 increases the neuronal differentiation of hAT-MASC. (**A**) Histograms showing the relative expression of transcripts of neuronal and glial markers in undifferentiated and differentiated hAT-MASC, exposed or not to E3330. (**B**) Immunofluorescence images of differentiated hAT-MASC that were either not exposed (upper 2 panels) or exposed (lower 4 panels) to E3330 during the differentiation protocol. Cells were stained for the glial marker MBP (green) and for the neuronal marker MAP2 (red). * p<0.05 vs Undifferentiated cells.
doi:10.1371/journal.pone.0089232.g006

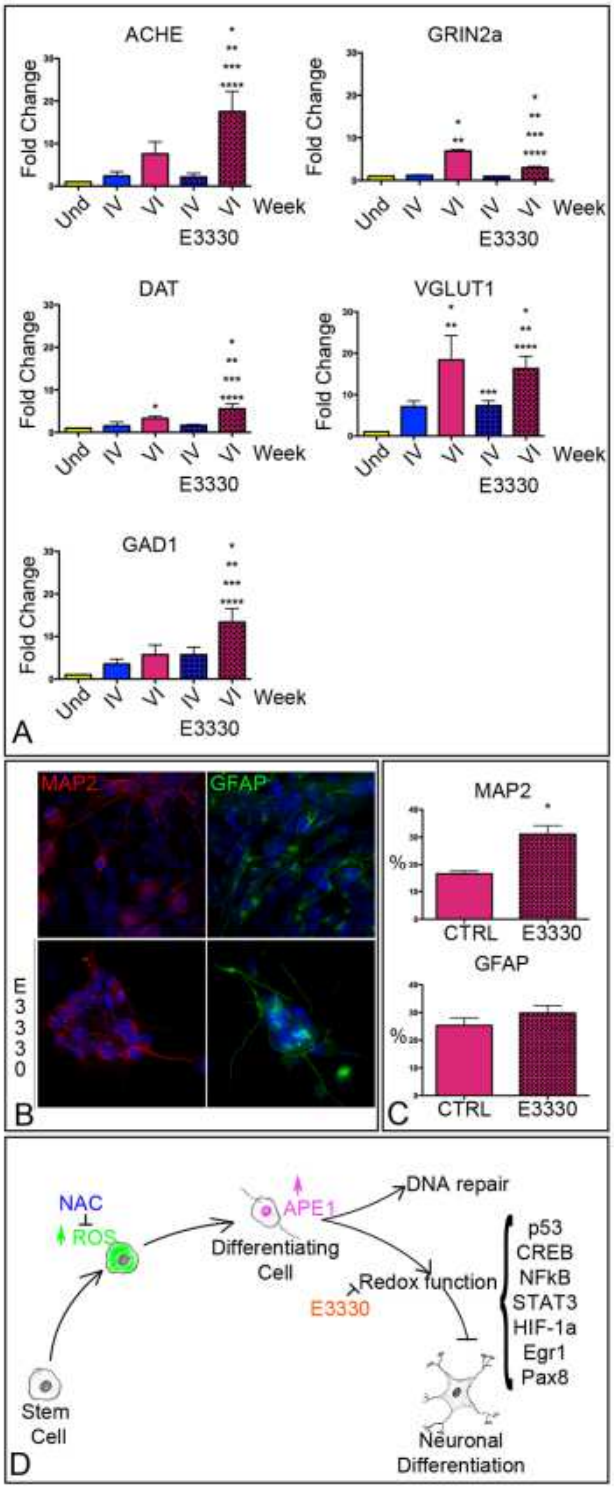

Figure 7. E3330 increases the neuronal differentiation of hAT-MASC. (**A**) Histograms showing the relative expression of transcripts of markers of specific neuronal subtypes in undifferentiated and differentiated NT2-D1, exposed or not to E3330, at the IV and VI week of differentiation. (**B**) Immunofluorescence images of differentiated NT2-D1 that were either not exposed (upper panels) or exposed (lower panels) to E3330 during the differentiation protocol. Cells were stained for the glial marker GFAP (green) and for the neuronal marker MAP2 (red). (**C**) Histograms summarizing the fraction of cells positive to MAP2 and GFAP at the end of the VI week of differentiation in the absence (−E3330) or presence (+E3330) of Ape1 inhibition. (**D**) Diagram summarizing the main findings of this work on the involvement of Ape1 in neuronal differentiation. Arrows with blunt ends indicate inhibition. * $p<0.05$ vs I column.
doi:10.1371/journal.pone.0089232.g007

Altogether these results indicate that the redox function of APE1 regulates stem cell differentiation towards a neurogenic fate, reducing it and modulating the differentiation towards specific neuronal subtypes.

Discussion

This work has several aspects of novelty that have been summarized in Figure 7D: i) APE1 accumulates, in a ROS-dependent fashion, into the nuclei and associates to the chromatin of adult stem cells differentiated towards a neuronal fate, ii) the redox function of APE1 plays a role in the neuronal differentiation of both adult and embryonic stem cells, and iii) the use of a specific inhibitor of the redox function of APE1 increases the extent of neuronal differentiation, facilitating the differentiation towards specific neuronal subsets.

A growing body of literature obtained on different cell models (most of which obtained from rodents) has demonstrated that low-to-moderate levels of ROS govern different steps of neurogenesis, ranging from progenitor cell proliferation to neuronal differentiation [34]. Consistently, we show in the present work that intracellular ROS levels significantly increase during the differentiation process of human AT-MASC towards a neural phenotype. However, we newly demonstrate that the addition of an antioxidant (NAC) to the culture medium of hAT-MASC may alter the extent of differentiation of this cell type. To gain insights into the mechanism involved in this process, we focused our attention on APE1, since Reactive Oxygen Species (ROS) may regulate the activity of this multifunctional protein both at the transcriptional level and at the post-translational one, promoting its cytoplasmic to nuclear translocation [2]. This latter event, which is regulated by acetylation of conserved K residues present in the N-terminal domain of APE1, has been associated to the functional activation of several target transcription factors [35]. In line, we found that hAT-MASC exposed to a neural differentiation protocol are characterized by a progressive nuclear accumulation of both APE1 and one of its target transcription factors (i.e. nuclear factor-kB, NF-kB). These events occur in the absence of a net increase in the total levels of APE1 and are paralleled by a progressive increase in the abundance of chromatin-bound APE1. Importantly, NAC can partially reduce the nuclear accumulation of APE1. Altogether our results support the hypothesized role played by redox-sensitive transcription factors on neurogenesis [34].

Given the complete independence of the two major functions of APE1 (i.e. the repair function and the redox one) [36], we took advantage of the ability of the drug E3330 to inhibit selectively this latter, without affecting the first one. Our results demonstrate that E3330, at a dose ranging from 10–100 μM, is not toxic, when given to undifferentiated cells. However, the addition of this compound to the differentiation media of either hAT-MASC or NT2-D1 significantly increases, in both cell types, the expression of markers of neuronal differentiation (e.g. MAP2). Altogether these results suggest that the redox function of APE1 exerts an inhibitory effect on the maturation of both adult and embryonic human stem cells towards the neuronal fate. Consistently, several transcription factors that are regulated by APE1 in a redox-dependent manner have been implicated in neurogenesis (e.g. p53,

CREB, NF-kB, STAT3, HIF-1α, Egr1, and Pax8). Among these, a primary inhibitory role on neural differentiation is played by p53. In fact, p53 deficiency leads to increased neurogenesis, biased differentiation *in vivo* and an incremented *ex vivo* proliferation of neural stem cells [37,38]. STAT3 too may bias stem cell differentiation, reducing neurogenesis, as shown by the observation that neural precursor cells differentiate into astrocytes after stimulation with CNTF or LIF via STAT3 activation [39,40].

Last, the addition of E3330 to differentiating cells modifies the expression of markers of specific neuronal subtypes, increasing the expression of cholinergic, dopaminergic and GABAergic markers. These results may be consistent with the observed effect of mild hypoxia on neural progenitor cell differentiation towards a dopaminergic phenotype [41] or with the effects of pollutants that increase intracellular ROS levels on the maturation of GABAergic neurons [42]. Less prominent are the effects observed on the expression of glutamatergic or serotoninergic markers. Intriguingly, although NT2-D1 cells may generate rare serotoninergic neurons [43], we observed that SERT expression peaked at a relatively early time-point (4 weeks) and significantly decreased after 2 additional weeks of culture. This event may be a consequence of the mechanical selection of cells that is performed after 4 weeks of differentiation. However, the addition of E3330 did not affect SERT expression levels at earliest time point.

In conclusion, we have demonstrated that APE1 is involved in the differentiation of adult and embryonic stem cells towards a neuronal fate. The inhibition of APE1 redox function, through the use of the specific inhibitor E3330, demonstrates that this factor may act by both repressing neuronal maturation and biasing the differentiation towards specific neuronal subtypes. The majority of the transcription factors that are regulated by APE1 in a redox-dependent fashion act mainly favoring progenitor cell proliferation and differentiation, while p53 and STAT3 exert a repressive effect on neurogenesis. E3330 may act either inhibiting these latter factors or shifting stimuli from proliferation to differentiation. Therefore, this work emphasizes the possible use of pharmacological strategies, based on modulation of APE1 redox functions, to boost neural differentiation and bias the differentiation potential of stem cells towards specific neuronal subtypes. In this regard, the possibility to employ a small molecule, such as E3330, to increase the extent of differentiation of stem cells towards a dopaminergic phenotype is a very attractive one.

Supporting Information

Figure S1 Immunofluorescence images of undifferentiated NT2-D1 cells (upper panels) and NT2-D1 cells exposed for 1 week to ATRA (lower panels). Typical markers of undifferentiated cells Nanog (purple), Nestin (green) and Sox2 (yellow) were tested. Histograms comprised in the mid box represent the fraction (%) of cells strongly positive to the tested markers. Histograms contained in the low box show the fraction of cells either strongly or weakly positive to Sox2.
(TIF)

Figure S2 Scheme showing the markers chosen to identify neural precursors, glial and neuronal subtypes.
(TIF)

Table S1 Primary and secondary antibodies utilized. RP = rabbit polyclonal; MM = mouse monoclonal.
(DOCX)

Table S2 Real-Time PCR primers.
(DOCX)

Author Contributions

Conceived and designed the experiments: DC GT APB. Performed the experiments: RD NB GG CV MR GV MF SR. Analyzed the data: RD NB CV MR DC GT APB. Contributed reagents/materials/analysis tools: MRK CAB PP. Wrote the paper: DC APB GT CAB.

References

1. Fung H, Demple B (2005) A vital role for Ape1/Ref1 protein in repairing spontaneous DNA damage in human cells. Molecular cell 17: 463–470.
2. Tell G, Damante G, Caldwell D, Kelley MR (2005) The intracellular localization of APE1/Ref-1: more than a passive phenomenon? Antioxidants & redox signaling 7: 367–384.
3. Su D, Delaplane S, Luo M, Rempel DL, Vu B, et al. (2011) Interactions of apurinic/apyrimidinic endonuclease with a redox inhibitor: evidence for an alternate conformation of the enzyme. Biochemistry 50: 82–92.
4. Fishel ML, Kelley MR (2007) The DNA base excision repair protein Ape1/Ref-1 as a therapeutic and chemopreventive target. Molecular aspects of medicine 28: 375–395.
5. Zhang J, Luo M, Marasco D, Logsdon D, LaFavers KA, et al. (2013) Inhibition of apurinic/apyrimidinic endonuclease I's redox activity revisited. Biochemistry 52: 2955–2966.
6. Shimizu N, Sugimoto K, Tang J, Nishi T, Sato I, et al. (2000) High-performance affinity beads for identifying drug receptors. Nature biotechnology 18: 877–881.
7. Nishi T, Shimizu N, Hiramoto M, Sato I, Yamaguchi Y, et al. (2002) Spatial redox regulation of a critical cysteine residue of NF-kappa B in vivo. J Biol Chem 277: 44548–44556.
8. Zou GM, Maitra A (2008) Small-molecule inhibitor of the AP endonuclease 1/REF-1 E3330 inhibits pancreatic cancer cell growth and migration. Molecular cancer therapeutics 7: 2012–2021.
9. Cesaratto L, Codarin E, Vascotto C, Leonardi A, Kelley MR, et al. (2013) Specific inhibition of the redox activity of ape1/ref-1 by e3330 blocks tnf-alpha-induced activation of IL-8 production in liver cancer cell lines. PLoS One 8: e70909.
10. Vascotto C, Bisetto E, Li M, Zeef LA, D'Ambrosio C, et al. (2011) Knock-in reconstitution studies reveal an unexpected role of Cys-65 in regulating APE1/Ref-1 subcellular trafficking and function. Molecular biology of the cell 22: 3887–3901.
11. Zou GM, Luo MH, Reed A, Kelley MR, Yoder MC (2007) Ape1 regulates hematopoietic differentiation of embryonic stem cells through its redox functional domain. Blood 109: 1917–1922.
12. Chung U, Igarashi T, Nishishita T, Iwanari H, Iwamatsu A, et al. (1996) The interaction between Ku antigen and REF1 protein mediates negative gene regulation by extracellular calcium. J Biol Chem 271: 8593–8598.
13. Kuninger DT, Izumi T, Papaconstantinou J, Mitra S (2002) Human AP-endonuclease 1 and hnRNP-L interact with a nCaRE-like repressor element in the AP-endonuclease 1 promoter. Nucleic acids research 30: 823–829.
14. Poletto M, Vascotto C, Scognamiglio PL, Lirussi L, Marasco D, et al. (2013) Role of the unstructured N-terminal domain of the hAPE1 (human apurinic/apyrimidinic endonuclease 1) in the modulation of its interaction with nucleic acids and NPM1 (nucleophosmin). Biochem J 452: 545–557.
15. Xanthoudakis S, Miao GG, Curran T (1994) The redox and DNA-repair activities of Ref-1 are encoded by nonoverlapping domains. Proc Natl Acad Sci U S A 91: 23–27.
16. Vascotto C, Fantini D, Romanello M, Cesaratto L, Deganuto M, et al. (2009) APE1/Ref-1 interacts with NPM1 within nucleoli and plays a role in the rRNA quality control process. Molecular and cellular biology 29: 1834–1854.
17. Tell G, Wilson DM 3rd, Lee CH (2010) Intrusion of a DNA repair protein in the RNome world: is this the beginning of a new era? Molecular and cellular biology 30: 366–371.
18. Ludwig DL, MacInnes MA, Takiguchi Y, Purtymun PE, Henrie M, et al. (1998) A murine AP-endonuclease gene-targeted deficiency with post-implantation embryonic progression and ionizing radiation sensitivity. Mutation research 409: 17–29.
19. Izumi T, Brown DB, Naidu CV, Bhakat KK, Macinnes MA, et al. (2005) Two essential but distinct functions of the mammalian abasic endonuclease. Proc Natl Acad Sci U S A 102: 5739–5743.
20. Kim MH, Kim HB, Acharya S, Sohn HM, Jun JY, et al. (2009) Ape1/Ref-1 induces glial cell-derived neurotropic factor (GDNF) responsiveness by upregulating GDNF receptor alpha1 expression. Molecular and cellular biology 29: 2264–2277.
21. Lin LF, Doherty DH, Lile JD, Bektesh S, Collins F (1993) GDNF: a glial cell line-derived neurotrophic factor for midbrain dopaminergic neurons. Science 260: 1130–1132.
22. Ono Y, Matsumoto K, Furuta T, Ohmoto T, Akiyama K, et al. (1995) Relationship between expression of a major apurinic/apyrimidinic endonuclease

(APEX nuclease) and susceptibility to genotoxic agents in human glioma cell lines. Journal of neuro-oncology 25: 183–192.
23. Wilson TM, Rivkees SA, Deutsch WA, Kelley MR (1996) Differential expression of the apurinic/apyrimidinic endonuclease (APE/ref-1) multifunctional DNA base excision repair gene during fetal development and in adult rat brain and testis. Mutat Res 362: 237–248.
24. Walton M, Lawlor P, Sirimanne E, Williams C, Gluckman P, et al. (1997) Loss of Ref-1 protein expression precedes DNA fragmentation in apoptotic neurons. Brain Res Mol Brain Res 44: 167–170.
25. Lewen A, Sugawara T, Gasche Y, Fujimura M, Chan PH (2001) Oxidative cellular damage and the reduction of APE/Ref-1 expression after experimental traumatic brain injury. Neurobiol Dis 8: 380–390.
26. Sakurai M, Nagata T, Abe K, Horinouchi T, Itoyama Y, et al. (2003) Oxidative damage and reduction of redox factor-1 expression after transient spinal cord ischemia in rabbits. J Vasc Surg 37: 446–452.
27. Marcon G, Tell G, Perrone L, Garbelli R, Quadrifoglio F, et al. (2009) APE1/Ref-1 in Alzheimer's disease: an immunohistochemical study. Neurosci Lett 466: 124–127.
28. Coyle DE, Li J, Baccei M (2011) Regional differentiation of retinoic acid-induced human pluripotent embryonic carcinoma stem cell neurons. PLoS One 6: e16174.
29. Beltrami AP, Cesselli D, Bergamin N, Marcon P, Rigo S, et al. (2007) Multipotent cells can be generated in vitro from several adult human organs (heart, liver and bone marrow). Blood 110: 3438–3446.
30. Bergamin N, Dardis A, Beltrami A, Cesselli D, Rigo S, et al. (2013) A human neuronal model of Niemann Pick C disease developed from stem cells isolated from patient's skin. Orphanet J Rare Dis 8: 34.
31. Zeppieri M, Salvetat ML, Beltrami AP, Cesselli D, Bergamin N, et al. (2013) Human adipose-derived stem cells for the treatment of chemically burned rat cornea: preliminary results. Curr Eye Res 38: 451–463.
32. Pines A, Perrone L, Bivi N, Romanello M, Damante G, et al. (2005) Activation of APE1/Ref-1 is dependent on reactive oxygen species generated after purinergic receptor stimulation by ATP. Nucleic acids research 33: 4379–4394.
33. Schneider CA, Rasband WS, Eliceiri KW (2012) NIH Image to ImageJ: 25 years of image analysis. Nature methods 9: 671–675.
34. Kennedy KA, Sandiford SD, Skerjanc IS, Li SS (2012) Reactive oxygen species and the neuronal fate. Cellular and molecular life sciences : CMLS 69: 215–221.
35. Tell G, Fantini D, Quadrifoglio F (2010) Understanding different functions of mammalian AP endonuclease (APE1) as a promising tool for cancer treatment. Cellular and molecular life sciences : CMLS 67: 3589–3608.
36. Tell G, Quadrifoglio F, Tiribelli C, Kelley MR (2009) The many functions of APE1/Ref-1: not only a DNA repair enzyme. Antioxidants & redox signaling 11: 601–620.
37. Liu H, Jia D, Li A, Chau J, He D, et al. (2013) p53 regulates neural stem cell proliferation and differentiation via BMP-Smad1 signaling and Id1. Stem cells and development 22: 913–927.
38. Gil-Perotin S, Haines JD, Kaur J, Marin-Husstege M, Spinetta MJ, et al. (2011) Roles of p53 and p27(Kip1) in the regulation of neurogenesis in the murine adult subventricular zone. The European journal of neuroscience 34: 1040–1052.
39. Bonni A, Sun Y, Nadal-Vicens M, Bhatt A, Frank DA, et al. (1997) Regulation of gliogenesis in the central nervous system by the JAK-STAT signaling pathway. Science 278: 477–483.
40. Rajan P, McKay RD (1998) Multiple routes to astrocytic differentiation in the CNS. The Journal of neuroscience : the official journal of the Society for Neuroscience 18: 3620–3629.
41. Liu S, Tian Z, Yin F, Zhao Q, Fan M (2009) Generation of dopaminergic neurons from human fetal mesencephalic progenitors after co-culture with striatal-conditioned media and exposure to lowered oxygen. Brain research bulletin 80: 62–68.
42. Addae C, Cheng H, Martinez-Ceballos E (2013) Effect of the environmental pollutant hexachlorobenzene (HCB) on the neuronal differentiation of mouse embryonic stem cells. International journal of environmental research and public health 10: 5244–5256.
43. Podrygajlo G, Tegenge MA, Gierse A, Paquet-Durand F, Tan S, et al. (2009) Cellular phenotypes of human model neurons (NT2) after differentiation in aggregate culture. Cell and tissue research 336: 439–452.